HAL
open science

Introduction of anisotropy in double network elastomers by orientation and two-step curing

Ludovic Feige

To cite this version:

Ludovic Feige. Introduction of anisotropy in double network elastomers by orientation and two-step curing. Material chemistry. Université Paris sciences et lettres, 2019. English. NNT : 2019PSLET030 . tel-02887289

HAL Id: tel-02887289

https://pastel.hal.science/tel-02887289

Submitted on 2 Jul 2020

HAL is a multi-disciplinary open access archive for the deposit and dissemination of scientific research documents, whether they are published or not. The documents may come from teaching and research institutions in France or abroad, or from public or private research centers.

L'archive ouverte pluridisciplinaire **HAL**, est destinée au dépôt et à la diffusion de documents scientifiques de niveau recherche, publiés ou non, émanant des établissements d'enseignement et de recherche français ou étrangers, des laboratoires publics ou privés.

PSL UNIVERSITÉ PARIS

THÈSE DE DOCTORAT
DE L'UNIVERSITÉ PSL

Préparée à l'Ecole Supérieure de Physique et de Chimie Industrielles de la ville de Paris (ESPCI Paris)

Introduction of anisotropy in double network elastomers by orientation and two-step curing

Introduction d'anisotropie dans des doubles réseaux élastomères par orientation et réticulation en deux étapes

Soutenue par
Ludovic FEIGE
Le 18 Décembre 2019

Ecole doctorale n° 397
Physique et chimie des matériaux

Spécialité
Chimie des Matériaux

Composition du jury :

Renaud, NICOLAY Professeur, ESPCI Paris	*Président*
Catherine, AMIEL Professeure, Université Paris 12	*Rapportrice*
Julie, DIANI Directrice de recherche, CNRS / Ecole Polytechnique	*Rapportrice*
Guillaume, MIQUELARD-GARNIER Maître de conférences Conservatoire National des Arts et Métiers	*Examinateur*
Meredith, WISEMAN Ingénieure de Recherche DSM	*Examinatrice*
Costantino, CRETON Directeur de recherches CNRS / ESPCI Paris	*Directeur de thèse*

ESPCI PARIS | PSL

Table of contents

Table of contents iii

Substantial summary in French vii

Acknowledgments xv

List of Symbols xvii

List of abbreviations xix

General introduction 1

Chapter 1: From chemistry and physics to the design of new double network elastomers 7

1. Introduction 11
2. Chemistry and physics of crosslinked elastomeric networks 13
   - 2.1. Synthesis of permanent polymeric networks 13
   - 2.2. From chain physics to network properties 19
3. Fracture of soft materials and how to reinforce them 27
   - 3.1. Description of fracture in soft materials, a matter of dissipation 27
   - 3.2. General guidelines for improving the fracture resistance of soft materials 32
4. The multiple network strategy: from the original concept to new properties 41
   - 4.1. Double network hydrogels 41
   - 4.2. From hydrogels to elastomers 47
   - 4.3. The challenge of describing the reinforcing mechanism theoretically 52
   - 4.4. Toward new properties for multiple network elastomers 55
5. Bringing anisotropy to double network elastomers 57
   - 5.1. Example of anisotropic polymeric systems 57
   - 5.2. Oriented chains in rubbers, a key element for some applications 60
   - 5.3. Battle plan, or how to make double networks anisotropic 63
6. Conclusions 67
7. References 69

Chapter 2: Design and preliminary study of two effective dual-curing systems 85

1. Introduction 89
   1.1. Overview of the requirements specifications 89
   1.2. Presentation of the thermal system 89
   1.3. Presentation of the UV system 90
   1.4. Outline 91
2. Generalities about chemistry and material preparation 93
   2.1. Chemicals and formulation 93
   2.2. Materials synthesis 94
   2.3. Characterization methods 96
3. Study of the thermal system 101
   3.1. A kinetic study of the system 101
   3.2. Variation of the initial formulation 106
   3.3. Partial conclusion and identification of a working point formulation 112
4. Study of the UV system 115
   4.1. Effect of crosslinker content 115
   4.2. Effect of initiator content 116
   4.3. Effect of allyl acrylate content 117
   4.4. The issue of sample-to-sample variability 121
5. Conclusions 125
6. References 127

Chapter 3: Application of the dual-cure systems to the preparation of prestretched filler networks 129

1. Introduction 133
2. Preparation process 135
   2.1. Initial network formulations 135
   2.2. Prestretching and second curing 135
   2.3. Problems encountered during the thermal second curing 135
3. Preparation of prestretched samples and measurement of prestretching 139
   3.1. Presentation of the results 139
   3.2. Comparison to Flory's model 140

3.3. Additional mechanical characterization for the thermal system 152
4. Prospective: what to expect in a double network structure? 155
4.1. Description of the approach 155
4.2. Derivation of the model 156
5. Conclusions 163
6. References 165

Chapter 4: Incorporation of prestretched filler networks into double network structures 167

1. Introduction 171
2. Preparation process and additional characterization tools 173
2.1. Filler networks 173
2.2. Preparation of double networks 173
2.3. Step-cyclic tests 174
2.4. Fracture tests 176
3. Study of two examples of prestretched DN 181
3.1. Relative changes in dimensions 181
3.2. Mechanical characterization 183
3.3. Toward a more detailed characterization? 186
3.4. Partial conclusion 193
4. Systematic study of the UV system 195
4.1. Identification of typical trends and odd ones 195
4.2. Study of unprestretched double network samples 196
4.3. Study of prestretched DN using envelope curves 201
4.4. Exploitation of the entire cyclic test 207
4.5. Suggested physical picture 222
5. Influence of damage on mechanical properties for the UV system 231
5.1. Study of viscoelastic properties 231
5.2. Study of fracture properties 234
6. Conclusions 239
7. References 241

Chapter 5: Toward glassy filler networks 243

1. Introduction and context 247
2. Materials preparation and characterization 249
   2.1. Overall presentation of the preparation strategy 249
   2.2. Materials preparation 250
   2.3. Dynamic Mechanical Analysis 254
   2.4. Tensile tests 257
3. Results regarding the materials preparation 259
   3.1. Overall overview of the synthesis 259
   3.2. Quantitative parameters associated to synthesis 260
4. DMA characterizations 263
   4.1. Effect of the nature of the crosslinker 263
   4.2. Effect of crosslinker content / UV synthesis / BDMA crosslinker 268
   4.3. Effect of initiation type 269
5. Tensile characterizations 273
   5.1. UV-polymerized DN with 0.75mol% BDMA 273
   5.2. UV-polymerized DN with 1.5 mol% BDA 274
6. Conclusions 277
7. References 279

General conclusions and prospects 281

Substantial summary in French

Chimie et physique au service de la conception de nouveaux doubles réseaux élastomères

Les élastomères sont des matériaux qui combinent deux propriétés très importantes : d'un côté un module bas et de l'autre une grande capacité de déformation. Ces propriétés sont dues à l'origine statistique de la déformation caoutchoutique. La compréhension fine de ce phénomène permet la conception de matériaux qui peuvent être utilisés dans un nombre toujours croissant d'applications.

Pour ce faire, il est intéressant de dépasser le compromis classique qui existe entre rigidité et ténacité. Dans un réseau élastomère simple, ces deux propriétés sont fondamentalement opposées, de sorte que de gros efforts de recherche ont été fournis pour trouver des matériaux à la fois rigides et résistants à la rupture. Jusqu'à maintenant, ces stratégies se sont concentrées autour de l'utilisation de charges minérales et de l'incorporation de dissipation d'origine viscoélastique. Toutefois, ces deux solutions ne sont pas toujours satisfaisantes et présentent le gros désavantage de rendre les matériaux opaques et leurs propriétés fortement dépendantes de la température et de la vitesse de sollicitation.

Parmi les nombreuses stratégies de renforcement qui ont été décrites dans la littérature, les élastomères à réseaux multiples sortent du lot par le fait qu'ils permettent une amélioration des propriétés mécaniques en jouant sur l'architecture du réseau de polymère, indépendamment de sa nature chimique. Cette stratégie a tout d'abord été développée par le groupe de Gong au Japon, et a depuis été largement étudiée, puis transposée aux élastomères il y a quelques années dans notre groupe.

Un double réseau élastomère est un ensemble de deux réseaux de polymères interpénétrés qui présentent des architectures différentes l'un de l'autre (Figure 1). L'un des réseaux dit « de charge » est fortement réticulé et contient des chaînes qui sont préétirées. Le deuxième réseau est dit « matrice » et présente au contraire une faible densité de réticulation. Ce réseau matrice est également présent en beaucoup plus grande quantité que le réseau de charge dans la structure en

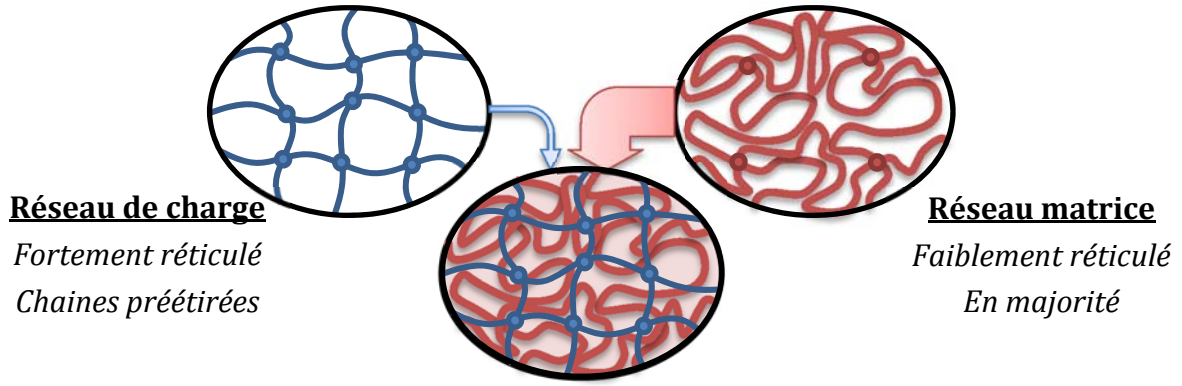

Figure 1: représentation schématique d'une structure de type "double réseau". Le réseau de charge est représenté en bleu, et le réseau matrice en rouge. Les deux réseaux sont interpénétrés à l'échelle moléculaire.

double réseau. La déformation de cette macroarchitecture à grande déformation provoque la rupture du réseau de charge qui dissipe de l'énergie mécanique et redistribue sa contrainte aux chaines très extensibles du réseau matrice. Dans cette structure, l'étirement des chaines du réseau de charge est un paramètre clé puisqu'il contrôle la capacité des chaines à casser et donc à dissiper de l'énergie.

La compréhension des mécanismes de renforcement des doubles réseaux élastomères permet aujourd'hui de se concentrer sur des matériaux qui sont plus proches des applications industrielles. Ainsi, la question de l'anisotropie est un aspect encore peu étudié des doubles réseaux élastomères. Qu'elle soit désirée ou subie, la dépendance des propriétés mécaniques avec la direction de sollicitation est une réelle problématique industrielle qui nécessite d'être étudiée plus en détails.

Dans la littérature, les matériaux polymères et leurs applications en lien avec l'anisotropie utilisent souvent un système qui permet de préétirer les chaines dans une direction donnée et de bloquer cet étirement par l'intermédiaire d'une réaction chimique ou d'une transition de phase. Dans un double réseau élastomère, la présence de chaines préétirées dans une seule direction dans le réseau de charge devrait donner un comportement anisotrope à grandes déformations pour le double réseau, et peut-être aussi à petites déformations. Le principal objectif de ce projet de thèse est donc de réaliser de tels matériaux en pratique et d'étudier leurs propriétés, notamment mécaniques.

Le principal verrou scientifique de ce projet est de trouver un système chimique qui permette de préétirer le réseau de charge et de garder les chaines pré-orientées dans une seule direction pour ensuite polymériser le réseau matrice. Cela nécessite de trouver une méthode pour réticuler le réseau de charge en deux étapes, le seconde étant réalisée à l'état étiré. Ce système dit de « double réticulation » est donc la combinaison d'une réticulation simultanée pour la première étape (i.e. les chaines sont synthétisées et réticulées en même temps) et d'une réticulation séquentielle pour la deuxième (i.e. on tire profit de groupements réactifs sur les chaines pour les coupler entre elles).

Conception et étude préliminaire de deux systèmes de double-réticulation

Dans ce premier chapitre expérimental, deux systèmes de double-réticulation ont été conçus, testés puis optimisés dans l'objectif de préparer des réseaux de charge présentant un préétirement uniaxial permanent. Pour les deux systèmes, on prépare tout d'abord un réseau initial par polymérisation radicalaire conventionnelle initiée par UV, en partant d'une formulation contenant un monomère acrylique, un initiateur et plusieurs additifs. La réaction de seconde réticulation est ensuite activée et le changement des propriétés mécaniques est étudié, d'abord sans préétirement.

Le premier système utilise deux comonomères (l'acide acrylique - AA - et le méthacrylate de glycidyl - GMA -), un catalyseur (la triethylamine) et une synthèse en « one-pot ». Le réseau initial est mou et extensible, et peut être rigidifié significativement par chauffage et condensation des groupements acides et glycidyl qui ont été copolymérisés dans le squelette carboné lors de la première étape de réticulation (Figure 2). Une expérience de DMA à déformation et température

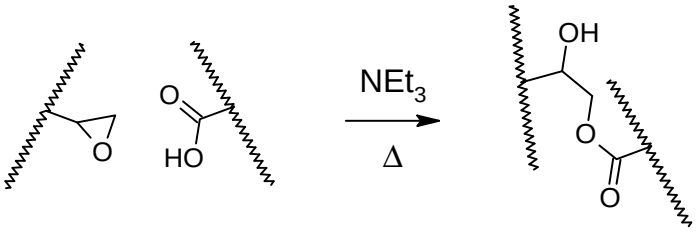

Figure 2: équation bilan de la réaction de double réticulation utilisée pour le système thermique. Les lignes en vague représentent des chaines de polymère préformées.

imposées est réalisée et comparée à un modèle cinétique. Un modèle du second ordre décrit bien nos mesures, et permet de déterminer une énergie d'activation de l'ordre de 70 kJ/mol. En utilisant ce modèle, des conditions optimales de chauffage ont pu être déterminées (2h de chauffage à 150 °C). Dans les formulations de ce premier système, le paramètre le plus utile pour piloter les propriétés des réseaux est la quantité de GMA et AA dans la formulation. Des mesures de gonflement à l'équilibre et des propriétés mécaniques ont permis de déterminer une formulation qui devrait être compatible avec une structure de type double réseau résistante à la rupture. Avec cette formulation, le module de Young du réseau de charge augmente typiquement de 0.20 à 0.82 MPa pendant la deuxième réticulation.

Le second système étudié utilise une formulation beaucoup plus simple avec un seul comonomère (l'acrylate d'allyle - ALA -). Ce comonomère contient deux fonctions avec deux réactivités différentes, ce qui permet d'envisager une réticulation en deux étapes (Figure 3). Afin d'assurer la réaction de toutes les unités allyle dans la deuxième étape, l'irradiation est effectuée avec une dose UV beaucoup plus élevée et est précédée par une étape d'infiltration d'initiateur. L'utilisation de BDA (le réticulant classique diacrylate utilisé dans nos synthèses) s'avère superfétatoire dans nos synthèses, alors que la baisse de la quantité de HMP s'avère néfaste pour le rendement de la réaction de polymérisation initiale. Le principal paramètre qui a été utilisé pour jouer sur les propriétés des réseaux est donc la quantité de ALA utilisée. Contrairement au système thermique, les propriétés des réseaux doublement réticulés préparés par le système UV sont beaucoup plus faciles à interpréter et à rapprocher des formulations qui ont été utilisées. Selon la formulation, le module de Young des réseaux réticulés une fois est de 0.56 à 0.89 MPa, alors que le module des réseaux doublement réticulés va de 0.86 à 1.5 MPa.

Au final, des points de fonctionnement ont été déterminés pour les deux systèmes de double-réticulation via l'étude des propriétés mécaniques de réseaux non préétirés. Ces propriétés sont cohérentes avec notre objectif d'utiliser ces systèmes pour préparer des doubles réseaux utilisant des réseaux de charges préétirés de façon permanente. Avant de se concentrer sur les doubles réseaux, le prochain chapitre s'intéresse d'abord aux réseaux de charge préétirés isolés et à la possibilité de modéliser leurs propriétés en petites et grandes déformations.

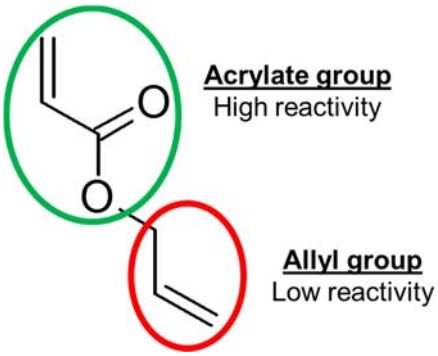

Figure 3: structure chimique de l'acrylate d'allyle. La molecule possède deux fonctions chimique, l'une (en vert) étant beaucoup plus reactive que l'autre (en rouge) vis à vis de la polymérisation radicalaire.

Application des systèmes de double-réticulation à la préparation de réseaux de charge préétirés

Dans ce chapitre, les conditions de double réticulation identifiées précédemment ont été appliquées à la préparation d'élastomères qui sont préétirés dans une direction de façon permanente.

D'emblée, la préparation de ces matériaux s'est révélée beaucoup plus compliquée que prévu. L'idée initiale (et naïve) était de préétirer les réseaux initiaux et de les soumettre simplement aux conditions nécessaires à la deuxième réticulation. Cette idée ignorait toutefois que les matériaux ne sont pas capables de supporter de forts niveaux d'étirement pendant des durées ou des températures trop grandes. Après optimisation, des réseaux étirés ont tout de même pu être obtenus, mais dans des gammes de préétirement relativement faibles. Le préétirement final λ^*, défini comme le changement relatif de longueur, augmente typiquement avec l'étirement imposé pendant la deuxième réticulation λ_{clamp}.

Le reste du chapitre est dédié à la présentation, à l'extension et à la comparaison du modèle de Flory à nos données expérimentales. Ce cadre conceptuel permet la modélisation de réseaux doublement réticulés. Il repose sur l'hypothèse selon laquelle la deuxième étape de réticulation est équivalente à la superposition d'un deuxième réseau (virtuel) au réseau initial (réel). Ce réseau supplémentaire est à l'équilibre dans l'état préétiré et a une densité de réticulation différente, de sorte qu'en équilibrant les forces entre le premier et le deuxième réseau on puisse prédire le préétirement final λ^* du réseau doublement réticulé.

La comparaison du modèle de Flory aux données expérimentales donne des écarts quantitativement significatifs, pour le système thermique (Figure 4) comme pour le système UV (Figure 5). Même en tentant de prendre en compte la variabilité inter-échantillon, les prédictions de λ^* basées sur des chaines gaussiennes sous-estime systématiquement les valeurs observées de préétirement. Cela peut être dû à la présence d'enchevêtrements qui tendent à surestimer la densité effective de réticulation du réseau initial. Une autre explication vient du fait que nos réseaux sont probablement hétérogènes et contiennent probablement des défauts et des chaines pendantes.

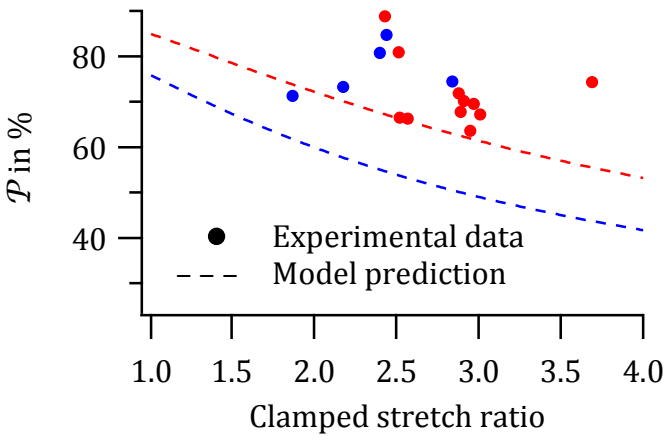

Figure 4: comparaison des données expérimentales au modèle de Flory pour le système thermique. $\mathcal{P}$ est la fraction de l'étirement imposé lors de la deuxième réticulation qui est toujours présent dans l'état pré-étiré final. Les deux couleurs représentent deux formulations différentes. Les lignes sont les predictions du modèle et les points sont les données expérimentales (un point = un échantillon).

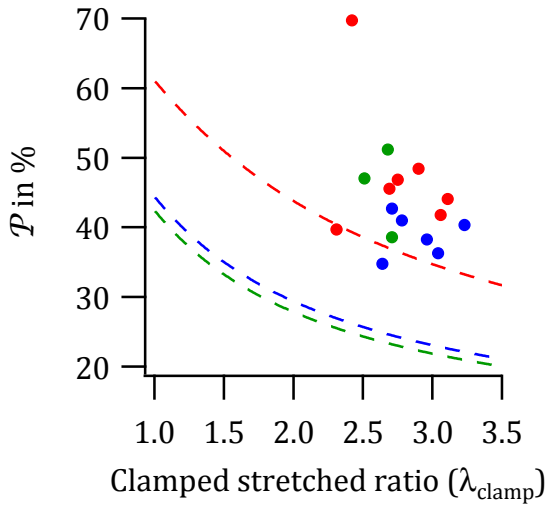

Figure 5: comparaison des données expérimentales au modèle de Flory pour le système UV. $\mathcal{P}$ est la fraction de l'étirement imposé lors de la deuxième réticulation (λ_{clamp}) qui est toujours présent dans l'état pré-étiré final. Les trois couleurs représentent trois formulations différentes. Les lignes sont les predictions du modèle et les points sont les données expérimentales (un point = un échantillon).

Des raffinements du modèle de Flory sont présentés et prennent en compte le caractère non-Gaussien des chaines. Toutefois, leur formalisme mathématique complexe et le fait qu'ils reposent toujours sur une approche de type champ moyen ne leur donne pas beaucoup de valeur ajoutée. A la place, nous proposons une approche basée sur une extension empirique du modèle de Flory et sur la prédiction des extensibilités limites des deux populations de chaines dans le réseau doublement réticulé. Ce modèle donne des résultats qualitativement similaires aux modèles rigoureux basés sur des chaines non-gaussiennes, et sera donc utilisé dans la suite du manuscrit pour interpréter les résultats expérimentaux.

Malgré l'incapacité du modèle de Flory à modéliser les réseaux de charge préétirés qui ont été obtenus, ces derniers peuvent tout de même être incorporés dans des structures de type double réseaux.

Incorporation des réseaux de charge préétirés dans des structures de type double réseaux

Dans ce chapitre, les réseaux de charge préétirés uniaxialement de façon permanente ont été incorporés dans des structures de type double réseau. Les réseaux préétirés des deux systèmes (thermique et UV) ont été utilisés, et les matériaux finaux ont été étudiés principalement en traction uniaxiale (monotonique et cyclique) et plus occasionnellement par DMA et via des tests de fracture. La première conclusion immédiate est que les doubles réseaux obtenus à partir de réseaux de charge doublement réticulés sont tenaces et présentent un raidissement marqué à grande déformation (Figure 6). Cela rend nos matériaux similaires aux doubles réseaux traditionnellement étudiés au moins sur le plan qualitatif. La présence de préétirement ne semble donc pas empêcher l'activation du mécanisme de renforcement. Cette étude confirme donc le caractère universel de la stratégie à base de réseaux multiples et le fait qu'elle devrait pouvoir être appliquée à des élastomères industriels qui ne sont pas aussi parfaits que des matériaux modèles de laboratoire.

Dans nos matériaux, il y a une différence fondamentale entre le comportement à petites et à grandes déformations. Peu importe le système de double-réticulation utilisé (thermique ou UV), la réponse à petite déformation des doubles réseaux préétirés est globalement isotrope. Le

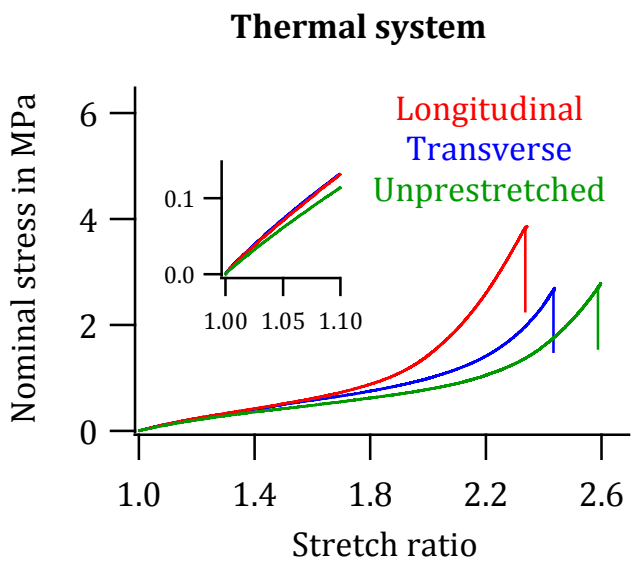

Figure 6: réponse mécanique de doubles réseaux basés sur le système thermique. Tous les doubles réseaux testés proviennent du même réseau initial qui est ensuite doublement réticulé soit à l'état pré-étiré soit sans préétirement. Les courbes rouges et bleues correspondent au matériau préétiré dans la direction longitudinale et transverse respectivement. La courbe verte correspond à un double réseau dont le réseau de charge est doublement réticulé mais pas préétiré (pour comparaison). L'insert de la figure est un zoom à faibles déformations. Les échantillons sont testés à 100 µm/sec.

préétirement n'est fondamentalement pas assez important pour changer la statistique des chaines qui demeure donc globalement gaussienne. A grande déformation par contre, l'effet du préétirement devient bien plus visible et induit par exemple une anisotropie au niveau de l'extensibilité limite des doubles réseaux préétirés. La séparation entre ces deux échelles de déformations différencie nos matériaux d'autres exemples d'élastomères résistants à la fracture.

Bien que l'effet du préétirement sur le comportement à grande déformation soit plutôt immédiat à visualiser, il est beaucoup plus difficile de l'interpréter en utilisant un modèle de type champ

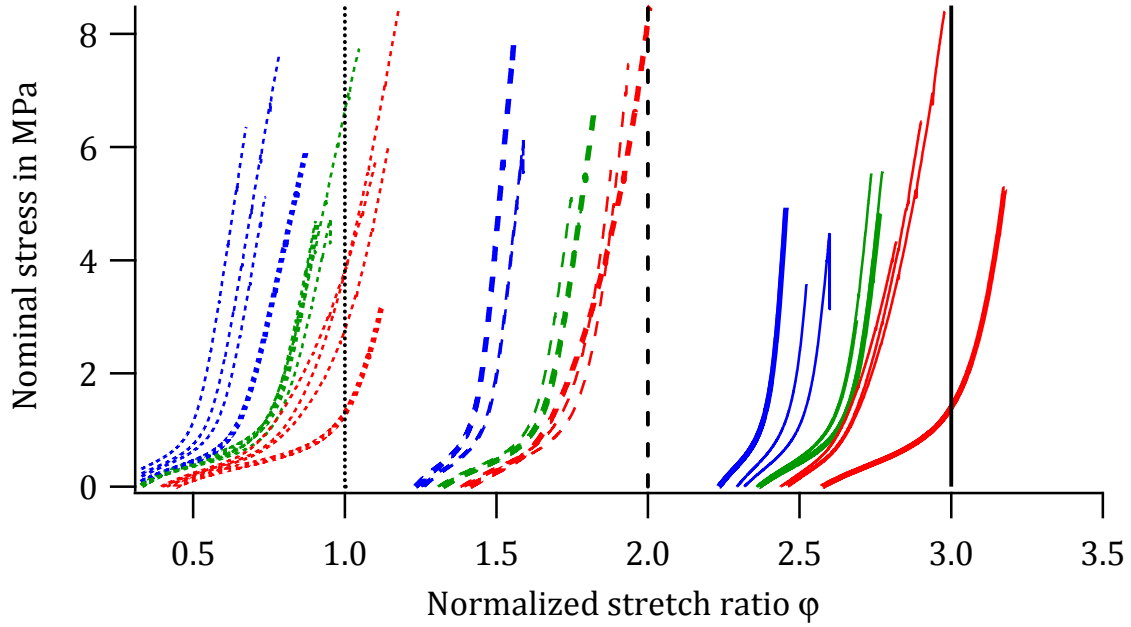

Figure 7: comparaison des résultats expérimentaux sur le système UV au modèle de Flory étendu. La contrainte nominale est représentée en fonction d'un paramètre qui représente l'écart entre l'étirement du réseau de charge et son extensibilité maximale modélisée ($\varphi = 1$ correspond donc à l'extensibilité maximale prédite par notre modèle). Le type de trait correspond à la formulation utilisée (point = 1 mol% ALA, tirets = 1.5 mol% ALA, trait plein = 2% ALA) , et la couleur correspond à l'échantillon testé (rouge = direction longitudinale, bleu = direction transverse, vert = échantillon non préétiré). Les courbes correspondant aux formulations à 1.5 et 2% en ALA sont décalées vers la droite d'une et de deux unités respectivement.

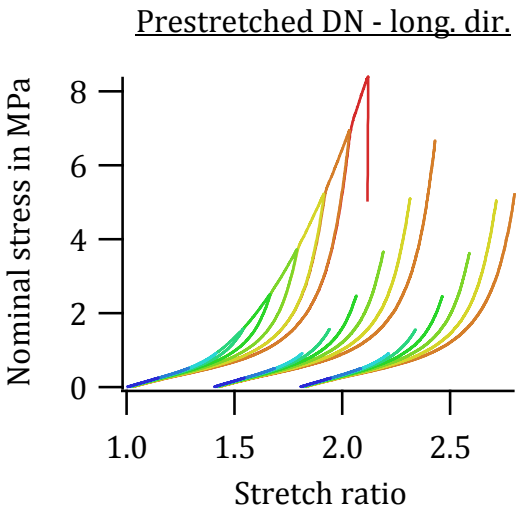

Figure 8: résultat d'un test cyclique sur la direction longitudinale d'un double réseau préétiré utilisant le système UV. Les courbes des deuxièmes et troisièmes cycles de chaque pallier de déformation ont été décalés de 0.4 et 0.8 respectivement vers la droite. En comparaison, la direction transverse ne montre aucun endommagement et toutes les courbes se superposent.

moyen. L'extension du modèle de Flory proposée dans le chapitre précédent donne une assez bonne explication qualitative des résultats obtenus dans la direction préétirée, mais échoue à modéliser la direction transverse (Figure 7). Cela indique que les détails de l'effet du préétirement sur les propriétés mécaniques des matériaux ne sont pas encore compris. Plus fondamentalement, cette divergence résulte probablement d'effets de directions croisées et/ou de l'influence du caractère fortement non-Gaussien des chaines lorsqu'elles approchent leur extensibilité limite.

Les deux systèmes de double-réticulation testés présentent des spécificités principalement visibles une fois que les réseaux préétirés sont incorporés dans des structures de type double réseau. Le système thermique est ainsi marqué par un très problématique manque de reproductibilité. Le système UV quant à lui présente un endommagement original et visible uniquement à grande déformation. Ce mécanisme d'endommagement est particulièrement visible en test cyclique et se traduit par un adoucissement et une augmentation de l'extensibilité maximale des doubles réseaux lorsque la déformation est augmentée (Figure 8). Cet endommagement est en partie similaire à l'effet Mullins traditionnellement observé dans les élastomères chargés. Il est également original dans le sens où il n'est normalement pas observé dans les doubles réseaux élastomères. Cette différence est attribuée à la présence d'une hétérogénéité importante dans nos matériaux.

L'effet de l'endommagement sur les propriétés des matériaux a également été étudié. L'endommagement n'affecte pas significativement le comportement des doubles réseaux, bien qu'il ait un effet évident sur les courbes de traction uniaxiale. Ni les propriétés viscoélastiques ni les valeurs d'énergies de fracture ne sont significativement affectées par l'endommagement. Cela s'explique par le fait qu'une toute petite fraction des chaines est en réalité cassée lors de l'endommagement cyclique. Ces chaines dissipent une quantité importante d'énergie mais ne sont pas assez nombreuses pour affecter les propriétés viscoélastiques du matériau ou sa capacité à résister à la propagation d'une fissure.

Vers des réseaux de charge vitreux

Ce chapitre correspond à un projet annexe et à un stage de master qui a été réalisé dans notre groupe. Jusqu'à maintenant, l'étude des doubles réseaux s'est focalisée sur des matériaux dans

lesquels les deux réseaux sont relativement similaires. Ces derniers sont choisis dans la famille des (meth)acrylates et dans des gammes de températures de transition vitreuse proches. Il est toutefois intéressant d'explorer de nouveaux types de réseaux de charge dans lesquels la Tg est beaucoup plus élevée. Ces réseaux hybrides devraient permettre d'obtenir des matériaux élastomères qui contiennent plus de dissipation d'origine viscoélastique, ce qui devrait aider à les renforcer encore plus vis-à-vis de la fissuration.

Des réseaux de PMMA avec différentes types et quantités de réticulants ont donc été préparés et incorporés dans des structures de type double réseau. La synthèse de ces matériaux s'est avérée compliquée, principalement à cause de la faible réactivité des méthacrylates et de la nécessité de synthétiser les réseaux en solution.

La caractérisation en petites déformations des matériaux révèle que le mélange entre les réseaux de charge et matrice joue un rôle très important. Dans la plupart des cas, un mélange partiel est obtenu ce qui donne des matériaux très dissipatifs avec une transition vitreuse très large et une rigidité élevée à température ambiante. Les détails de la microstructure du réseau de charge influencent très fortement les propriétés viscoélastiques des doubles réseaux. Dans certains cas par exemple, la réponse en DMA de nos matériaux suggère l'existence de régions très riches en PMMA ou la présence de chaines courtes. L'hétérogénéité de la réticulation induit un gonflement hétérogène et donc une composition hétérogène dans la structure double réseau.

Pour un jeu de paramètres particulier, un double réseau dans lequel les deux réseaux sont particulièrement bien mélangés a été obtenu. Ce matériau est globalement mou et élastomérique, bien que sa réponse en grandes déformations montre des signes d'hystérèse mécanique et de déformation résiduelle. Des études plus poussées pourraient se focaliser sur cette formulation particulière pour tenter d'identifier la raison pour laquelle un si bon mélange est obtenu.

Acknowledgments

Aaaah, la page des remerciements… la fameuse… Parce que sans se mentir, les remerciements, c'est les pages qui doivent être le plus lues dans un manuscrit de thèse après la page de garde. Franchement, je crois qu'à certains moments pendant la thèse j'ai dû en rêver la nuit. Je me suis dit « tu verras, quand tu y seras, tu écriras un truc de fou, super original, pour vraiment remercier les gens qui ont compté pendant ces trois ans ». Oui, clairement, je me voyais écrire du Chateaubriand (rien que ça).

Et puis là, maintenant, devant mon ordi, je me rends compte que finalement je risque de pas être super original. Parce que bon, mes piètres qualités de poète m'empêchent d'écrire mes remerciements en alexandrins, et puis je ne vais pas faire une BD ou une estampe de remerciement non plus. Donc désolé, cher lecteur, mais ce sera des remerciements très classiques, neutres, sobres et sans fioritures. Zéro blague, zéro trait d'humour, un truc un peu chiant quoi. Quoique…

Déjà, un immense merci à mon directeur de thèse Costantino Creton pour m'avoir choisi comme thésard et m'avoir laissé autant de liberté pendant ces trois ans. J'ai vraiment énormément appris pendant ces trois ans et c'est grâce à ta supervision bienveillante (et jamais intrusive), à tes conseils avisés, et même à tes remarques un poil sarcastiques sur mes cheveux ou mes chemises (toujours respectables, évidemment). J'ai peut-être bien failli « remporter le titre de thésard le plus malchanceux » (sic), mais j'ai fini par m'en sortir et tu n'y es pas pour rien, loin de là. Et je jure que ce n'est pas (que) grâce aux soirées wine tasting et aux conférences à l'étranger ☺

Merci à DSM pour avoir financé ce projet et pour l'avoir suivi, toujours de façon bienveillante et stimulante, jamais de façon envahissante et directive.

Merci à Pierre Millereau qui m'a accepté en projet de recherche avant ma thèse et m'a fait découvrir les doubles réseaux et la vie quotidienne du thésard qui fait avec les moyens du bord (grâce à toi je sais qu'un sac à gants ne suffit pas à créer une atmosphère inerte, c'est toujours utile comme apprentissage). Merci aussi à Maeva Balima pour avoir accepté de venir en stage au SIMM avec moi et m'avoir permis de passer de l'autre côté du miroir (apparemment j'ai été à la hauteur et ne t'ai pas dégoutée de la thèse, donc ça va).

Merci aux membres du jury pour avoir pris le temps de lire mon manuscrit ainsi que pour les questions, suggestions et commentaires très constructifs et stimulants pendant la soutenance (et désolé pour le pavé, je jure qu'à la base je visais moins de 200 pages !).

Merci à tous les membres du groupe Soft Polymer Networks, permanents et non-permanents, pour leur aide, leurs suggestions et leur bienveillance. Merci à tout le laboratoire SIMM en général, en particulier aux directeurs successifs du laboratoire pendant ma thèse (Christian et Etienne) qui accomplissent un travail titanesque pour que le labo tourne, et aux personnels techniques et administratifs (les gars de l'atelier, Pierre, Gilles, les gestionnaires, Armand et bien sûr Freddy). Merci en particulier à Hélène Montes qui en plus de sa bonne humeur communicative m'a permis de faire les tutorats de physique des polymères à l'ESPCI.

Un immense merci général à tous les non-permanents du laboratoire, passés et présents. Il y a au labo une ambiance assez exceptionnelle et des gens qui se soutiennent les uns les autres. Ce n'est pas dans tous les labos qu'il y a des WE d'organisés tous les 6 mois par exemple, et sur une thèse qui se passe pas tous les jours de façon optimale ça fait très clairement la différence. Un merci particulier à mes co-bureaux successifs, en particulier ceux qui ont supporté le bruit tonitruant de mon clavier pendant la rédaction (enfin, je suis sûr qu'ils exagèrent). Mention spéciale également à tous les thésards qui ont soutenu la même année que moi et avec qui j'ai pu partager ces trois ans de thèse de A à Z, et en particulier Julie et Valoche (#TeamDerniersASoutenir). Un merci tout particulier à mes deux acolytes Juliette et Paul : vous avez été ma famille de thèse, mes cobayes de pâtisserie, l'Imperial Stout de ma carte des bières, le jour qui se lève sur ma jeunesse France, juste merci.

Merci à tous mes amis extérieurs au labo… et non, je vais pas me lancer dans une liste exhaustive, j'ai trop peur de me planter et en plus il y aurait une trace écrite. Je vais plutôt me contenter de remercier de façon générale les copains du Bar (de l'Amour, et de tous les autres bars moins bien que le nôtre), du groupe vocal, du BDE, de la JE, de la coloc (y compris monsieur Poney), de la promo 130 (un poil snobs mais assez sympas), de la promo 133 (globalement sympas aussi), de la promo 132 (moins sympas, sauf certains), de la CNJE, du club de natation (même les lâcheurs qui sont partis voir si l'eau est plus claire ailleurs), du lycée, et de tous les autres groupes que je pourrais oublier.

De façon générale, merci à toi qui as essayé de t'intéresser à mes histoires d'élastiques, merci à toi qui m'a écouter te raconter à quel point ma thèse avançait pas, merci à toi qui m'a permis de m'amuser et d'oublier un peu ma thèse pour mieux y revenir ensuite, merci à toi pour la musique, pour la bouffe, pour les soirées, pour les bières, pour les blagues, bref pour tous ces à-côtés qui font que je suis aujourd'hui docteur (comment ça claque d'écrire ça, je m'y fais pas encore).

Et enfin, le plus important, merci à ma famille pour m'avoir toujours soutenu et encouragé. Merci à ceux qui étaient présents pour ma soutenance, y compris par la pensée, et merci à ceux qui ne sont plus là mais qui continuent de compter pour moi.

Et merci à Baby Shark (tu tu tudu tu). En espérant te l'avoir mise dans la tête 😸

Et merci d'avoir lu ces deux pages jusqu'au bout… et bon courage pour la suite cher lecteur : ça se lit bien, mais c'est pas une sinécure non plus ☺

List of Symbols

C_1 and C_2	Constants from Mooney-Rivlin's model
C_∞	Characteristic ratio
$\chi_T(t)$	Predicted extent of reaction based on the kinetic model
E	Young's modulus
E'	Storage modulus / real part of the complex modulus
E''	Loss modulus / immaginary part of the complex modulus
E_a	Arrhenius activation energy
η	Estimated yield of polymerization reactions
φ	Ratio of stretch ratio over predicted maximum extensibility
Γ	Fracture energy (or tearing energy)
Γ_0	Threshold value of fracture energy from Lake and Thomas model
Γ_{virgin}	Fracture energy of an undamaged double network sample
Γ_{damaged}	Fracture energy of a damaged double network sample
G_c	Critical value of the strain energy release rate
G_x	Shear modulus due to crosslinks
J_1	Reduced value of the first strain invariant ($I_1 - 3$)
J_m	Maximum value of J_1 in Gent's model
k	Boltzman's constant
k_{app}	Apparent rate constant in kinetic models
$\lambda, \lambda_x, \lambda_y, \lambda_z$	Stretch ratio (current length over initial length)
$\lambda_{\text{swelling}}$	Stretch ratio due to swelling during the matrix network polymerization
λ_{clamp} or λ_c	Stretch ratio at which the single-cured sample is clamped
λ^*	Final stretch ratio of the dual-cured sample / permanent prestretching
λ^*_{Gauss}	Prediction of λ^* based on a Gaussian version of Flory's model
Λ^*	Overall stretch ratio due to prestretching in Flory's model
λ_{max}	Maximum extensibility of a network strand
λ_m	Maximum stretch ratio of a material (as defined in Gent's model)
λ_{step}	Maximum applied stretch ratio during a step-cyclic test
$l_{\text{C-C}}$	Length of a carbon-carbon bond
$\mathcal{M}_0$	Molar mass of a monomer
$\mathcal{M}_x$	Molar mass between two crosslinks
N_x or N_{mono}	Number of monomers between two crosslinks
$N_{\text{C-C}}$	Number of carbon-carbon bonds between crosslinks
$\mathcal{N}_A$	Avogadro's number

ν_1 and ν_2	Crosslinking densities of the two populations from Flory's model
ν_x	Number density of elastic chains or crosslinks
$\mathcal{P}$	Extent of prestretching
Q_{mass} or Q_w	Mass swelling ratio
R	Perfect gas constant
R_0	Average end-to-end distance of a Gaussian chain
R_{max}	Maximum size of a polymer chain
ρ	Density
σ_N	Nominal stress
T_g	Glass-transition temperature
$\tan(\delta)$	Tangent of the loss angle / loss tangent
θ	Valence angle
U_b	Energy dissipated by a bond in Lake and Thomas model
W	Strain energy density
x_i	Molar fraction of component i
ξ	Quantity of crosslinker that gives elastically active network strands
Ξ	Ratio of ξ to the total amount of crosslinker that is used

List of abbreviations

AA	Acrylic acid
AcOEt	Ethyl acetate
AIBN	2,2′-Azobis(2-methylpropionitrile)
ALA	Allyl acrylate
BDA	1,4-Butanediol diacrylate
BDMA	1,4-Butanediol dimethacrylate
DMA	Dynamic Mechanical Analysis
DN	Double Network
EA	Ethyl acrylate
GMA	Glycidyl methacrylate
HEA	2-Hydroxyethyl acrylate
HMP	2-Hydroxy-2-methylpropiophenone
IPN	Interpenetrated Network
LCE	Liquid Crystal Elastomer
MA	Methyl acrylate
MMA	Methyl methacrylate
NEt3	Triethylamine
PAAm	Poly(acrylamide)
PAMPS	Poly(2-acrylamido-2-methyl-1-propanesulfonic acid)
PEA	Poly(ethyl acrylate)
PEG	Poly(ethylene glycol)
PET	Polyethylene Terephtalate
PMA	Poly(methyl acrylate)
PMMA	Poly(methyl methacrylate)
SMP	Shape memory polymer

General introduction

Simple elastomers are either stiff or tough, but not both

Elastomers are materials that have a lot of industrial applications due to their original set of properties. They are very extensible, up to several times their initial length, and their deformation is often almost completely reversible. Beside their mechanical properties, they are also easy to manufacture and relatively inexpensive. As a result, they suit a variety of different applications, from tires and seals to sports and commodity goods.

From the chemical point of view, elastomers are networks of polymer chains that are linked together via chemical or physical bonds called crosslinks. The deformation of amorphous elastomers involves the unfolding and progressive extension of molecular chains. This deformation is primarily entropic and associated to a low energetic cost, thus explaining the relative softness of elastomers compared to crystalline or glassy materials. The stiffness of an elastomer is controlled by the density of elastic strands, which in turn is linked to the amount of crosslinks per unit volume in the material.

In most applications however, stiffness is not enough. As in most materials, there is a compromise in elastomers between stiffness and toughness. Basically, increasing the crosslinking density increases the modulus of the material but conversely decreases its maximum extensibility and resistance to crack propagation. A simple elastomeric network therefore cannot be stiff and tough at the same time, unless the material scientist finds a way to circumvent this compromise.

The rupture of an elastomer is the result of the catastrophic failure of the polymer chains because of the excessive load that is applied. Schematically, there is an input of elastic energy that needs to be dissipated. In the absence of any dissipative process, the only way to do so it so break the chemical bonds that bear the load, leading to the propagation of a crack. The basic idea to toughen elastomers is therefore to channel part of the elastic energy into dissipative mechanisms that do not lead to the breakage of all the elastic strands at once.

The double network toughening strategy

Among the many possible dissipative mechanisms, our group has focused on a strategy inspired by the hydrogel community that involves the breaking of covalent bonds via a clever design of the polymeric network. Contrary to conventional elastomers, the ones we study are made of two interpenetrated polymeric networks, as depicted in Figure 1. The first network is referred to as “filler network” and made of relatively highly-crosslinked chains. The second network is referred to as “matrix network” and made of long and loosely crosslinked chains that are entangled within the mesh of the filler network. The matrix network is in vast majority compared to the filler network and plays the role of a “molecular stent” by filling the space in the filler network. As a result, the chains of the filler network are swollen and extended by the chains of the matrix network. The more matrix network there is in the double network structure, the lower the mass fraction of the filler network and the larger the isotropic swelling stretch ratio of the filler network chains.

Not only is the filler network intrinsically brittle because of the large crosslinking density, but the chains of the filler network are also extended by the presence of the matrix network. They are

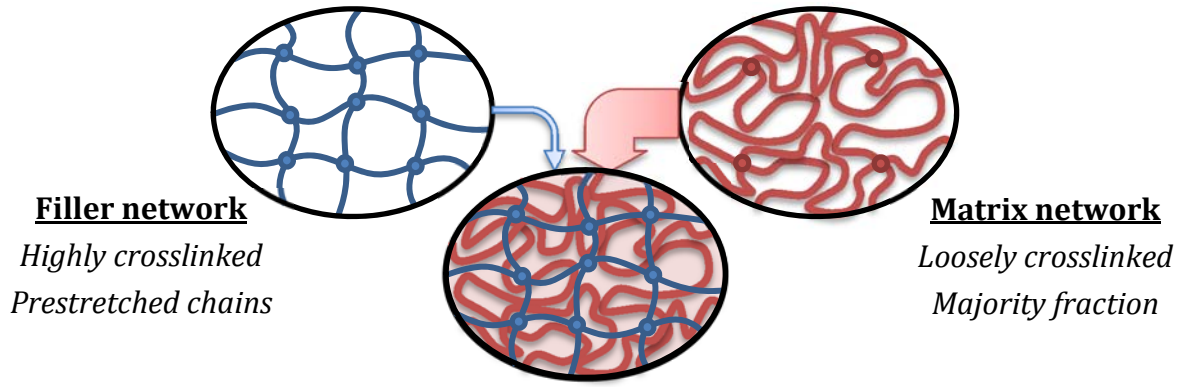

Figure 1: schematic representation of the double network architecture. The filler network is represented in blue, the matrix network is represented in red. Both networks are interpenetrated at the molecular scale.

therefore close to their maximum extensibility and may break when the material is stretched, thus dissipating energy. The trick that enables energy dissipation without breaking the entire material macroscopically is that the filler network chains are overall in minority and that the stress may be redistributed from the filler to the matrix network when the bonds break. Double networks therefore exhibit a much larger fracture energy, as quantified by the amount of energy necessary to propagate a crack in the material. Meanwhile, they are stiff thanks to the presence of the highly crosslinked filler network and the presence of a lot of entanglements between the filler and matrix networks.

The mechanical properties of double networks have been shown to primarily depend on the properties of the filler network. Namely, for a given crosslinking density, the level of prestretching is the main parameter that controls the distance of the filler network chains to their maximum extensibility. The large strain response of the material and the toughening effect of the double network structure therefore primarily depends on this parameter.

The double network strategy to reinforce elastomers against fracture propagation is very original, in the sense that it relies on a specific network design and not on a specific polymer chemistry. Provided the filler network may be swollen by the matrix network, any type of polymer could be used. Until now, only simple acrylic networks have been used, but the wide applicability of the strategy makes it interesting for industrial and applicative purposes.

Toward more realistic situations

Now that the behavior of double network elastomers is fairly well understood at the lab-scale, it becomes interesting to evaluate their potential in light of real-life applications and materials. For instance, the toughening strategy could be appealing for the reinforcement of soft coatings against fracture. In this case however, the material to reinforce is going to contain defects and its structure is most likely not going to be homogeneous. More generally, usual elastomeric materials are not fabricated by solution molding as in our case, but rather by much more efficient techniques such as extrusion. In particular, most of these techniques yield polymer chains that are at least partly oriented during the process. Yet, the reinforcing mechanism of double network heavily relies on the state of stretch of the filler network.

The present research project therefore focuses on new filler networks in order to expand the range of materials that can be obtained with a double network structure. In particular, filler networks in which the chains are not isotropically prestretched are studied in details. The idea is to start with a network structure that is already preoriented in a specific direction and to examine how it influences the properties of the final double network material.

To this intent, permanently prestretched elastomeric filler networks first need to be prepared. Hopefully, polymer chemistry provides ways to prepare materials that can be crosslinked in two steps, using a so-called "dual-curing system". These materials are initially soft and extensible and may be prestretched in one direction specifically. In the prestretched state, they can then be further crosslinked in order to prevent the material from returning to its original shape. The polymer chains therefore retain some of their orientation, thus resulting into a permanent stretch ratio. These prestretched filler network can then be incorporated in soft, extensible and isotropic matrix networks. The resulting double networks can then be studied and reveal the influence of the additional prestretching that has been applied.

Scientific questions and outline of the manuscript

The scientific challenges and conceptual questions that are raised by this research project may be roughly divided in two parts. The first one addresses the chemistry and fabrication of the materials, and the second part focuses on the characterization of their mechanical properties and the analysis of the physics behind them. More specifically, the present manuscript aims to answer the following questions:

1. How to prepare elastomers that can be crosslinked in the stretched state in order to obtain permanently prestretched filler networks? In other words, can we find dual-curing systems that can be adapted to the acrylate chemistry we traditionally use in the fabrication of double network elastomers?
2. What are the properties of the dual-cured and permanently prestretched filler networks that are obtained? Can we rationalize their properties by using usual models of dual-cured elastomers from the literature? Can we expand these models in order to have some insights about the possible mechanical properties of double network elastomers in large strains?
3. What are the actual properties in small and large strains of double networks that contain a filler network that has been non-isotropically prestretched? Can we relate these properties to the assumed molecular structure of the filler network? How is the behavior of double networks influenced by the presence of an additional unidirectional prestretching?

The present manuscript is therefore divided in five chapters. The first chapter gives a detailed review of the literature and state of the art. It is designed to give the reader a broad overview of the theoretical and practical background linked to the project. The three main scientific questions stated above are then treated sequentially in chapters two to four, following the fabrication process of these new prestretched double network elastomers.

Chapter two focuses on the design and optimization of two effective dual-curing systems. Chapter three presents the preparation and characterization of permanently prestretched filler networks as well as the modelling and prediction of their properties in large strains. The fourth chapter focuses on the actual prestretched double networks, from their preparation to the characterization of their properties and comparison to the models exposed in the previous chapter.

The fifth and last chapter is a side-project and preliminary study of novel hybrid double networks in which the filler network is not purely elastomeric at room temperature. In this project, a glassy filler network is incorporated in a rubbery matrix, thus expanding further the range of materials that may be obtained with the double network architecture.

Chapter 1

From chemistry and physics to the design of new double network elastomers

Table of contents

1. Introduction 11
2. Chemistry and physics of crosslinked elastomeric networks 13
2.1. Synthesis of permanent polymeric networks 13
2.1.1. The simultaneous route: kinetics matters 13
2.1.2. The sequential route: chemistry matters 15
2.1.3. The mixed route using dual-curing systems 16
2.2. From chain physics to network properties 19
2.2.1. Physics of isolated polymer chains 19
2.2.2. Assembly of chains and network elasticity 20
3. Fracture of soft materials and how to reinforce them 27
3.1. Description of fracture in soft materials, a matter of dissipation 27
3.1.1. From LEFM to a modern description of soft material fracture 27
3.1.2. Measurement of fracture energy 29
3.1.3. Molecular description of fracture in polymeric materials 30
3.1.4. The case of cyclic fatigue 30
3.2. General guidelines for improving the fracture resistance of soft materials 32
3.2.1. Delaying the onset of fracture 33
3.2.2. Increasing the cost of propagation by adding dissipation 34
3.2.3. Specificities of elastomers 34
4. The multiple network strategy: from the original concept to new properties 41
4.1. Double network hydrogels 41
4.1.1. A seminal paper and its first results 41
4.1.2. Toward the understanding of the toughening mechanism 42
4.1.3. Use of new characterization techniques 46
4.2. From hydrogels to elastomers 47
4.2.1. Translation of Gong's concept by Ducrot 47
4.2.2. Finer understanding by Millereau and Chen 48
4.2.3. A not-so-new concept 50
4.3. The challenge of describing the reinforcing mechanism theoretically 52
4.4. Toward new properties for multiple network elastomers 55
5. Bringing anisotropy to double network elastomers 57

5.1. Example of anisotropic polymeric systems 57
5.1.1. In composite materials 57
5.1.2. In polymer glasses and hydrogels 57
5.1.3. In dual-cured elastomers 60
5.2. Oriented chains in rubbers, a key element for some applications 60
5.2.1. Shape-memory polymers 60
5.2.2. Liquid crystal elastomers 61
5.2.3. Dielectric elastomers 62
5.3. Battle plan, or how to make double networks anisotropic 63
5.3.1. The first naïve idea: swelling in the stretched state 64
5.3.2. The more subtle strategy: dual-cure chemistry and then swelling 64
6. Conclusions 67
7. References 69

1. Introduction

Compared to other scientific fields, polymer science is a relatively recent research area, fueled in great part by the works of Pierre-Gilles de Gennes [1]. Although polymers were already man-made in the nineteenth century, the real understanding of their properties only began in the early twentieth century. Benefitting from the progress in statistical thermodynamics, modern polymer physics was developed progressively throughout the twentieth century to give what is now considered as an established theory.

Among the many advantages of polymers, one that is particularly useful is their versatility. Use of organic chemistry in particular gives to the polymer scientist the ability to obtain virtually any final property by playing on the (macro)molecular architecture. The entire challenge is then to relate what is done with chemistry to what is obtained in terms of mechanical, optical, thermal or chemical properties to name only a few.

The present chapter gives a broad overview of the theoretical, conceptual and practical tools that are used in this project. First, some fundamental aspects of polymer chemistry and physics are presented, starting from the preparation of a crosslinked elastomeric network to the study of its mechanical properties. The second part of this chapter gives more details on the study of fracture of elastomers and soft materials in general. Then, a third part focuses on a specific strategy that may be used to toughen elastomers, from its origins to its latest developments. A final part shows how this concept may be associated to new properties such as anisotropy, and how to design the material to reach this goal.

2. Chemistry and physics of crosslinked elastomeric networks

2.1. Synthesis of permanent polymeric networks

A polymeric network is a set of macromolecules that are linked together to form a three-dimensional structure. The term "permanent" means that the attachment points cannot break and reform in normal use conditions. The most basic way to do so is to link the chains with covalent bonds, in which case the final material is a thermoset.

There are basically two ways to prepare a chemically-crosslinked polymer network (see Figure 1). The first and simplest is to polymerize and crosslink the material at the same time by using a mix of mono and multi-functional monomers. The second consists in polymerizing the chains, and then couple them in a second step to get a three-dimensional network. In some specific cases, a combination of the two previous routes may also be needed.

2.1.1. The simultaneous route: kinetics matters

The major advantage of this strategy is its simplicity, which comes at the expense of the control of the final architecture. Since the main monomer and the bifunctional crosslinking agent are polymerized at the same time, the final structure strongly depends on the details of the polymerization reaction.

Thermosets can be made by free radical polymerization. The network formation mechanism may roughly be described by three steps [2] (see Figure 2):

- First, the initiator decomposes and reacts with mono or multifunctional monomers (crosslinkers). Since the chains are diluted in the reactive medium, most of crosslinkers react in intramolecular reactions leading to chains with loops and defects.

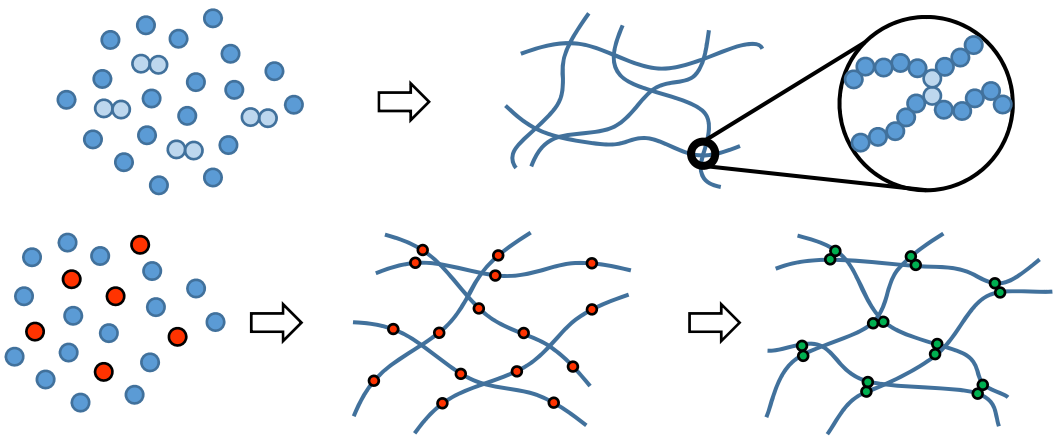

Figure 1: schematic representation of network formation strategies. Blue circles represent monomers. Top: simultaneous route, light blue circles represent bifunctional monomers. Bottom: sequential route, red circles are reactive comonomers that are incorporated in the polymer chains during polymerization and then reacted together to give crosslinks (green circles).

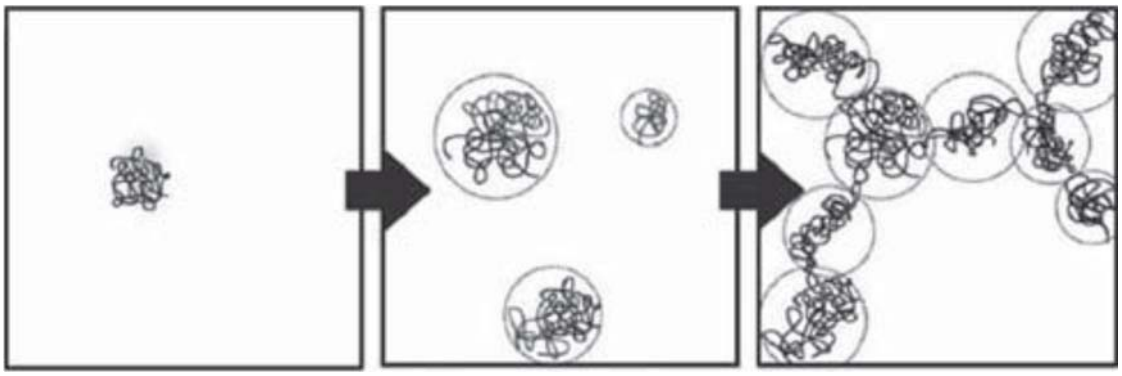

Figure 2: schematic representation of the gelation process in free radical polymerization. In the first stage, only intramolecular crosslinking occurs. In the second stage, microgels are formed. In the third stage, microgels are connected to yield the networks

- As the reaction proceeds, the polymer concentration increases and chains start overlapping. Intermolecular reactions become possible and crosslinked microgels form.
- When the polymer concentration is high, microgels start to entangle and connect with each other with their remaining pendent reactive groups. At this stage, a network is formed and keeps densifying as the reaction continues

This mechanism obviously leads to networks that are intrinsically poorly defined. Other factors may add up and impair the network ideality.

- First, the presence of two reactive groups makes the crosslinker roughly twice as reactive as a monomer, even if the functional groups are the same. The crosslinker is thus mainly incorporated in the first stages of the reaction leading to a heterogeneous distribution of crosslinker molecules in the final material.
- Second, different functional groups lead to differences in terms of kinetics of polymerization. This may be anticipated by studying the values of reactivity ratios [3] defined as follows:

$$r_i = k_{p_{ii}}/k_{p_{ij}} \qquad \text{Eq. 1}$$

  where $k_{p_{ij}}$ is the rate propagation constant of the reaction of monomer i with monomer j. Based on the knowledge of the 4 propagation constants, several situations may occur, as shown in Table 1. In most cases however, the precise knowledge of reactivity ratios is not necessary since monomers from the same family (acrylates for example) usually exhibit reactivity ratios close to 1 [3,4].

- Third, when polymerization is performed without a large excess of solvent, transfer reactions occur and bring another level of complexity to the final macroarchitecture [5].

To sum up, the simultaneous route involves the polymerization of the network chains at the same time as their crosslinking. The resulting network necessarily contains defects for kinetic reasons and the final molecular architecture is thus heterogeneous.

r_1 vs r_2	Interpretation	Consequence
$r_1 \approx r_2 \approx 1$	No preference for both monomers	Statistical incorporation of the crosslinker
r_1 and $r_2 \gg 1$	Each monomer prefers to react on himself	Blocky structure
r_1 and $r_2 \ll 1$	Each monomer prefers to react on the other one	Alternated structure
$r_1 \gg 1$ and $r_2 \ll 1$	Both monomers prefer to react with the same monomer	Strong compositional drift: chains that formed first will contained much more preferred monomer than chains that formed later

Table 1: recap of the effect of the relative values of reactivity ratios in the final polymeric network architecture.

2.1.2. The sequential route: chemistry matters

By opposition to the simultaneous route, the sequential route involves the synthesis of the polymer chains first, and then their coupling in a second separate step. This second step may have different names depending on the type of chemistry: crosslinking, curing, vulcanization, etc.

Although the simultaneous route is arguably more straightforward, the sequential route is usually applied in the rubber industry. In the case of unsaturated polymers in particular, the polymer chains contain reactive double bonds that can easily be reacted with sulfur (i.e. by vulcanization, as originally patented by Goodyear [6]) or peroxides [7].

Saturated chains like polyacrylates are more complicated to handle since usual crosslinking agents are not effective on the pristine polymer [8]. It is thus necessary to use comonomers to incorporate new reactive groups in the polymer chains in order to react them together in the second stage, using a crosslinking agent. Table 2 shows some traditional couples of comonomers and crosslinking agents that are used in the literature [8–11]. Note that the sequential route does not completely avoid kinetic issues since the way the comonomer incorporates strongly impacts the final material architecture.

More original strategies may be used to crosslink saturated polymer chains. For instance, the thiol-ene reaction is frequently encountered in the field of polymer chemistry [12,13]. This reaction enables the direct connection of double bonds that may be incorporated in the polymer backbone, using comonomer like allyl methacrylate [14,15]. Another interesting strategy consists in tethering a photoinitating group to the polymer backbone [16]. These units may then be activated by UV light and lead to crosslink points, either by hydrogen abstraction or direct coupling to another unit.

The sequential route therefore gives a lot of control to the polymer scientist provided the right chemical system can be found. The success of this approach relies on the choice of the adequate chemical reaction, comonomer, initiator and formulation. Better control usually means more complexity in the synthesis.

Comonomer	Crosslinking agent
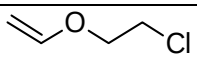 2-chloroethyl vinyl	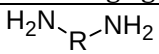 Diamine
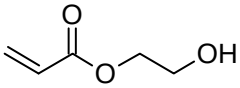 2-hydroxyethyl acrylate (HEA)	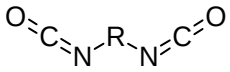 Diisocyanate
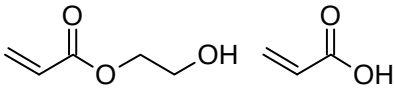 HEA or acrylic acid (AA)	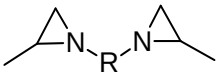 Bisaziridine
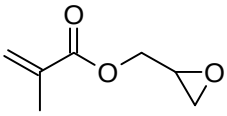 Glycidyl methacrylate (GMA)	Amine

Table 2: some common strategies used for the crosslinking of polyacrylates using a sequential route.

2.1.3. The mixed route using dual-curing systems

In some cases it becomes interesting to first prepare a crosslinked network, and then crosslink it further in a second separate step. This synthetic strategy may be called a "dual-curing system", i.e. a chemical system that enables one to cure the material twice in two separate steps.

Typical dual-cure mechanisms rely on reactions that are different in nature. The first reaction may for instance be cationic polymerization and the second one radical, or vice versa. First examples in the literature make use of the difference in reactivity of vinyl and acrylate carbon-carbon double bonds [17,18]. In the late 20th century, Decker and Decker studied a mixture composed of vinyl ethers and acrylates with radical and cationic photoinitiators [19]. They demonstrated a dual-cure behavior by first activating the radical initiator and then the cationic one using two different UV wavelengths.

The idea of using two different reactions was also exploited using epoxies for the cationic reaction, using either a radical and a cationic initiator [20], or only a cationic initiator since the latter also generates free radicals when there are hydrogen donor molecules nearby [21–23]. In the field of adhesives, Kim's group published a series of papers about epoxy-acrylate dual-curable pressure-sensitive adhesives [24,25]. Figure 3 gives a schematic representation of their system: acrylate functions are reacted in a first step, and epoxy functions are then reacted either together or with a carboxylic counterpart in a second cationic step.

Interestingly, the series of papers from Kim's group began with a dual-cure mechanisms relying on largely different chemistries (see Figure 4) [26]. In a first step, a copolymer comprising benzophenone (a photoinitiating unit) and alcohol pendent groups was synthesized and isolated. The copolymer was then coated with a multifunctional isocyanate and UV-cured to crosslink the benzophenone groups. In a third step, the material was heated up to 60°C for 6 hours to react the isocyanate with alcohol groups. In this paper, the authors demonstrated that the two steps are well-separated but also reported a large decrease in the extent of reacted benzophenone groups with thickness.

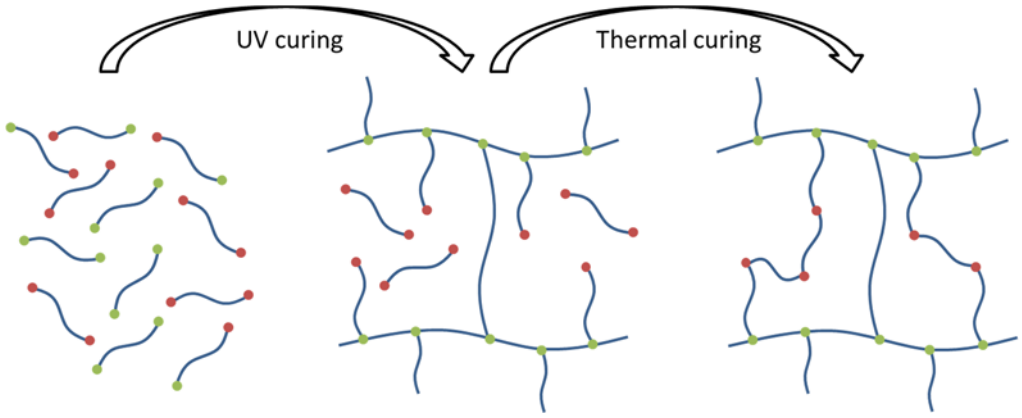

Figure 3: simplified picture of the mechanism used by Kim et al. for the synthesis of dual-curable adhesives. Red dots represent epoxy functions and green dots represent acrylate functions. Initiator and curing agent are not represented. Also, the initial composition includes a triacrylate which react in the first step to bring additional crosslinks in the system.

More recent studies about dual-cure systems involving radical and cationic reactions are based on "click" chemistry [27], in link for instance with applications in shape-memory materials [28,29]. The aza-Michael addition between acrylates and amines may also be used. The main advantage of this reaction is that it proceeds at room temperature in oxygenated conditions without the use of any catalyst [30].

From these examples from the literature (summarized in Table 3), two general rules of thumb may be identified for efficient dual-curing systems. First, the two steps should rely on very efficient chemical reactions. For this, click chemistry is a great help and extensively used in the

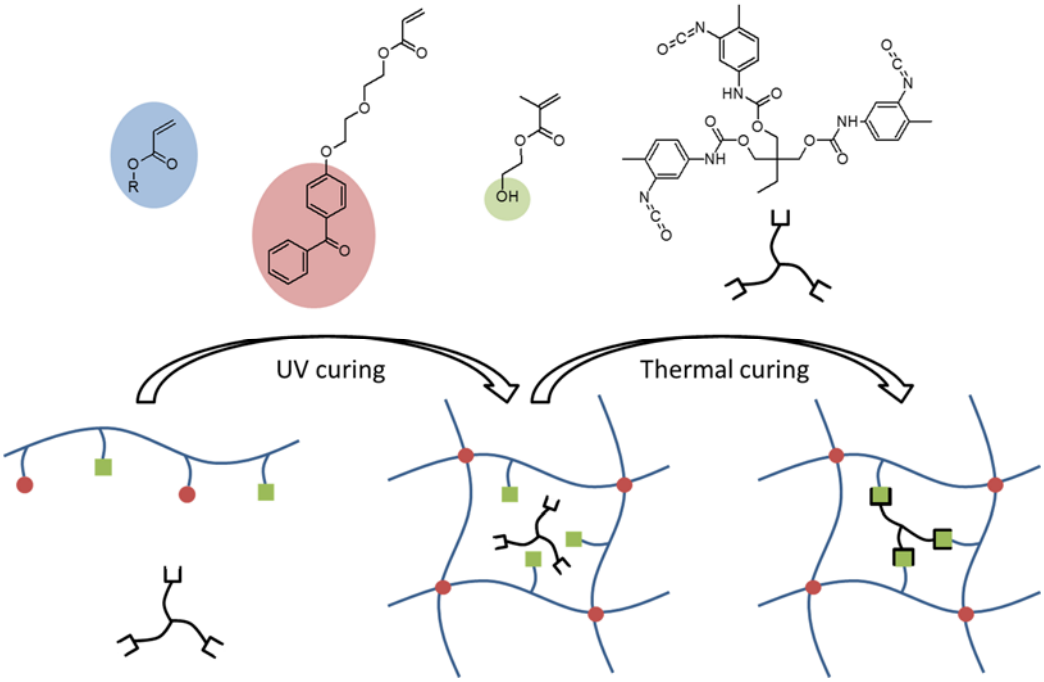

Figure 4: schematic representation of Kim et al's dual cure system based on pendent benzophenones and isocyanate conjugation. The acrylic backbone is represented by a blue line, and each reactive group by a different shape/color (red dots: pendent benzophenone groups, green squares: alcohol groups, black forks: isocyanate group). The group R is either butyl, hydrogen or 2-ethylhexyl.

recent literature. Second, the two stages should be as well separated as possible, ideally using orthogonal chemistries in order to avoid any interference between the two reactions.

All these synthetic strategies make a toolbox the chemist can use to prepare covalently crosslinked networks. Knowing the details of the preparation process is a key to precisely understand the final material properties. The next section will now focus on mechanical properties and how to relate them to the details of the molecular architecture.

First step		Second step		Refs.
Chemical function(s)	Reaction type	Chemical function(s)	Reaction type	
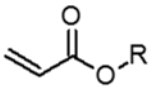	Radical photopolymerization	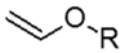	Cationic photopolymerization	[17–19,31,32]
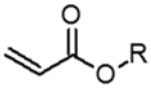	Radical photopolymerization	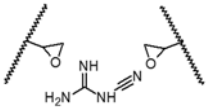	Epoxy condensation via dicyandiamide	[20–23,33]
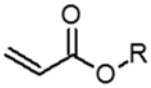	Radical photopolymerization	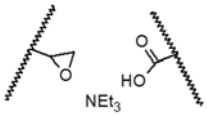	Epoxy-acid condensation	[24,25]
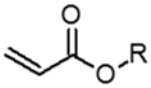	Radical photopolymerization	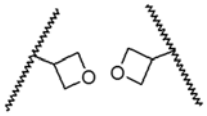	Cationic photopolymerization	[34,35]
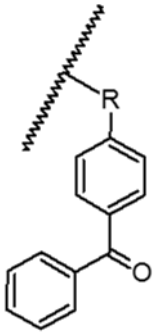	Radical polymerization	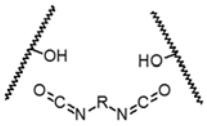	Urethane formation	[26]
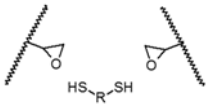	Thiol-epoxy click reaction	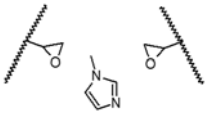	Epoxy condensation	[27–29]
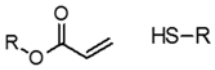	Thiol-ene Michael addition	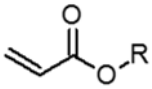	Radical polymerization	[36,37]
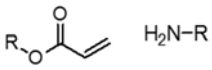	Aza-Michael addition	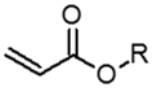	Radical polymerization	[30,38,39]
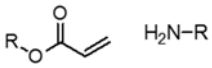	Aza-Michael addition	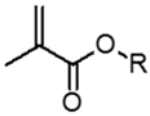	Radical polymerization	[38,40,41]

Table 3: Recap of dual-cure system described in this review. Chemical functions as well as reaction types are given. In the schemes, wavy lines represent pre-existing polymer chains.

2.2. From chain physics to network properties

Polymeric materials are used in a large variety of applications because of their original mechanical properties. These properties stem from the basic physics of polymer chains, and several models have been developed throughout the years to understand the behavior of polymeric networks. These topics are extensively covered in a reference textbook from Colby and Rubinstein that is used throughout this part of the chapter [42].

In this part, the physics of isolated polymer chains is first reviewed. From this basis, the mechanical properties of polymeric networks are modelled. Most basic models are useful since they contain all the physics of the problem, but they can also be refined to take more aspects of polymer mechanics into account.

2.2.1. Physics of isolated polymer chains

A polymer chain is described as an assembly of $N_{\text{C-C}}$ bonds of length $l_{\text{C-C}}$, as depicted in Figure 5. The most obvious characteristic length that comes in mind is the contour length of the chain:

$$R_c = N_{\text{C-C}} \times l_{\text{C-C}} \qquad \text{Eq. 2}$$

This length represents the maximum size of the chain if all monomers were perfectly aligned. In practice, the maximum size of a chain is smaller than R_c because the valence angle between consecutive monomers is fixed by quantum mechanics rules. Introducing the tetrahedral angle θ (see Figure 6), the maximum size of a chain is given by

$$\text{R}_{\text{max}} = \cos\left(\frac{\theta}{2}\right) N_{\text{C-C}}\, l_{\text{C-C}} \qquad \text{Eq. 3}$$

For instance, in many usual polymers (polystyrene, polyacrylates, polyethylene to name only a few), the backbone of the chain is made of carbon-carbon bonds with hybridization states sp3. In these conditions, the valence angle is 109.5° and $R_{\text{max}} = 0.82 R_c$.

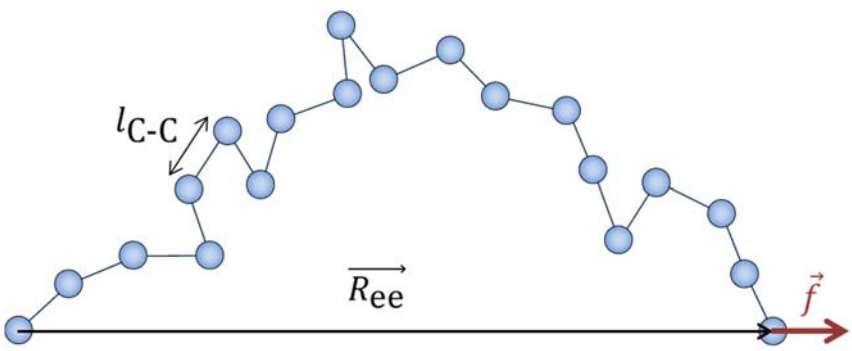

Figure 5: schematic representation of a polymer chain containing $N = 20$ monomers. A force $\vec{f}$ is applied at one end of the chain.

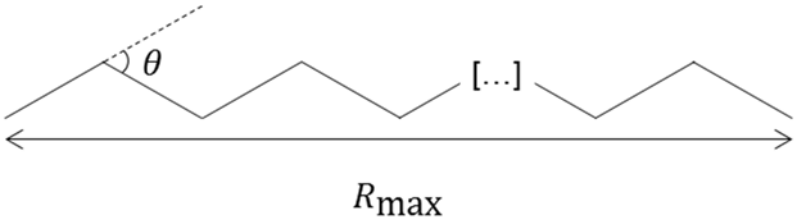

Figure 6: schematic representation of the maximum size of a polymer chain with fixed valence angle. θ is the tetrahedral angle.

A fundamental characteristic length of a polymer chain is the average end-to-end distance, which represents the average size of the chain at rest. In short, a polymer chain may be described as a random walk, possibly with constraints between adjacent monomers. In the case of ideal chains made of independently-linked segments (which is a very common assumption in the study of polymeric materials), it is given by

$$R_0^2 = \left\langle \overrightarrow{R_{\mathrm{ee}}}^2 \right\rangle = C_\infty \, N_{\text{C-C}} \, l_{\text{C-C}}^2 \qquad \text{Eq. 4}$$

where $\overrightarrow{R_{\mathrm{ee}}}$ is the end-to-end vector (see Figure 5) and C_∞ is the structure factor of the chain, a coefficient greater than 1 that quantifies how extended is the chain compared to a perfectly random walk.

In between R_0 and $R_{\max}$, a polymer chain may be partially extended by applying a force (as in Figure 5). Contrary to crystalline materials like ceramics or metals, deforming a polymer chain does not require to break any bond. Instead, the chain unfolds and changes conformations, which implies a much lower energetic cost. This explains why polymeric materials are so easy to deform compared to crystalline materials. For ideal chains and low deformations, the relationship between the end-to-end vector and the force applied to the chain is given by

$$\vec{f} = \frac{3kT}{C_\infty \, N_{\text{C-C}} \, l_{\text{C-C}}^2} \, \overrightarrow{R_{\mathrm{ee}}} \qquad \text{Eq. 5}$$

where $\vec{f}$ is the force applied, k is the Boltzmann's constant and T is the absolute temperature. This linear equation is the molecular equivalent of Hooke's law: a polymer chain behaves like a spring with increasing stiffness when either the temperature increases or the number of monomer decreases.

2.2.2. Assembly of chains and network elasticity

The physics of an assembly of chains ensues from the physics of isolated chains. In order to scale up from the chain to the network, the key question to address is how the chains are connected together. The links may be well defined as when chains are crosslinked, or more subtle as when molecular friction is considered.

Viscosity and molecular friction

In the absence of solvent, polymer chains may exert friction forces onto each other. The magnitude of the friction forces depends on the temperature and on the speed at which the chains deform. This dependence leads to the concept of glass transition temperature T_g, which is basically the temperature below which polymer chains do not have enough thermal energy to move and

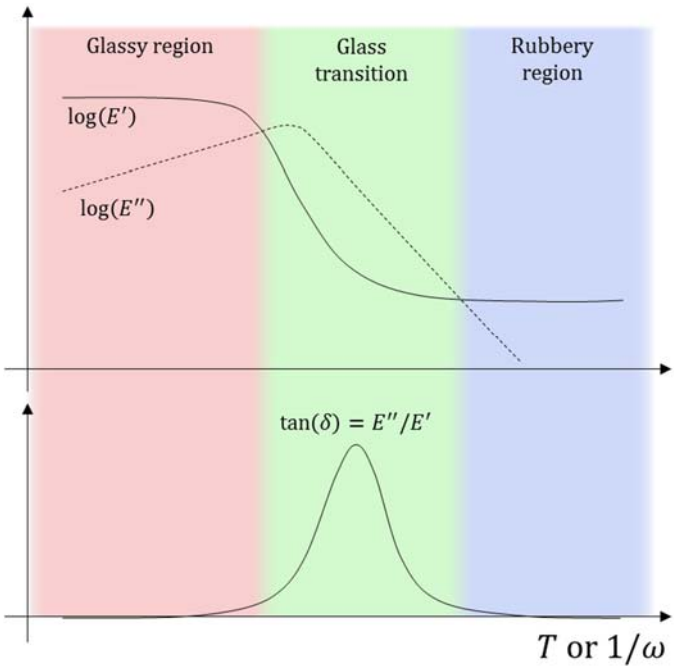

Figure 7: schematic representation of the evolution of complex modulus with temperature or frequency for a viscoelastic material. Top part shows the real and imaginary parts of the complex modulus, bottom part shows the tangent of the loss angle. Bottom axis is either temperature or time/inverse of frequency according to time-temperature superposition principle.

overcome the friction forces. An easy way to visualize the viscoelastic nature of an assembly of polymer chains is to deform it periodically and measure the resulting force or vice versa. The resulting modulus E^* may be decomposed in a real part E' called the storage modulus and an imaginary part E'' called the loss modulus. The ratio between the two is called the loss tangent and represents the fraction of energy dissipated in the material at a given time and frequency. Figure 7 shows the viscoelastic spectrum of a typical polymer network, which may be roughly decomposed in three regions.

- Below T_g, the network behaves like a rigid glass and cannot be deformed easily. The modulus is high (about 1 GPa) and the structure is frozen.
- In the other extreme case, well above T_g, friction forces are so low that they may be neglected. The material is rubbery, fully elastic, and the material behaves like a fluid at long times unless the chains are somehow attached together. The modulus is much lower (about 1 MPa).
- In between these two extreme cases, the chains may move but their motion is partially constrained. As a result, a significant part of the elastic energy that is brought to the material is dissipated.

The presence of viscoelasticity therefore strongly impacts the way the material behaves. The description of the behavior of a material in the transition region is not an easy task. The description of structure-relationship properties in the rubbery region however is much easier, which makes elastomers well above their T_g good model materials for academic studies. It is important however to keep in mind that most industrial elastomers are actually viscoelastic, since it is a very efficient way to tune their properties and in particular their resistance to fracture, as explained later.

The affine model of rubber elasticity

We now consider independent chains well above their T_g and linked together by covalent (i.e.permanent) bonds. In order to model the behavior of an ensemble of chains, one needs a fundamental assumption regarding the relationship between the deformation of the global material and the deformation of a single network strand. The simplest assumption is the affine model, which states that individual chains deform proportionally to the macroscopic material (see Figure 8). Mathematically, defining λ_i as the relative change in dimensions in the direction i, this means that if the material deforms by λ_x, λ_y and λ_z in the x-, y- and z-directions respectively, then the molecular chains deform by the same three ratios. With this assumption, an expression for the change of free energy ΔF may be given:

$$\Delta F = \frac{nkT}{2}\left(\lambda_x^2 + \lambda_y^2 + \lambda_z^2 - 3\right) \qquad \text{Eq. 6}$$

where n is the number of elastic strands in the network. In the case of uniaxial tension, since polymeric materials are incompressible (i.e. $\lambda_x\lambda_y\lambda_z = 1$), a stress-strain relationship may be derived from Eq. 6:

$$\sigma_N = \frac{f}{\mathcal{A}_0} = \nu_x kT\left(\lambda - \frac{1}{\lambda^2}\right) = G_x\left(\lambda - \frac{1}{\lambda^2}\right) \qquad \text{Eq. 7}$$

where σ_N is the nominal stress, $\mathcal{A}_0$ is the initial cross-section of the material, ν_x is the number density of elastic chains in the network and G_x is the shear-modulus of the material. Note that due to incompressibility, Young's modulus and shear modulus are linked by a constant proportionality factor of 3 ($E = 3G_x$). Also, the shear modulus of the material may be expressed as:

$$G_x = \nu_x kT = \frac{\rho RT}{\mathcal{M}_x} = \frac{\rho RT}{\mathcal{M}_0 N_x} \qquad \text{Eq. 8}$$

where ρ is the density of the material, R is the perfect gas constant, $\mathcal{M}_x$ is the molar mass between crosslinks, $\mathcal{M}_0$ is the molar mass of a monomer and N_x is the number of monomers between two crosslinks.

Two very fundamental aspects of rubber elasticity may be seen in Eq. 8. First, the stiffness of an elastomer increases linearly with temperature, which is the physical signature of the entropic origin of rubber elasticity. The second aspect is the dependence on N_x. Since rubber elasticity is a purely entropic phenomenon, the only physical parameter that impacts the value of the modulus is the number of chains (or equivalently crosslinks) per unit volume. In the frame of the affine model and in elastomers specifically, since there is no solvent, the modulus solely depends on the average molecular mass of the network strands. The longer the network strands, and the softer the final elastomeric network. The chemical nature of the polymer does not play any role, provided the material is well above its glass transition temperature. In other words, the strength of the covalent bonds that constitutes the polymer chains have no impact on the modulus.

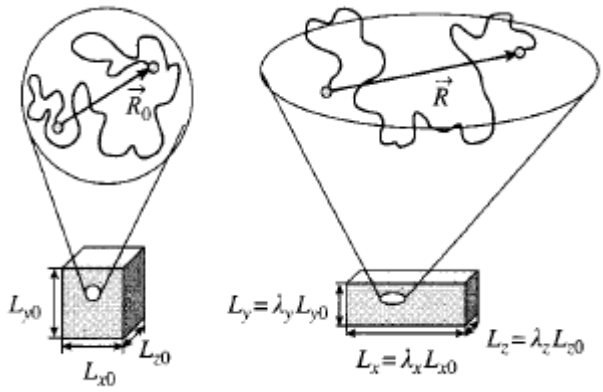

Figure 8: schematic representation of the affine model. In this representation, $\overrightarrow{R_0}$ is the end-to-end vector in the unstretched state and $\vec{R}$ in the stretched state. Taken from [42].

The question of entanglements

Entanglements are topological constraints due to the fact that molecular chains are long enough to entangle. They prevent the chains from moving freely and add some links between the chains, which gives additional rigidity to the material. Qualitatively, it is fairly intuitive that entanglements can slide along the chain when the material is being deformed, contrary to chemical crosslinks that are fixed. The effect of entanglements on modulus is thus strain-dependent and should decrease as strain increases.

The simplest way to take entanglements into account at low strain is to consider them as transient crosslinks and summarize their action with an additional contribution to the shear modulus $G_e = \nu_e kT$ where ν_e is the number density of entanglements. The overall shear modulus of the material is then given by $G = G_x + G_e$. However, this does not model the effect of entanglements at larger strains.

An alternative empirical approach was given by Mooney and Rivlin [43,44]. In the affine model, the reduced stress $\sigma_{\text{Mooney}} = \frac{\sigma_{\text{nominal}}}{\lambda - 1/\lambda^2}$ is a constant (of value G). Mooney and Rivlin consider instead that this reduced stress evolves linearly with $1/\lambda$, which gives the following expression:

$$\sigma_{\text{Mooney}} = \frac{\sigma_{\text{nominal}}}{\lambda - 1/\lambda^2} = 2C_1 + \frac{2C_2}{\lambda} \qquad \text{Eq. 9}$$

This non-linear modification catches fairly well the behavior of crosslinked and entangled materials [45] and more importantly provides a simple mathematical form to take into account the softening that may be observed at small strain. It however does not work in other deformation modes, like compression or biaxial extension. Mooney-Rivlin model is therefore useful because it is easy to handle mathematically, but it is also intrinsically erroneous.

A molecular model was more recently proposed by Rubinstein and Panyukov [46]. Entanglements are modeled as originally proposed by Edwards [47]: a topological potential is applied all along the chains and adds an unfavorable energetic contribution to monomer movement perpendicular to the chain. The chain behaves as if constrained in a tube (see Figure 9). Rubinstein and Panyukov's model also proposes that this tube fluctuates randomly and that the amplitude of these fluctuations depends on the strain tensor. In uniaxial deformation, this model leads to a semi-analytical stress-strain equation:

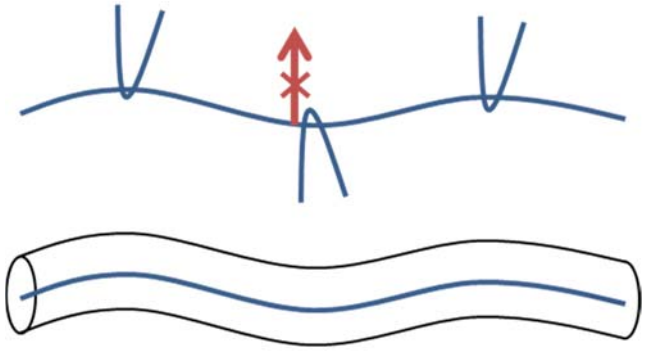

Figure 9: schematic representation of an entangled chain. Top: entanglements hinders mouvements perpendicular to the direction of the chain. Bottom: "tube representation" of entanglements, the contribution of all entanglements is summarized by a constraining potential perpendicular to the direction of the chain.

$$\sigma_{\text{Mooney}} = \frac{\sigma_{\text{nominal}}}{\lambda - 1/\lambda^2} = 1/3\left(E_x + \frac{E_e}{0.74\lambda + 0.61\lambda^{-1} - 0.35}\right) \qquad \text{Eq. 10}$$

where E_x (respectively E_e) is the Young modulus attributed to crosslinks (resp. entanglements). This model is especially useful to extract the respective contributions of crosslinks and entanglements from the nonlinear elastic response of a polymer network at intermediate strain, measured by uniaxial tensile or compressive test for example.

The end of the Gaussian regime

All the previous expressions are based on the fundamental assumption that the extension of the chains are well below their contour length. At large extensions, this is no longer true and the previous calculations break down. Intuitively, the number of possible conformations at large extension becomes so small that a very high amount of free energy has to be spent to deform the chains further. One thus expects an increase in rigidity when stretching the chain close to its maximum size. This translates experimentally to an increase in the local slope of the stress-strain curve, a phenomenon called strain-hardening.

A very general way of taking this effect into account is to use concepts of statistical thermodynamics to compute the free energy of a chain via the partition function and theorem of fluctuation-dissipation. This eventually leads to an equation that links the average end-to-end length to the applied force via a Langevin function $\mathcal{L}$:

$$\frac{\langle R_{\text{ee}} \rangle}{\mathcal{N} b} = \mathcal{L}\left(\frac{fb}{kT}\right) = \coth\left(\frac{fb}{kT}\right) - \frac{1}{fb/kT} \qquad \text{Eq. 11}$$

where $\mathcal{N}$ and b are the number and size of Kuhn segments.

In the case of small deformations, this equation reduces to Eq. 5. Note that this model is still purely entropic although it takes finite extensibility into account. The increase in force with extension has a statistical origin (reduction in number of available conformations) and not energetic (pulling on bonds). In other words, this model does not describe a regime where covalent bonds between segments are stretched. Thus explains why the bond energy does not appear in the force-extension relationship.

Eq. 11 can (at least in theory) be included in any of the previously exposed network models to take the finite extensibility of the chains into account, as for example in Arruda-Boyce's model [48]. In practice stress concentration effects and interactions between chains cannot be neglected

in highly stretched polymer networks. Thus, summing up the free energy of each individual chain does not really work.

Instead, an alternative approach consists in using an empirical expression. Gent's constitutive model [49] for instance describes the increase in stress by an equation expressed in terms of the strain invariant $J_1 = \lambda_x^2 + \lambda_y^2 + \lambda_z^2$. In uniaxial traction, this gives the following expression:

$$\sigma_{\text{nominal}} = G\frac{\lambda - 1/\lambda^2}{1 - \frac{J_1 - 3}{J_m - 3}} = G\frac{\lambda - 1/\lambda^2}{1 - \frac{\lambda^2 + 2/\lambda - 3}{\lambda_m^2 + 2/\lambda_m - 3}} \qquad \text{Eq. 12}$$

where J_m is the value of the first strain invariant when the chains are stretched at their maximum and λ_m is the modelled maximum extensibility of the material.

Fracture, or when reality meets theory

Up to this point, the mechanical properties of polymeric materials are fairly well understood. Above the glass transition, the mechanical properties of a network are dictated by the physics of its polymer chains. Using a combination of theoretical and empirical models, the network mechanics may be described and possibly linked to what happens at the chain length scale.

But this description ignores two very fundamental points. First, a network is never perfect and heterogeneities in the architecture may change the material properties significantly. For instance, the number of monomer between crosslinks may not be constant. Second, chains are not indefinitely deformable and may break when they are brought close to their limit of extensibility. This creates defects that can then turn into cracks.

The understanding of materials fracture properties is therefore vital to the engineering of new polymeric materials and to their use in specific applications.

3. Fracture of soft materials and how to reinforce them

Fracture of soft materials is a seemingly simple topic that is the focus of a lot of recent research, both from the theoretical and applicative points of views. First, a brief recap of the current vision of fracture of soft materials is given. Then, common strategies to toughen soft materials will be highlighted.

3.1. Description of fracture in soft materials, a matter of dissipation

3.1.1. From LEFM to a modern description of soft material fracture

The description of fracture consists in studying the amount of mechanical energy that is brought to the material and how it evolves when a crack propagates in the material. Formally, the strain energy release rate is defined as the change in total mechanical energy W_{tot} with change of crack area A:

$$G = \frac{dW_{\text{tot}}}{dA} \qquad \text{Eq. 13}$$

Defined like this, W_{tot} includes the work done to the system and the strain energy released by the system as the crack advances.

A simple criterion for crack propagation is Griffith's model [50], which states that a crack propagates when G reaches a critical value G_c that corresponds to the reversible work of adhesion of the material, also called Dupré energy of adhesion. In other words, the crack propagates when there is enough available energy to create new surfaces of material.

Despite its simplicity, Griffith's model is a very powerful way of describing fracture and is the basis of Linear Elastic Fracture Mechanics (LEFM) [51]. In particular, its combination with Irwin's model [52] which describes the stress concentration at the vicinity of a sharp feature such as a crack successfully describes fracture in brittle materials like glasses or ceramics. Simply speaking, LEFM describes fracture resistance as the ability for a material to store reversibly a large amount of elastic energy before breaking.

LEFM however is not a suitable tool to describe fracture in soft materials such as elastomers and gels. The main reason is that contrary to brittle materials the energy is not solely dissipated at the crack tip by breaking bonds, and therefore the behavior at the crack tip does not entirely control the fracture phenomenon [53].

More specifically, the fracture of soft materials involves several sources of energy dissipation, and at different length scales, as depicted in Figure 10:

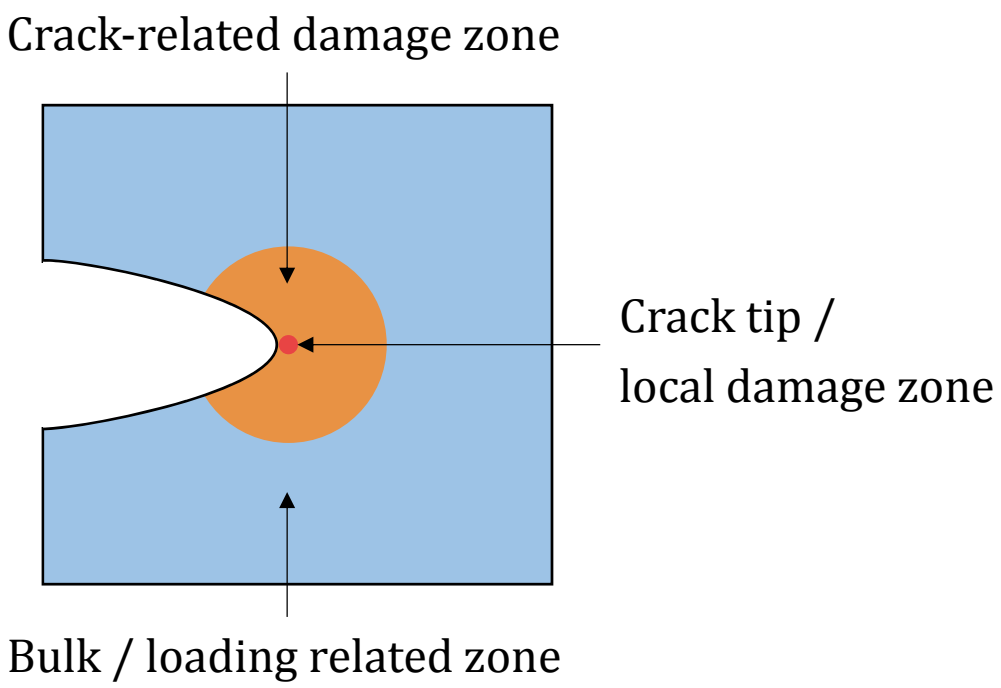

Figure 10: schematic representation of the different zones where energy may be dissipated during crack propagation. At the crack tip, the local damage zone (in red) is where bonds are broken to propagate the crack. The crack-related damage zone (in orange) is where energy may be dissipated without helping the crack to advance. In the bulk of the material (blue), viscoelasticity or other dissipative mechanisms may appear simply because of the loading. Image adapted from [53].

- In the bulk of the material, far from the crack tip, the material may dissipate energy because of non-reversible phenomena such as viscoelasticity or plasticity. Note that the concept of J-integrals is a way to account for these phenomena theoretically [54] and experimentally [51].
- At the crack tip, the shape of the crack may evolve because of the large deformability of the material. This can induce crack blunting for instance, i.e. a deformation of the crack tip that removes stress concentration and hinders crack propagation [55].
- In a neighboring region, the propagation of the crack may trigger dissipation phenomena that are not useful for crack propagation (and thus beneficial for resistance against fracture).

All these specificities strongly impact the way energy is used to propagate the crack. The concept of G_c from LEFM therefore needs to be extended. The tearing energy Γ is thus defined in a similar way as G_c except that all different types of energy losses are considered [56]. For elastomers, the tearing energy is usually referred to as the fracture energy, in a sense similar to the critical strain energy release rate.

In practice, it is very difficult to separate the contributions of the various sources of energy dissipation in Γ. In addition to this, the presence of time-dependent phenomena like viscoelasticity implies that Γ is not a constant but may strongly depend on the experimental conditions.

Despite its commonness in nature and industrial applications, soft material fracture is a complex topic that is the object of intense research work. LEFM may provide a conceptual framework but does not suffice to describe completely experimental observations.

3.1.2. Measurement of fracture energy

Now that the concept of fracture energy has been covered, it becomes necessary to elaborate on the methods used to measure it. Over the years, some reliable experimental configurations have been found and extensively described in the literature.

The measurement of fracture energy is made by pre-notching a sample and loading it in uniaxial tension or pure shear until rupture. The sample may be notched on one or two sides (see Figure 11). Tear test can also be used for tough samples.

In the case of single edge notch test, Greensmith proposed an empirical expression giving the strain energy release rate with respect to the deformation of the sample [57]:

$$G(\lambda) = \frac{6\,c\,W(\lambda)}{\sqrt{\lambda}} \qquad \text{Eq. 14}$$

where c is the initial crack size, λ is the stretch ratio and W is the strain energy density defined as the integral of the stress-strain function of the unnotched sample. In practice, Γ is estimated by measuring the stretch ratio at which a notched sample fails λ_{rup} and then use this value to calculate $W(\lambda_{\text{rup}})$, using the stress-strain curve of an unnotched sample.

In the case of pure-shear geometry and provided $c > h_0$, where c is the crack length and h_0 the initial height of the sample, the strain energy release rate is simply given by:

$$G = W(\lambda)h_0 \qquad \text{Eq. 15}$$

This expression is usefully not dependent on the crack length c, in contrast with the single-edge notch test configuration in which $dG/dc > 0$. In the latter case, the propagation of the crack is always catastrophic, while in the former case a constant crack speed may be observed.

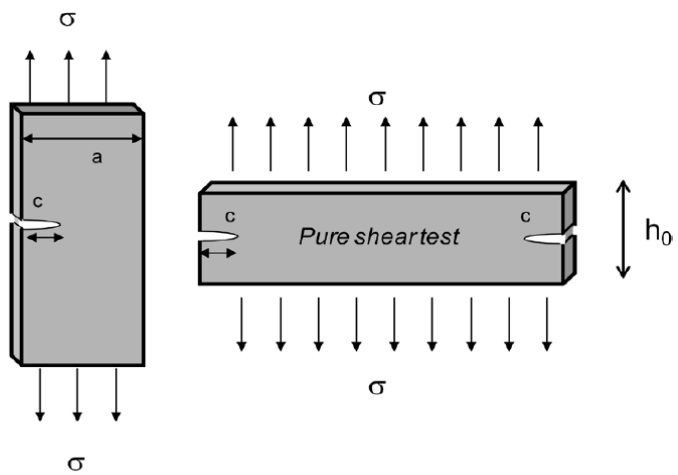

Figure 11: two possible configurations to measure the fracture energy of soft polymeric materials. Left: single-edge notched test. Right: pure-shear test. Taken from [53].

3.1.3. Molecular description of fracture in polymeric materials

The description of fracture is a complex issue, and in practice it is difficult to have a top-down approach, i.e. to try to decompose the various contributions to Γ. Instead, an alternative way is to study fracture from a molecular point of view using a bottom-up approach.

Quite obviously, the propagation of a crack requires to break all the chains in the plane perpendicular to the principal tensile direction. These chains carry an energy U_{chain} that is dissipated once the bond is broken. The fundamental question is then to relate U_{chain} with the energy of a carbon-carbon bond U_{b}. A naïve (and false) idea is to consider that U_{chain} corresponds to U_{b}, i.e. that the only price to pay to break the chains is the dissociation energy of the weakest covalent bond.

This is wrong because the chains need to be stretched before breaking. In their pioneering article, Lake and Thomas explain that in order to break one of the bonds of an elastic chain between two crosslinks, the entire strand must be stretched and all bonds must be loaded up to an energy that corresponds to U_b. Eventually, when any of the bonds breaks, the entire chain relaxes and all the stored energy is lost. Mathematically, neglecting all other sources of energy dissipation, fracture energy may thus be expressed as

$$\Gamma_0 = 2N_x U_b \Sigma \qquad \text{Eq. 16}$$

where N_x is the average number of monomers between two crosslinks and Σ the areal density of chains in the fracture plane. Note that a recent research article suggests that using the dissociation energy for U_b over-estimates the value of Γ_0 [58]. This is because it neglects the contribution of the force to the chemical reaction of the cleavage of the carbon-carbon bond. They suggest instead to use a value of about 60kJ/mol, which in any case changes only the numerical values and not the scaling laws described here.

One can further show that $\Sigma = \nu_x a\sqrt{2N_x}$, for geometrical reasons. By using the expression of the modulus given by the affine model (see Eq. 8), one can show that Γ is proportional to the inverse of the square root of the Young's modulus. This key result basically states that the stiffer the material is, the less resistant to fracture it is. When considering only dissipation due to bond scission, there is a clear tradeoff between stiffness and toughness. In order to circumvent this compromise, one must find strategies that involve other sources of dissipation at larger length scales.

3.1.4. The case of cyclic fatigue

Cyclic fatigue is a phenomenon that corresponds to a loss of mechanical properties caused by repetitive deformations at small to intermediate levels. In crosslinked polymer networks, fatigue usually leads to propagation of pre-existing cracks, but at deformation levels well below the critical threshold G_c. Fatigue is therefore an important industrial parameter to assess since it strongly conditions the lifetime of the final product.

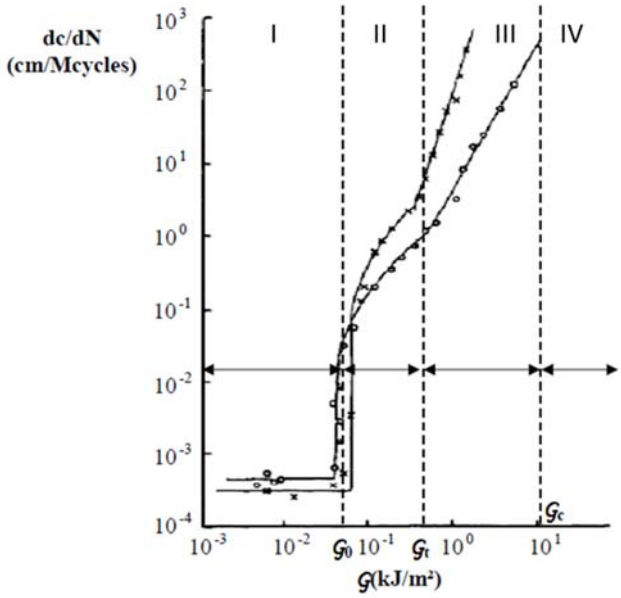

Figure 12: typical fatigue curves obtained from crosslinked elastomers. The vertical axis shows the crack propagation rate. Circles corresponds to natural rubber, crosses to styrene-butadiene-acrylonitrile. Four regimes may be distinguished depending on the applied strain energy release rate. Taken from [59].

Figure 12 is taken from Mzabi's PhD work [59] and shows a set of typical curves of fatigue testing (data are taken from [60]). Four typical regimes may be distinguished depending on the value of G that is imposed:

I. For very low values of G, virtually no propagation is observed.
II. For values of G between G_0 (the crack propagation threshold) and G_t (the transition threshold), propagation is observed and the speed scales linearly with G.
III. For values of G between G_t and G_c (the critical strain energy release rate, or fracture energy), propagation speed follows a power-law of G called Paris law. The exponent of G is usually noted β and ranges from 2 to 4 for elastomers[61]. This regime is the one that is typically characterized in most fatigue tests and is the only one described in normalized tests [62].
IV. For values of G larger than G_c, catastrophic failure occurs, as described previously.

A material that has good properties with respect to fatigue exhibits a large threshold energy G_0 and a low exponent β at working temperature. Although fatigue resistance is vital to assess for industrial applications, it is not commonly done in practice for lab-scale materials. The practical assessment of fatigue lifetime not only requires lots of material, but also needs to follow a precise methodology to avoid experimental bias.

Also, it is worth pointing out that fatigue properties cannot a priori be anticipated from tensile and fracture tests. For example, the fatigue threshold of natural rubber at about 50 J/m^3 on Figure 12 whereas measurements of tearing energies give values ranging from 1 to 20 kJ/m^2 [56]. This low value explains the use of carbon black fillers in the tire industry, which raises the threshold value by 50% [61]. The discrepancy between the values of G_0 and Γ is explained by the presence of dissipation mechanisms that raises the value of Γ whereas G_0 is intrinsically linked to the pristine material ability to resist fatigue, which is more accurately estimated with Lake and Thomas model.

Contrary to what is sometimes found in the literature, it is useful to point out that weakness in fatigue is not a priori correlated to the presence of permanent damage in the material during

deformation [63–65]. As a counterexample, natural rubber filled with carbon black exhibits a large Mullins effect which is linked to damage in the material that cannot be recovered unless the material is heated or left at rest for a very long time [59]. Yet, once the energy associated to Mullins effect is dissipated, the material still has good properties in fatigue as illustrated by its widespread use in the tire industry whenever a high mechanical strength is required.

3.2. General guidelines for improving the fracture resistance of soft materials

Several recent reviews address the different strategies that can be used to increase the fracture energy of soft materials [53,66,67], and they are extensively used in this exposition of the state of the art.

The fracture of a material may be roughly separated in two events. First, a defect is created somewhere in the material. Then, when a critical force is reached, this defect propagates into a crack and the material fails. Logically, there are thus two main ways to toughen a soft material, playing either on the initiation or on the propagation of defects.

In order to study the toughening of soft materials, hydrogels are often used as a model material. Hydrogels are polymeric materials that contain a significant fraction of water [68]. They concentrate large research efforts due to their ability to combine high affinity with water (hydrophilicity) and solid-like character (hydrogels are not soluble in water). For example, hydrogels are massively used as soft lenses where hydrophilicity is a key property to achieve biocompatibility [69]. Other applications can be found in the fields of cosmetics, drug delivery and biomedicine among others [68,70,71]. In particular, synthetic hydrogels are good candidates for the production of biomaterials like artificial tendons or cartilage.

Beside their applicative interest, there are at least three reasons that make hydrogels good model materials to study fracture. First, the chemistry behind hydrogels is versatile since it is based on organic chemistry. It is therefore possible to tune precisely the architecture of the polymeric network and to incorporate reactive functions or functional groups in the backbone structure of the gel. Second, highly swollen hydrogels are fully elastic (negligible internal friction) and disentangled thanks to the presence of water. This makes their structure much simpler than a dry soft material and makes structure-property relationship much easier to establish. Third, because hydrogels are swollen with water, their intrinsic fracture resistance is very weak. A basic hydrogel shows a fracture energy of about 10 J/m2 for instance [72]. Therefore, any reinforcing or toughening effect should be easy to visualize.

Some general paths for the reinforcement of soft materials are now given, some of them stemming from the field of hydrogels. First, examples of systems that play on the initiation of cracks are given, then examples playing on the propagation of existing defects. Finally, a third part focuses more specifically on elastomers and highlights the differences with hydrogels and some of the original strategies that may be used on them.

3.2.1. Delaying the onset of fracture

In soft materials, the initiation of the crack is typically linked to the fracture of the shortest polymeric chains of the network. A way to increase the material's extensibility (and hence the material's fracture energy) is thus to delay the generation of cracks by homogenizing the length of the different network strands. For example, 4-arm polyethylene glycol (tetra-PEG) macromonomers may be prepared and coupled to each other to form a more homogeneous polymeric network [73–75]. Provided the arms are exactly the same size (using living polymerization techniques for instance), the final network has a controlled structure and resists high levels of strain and stress [73,76]. Alternatively, telechelic chains may be used and cross-linked, for instance using click chemistry [77].

Another well-explored technique consists in using crosslinks that can slide along the polymeric network. These structures are called topological gels or polyrotaxane gels and were first synthetized by Okumura and Ito in 2001 [78]. When the network is stretched, it accommodates the deformation by increasing the distance between crosslinks of the shortest chains until all network strands are the same size (a phenomenon referred to as "Pulley effect", see Figure 13) [79,80].

These two examples illustrate that the uniformization of the network strand is an effective strategy to avoid the onset of fracture at low stretch ratios. It however does not really impact the resistance of the material to the propagation of an existing crack or defect. Sakai's group reports

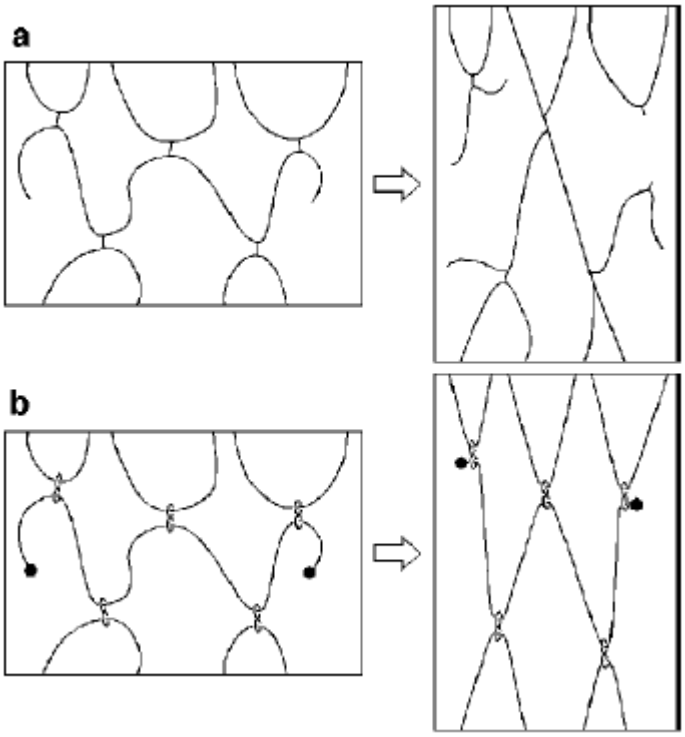

Figure 13: illustration of the Pulley effect from Ito and Okamura's tough hydrogels. a) case of a crosslinked networks, fracture occurs from the smallest strands. b) case of polyrotaxane gels, crosslinks slide until all strands are about the same size, thus delaying the fracture onset.

fracture energies ranging from 5 to 40 J/m^2 depending on the size of the PEG arms, in agreement with Lake and Thomas predictions [81,82]. Ito's group also studied the fracture energy of their rotaxane sliding gels and found values as low as 4 J/m^2 [83]. As a side note, they also find that in their system Γ is constant and independent from the modulus of the gel (contrary to Lake and Thomas prediction). This is interpreted by the authors as a result of the sliding character of the crosslinks.

3.2.2. Increasing the cost of propagation by adding dissipation

As reviewed earlier, the ability of a material to resist the propagation of a crack may be improved by adding sources of energy dissipation. The basic idea is to channel part of the released elastic energy into something else than the creation of two new surfaces.

In a recent review article focusing on tough hydrogels, Zhao details different possible strategies to get additional toughness [67]. He summarizes them by considering that an efficient strategy should combine two aspects: dissipating a large amount of energy during stretching on the one hand, and maintaining a large reversible deformation of the network on the other hand.

A way to do so is to combine transient (or "physical") and permanent (or "chemical") crosslinks, so that the breakage of physical bonds may dissipate energy. These transient bonds may be incorporated via ionic groups in the network that can be further crosslinked reversibly with metal cations [84–87]. Metal-ligand complexes [88], hydrogen bonds [89] or hydrophobic interactions [90,91] may also be used.

The physical integrity of the material may also be kept by having enough bonds at a given time, such that even if some of them break and reform there is always enough crosslinks to avoid creep and permanent deformation. For instance, this can be performed by using nanoparticles to crosslink the networks which act as multi-functional crosslinks. Chains may thus be individually broken without breaking the entire specimen. Such highly-functional materials may involve the use of various clays or silica nanoparticles [92–95], graphene oxide [96], crystalline domains [97–99], microspheres [100] or glassy spheres [101].

3.2.3. Specificities of elastomers

Elastomers share with hydrogels the fundamental property that the polymer chains are organized in a three-dimensional network. The main difference however is that elastomers are dry, so that the chains may entangle and rub against each other. This brings an additional level of complexity that may be exploited to find additional sources of energy dissipation.

Viscoelasticity, an ambiguous help for toughness improvement

Tuning the glass transition (and thus the amount of energy dissipated by viscoelasticity) in elastomers is one of the easiest tools to increase the fracture energy of elastomers. Contrary to hydrogels, the polymer chains in elastomers are in contact with each other, and as a result there is a friction force that applies on the chains when they deform.

The effect of viscoelasticity on fracture has been extensively studied both experimentally and theoretically. Gent is one of main scientists who studied the relationship between the toughness

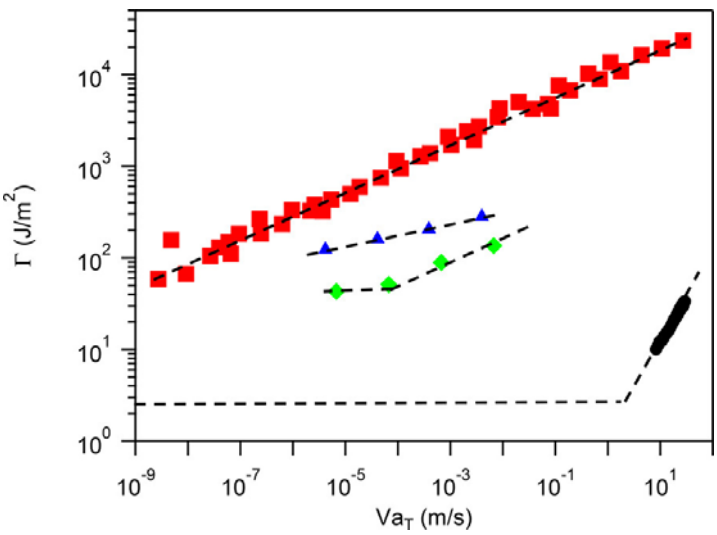

Figure 14: fracture energy as a function of reduced propagation velocity for various elastomers. (red squares: SBR, green diamonds: polyurethane rubber, blue triangles: double network elastomer, black circles: gelatin circle). Taken from [66].

in rubbers and molecular friction [102–104]. He showed that bringing an elastomer closer to its glass transition temperature increases its fracture energy by two orders of magnitude. This is a very generic result that is valid for any elastomer, as shown in Figure 14 which shows the change in Γ with reduced crack velocity for 4 different elastomers [66]. Viscoelasticity may also be associated to other toughening strategies in order to further increase the resistance to fracture. As an illustrating example, Ito's group have recently developed elastomers crosslinked with sliding rings, similarly to their polyrotaxane hydrogels [105]. In their article, they report large values of fracture energy, up to 1300 J/m². They attribute this increase to an increase in viscous dissipation, triggered by the presence of sliding crosslinkers.

An interesting side note is that some of the previously mentioned strategies to reinforce hydrogels may actually be seen as the incorporation of an artificial friction in a lubricated system where these forces are not naturally present. Such an example is the dual-crosslinked hydrogels studied in our group [106] (see Figure 15). On the graph, the complex modulus of a chemically crosslinked network (black line) is compared with a dual-crosslinked network where some of the crosslinks are permanent and some are transient (due to association of alcohol functions of poly(vinyl alcohol) and borax molecules). The presence of transient bonds leads to an increase in modulus but also to a dependence of storage modulus on frequency. This is equivalent to going from a perfectly rubbery situation to a transition situation where viscous forces are active. In a recent article, it has indeed been shown that the change in properties of PVA-borax networks could be explained on the basis of time-temperature superposition [107] which goes in the sense of a viscoelastic dissipation.

Coming back to elastomers, using viscoelasticity to increase the fracture energy actually comes with several drawbacks. One of them is that viscoelasticity renders the material mechanical properties dependent on time and temperature. From an applicative point of view, this means that considering a specific application one must find and/or prepare a specific polymer with a given glass transition temperature. This may become an uphill battle when said application implies a large range of temperature and/or loading rates.

Another problem is that energy dissipation is necessarily associated to a local increase in temperature. In most cases, this is not an issue because the generated heat has enough time to

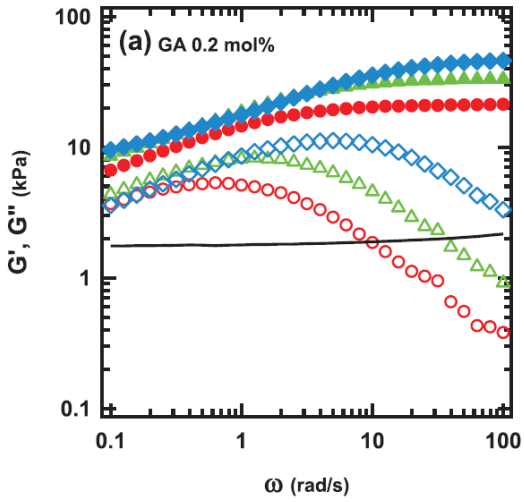

Figure 15: angular frequency dependence of the storage and loss shear moduli of a poly(vinyl alcohol) gel crosslinked with 0.2 mol% glutaraldehyde (black line) with dual crosslink gels crosslinked with 0.2 mol % glutaraldehyde and borax at three different concentrations (red: 1 mM, green: 5 mM, blue: 50 mM). Taken from [106].

diffuse in the material, leading to an increase of temperature of a few degrees at most [108]. When the strain rate becomes larger however, the build-up of heat may ruin the material's ability to resist crack propagation [109]. This may also be the case when a thick material is cyclically loaded, a phenomenon called "thermal runaway" [61].

Viscoelasticity is also associated to other effects that may be desirable to avoid, like the presence of residual deformation. For instance, coming back to Ito's sliding elastomers [105], the sliding nature of the crosslinks results in an increase in E'' above T_g, which probably explains the observed increase in fracture energy. Materials are tougher, but they also show a significant hysteresis and residual deformation when deformed cyclically (see Figure 16). This is a very general feature of viscoelastic elastomers, and may be detrimental for some applications (e.g. sealants)

To sum up, viscoelasticity is always an effective strategy to increase the fracture energy of an elastomer. Choosing the right glass transition temperature is a way to tune the resistance to fracture but it comes with some drawbacks. Dependence of properties on temperature and frequency is one of them, and may requires to find alternative strategies to enhance Γ.

Use of fillers, the classical approach for reinforcing elastomers

The reinforcement of rubber materials using inorganic fillers is almost as old as the use of elastomers in industrial applications. This paragraph only aims to give a broad overview of the important features of filled elastomers and is in large parts based on a book chapter [110] by Chazeau et al.

Very basically, filled rubbers are prepared by mixing a gum with curing agents and inorganic particles, most often carbon black or silica. Use of hard particles in a soft matrix significantly changes the properties of the material, as shown in Figure 17 which compares the stress-strain curves of an unfilled and a filled elastomer [111]. The modulus, stress and strain at break increases simultaneously when the inorganic load is added. Filled rubber also show significantly better properties regarding crack propagation experiments. For instance, the threshold tear energy of styrene-butadiene rubbers filled with carbon black is five to ten times better than their unfilled counterparts [112], the threshold energy being the minimum energy required to propagate a

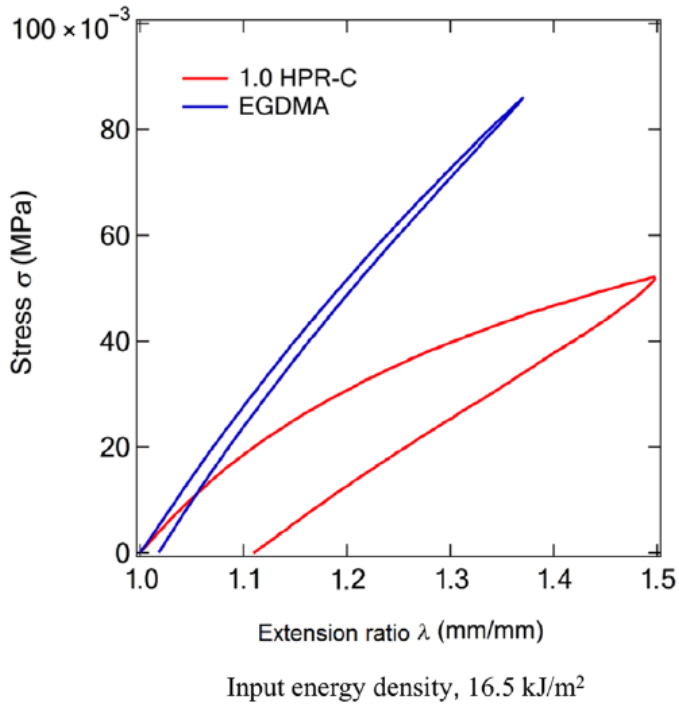

Figure 16: comparison of stress-strain curves in cyclic loading for two elastomers. Blue curve is a classically crosslinked elastomer, red curve is an elastomer crosslinked with rotaxane crosslinkers that can slide along the chain. Taken from [105].

crack when molecular friction (i.e. viscoelasticity) is removed. With the addition of viscoelasticity, the gain in fracture toughness is tremendous.

But the addition of fillers in the elastomer structure also triggers some hysteretic processes that are not without consequences on the material. First, at small strain, a strong non-linearity of the modulus is observed. This phenomenon is referred to as "Payne effect" and depends both on the maximum applied strain and strain rate [113,114]. A decrease in stiffness and an increase in viscous losses are observed when the strain increases. The magnitude of this effect strongly depends on the filler fraction and vanishes when the temperature is increased or when the strain rate approaches zero, making it very similar to classical viscoelasticity. The other dissipation mechanism specific to filled rubbers has originally been observed by Holt but is commonly referred to as the Mullins effect [115–117]. It consists in a significant softening at large strain after the first elongation of the material. This softening is accompanied by a residual deformation and can be partially recovered after either heating or long time at rest [118].

A lot of research has been devoted to the understanding of the reinforcement of elastomers by fillers and the identification of the main parameters behind the process. First, the quantity of filler plays an important role, and the best reinforcements are achieved when the filler is relatively homogenously distributed and in large enough amount so that a percolating network of filler particles may form [119]. By playing on the surface chemistry of fillers, some authors also demonstrated that the filler-filler and filler-matrix interactions play a major part in the reinforcing mechanism [120,121]. The question of the physical state of polymer chains at the interface with particles is also a topical research subject. One of the current views describes some of the properties of filled elastomers as the consequences of frozen and bound polymer chains that form glassy domains at the vicinity of inorganic particles [122–125].

Adding filler particles to elastomers is therefore an immediate strategy to increase the stiffness and the toughness of the material. It however brings additional levels of complexity to the dynamic

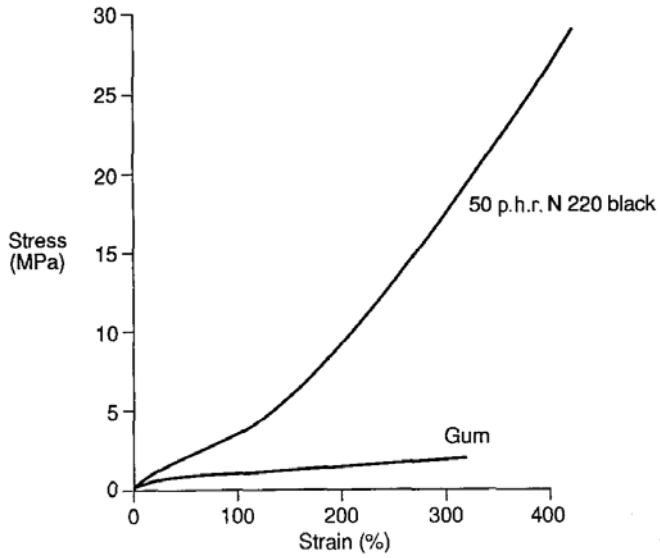

Figure 17: comparison of the stress strain curves of an unfilled and a filled rubber. The matrix is a styrene-butadiene rubber ("Gum") and the filler is a carbon black. The actual formulation is more complex than that and given in the original reference of the graph [111].

properties of the material. It also imposes to control the processing very well since the dispersion of the particles greatly influences the properties of the final material. Another obvious drawback of this method is that it yields materials that are not transparent, which is detrimental to some applications.

Some other strategies to dissipate energy in elastomers

Similar to the previously mentioned strategy for hydrogels, polar groups may be incorporated in the elastomer structure to promote weak interactions and physical bonds. The resulting materials are called ionomers and are widely used in the fields of packaging, coatings and adhesives [126]. There is however a major difference with hydrogels, since elastomers do not contain any solvent and are thus mainly hydrophobic. The polar groups therefore tend to phase separate and form clusters [127]. The fracture of these materials has not been studied in detail [126] but some recent research has been conducted in this field. In particular Shabbir et al. studied ionomer melts and found unusually slow propagation speeds, which would indicate that dissipation processes are present [128].

Another possibility to add sources of energy dissipation, once again by analogy with hydrogels, is to use dynamic bonds. The breaking and reforming of the bonds could dissipate some energy and increase the apparent fracture energy of the material. Additionally, this brings a self-healing property, i.e. the material becomes recyclable (which is not the case of conventional elastomers). For instance, Li et al. showed that a fracture energy of several kJ/m^2 could be obtained by incorporating pyridinedicarboxamid moieties in the backbone of a silicone elastomer using metal ions as crosslinking agents [129]. In this example, the modulus of the material (about 0.5 MPa) does not depend on the strain rate indicating a perfectly elastic behavior. In another recent example, authors combined covalent crosslinks with transient ones using the interaction between amide groups [130] and observed fracture energies up to 13.5 kJ/mol. Another promising class of materials for energy dissipation via dynamic bonds is vitrimers, a specific kind of materials where crosslinks are covalent, reversible, and most importantly based on exchange reactions [131,132]. The latter means that at any time the crosslinking density and network topology are identical, by opposition to reactions based on fragmentation-recombination reactions where the crosslinks are

broken at some point. This gives a much better creep resistance to these materials at ambient temperatures while maintaining their self-healing properties at higher temperatures. The fracture of this class of materials have not really been studied but is believed to give interesting properties [66].

Before moving to the next part, an additional mechanism may be stated although it only concerns some very specific materials. Strain-induced crystallization is a phenomenon that is observed in only a very limited set of elastomers, a famous example of which is natural rubber [133,134]. By comparing strain-crystallizable elastomers to non-crystallizable ones, Le Gac et al. showed that this phenomenon could be responsible for an increase of Γ by three orders of magnitude by itself [135].

Up to now, the strategies that have been covered to reinforce elastomers against fracture include viscoelasticity, use of fillers and incorporation of dissipation via physical bonds. In these three cases, the response of the material becomes widely strain-rate dependent and may impose some processing constraints to control the morphology of the material. This raises the question of the possibility of finding a dissipation mechanism that relies only on the architecture of the network, without involving any filler or increase in viscous dissipation. Such a strategy exists and has been adapted from the hydrogel literature a few years ago in our group.

4.The multiple network strategy: from the original concept to new properties

4.1. Double network hydrogels

4.1.1. A seminal paper and its first results

In 2003, Gong published a seminal paper reporting the synthesis of a new hydrogel exhibiting a high toughness [136]. In the original paper, a first polyelectrolyte network is synthesized in water by UV-initiated free-radical polymerization. The network is then immersed in a mix of monomer and water until osmotic equilibrium is reached, and the second network is subsequently synthesized (see Figure 18).

The resulting network exhibits a large increase in extensibility at break compared to individual single networks (see Figure 19). Gong et al. showed in the article that the first to second network crosslinking density ratio was an important parameter, and that this ratio should be kept high in order to reach significant mechanical reinforcement. This led them to hypothesize that the first network would dissipate energy and relax the local stress while the second network would avoid the crack from growing macroscopically.

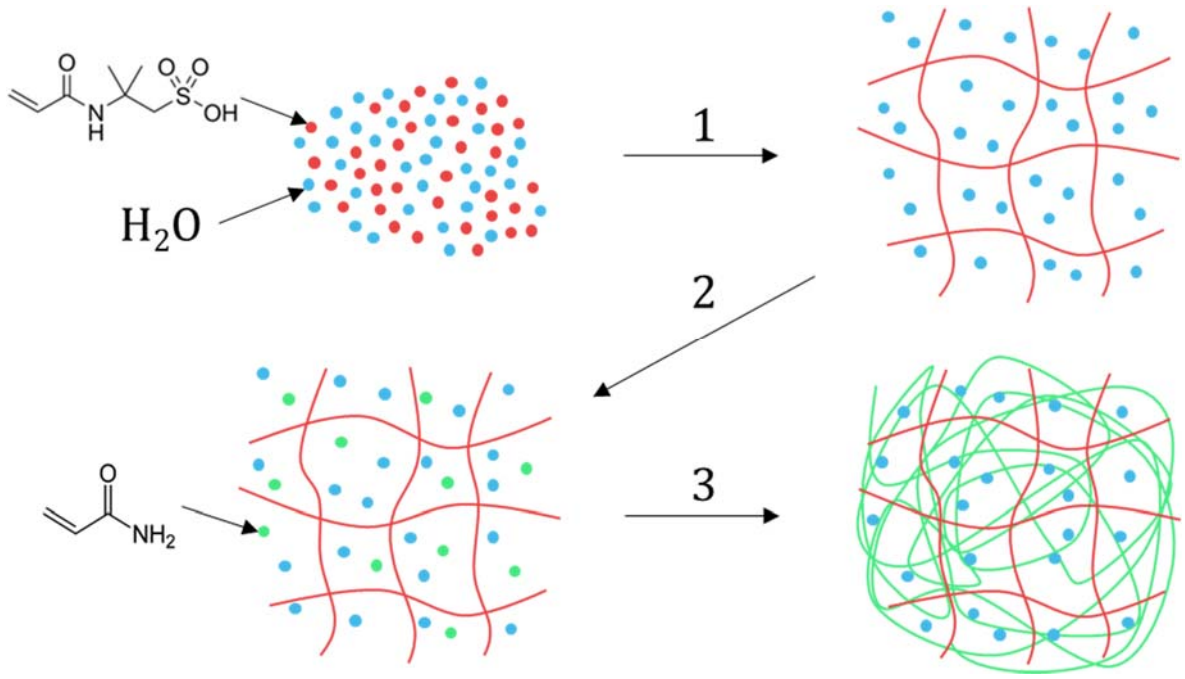

Figure 18: schematic representation of the experimental procedure used by Gong et al. in their original paper [136]. Numbers are the different steps of the process: 1) polymerization of the first network, 2) equilibrium in a bath containing the monomer of the second network, 3) polymerization of the second network.

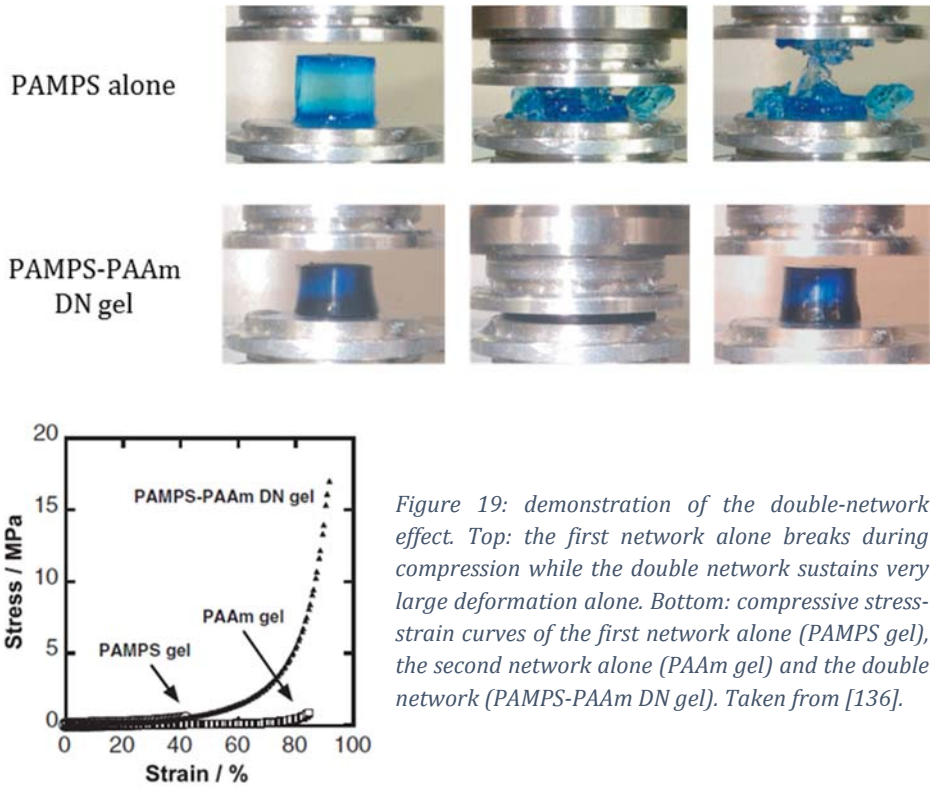

Figure 19: demonstration of the double-network effect. Top: the first network alone breaks during compression while the double network sustains very large deformation alone. Bottom: compressive stress-strain curves of the first network alone (PAMPS gel), the second network alone (PAAm gel) and the double network (PAMPS-PAAm DN gel). Taken from [136].

4.1.2. Toward the understanding of the toughening mechanism

From then, a series of papers mostly published by Gong's group attempted to understand, explain and model the mechanism responsible for the mechanical reinforcement. Using Dynamic Light Scattering, they studied relaxation in double networks and observed a slow relaxation mode above the gel point [137]. This indicated the presence the presence of clusters of second network in the deformed state which were suggested to act as "crack-stoppers".

One major step forward was made by Tanaka in 2005 who first applied the concept of tearing energy to double networks [138]. He obtained a much higher value for double network compared to single networks. Interestingly, Tanaka did two other important observations. First, fracture energy did not significantly change with strain rate, and second, the measured values of fracture energy could not be explained only by Lake and Thomas mechanism (i.e. fracture of chains solely in the crack plane). This suggested the existence of a dissipative mechanism other than viscoelasticity on a length scale larger than the close vicinity of the crack tip.

Two experimental articles then followed and gave additional information about the reinforcement mechanism of double networks. The first one reported the synthesis of tough double networks in which the second network is actually composed of linear uncrosslinked polymer chains that are long enough to entangle [139]. The second one reported the observation of necking in double network hydrogels where the first network concentration is very low with respect to the second one [140]. On the graph in Figure 20, one can clearly identify the existence of a level of stress above which the strain increases while the stress remains constant. Macroscopically, this corresponds to the appearance of a necked region (i.e. a zone with smaller width on the sample)

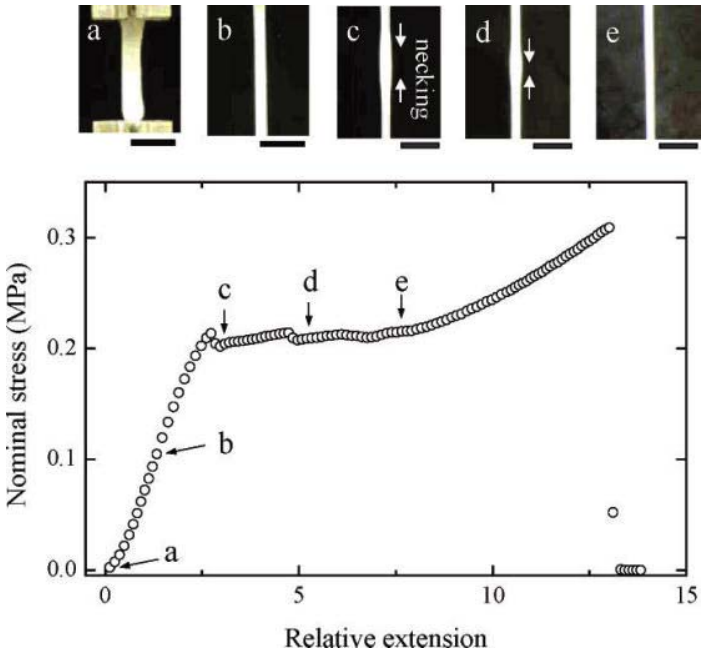

Figure 20: illustration of the necking phenomenon. Top: pictures of the sample at increasing levels of strain. Bottom: stress-strain curve exhibiting a yield stress of about 0.2MPa at which the stress saturates while the extension increases. Taken from [140].

that propagates along the tensile direction as the sample is further stretched. This phenomenon was presumably linked to the fragmentation of the first network.

An experimental evidence for this hypothetic internal fracture mechanism was finally brought by the work of Webber et al. in 2007 [141]. Using cyclic compression and tensile tests, they showed the existence of large hysteretic cycles that could not be recovered (see Figure 21). This clearly demonstrated the existence of permanent damage in the material. Additionally, almost all the energy was dissipated during the first cycles, meaning that the dissipation process occurs irreversibly at once. Finally, the elastic modulus dropped significantly after the first cycles whereas the amount of broken bonds (derived from the hysteresis area and Lake and Thomas theory) remained low (less than 1% of broken bonds). This is fully consistent with the hypothesis of breakage of the first network, since the latter is very stiff and highly diluted by the presence of second network. A large amount of broken bonds of first network thus represents only a small fraction at the scale of the entire material, but also a large drop in elastic modulus.

On the basis of these experimental observations, Tanaka [142] and Brown [143] simultaneously proposed a similar model for the double network hydrogels reinforcing mechanism. The propagation of a crack is described as a two-step process. First, the local high strain at the crack tip triggers the local failure of the first network. This generates a damage zone close to the crack

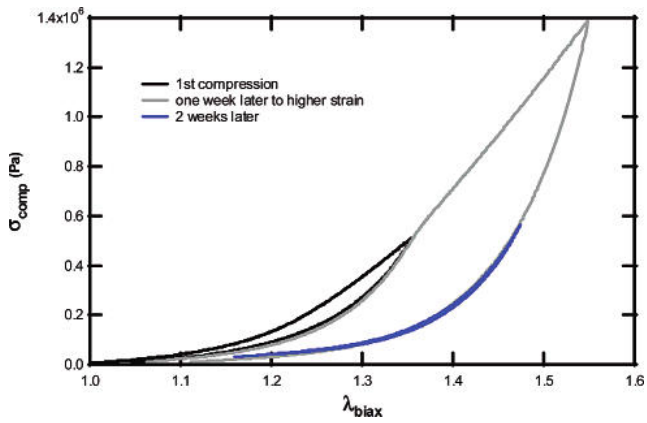

Figure 21: stress-strain curve of a double network loaded cyclically in compression three times within a week time interval. Black curve is the initial loading, grey curve is a second loading at a higher strain and blue curve is a third loading performed 2 weeks after. The sample showed large hysteresis no recovery after the first cycle. The loading curve the subsequent cycles matched the unloading curve of the previous cycle. Taken from [141].

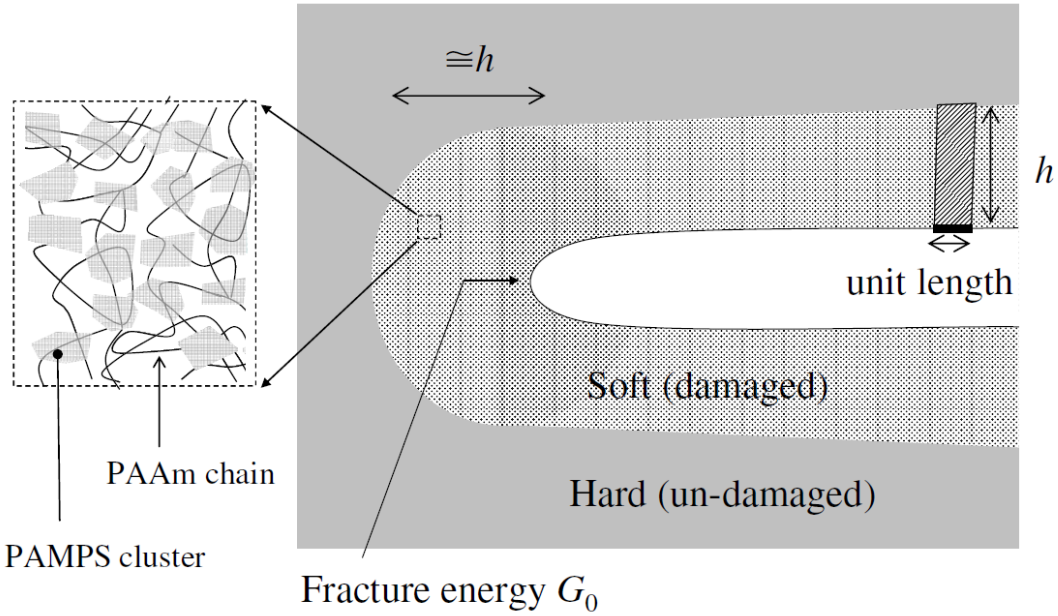

Figure 22: schematic representation of Tanaka's model. A damaged/yielded zone is formed in the area close to the crack. In order to propagate though the material, the crack must cross this damaged zone. The creation and the crossing of the damaged zone both consume energy, thus explaining the high level of fracture energy observed in double network hydrogels. Taken from [142].

tip that must be crossed during the second step, thus costing additional energy (see Figure 22). The experimental observations were satisfactory explained, although direct observation of damaged zone via Atomic Force Microscopy and laser scanning microscopy was only performed two years later [144,145]. However, none of the models accounted for the existence of double networks where the second network is only entangled but not crosslinked. Brown indeed assumed that crosslinks were generated in situ by recombination of radicals after breakage of first network chains.

In the following year, Gong's group published a communication [146] and an article [147] about a neutron scattering study on double network hydrogels. This study showed the existence of composition fluctuations along the traction direction with a characteristic length of 1.5 micron. These observations were accounted for in a model that described the stress transfer between the first and second network in a way similar to fiber-reinforced composites [148].

A new key for understanding the concept of double networks was brought by Nakajima seminal paper on the true chemical nature of double networks [149]. By suppressing all unreacted carbon-carbon double bonds prior to the polymerization of the second network, they prepared independent double networks, i.e. networks that are not chemically connected with each other. They showed that in the previous double networks with uncrosslinked second network, the stress transfer was actually due to unreacted double bonds that linked covalently the two networks. This paper thus validated Brown and Tanaka's approaches to explain the double network effect. In light of all these experimental and theoretical studies, Gong published a review paper in 2010 that summarized the key points explaining the toughness of double network hydrogels [150]. Interestingly, Gong stated in this review that double network hydrogels exhibited very low fatigue resistance, though no experimental evidence had ever been published on this topic.

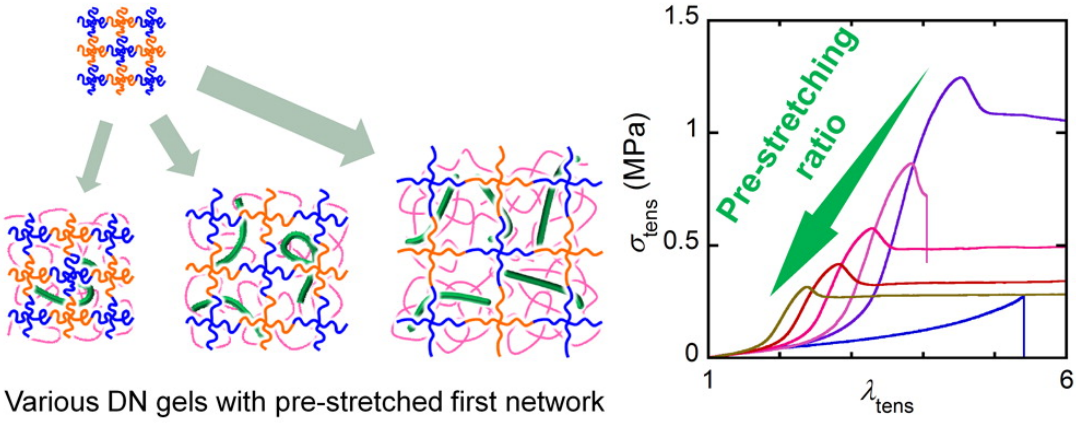

Figure 23: use of molecular stents to control the level of prestretching in double network hydrogels. Left: illustrtation of the concept of molecular stent. An initial tetra-PEG network is prepared. Polyelectrolyte chains are then diffused in the network to increase the swelling ability of the network and tune the prestretching of the chains. Right: the shape of the stress-strain curve is shown to depend on the prestretching ratio. More specifically, the onset of necking is primarly dictated by the level of prestretching of the chains. Taken from [152].

At this stage, two main questions remained regarding the toughening mechanism in double network hydrogels. The first one dealt with the precise chronology of events, i.e. when bonds break exactly. In order to answer this question, Nakajima et al. performed cyclic tests and reswelling experiments on double network showing necking to measure the amount of damage in the first network [151]. Using a method similar to Webber et al., they first showed that bonds started to break well before yielding, and that bonds kept breaking until the macroscopic failure of the sample. The first bonds breaking being elastically active, the onset of necking was associated to a drop in modulus. The rest of the necking process was associated to a lot of damage in the first network, and the softening stopped at the end of the plateau. This led the authors to hypothesize that necking was associated to the clusterization of the first network, and that by the end of the necking the PAMPS fragments were completely discontinuous. Finally, they showed that bond breakage was an anisotropic phenomenon, and that bonds oriented parallel to the stretching directions were more likely to break. These experimental observations enabled the authors to describe a refined version of Brown and Tanaka's models where this two-step process is taken into account.

The other main grey area was the precise criterion for yielding, i.e. how to discriminate networks that exhibit yielding from the ones that do not. The key to this problem came from previously exposed tetra-PEG homogeneous networks (see 3.2.2). Using these materials as first networks, Matsuda et al. synthetized double networks with a well-controlled structure [152] (see Figure 23). The swelling of the first network was made possible by so-called molecular stents which are polyelectrolyte chains that were incorporated in the network structure to artificially increase osmotic pressure. They observed a significant and continuous decrease of the yield stress with increasing prestretching and explained it using simple geometrical arguments, showing that the finite extensibility of the chains was the driver for the onset of yielding. They eventually obtained a master curve for stress and strain by taking into account the dilution of elastic chains due to prestretching in the plane perpendicular to traction, thus validating their theory.

4.1.3. Use of new characterization techniques

Now that the mechanism is fairly well understood, more recent articles focus on the study of double networks in the light of new characterization techniques. In 2018, Gong published an article in collaboration with Urayama in which double networks are subjected to cyclic tests in various loading geometries including biaxial extensions [153]. In this article, the authors show that the reduction in initial modulus and dissipated mechanical energy depend on the loading geometry. Using a combination of first and second invariants of deformations, they rescale these quantities and obtain a universal relationship. They draw two important conclusions from this. First, they claim that this proves the existence of cross-directional effects, i.e. that stretching in the x-direction has an effect on the stress in the y-direction that is not only due to Poisson's ratio. Second, by comparing double networks to a classically silica-filled silicone rubber, they state that the origin of reinforcement is intrinsically different. This paper has been recently followed by another one [154] studying more specifically the cross-directional effect and the anisotropy that results from the breakage of the first network. The authors propose an explication for this directional coupling based on the existence of chains that are not aligned with the principle directions of the sample. In filled rubbers, the softening is multi-factorial which makes the issue of alignment less predominant.

Last but not least, cyclic fatigue properties of hydrogels have recently been studied by Suo's group [155]. They show that the fatigue threshold of double network hydrogels is almost insensitive to the concentration of second network (see Figure 24), with a measured threshold value close to 400 J/m^2 for all samples tested after 50k cycles. This value scales well with predictions based on Lake and Thomas model and is much lower than the fracture energy in monotonic traction (3.1 to 3.8 kJ/m^2). It is however much higher than the fatigue threshold of simple polyacrylamide gels (below 10 J/m^2 for water contents above 90% [156]), and the slope of the crack speed versus strain energy release rate is also much lower for DN hydrogels. This means that fatigue crack propagation rate is much less sensitive to the strain energy release rate for double networks. One can therefore conclude that contrary to what has often been said in the literature, double network hydrogels show relatively good fatigue properties. Interestingly, Suo's hydrogels containing polyacrylamide and alginate have a fatigue threshold of about 50 J/m^2 [157] which is much lower than DN hydrogels, despite the fact that fracture energy is much higher in acrylamide/alginate gels (about 10kJ/m^2). The presence of reversible bonds that are able to reform thus does not correlate with good resistance to cyclic fatigue.

All in all, the development of double network hydrogels in 2003 introduced a new kind of materials that are both tough and stiff. Their original toughening mechanism relies on the macroarchitecture of the network and not on viscous dissipation phenomena like many other tough hydrogels. The understanding of their properties took a few decades and results nowadays in more application-oriented research [158] and extensions of the initial concept using for instance mechanochemistry [159] or particles in lieu of the first network [160]. An example of such an extension is double network elastomers, a class of materials developed in our group and directly inspired from Gong's research.

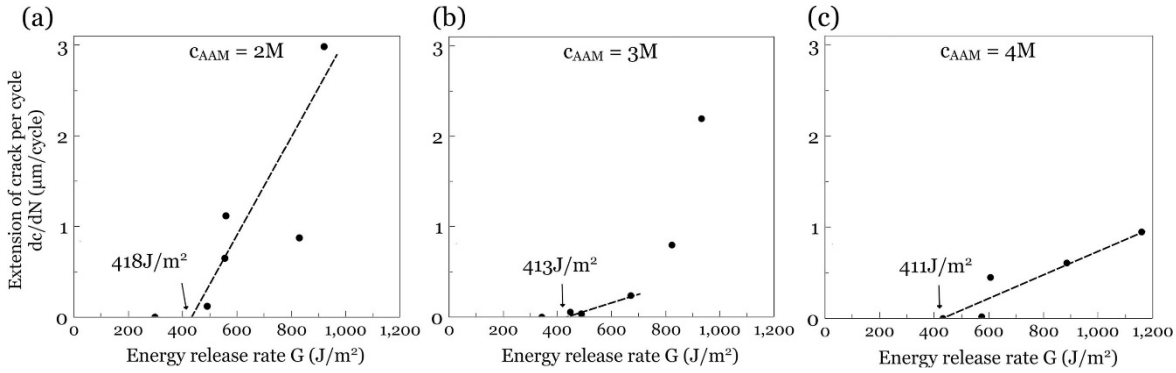

Figure 24: study of fatigue properties of double network hydrogels with 3 different concentrations of second network. The graphs show the crack growth rate versus the strain energy release rate. Taken from [155].

4.2. From hydrogels to elastomers

4.2.1. Translation of Gong's concept by Ducrot

Using a synthetic method inspired from Gong's work, Ducrot prepared multiple network elastomers based on ethyl acrylate (EA) and methyl acrylate (MA) [161]. Contrary to Gong's synthesis however, the swelling/prestretching step was performed multiple times thus giving double/triple/quadruple networks. A mechanical reinforcement very close to what is observed on double network hydrogels was obtained (see Figure 25). Fracture experiments gave energy values as high as several kJ/m² which is comparable to that of some filled elastomers. Chain pre-stretching was also shown experimentally by Small Angle Neutron Scattering [162].

Ducrot et al. initially hypothesized a reinforcing mechanism similar to what Gong described, namely that first network chains were breaking while second network chains were preventing the crack from macroscopically propagating. Using mechanoluminescence, they proved unambiguously this model and mapped the intensity of the bond scission in what can be called a damage zone (see Figure 26) [163]. Despite some differences with hydrogels (as for instance the change in modulus with network multiplicity), multiple network elastomers are conceptually similar to double network hydrogels. The subsequent research on these materials focused on a more thorough investigation of their properties.

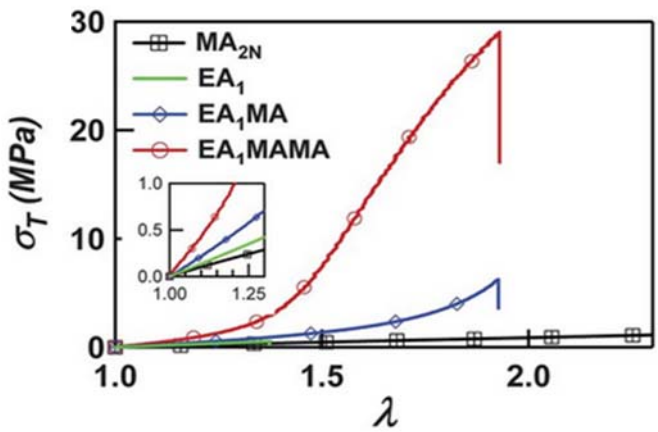

Figure 25: mechanical characterization of multiple network elastomers.MA2N is a network with same composition as the second network used in the multiple network structures (0.01 mol% crosslinker and 0.01 mol% initiator). EA1 is a first network prepared with 1.45 mol% crosslinker and 1.16 mol% initiator. Taken from [163].

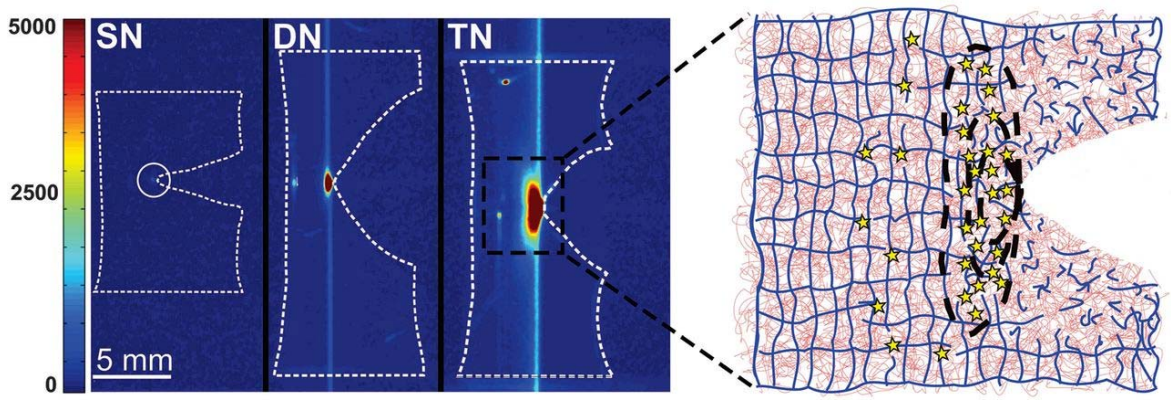

Figure 26: colorized images of mechanoluminescent notched samples during crack propagation. The color bar corresponds to the number of emitted photons and the edges of the samples are showed by white dashed lines. Taken from [163].

4.2.2. Finer understanding by Millereau and Chen

A few years later, Millereau pursued these efforts and carried out a systematic study of the system [164]. Instead of using a swelling bath with only monomer, he used solvent to better control the monomer concentration and the level of pre-stretching of the chains of the first network. Starting from the same piece of first network, he performed some uniaxial tensile tests, obtained a set of stress-strain curves (see Figure 27-left) and identified 4 different types of mechanical behavior depending on the level of pre-stretching:

- Type 1: for low levels of pre-stretching, no significant reinforcement is observed. This is actually the range of relative concentrations that corresponds to conventional IPN.
- Type 2: for prestretching levels between 1.5 and 2, the samples show strain-hardening but no damage is observed in the bulk before macroscopic failure. Chains from first network reach their maximum extensibility.

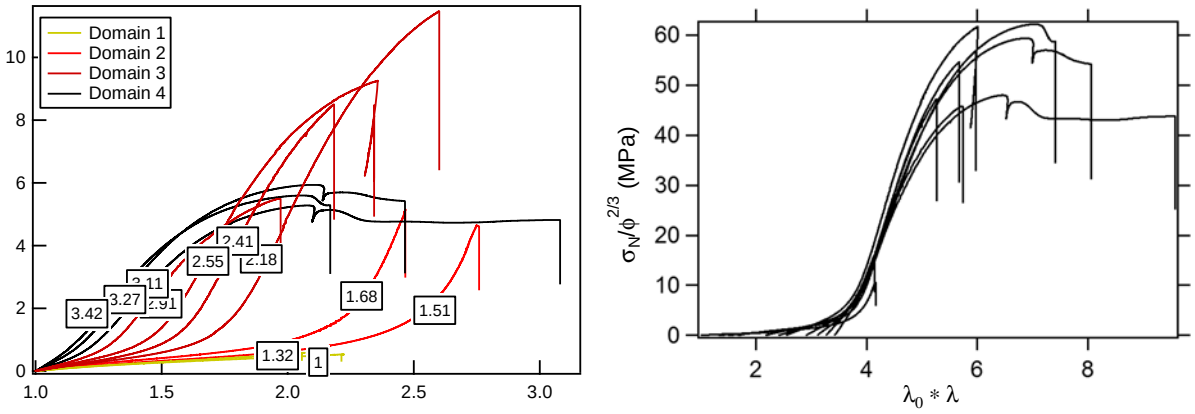

Figure 27: Millereau's systematic study of multiple network elastomers. Left: stress-strain curves of samples prepared from the same first network (1.45 mol% crosslinker) and pre-stretched up to different levels (the squared numbers on the curves). The same strain rate of 2.1% s^{-1} is used for all curves. Right: master curve showing the corrected nominal stress versus the total deformation of the first network. λ_0 is the prestretching level and ϕ is the mass fraction of first network. Taken from [164].

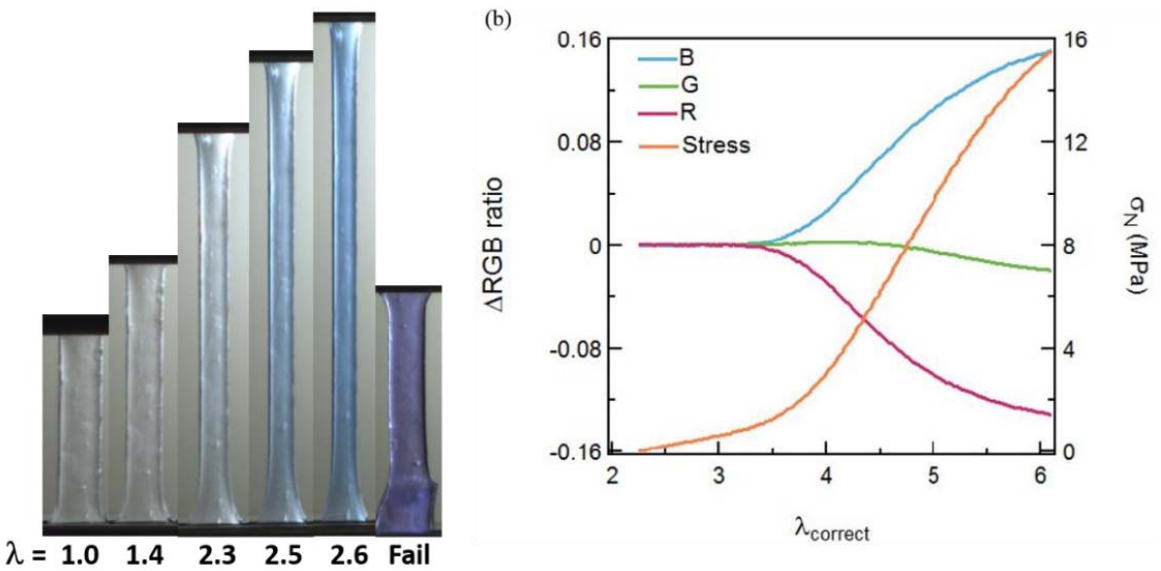

Figure 28: basic tensile experiment on a double network elastomer containing spyropyran crosslinker in the first network. A) Pictures of the sample during the test. When activated, spyropyran becomes blue. When unloaded, it becomes purple. B) Superposition of stress-strain curve (orange) with variation of red, blue and green ratios measured using an image analysis software from a film taken during the test. The visual change in color on the left translates to quantitative change in RGB ratios.

- Type 3: for pre-stretching levels between 2 and 3, there is both a strain-hardening and then a strain-softening. The latter is the consequence of the progressive rupture of the first network, and during cyclic loadings a large hysteresis is incidentally observed after the inflection point.
- Type 4: for large prestretching (above 3), necking is observed.

In a way very similar to Matsuda et al., he subsequently plotted the normalized stress versus the elongation of the first network, taking into account the prestretching of the chains and the dilution of elastically active chains. This resulted in a master curve (see Figure 27-right) demonstrating that the level of prestretching in the first network is the key ingredient to tune the mechanical response of the system.

The damage process in multiple network elastomers was also studied by Yinjun Chen in his PhD work [165]. He used spyropyran as force sensing molecules in order to study the mechanical behavior of double network elastomers. Spyropyran is a chemical function that changes light absorption when subjected to force [166] and as a result changes color. It can be chemically modified in order to bear acrylate functions, and then polymerized in a rubber network acting as a crosslinker. In the end, a tagged material is obtained, which changes color when deformed (see Figure 28). Spyropyran may be incorporated in any of the networks of the multiple network structure, which makes it a unique tool to follow the distribution of stress throughout the deformation process.

Using this system, Chen studied the behavior in traction of multiple network elastomers. He proved that in type 4 multiple elastomers, the breakage of the first network at the yield point is accompanied by a stress transfer from the first to the second network. More importantly, he showed that in the necked region, this transfer is not complete: the first network releases a part

of its mechanical load, but it is not completely unloaded at the end of the yielding zone. This implies that the filler network is still percolating in the yielded structure although it is highly damaged. This is contrary to what is commonly found in the literature, and proves wrong Gong's original hypothesis that the first network breaks into pieces ("clusters").

To conclude, recent studies from our group in the field of multiple network elastomers showed that they behave very much like molecular nanocomposites [167]. The first sacrificial network plays the role of the filler, bringing stiffness as well as possible energy dissipation to the system. Chains from the filler network are brought close to their maximum extensibility via swelling, which brings stiffness to the system (filler effect) and makes them ready to break in order to dissipate energy (sacrificial role). Subsequent networks in vast majority play the role of the soft, extensible matrix. Its main role is to sustain the stress carried by the filler network once it is extensively damaged. Like in nanocomposites, the filler network drives the mechanical properties of the system.

4.2.3. A not-so-new concept

Before moving to the next part, it is important to open a parenthesis to present concepts and materials from the literature that are somehow connected to multiple network elastomers.

Interpenetrated networks (IPN)

In spite of the relative recentness of double networks, the concept of interpenetrating two polymeric networks was covered many years ago as an alternative to conventional polymer blends. Aylsworth invented this type of materials in 1914 [168] and since then many papers and books were published on the topic of interpenetrated networks (IPN). IPN can typically be synthetized in two ways: either networks are polymerized sequentially, in a way very similar to double network hydrogels, or they can be polymerized at the same time with orthogonal chemistries [169]. There are however two major differences between IPN and double networks:

- Both networks are in relatively similar proportions in IPNs, whereas in Gong's hydrogels the relative concentration of first network is very low.
- In most IPN, there is no difference in crosslinking density, with the notable exception of so-called semi-IPN where the second network is completely uncrosslinked.

As a result, previously developed IPN do not show the large increase of toughness that is observed for double network hydrogels. IPN are actually used to mix polymers with very different glass transition temperatures (a rubber and a glass typically). The resulting glass transition may be tuned this way and as a result IPN are used in applications like vibration damping [170].

Multiple network elastomers are therefore IPNs, but of a very specific kind which confers them additional properties that differentiates them from the rest of the IPN literature.

Historical "Double network elastomers" and prestressed thermosets

Although Gong et al. published their seminal paper in 2003, the term "double network" was actually already used in the literature. In the middle of the twentieth century, double networks

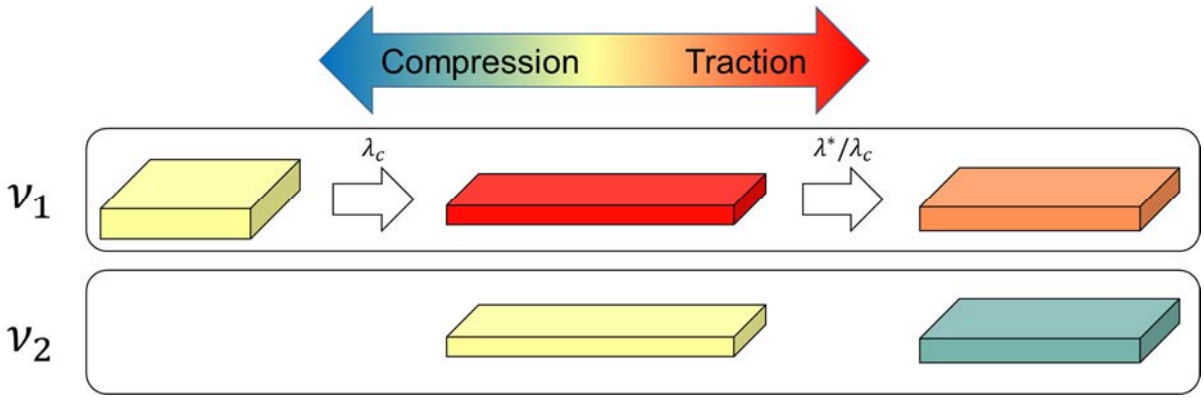

Figure 29: schematic representation of the "independent network hypothesis". Top line represent the stress state seen by the first/initial population of crosslinks. Bottom line represents the stress state of the second population. A color code indicated by the top arrow is used for compression/traction.

were rubbers that were cured twice. In the original sense, "double network elastomers" are therefore rubbery materials with two different populations of chain lengths.

The original description of this concept may be attributed to Andrews, Tobolsky and Hanson who studied the permanent set of stretched elastomers subjected to high temperatures for extended periods of time [171]. Andrews et al. attributed this change in length to chemical modifications of the rubber material and developed a model to explain and predict it. The model was later refined and confronted to experiments by other scientists including Flory [172–174]. The model is sometimes referred to as "Flory's model" although Flory merely provided a rigorous analytical framework.

The main conceptual framework that is used to model networks that have two different populations of crosslinks uses an "independent network hypothesis". Each population of crosslinks is considered to contribute to the free energy of the network, and these contributions are calculated separately and linearly superimposed. The final state is reached when the contribution of the first population of crosslinks (or "initial network") balances the contribution of the second population ("second network"). It has to be emphasized that this "network superposition" framework is entirely different from that of interpenetrated double networks. In the present case, the denomination of "initial" and "second" network is purely conceptual. There is only one polymeric network although there are two different populations of chain lengths.

Let us consider that there are ν_1 crosslinks per unit volume in the initial state. ν_2 crosslinks are added during second curing in the stretched state. A key point is that crosslinks that are added in the second step are at rest when the overall network is stretched by λ_c. When the material is unclamped, the first crosslinks thus relax while second crosslinks enter compression (see Figure 29). By equilibrating forces, one can derive a relationship between λ_c and λ^*:

$$\lambda^* = \lambda_c \left(\frac{\nu_2/\nu_1 + 1/\lambda_c}{\nu_2/\nu_1 + \lambda_c^2} \right)^{1/3} \qquad \text{Eq. 17}$$

The final stretch ratio mainly depends on the ratio of crosslink densities. If there is a very strong asymmetry in crosslinking (i.e. $\nu_2/\nu_1 \to \infty$), then the material does not relax and keeps the

clamped stretch ratio entirely ($\lambda^* \rightarrow \lambda_c$). If on the contrary almost no crosslinks are added in the second stage (i.e. $\nu_2/\nu_1 \rightarrow 0$), then the material relaxes back to its original shape ($\lambda^* \rightarrow 1$).

Many refinements and generalizations [175] of this model have been proposed, for example including the non-Gaussian behavior of chains [176–178] or their finite extensibility [179]. The comparison of theoretical models with experimental data have also been the focus of many research articles. Most of them are based on natural rubber, with crosslinking achieved either by heating and use of a peroxide [180–182] or using high energy radiation [183–185]. An overall good agreement with the two-network framework is found, although some discrepancy appears when networks with different entanglement structures are compared. Most of the studies focus on standard tensile tests and compare the stiffness of the materials with models, but some authors have also studied the ultimate properties and find an improvement in the resistance to cyclic fatigue crack propagation in the transverse direction specifically [186,187]. Among the other experiments used to characterize these materials, birefringence has been used by Roland et al. to investigate the molecular orientation in the elastomer structure [188,189]. More recently, theoretical models have been confronted to molecular dynamics simulations by Rottach et al. [190,191].

The concept of "double network elastomers" has also been adapted to systems where chemical crosslinks are introduced in the second step only. Specifically, a polymer melt close to its glass transition is used so that the elasticity of the initial network is only due to the presence of entanglements [192–194]. In the same vein, thermoset elastomers may be used and crosslinked in the stretched state taking advantage of the remaining insaturations of the polymer backbone [195,196].

Incidentally, the theoretical framework of "double network elastomers" has recently resurfaced in a recent article from Katashima et al. [197]. In the paper the authors report the preparation and study of mechanical properties of hydrogels based on 4-arm PEG chains that are crosslinked twice by playing on the extent of the gelation reaction. They globally find a good agreement with Flory's model regarding the residual strain and change in modulus with prestretching and crosslinking asymmetry.

Despite its anteriority, the term "double network" in the sense of a "network with two different populations of network strands" is arguably misleading. Although the theoretical description of these materials involves two networks, the material is actually made of only one polymeric network. For this reason, in the rest of the manuscript, the term "double network" is used to refer to materials with two distinct interpenetrated networks. In the other case, the term "dual-cured network" is used.

4.3. The challenge of describing the reinforcing mechanism theoretically

In addition to experimental work, a lot of efforts has been devoted to the mathematical representation of double network system. This raises interesting conceptual questions such as modelling polymeric networks close to their maximum extensibility and modeling the damage of

a network. Note that models only attempting to provide constitutive laws [198,199] are not reviewed in details here. Although they provide interesting results and may be implemented in a Finite Element Analysis, they do not give any insight on the underlying physics and deformation/reinforcement mechanisms.

There are to the best of our knowledge four main strategies that have been explored to model the behavior of double networks. Wang and Hong choose to base their approach on Gent's phenomenological model of strain hardening [200]. Instead of using fixed parameters like in Eq. 12, they consider that the modulus and maximum extensibility are functions of the maximum elongation experienced by the material $\lambda_{\text{max applied}}$:

$$\sigma_{\text{nominal}} = G\left(\lambda_{\text{max applied}}\right)\frac{\lambda - 1/\lambda^2}{1 - J_1/J_m\left(\lambda_{\text{max applied}}\right)} \qquad \text{Eq. 18}$$

Damage is then modelled as a random process with a probability that depends on the elongation. The authors derive a "damage function", $\eta\left(\lambda_{\text{max applied}}\right)$, ranging from 0 to 1 and scaling like an error function. They use this function to compute the modulus as a function of $\lambda_{\text{max applied}}$. Using a phenomenological analytical form for $J_m\left(\lambda_{\text{max applied}}\right)$, they eventually derive an expression for the stress and compare it to experiments. They get good agreement with experimental data from Webber's experimental work and even predict necking. Wang and Hong's model is therefore mainly phenomenological but yields parameters with physical meaning. On the other hand, Zhao's model relies on Langevin's statistics [201]. It assumes that the free energy of double networks is a linear superposition of the free energy of both sub-networks. Each free energy is derived by considering the free energy of a single chain (captured by Langevin's statistics, see 2.2.2) and made into a network via a model similar to the affine model. The damage of the first network is modelled with two possible mechanisms, each associated to an arbitrary probability of occurrence modelled as an exponential function of the maximum deformation experienced by the network:

- If an elastic chain of the network is broken, then the chain density decreases.
- If the fracture occurs on a crosslink, the size of the elastic chains as well as the maximum chain size used in Langevin's statistic increases.

Eventually, the model qualitatively predicts the hysteretic cycle and loss of modulus in cyclic tests. Also, necking can be modelled by a specific choice of parameters. Although Zhao's model relies on a molecular description of the toughening mechanism, its heavy mathematical formulation makes the physical interpretation of the parameters difficult.

More recently, Vernerey developed a statistical model for transient networks [202,203] and adapted it to multiple network elastomers [204]. The specificity of this approach is that it follows the distribution of chain lengths of all networks throughout the deformation process and applies a molecular-based damage mechanism to it. Chains are considered to have an increasing probability to break while they approach their contour length, and the shape of the end-to-end vector probability distribution thus evolves from a Gaussian distribution to a truncated distribution when the network is deformed. Vernerey uses this distribution to calculate the stress applied to the material using Langevin's distribution to link the chain size distribution to the

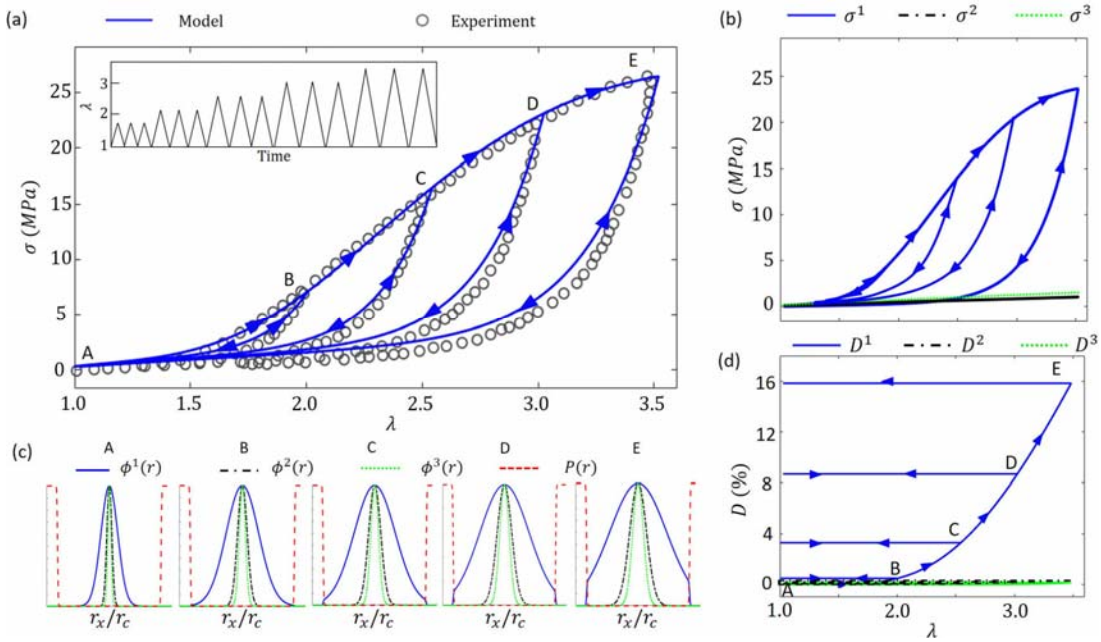

Figure 30: Example of comparison of Vernerey's model with experimental data of a triple network elastomer. The top left graph shows the comparison of stress strain curves. The bottom left graphs are computation of the distribution of chain lengths in each network. The top right graph is a superposition of the computed stress bore by each network of the triple network structure. The bottom right graph is the damage function. Taken from [204].

elastic energy stored in the material. Eventually, the Cauchy stress is derived and the entire stress-strain curve is modelled and compared to experimental data.

Beyond fitting stress-strain data (see Figure 30), Vernerey's model brings new conceptual tools for the theoretical study of multiple network systems. Mainly, the damage function is an experimentally-accessible parameter (via mechanochemistry for example) and provides an additional tool to check the consistency of the model. For instance, Vernerey's model accurately predicts that:

- Less than 1% of the filler network break in weakly prestretched double networks, although a significant mechanical reinforcement is observed
- In all cases, matrix networks are almost intact throughout the process, with less than 0.5% of broken bonds

However, some quantitative information of the failure process is not caught by the model. For instance, in largely prestretched multiple networks, Vernerey's model predicts that approximatively 4 to 5% of the bonds are broken at the onset of yielding, and that this amount raises to 35% at the end of yielding. Instead, Millereau's mechanochemistry data show that most of the bonds are broken before the onset of the yielding [167]. Besides, a rough estimate of the fraction of broken bonds in the filler network based on the hysteresis in cyclic mechanical tests give fractions close to a few percent [164] which is much lower than Vernerey's estimation.

It is useful to keep in mind that this approach is necessarily limited. Important aspects, such as chain polydispersity, damage localization (Vernerey's model is a mean-field approach), chain connectivity and non-affine motions are not included. These factors are all important to describe

crack propagation. The ability of the model to fit experimental data should therefore not be taken as a confirmation of its physical soundness, especially since Vernerey's approach has not been reproduced yet.

Last but not least, two recent models have been proposed using a slightly different approach [199,205]. In these models, contrary to the previous cases, the behavior of the multiple network is not fitted but predicted. By fitting the mechanical responses of the filler and matrix networks, the authors extract parameters that represent the architecture of the two types of networks. These parameters are then used to predict the behavior of the multiple network, which gives stress-strain curves that are very close to reality. These models confirm that the filler network is the one that controls the properties of the multiple network assembly, and that the physics of the filler network chains explains well the different observed phenomena (strain-hardening, hysteresis, etc.)

To sum up, modelling of multiple network systems is a topical research area that aims to develop tools to help studying the actual materials. The development of damage-based mechanisms seems to confirm the experimentally-based mechanisms that have been proposed first.

4.4. Toward new properties for multiple network elastomers

Multiple network elastomers are interesting model materials in the sense that their toughness originates from the architecture of the network. The way the material is prepared triggers the possibility to break bonds and dissipate energy independently from the polymer chemical nature. Of course, one way to push this concept further is to add new sources of energy dissipation. The first one that comes in mind is viscoelasticity, and incidentally the study of its relation to molecular damage in double networks is one of the aspects of a recent PhD project from our group [206].

In the present project, we aim to use the previously mentioned knowledge of the physics of multiple network elastomers in order to give them new mechanical properties. In particular, the mechanical response of multiple network elastomers is primarily dictated by the level of prestretching of the filler network chains [167]. This prestretching is achieved by swelling to equilibrium, taking advantage of osmotic pressure. The prestretching is thus isotropic. There are several reasons that makes it interesting to study the behavior of multiple networks elastomers in which the filler network have been prestretched unidirectionally in addition to osmotic pressure:

- There is a practical aspect in adding an additional prestretching. Up to now, large prestretching requires several synthesis steps which is time-consuming and costly. If the prestretching may be applied manually (by simply stretching the filler network) instead of chemically (by using osmotic pressure), then any mechanical behavior could be obtained in only one step in principle.
- One can also imagine that prestretching the filler network in only one direction could result in a prestretching state that changes with the orientation. One could therefore

expect to get anisotropic double network elastomers, which can be interesting for some applications like dielectric elastomers.

- In real manufacturing processes of rubbers, a unidirectional prestretching may be incurred instead of desired. For example, elastomer sheets are often produced by calendering, making the polymer chains more extended in the stretched direction at the end of the process [172,207]. If the multiple network strategy is to be used in an industrial context, it is therefore necessary to validate the fact that the reinforcing mechanism is still active when an additional unidirectional prestretching is applied.

The next section therefore focuses more specifically on the idea of making anisotropic elastomers using the multiple network strategy.

5.Bringing anisotropy to double network elastomers

5.1. Example of anisotropic polymeric systems

Anisotropy is a generic term that refers to material properties that are not the same in all directions. It is very generic and can apply to virtually all physical phenomena. In mechanics, anisotropy usually means a different modulus depending on the strain direction. This is actually a very frequent phenomenon both in natural or synthetic polymers. For example, wood has a modulus approximatively 20 times higher in the longitudinal direction than in the tangential direction, and 10 times higher than in the radial direction (see Figure 31) [208]. Same goes for strength which is much higher in the longitudinal direction. This is obviously due to the fibrous structure of the material: wood is actually a nanocomposite made from a basic reinforcing fiber: cellulose [209]. This complex architecture gives to the wood its very high stiffness and resistance.

5.1.1. In composite materials

Actually, using a composite structure often gives anisotropic properties. In a polymer-matrix composite, the filler phase may bring anisotropy to the entire system if it is oriented. This is the case for example of fiber-reinforced polymers in which properties are much better in the direction of the fibers compared to the transverse direction [210]. More subtly, nanocomposites may also be anisotropic due to the alignment of filler particles [211]. Particles may be aligned during the processing of the material, for example when calendering or molding is used [172,212,213]. Mullins effect may also be a source of anisotropy in filled rubbers which become softer in the loaded direction [116,214]. The underlying mechanism could be that first stretching changes the local topology of the polymer chains close to the particles, which causes softening in a preferential direction [215].

5.1.2. In polymer glasses and hydrogels

Purely polymeric systems have also been reported to exhibit anisotropic mechanical properties when subjected to pre-strain. Examples in the field of glassy polymer includes PMMA and

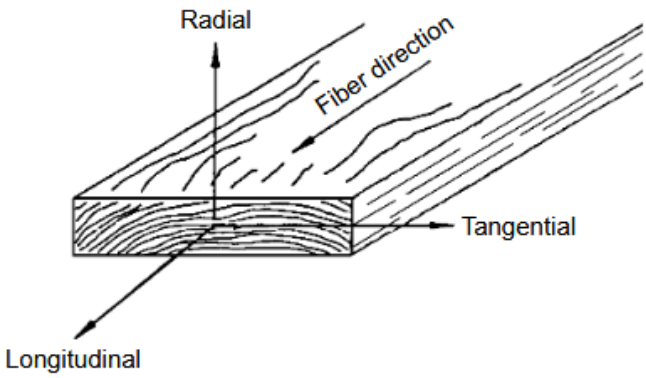

Figure 31: definition of the principle direction of wood. Modulus in the longitudinal direction is the largest by far. Taken from [208].

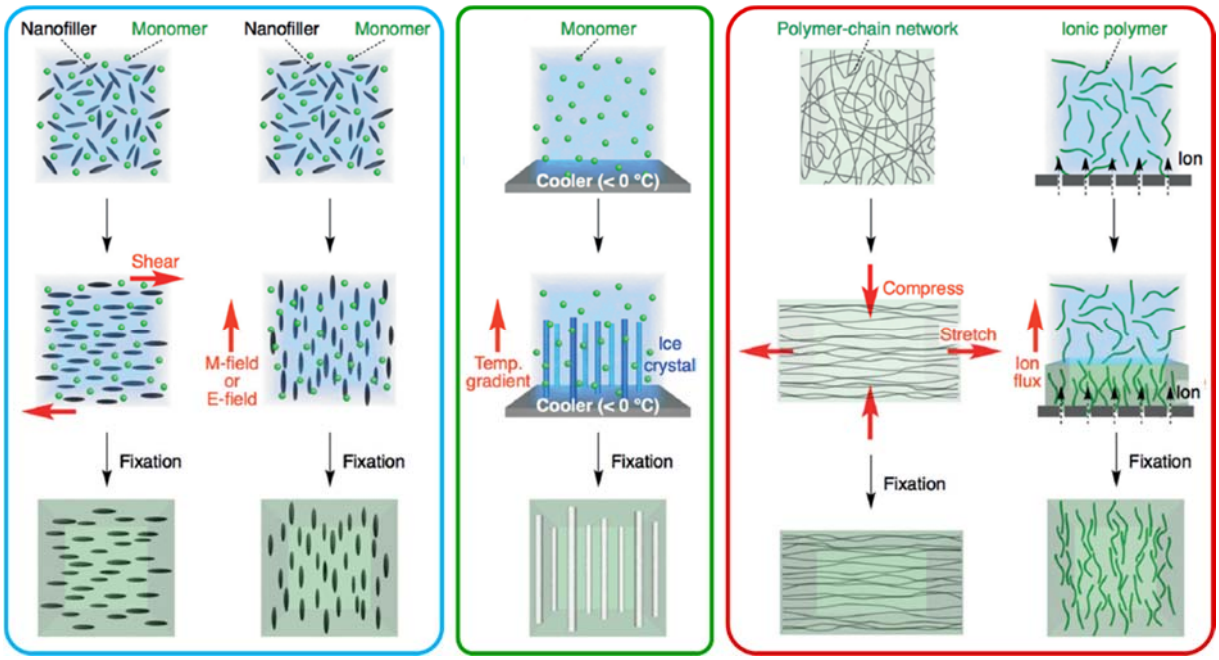

Figure 32: schematic illustration of various techniques used in order to prepare anisotropic hydrogels. Left/blue frame: nanofillers may be incorporated in the network structure and oriented either using shear flow or electromagnetic field. Center/green frame: aligned nanopores may be generated in situ by ice-templating. Right/red frame: chains may be stretched in one direction and fixed using supramolecular structures or by crosslinking the material using ion diffusion. Images taken from [219].

polycarbonate [216,217]. The field of anisotropic hydrogels is also particularly well-documented in the literature because of the possible bio-applications. One major difference between hydrogels and natural biomaterials like muscles, tendons or cartilage is that the latter are mechanically anisotropic thanks to a fibrous structure [218]. There is therefore an interest in preparing and studying hydrogels with anisotropic mechanical properties. In their recent review article [219], Sano et al. have summarized the recent research outputs from the field (see Figure 32). They distinguish three main routes to produce anisotropic hydrogels:

- Use of an oriented filler, using for instance a flow [220], an electric [221] or a magnetic field [222].
- Use of parallel nanovoids generated in the network structure by "ice-templating". This method consists in growing ice crystals in a preferential direction using a temperature gradient. Ice is then sublimated yielding a porous structure with oriented voids. This method gives easily tunable properties and may be used with a variety of different polymers [223–225].
- Stretching, alignment and freezing of the polymer chains in the stretched state using a second crosslinking step. Both alignment and fixture may be performed in one step using semirigid polymers and ions to complex the chains. In this case, chains orient themselves as the ions diffuses in the structure [226]. Stretching and crosslinking may also be performed in two successive steps using for example the complexation of alginate chains by barium cations [227] or physical crosslinking of acrylic acid groups by Fe^{3+} ions [228].

The latter strategy of stretching and fixing the orientation of polymer chains has been recently exploited by Gong's group [229]. In their article, they report the preparation of anisotropic

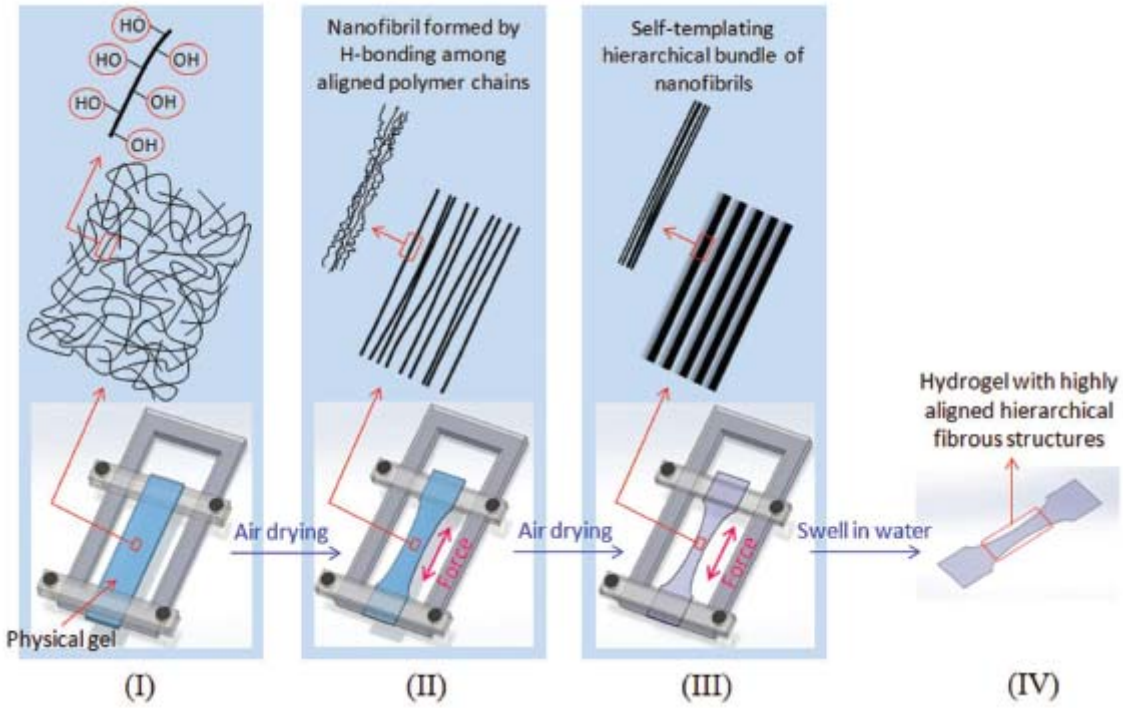

Figure 33: schematic illustration of the method used by Gong et al. to prepare highly anisotropic hydrogels with fibrous structures. I: initial situation, the gel is swollen by water and clamped on a fixed frame. II: drying begins, chains are brought close together and start forming fibrils thanks to attractive H-bonding interactions. III: as drying continues, fibrils aggregate in a hierarchical structure. IV: eventually, the dry fibrous network may be reswollen in water yielding an insoluble anisotropic hydrogel. Taken from [229].

hydrogels via a very simple method of drying under strain (see Figure 33). The principle is to clamp a swollen hydrogel on a rigid frame and to leave it dry and self-assemble. Eventually, a network is obtained with a well-aligned fibrous structure. When immersed in water, the material swells but does not dissolve, yielding an elastic hydrogel with anisotropic mechanical properties. Although this method is very simple and straightforward, it does not work for any polymer and any drying conditions. Gong specifies that the method requires the initial polymer to be diluted and loosely crosslinked with transient bonds. This gives enough mobility to the chains to aggregate and form the fibrous structure. Also, the polymer chains need to be semi-flexible and should contain lots of functional groups that promote H-bonding in order to form hierarchical structures. Finally, stretching is limited to 50% deformation, otherwise the material breaks during the drying phase. The strategy is thus “facile” but also not easily adaptable to other types of networks.

Several design strategies therefore exist in the field of hydrogels to get anisotropic and soft materials. Most of them rely on the coexistence of different phases: anisotropy may for instance come from the alignment of filler particles or nanovoids, or through a hierarchical supramolecular structure. One common feature and key step to obtain anisotropy is the alignment of these features and subsequent fixture using a chemical reaction of physical interactions.

5.1.3. In dual-cured elastomers

The question of anisotropy in rubber that are crosslinked in two steps has been raised by several authors, both experimentally and theoretically. Most of the authors who studied anisotropy in dual-cured elastomers report an increased stiffness in the longitudinal direction compared to the transverse one [172,173,181,184–186]. Ferry et al. on the other hand report a larger stiffness in the transverse direction on its materials where the initial network is only entangled and close to its glass transition [192,194].

From the modelling point of view, accounting for anisotropy is a sensitive task. First of all, in the frame of Flory's model, use of Gaussian statistics automatically leads to an isotropic solution for the stress-strain behavior [174,230]. A model that features anisotropy requires to take into account two additional characteristics, the non-Gaussian behavior of the chains and the non-uniform aspect of the chain size distribution [176–178]. Even with these elements, the models predict an increase in stiffness in the transverse direction, which is not what is usually observed. Note that in all these models and observations only the modulus (i.e. the small strain response of the material) is considered in the study of anisotropy.

The anisotropic behavior at small strain is therefore not a trivial phenomenon and its modelling seems to be a delicate task. Entanglements is most certainly an important aspect in this and is likely to complexify the analysis and modelling of dual-cured systems.

Once again, the key to get anisotropy in dual-cured elastomers is the concept of stretching and fixing using a dual-cure system. The next part therefore focuses on applications that involve the concept of stretching-and-fixing in order to give a complete picture of the interest of dual-curing chemistry.

5.2. Oriented chains in rubbers, a key element for some applications

5.2.1. Shape-memory polymers

Shape memory polymers (SMP) are stimuli-responsive materials that are able to change shape spontaneously [231]. They are characterized by the fact that they have two possible shapes, one that is permanent and one that is temporary. The temporary shape may be programmed and retained by the material until the stimulus is activated. Then, the material changes shape and returns to its permanent shape. With this very general definition, lots of materials may be considered as SMP [232]. For instance, a basic crosslinked thermally-responsive hydrogel like poly(N-isopropylacrylamide) has a permanent swollen state at low temperature and a transient collapsed shape at high temperature. In this case though, the temporary shape cannot be chosen, so the material is called "non-programmable SMP".

Using more subtle systems, it is possible to fabricate programmable SMP. For instance, one may use block copolymers or composites with different physical transition temperatures. By deforming the material above the transition and subsequently quenching the material, the

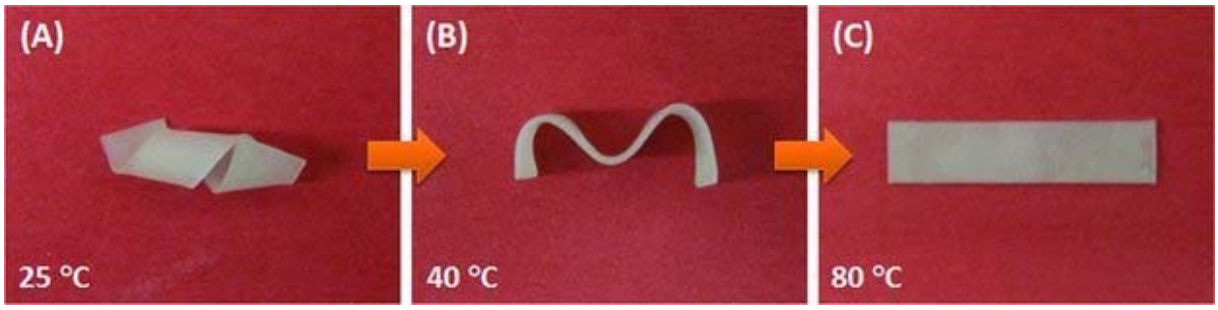

Figure 34: pictures from Luo and Mather showing the temporary shape relaxation of a triple SMP based on a fibre composite structure. A and B are temporary shapes, C is the permanent shape. The matrix exhibits a glass transition temperature at 30.5°C and fibres exhibit a melting temperature at 64.4°C. Pictures from [233] .

temporary shape may be retained and relaxed when the material is heated again. This concept has been used in the literature to prepare SMP with 2 temporary shapes, using a fiber composite [233] (see Figure 34). Interestingly, programmable SMP have been reported to exhibit anisotropic mechanical properties when in their temporary shape [234]. Beblo et al. use in their article a styrene-butadiene rubber and strain it uniaxially above the glass transition. The material is then quenched and studied in the two principal directions. They find a dramatic loss of modulus in the transverse direction and a significant increase in toughness.

Many different chemistries may be used to obtain shape-memory effects [235]. The common point between all these techniques is that the temporary shape is fixed by the generation of either physical or chemical constraints (covalent crosslinks, crystalline domains, glassy domains, etc.) in the deformed state. Another key element is that a fully functional SMP requires these constraints to be temporary. The connection between the elastomer chains must therefore be reversible, which limits the scope of possible chemical systems and makes them not easily translatable to another application in which the anisotropy must be permanent.

5.2.2. Liquid crystal elastomers

Liquid crystal elastomers (LCE) are rubbery materials in which rigid and elongated molecular segments (called “mesogens”) are attached to an elastomeric polymer backbone [236]. When these segments are aligned, they exhibit a preferential orientation which may strongly impact the material properties (like optical properties for example). The alignment of the rigid groups is temperature dependent such that the final material exhibits a phase transition from nematic to isotropic when the temperature increases. Mesogens may also be aligned using external stimuli such as stress or polarized light.

The fields of shape memory polymer and liquid crystal elastomers may interestingly converge by using the transition from the isotropic to the nematic state as a way to temporarily fix a geometrical shape. Saed et al. demonstrated a shape-memory effect on liquid-crystalline elastomers with the possibility to change the permanent shape by irradiating the material with UV light [237]. The recovery of the permanent shape is then achieved by the phase transition from the nematic to the isotropic state. Ware et al. used the same kind of phase transition to prepare films that can fold in a controlled way toward a programmed shape (see Figure 35) [238]. Using an optical device, they illuminated the surface of their samples using a specific spatial pattern of

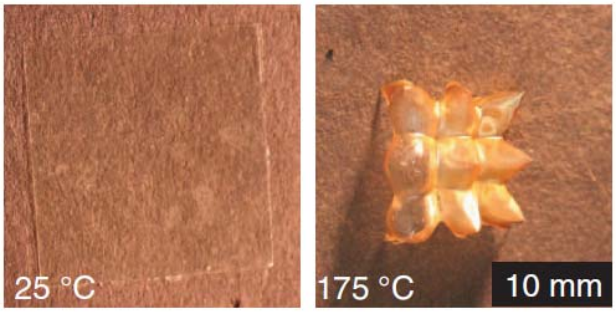

Figure 35: pictures of liquid crystalline films that exhibit a shape-memory effect on their surface. Films are programmed using a pattern of polarization state which induces a pattern of mesogen alignment. Pictures taken from [238].

polarization state. This resulted in controlled alignment of the mesogens at the surface of the films. When the material is heated above the nematic to isotropic transition, macromolecules shrink differently depending on the alignment of the mesogens. As a result, the film exhibits spatially controlled curvature and folds onto a specific shape.

Liquid crystal elastomers are therefore materials that can exhibit substantial and anisotropic shape change upon heating. The latter is induced by the orientation of rigid segments within the molecular structure. The anisotropic effect is thus the result of the combination of the flexibility of the elastomer chains and the rigidity of the mesogen groups.

5.2.3. Dielectric elastomers

Dielectric elastomers or dielectric elastomer actuators are electroactive polymers that are able to change size when subjected to an electrical field [239]. They are considered as candidate materials for flexible actuators, i.e. for the conversion of a mechanical deformation into an electrical signal or vice versa. Example of applications are highly sensitive sensors [240] or artificial muscles [241].

The working principle of purely amorphous dielectric elastomers is based on the Maxwell stress effect [239]. When a dielectric material is subjected to an electric field, the electric field distribution in the material is not homogeneous and induces a change in dimensions due to Coulomb's force. The resulting strain has a quadratic dependence with the electric field and scales linearly with the dielectric permittivity and the compliance of the material. Elastomers are soft and good dielectrics (i.e. they have large permittivity and high compliance) which makes them good candidates to get large strains by application of a "moderate" electric field (in the order of 10 V/µm).

In 2000, Pelrine et al. published a seminal paper about dielectric elastomers exhibiting electrically-induced strains larger than 100% [242]. They reported that prestraining the material perpendicular to the field direction increased significantly the actuation response. The question of how prestrain could foster the material response has been the focus of many studies and reviews [243,244] but does not seem to be fully understood. Presumably the main effect of prestrain is the change in geometrical dimensions that reduces the required voltage for actuation. Additionally, prestretching the elastomer increases the breakdown strength, i.e. the voltage at which the dielectric material starts being conductive. The mechanism behind this effect is however not well understood [239].

Dielectric elastomer actuators rely on the coupling of an electric field to the mechanical response of the material. As a result, the material properties greatly influence the actuation. In their review article [245], Zhao and Suo state that the following properties are required to achieve large voltage-induced strains: 1) large compliance at small strain, 2) large extent of strain-hardening and 3) not too large finite extensibility. These ideal properties are achieved in the most commonly used commercial dielectric elastomer (VHB 4910 from 3M) thanks to a grafted network architecture. Long side chains are grafted on the elastic strands which have three beneficial effects for the actuation properties: they ease the motion of chains thus lowering the glass transition temperature, they dilute the elastically active chains which decreases the modulus at low strains, and they extend the chains thus amplifying the strain-hardening at moderate stretch [246].

As a side note, some very efficient dielectric elastomer actuators has been reported using an interpenetrated network design [247–249]. VHB dielectric elastomer is strained biaxially and infiltrated with very short diacrylate chains (typically 1,6-hexanediol diacrylate) and radical initiator. The second network is subsequently polymerized thus freezing the prestrain. Electric strains up to 300% have been reported using this design. This preliminary study could open new applications for our multiple network elastomers in the future.

5.3. Battle plan, or how to make double networks anisotropic

The previous examples clearly show that anisotropy is very often the result of the alignment of hard or stiff segments in the material structure. In this project, we aim to combine this idea with the design strategy of multiple network elastomers. More specifically, the idea is to stretch the chains of the filler network in one direction, so that the ultimate extensibility of the filler network becomes different in the longitudinal/stretched direction and in the transverse direction. This difference at large strain may possibly be accompanied by a difference in stiffness. The literature does not systematically predict it, but in our case we imagine that chains very close to their limiting extensibility in the longitudinal direction could induce an increase in stiffness at small strains.

An enlightening way of seeing the problem is to consider the multiple network strategy as an amplifier of large strain effects in the filler network [250]. The filler network has a given maximum extensibility that comes from the crosslinking density and maximum extensibility of the network strands. When on its own, this large strain effect cannot be observed because the material fails at low stretch ratios because of stress concentration and network heterogeneities. By embedding it in a multiple network structure, the prestretching of the chains as well as the dissipating mechanism make this observation possible. The maximum extensibility of the filler network now corresponds to a visible phenomenon on the stress-strain curve of the double network, namely the strain-hardening.

In light of these considerations and having regard to the state-of-art that have been exposed previously, it seems that two possible ways may be used to prestretch the filler network unidirectionally.

5.3.1. The first naïve idea: swelling in the stretched state

One first strategy consists in stretching the crosslinked filler network and clamp it at a given extension ratio. The material could then be placed in a bath containing the matrix network formulation and be swollen to equilibrium. Once swollen, the matrix network could be polymerized yielding a double network structure.

The question of how equilibrium swelling and strain may be connected has already been covered in the literature. The effect of mechanical work has been included in the calculation of equilibrium swelling by Flory, the main result being that the application of strain increases swelling [251,252]. This prediction has been confirmed experimentally by several authors [253–255]. Note that the influence of the limiting extensibility of the chains is never studied in these articles.

There is however a huge practical limitation with this approach. On the one hand, the double network toughening strategy requires a large crosslinking asymmetry between the filler and the matrix network [136]. The filler network needs to be tightly crosslinked so that chains can break easily in the multiple network architecture and dissipate energy. On the other hand, swelling makes rubbery materials more brittle, like in hydrogels for example [67]. The presence of solvent suppresses molecular friction and the dilution of elastic chains increases the stress carried by each chain. This strategy therefore seems to be delicate to implement. Incidentally, experimental studies about swelling under strain very clearly state this issue. This limits the range of tested strains [253] or imposes the use sophisticated devices and very soft rubbers to perform the experiments [254].

As a matter of fact, all attempts to use this strategy with a standard filler network have resulted in fracture at the level of the clamps, i.e. where the deformation gradient is the largest. This approach is thus tempting but apparently bound to fail and will not be further elaborated in the manuscript.

5.3.2. The more subtle strategy: dual-cure chemistry and then swelling

If swelling need to be performed without any clamp, then the filler network must be prestretched in a first separate step. To do so, the solution that comes in mind is to use the concept of dual-cure chemistry. Starting from an initially loosely crosslinked filler network, a first stretch can be applied and the second curing reaction may be performed in the stretched state. The resulting material is therefore stiff and oriented at rest. It may then be used in a multiple network structure after swelling and polymerization of the matrix network. The final elastomer would therefore be a dual-cured double network. Funnily enough, the dual-cured filler network would be a “double network” in the historical sense of the term. As a recap of the synthetic strategy that is envisioned, Figure 36 gives a schematic representation of the different preparation steps that are studied in the project.

Of course this strategy is much more complex that the previous one in terms of chemistry. One must find a chemical system that gives the possibility of partially crosslinking the material in a first step, and then complete the crosslinking in a second step. As previously stated, the properties of the dual-cured elastomer are already complex by themselves, most probably because of the presence of entanglements. To simplify the problem, the initial filler network may be prepared in

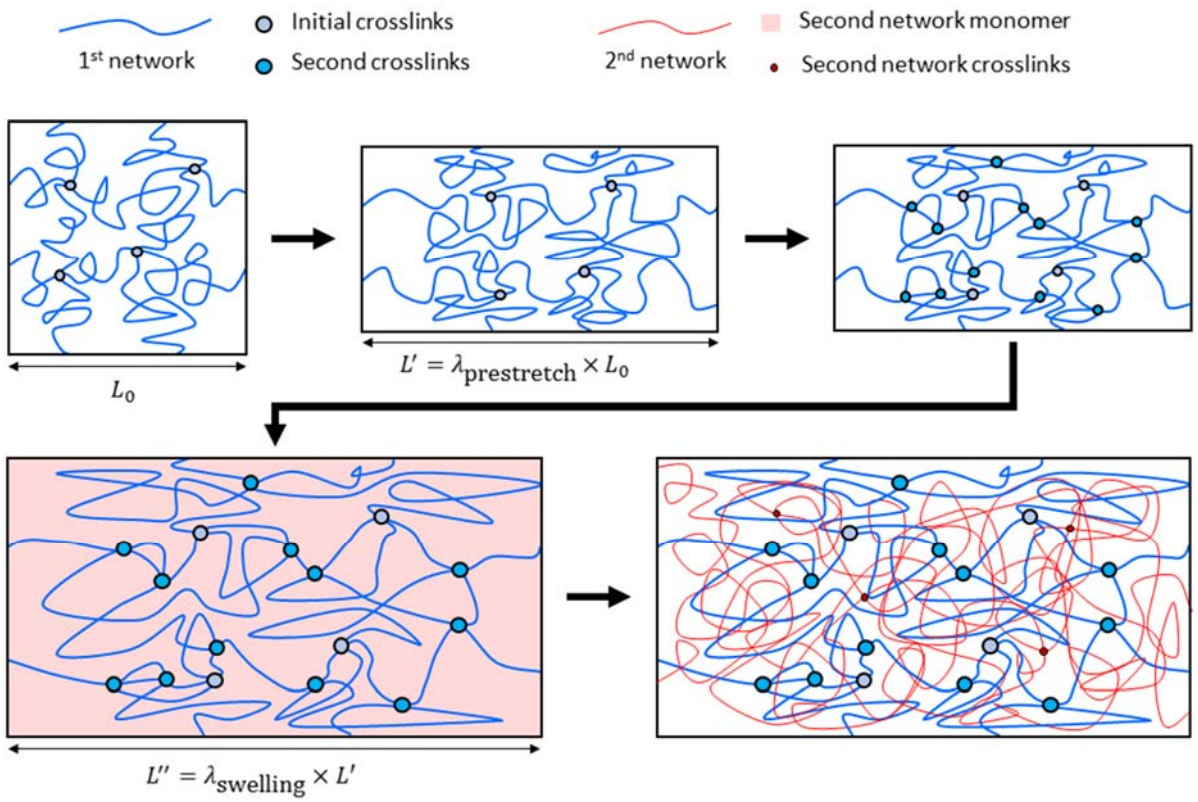

Figure 36: schematic representation of the synthetic strategy that will be used in this project. The initial network is first stretched and crosslinked in the stretched state. The resulting network is a dual-cured elastomer with oriented chains in the prestretched direction. This material may then be swollen in the matrix network formulation, thus adding an isotropic prestretching. After polymerization of the matrix network, a double network structure is obtained.

the presence of solvent. The latter dilutes the entanglements and makes the mechanical properties easier to understand by being closer to the affine model of elasticity [256].

6.Conclusions

Elastomers are materials that combines two very important properties: relatively low modulus and large extensibility. These properties are the result of the statistical origin of rubber elasticity. Its precise understanding gives keys for the design of materials that suit an always increasing number of applications. To this intent, it is interesting to tackle the classical paradigm of stiffness/toughness. These two properties are fundamentally predicted to go in opposite directions, so that stiff and tough materials require clever material design and concentrate a lot of research effort. Up to now, this is traditionally achieved by use of inorganic fillers or incorporation of viscous dissipation. These two solutions however are not always satisfactory since they give opaque materials with mechanical properties that may be too strongly rate and temperature dependent.

Among the many toughening strategies that have been reported in the literature, multiple network elastomers stand out by the fact that they bring a way to toughen brittle elastomers by playing on their macroarchitecture, independently from the polymer chemical nature. This strategy has been pioneered by Gong in the field of hydrogels and has been studied in large details before being translated to elastomers a few years ago in our group. The comprehensive study of these materials now gives new levers to double network elastomers closer to real applications.

One way to do so is to confront the multiple network architecture with anisotropy. Whether it is desired or not, the dependence of mechanical properties with strain direction is an actual applicative issue that needs to be studied in more details. In the literature, polymeric materials and applications that deal with anisotropy often use a chemical system that enable polymer chains to be prestretched and frozen in an oriented configuration. In the case of multiple network elastomers, the presence of filler network chains that are prestretched in one direction should give materials that have an anisotropic response at large strain, and possibly at small strain too. The main focus of this project is thus to make such a material in practice and to study its properties.

The main scientific challenge is to find a synthetic way that gives the possibility of prestretching and fixing the orientation of filler network chains. Such a crosslinking technique differs from the traditional crosslinking of elastomers in the sense that two crosslinking steps must be performed, and in two separate steps. What we need is therefore a dual-curing system, i.e. the combination of a simultaneous and a sequential crosslinking strategy.

7.References

1. Gennes PG de. Scaling concepts in polymer physics. Ithaca, N.Y: Cornell University Press; 1979. 324 p.
2. Hernández-Ortiz JC, Vivaldo-Lima E. Crosslinking. In: Handbook of Polymer Synthesis, Characterization, and Processing [Internet]. John Wiley & Sons, Inc.; 2013. p. 187–204. Available from: http://dx.doi.org/10.1002/9781118480793.ch9
3. Dubé MA, Saldívar-Guerra E, Zapata-González I. Copolymerization. In: Handbook of Polymer Synthesis, Characterization, and Processing [Internet]. John Wiley & Sons, Inc.; 2013. p. 105–25. Available from: http://dx.doi.org/10.1002/9781118480793.ch6
4. Brandrup J, Immergut EH, Grulke EA, Abe A, Bloch DR. Polymer handbook. 4th ed. Vol. 7. Wiley New York etc; 1989.
5. Guerrero-Santos R, Saldívar-Guerra E, Bonilla-Cruz J. Free Radical Polymerization. In: Handbook of Polymer Synthesis, Characterization, and Processing [Internet]. John Wiley & Sons, Inc.; 2013. p. 65–83. Available from: http://dx.doi.org/10.1002/9781118480793.ch4
6. Charles Goodyear. Improvement In India-Rubber Fabrics [Internet]. US3633A, 1844 [cited 2018 Nov 7]. Available from: https://patents.google.com/patent/US3633A/en
7. Kruželák J, Sýkora R, Hudec I. Sulphur and peroxide vulcanisation of rubber compounds – overview. Chem Pap. 2016;70(12):1533–1555.
8. Saunders KJ. Acrylic Polymers. In: Organic Polymer Chemistry [Internet]. Springer, Dordrecht; 1988 [cited 2017 Aug 30]. p. 125–48. Available from: https://link.springer.com/chapter/10.1007/978-94-009-1195-6_6
9. Hamed GR. Materials and compounds. In: Engineering with rubber: How to design rubber components [Internet]. 1992 [cited 2017 Jun 22]. p. 11. Available from: http://files.hanser.de/hanser/docs/20040401_244515439-6683_3-446-21403-8.pdf
10. Asahara J, Hori N, Takemura A, Ono H. Crosslinked acrylic pressure-sensitive adhesives. I. Effect of the crosslinking reaction on the peel strength. J Appl Polym Sci. 2003 Feb 28;87(9):1493–9.
11. Tillet G, Boutevin B, Ameduri B. Chemical reactions of polymer crosslinking and post-crosslinking at room and medium temperature. Prog Polym Sci. 2011 Feb 1;36(2):191–217.
12. Hoyle CE, Lee TY, Roper T. Thiol-enes: Chemistry of the past with promise for the future. J Polym Sci Part Polym Chem. 2004 Nov 1;42(21):5301–38.
13. Hoyle CE, Bowman CN. Thiol–Ene Click Chemistry. Angew Chem Int Ed. 2010 Feb 22;49(9):1540–73.
14. Mennicken M, Nagelsdiek R, Keul H, Höcker H. ATRP of Allyl Methacrylate with Alkyl Methacrylates – Crosslinking of Poly(methacrylate)s with Allyl Ester Side Groups. Macromol Chem Phys. 2004;205(18):2429–37.

15. Delavoipière J, Tran Y, Verneuil E, Chateauminois A. Poroelastic indentation of mechanically confined hydrogel layers. Soft Matter. 2016;12(38):8049–58.
16. Christensen SK, Chiappelli MC, Hayward RC. Gelation of Copolymers with Pendent Benzophenone Photo-Cross-Linkers. Macromolecules. 2012 Jun 26;45(12):5237–46.
17. Aoshima S, Hasegawa O, Higashimura T. Living cationic polymerization of vinyl ethers with a functional group. Polym Bull. 1985 Nov 1;14(5):417–23.
18. Itoh H, Kameyama A, Nishikubo T. Synthesis of new hybrid monomers and oligomers containing cationic and radical polymerizable vinyl groups and their photoinitiated polymerization. J Polym Sci Part Polym Chem. 1996 Jan 30;34(2):217–25.
19. Decker C, Decker D. Photoinitiated Polymerization of Vinyl Ether and Acrylate Monomer Mixtures. J Macromol Sci Part A. 1997 Apr 1;34(4):605–25.
20. Touhsaent RE, Thomas DA, Sperling LH. Epoxy/acrylic simultaneous interpenetrating networks. J Polym Sci Polym Symp. 1974 Jan 1;46(1):175–90.
21. Vabrik R, Czajlik I, Túry G, Rusznák I, Ille A, Víg A. A study of epoxy resin–acrylated polyurethane semi-interpenetrating polymer networks. J Appl Polym Sci. 1998 Apr 4;68(1):111–9.
22. Decker C, Nguyen Thi Viet T, Decker D, Weber-Koehl E. UV-radiation curing of acrylate/epoxide systems. Polymer. 2001 Jun 1;42(13):5531–41.
23. Decker C, Nguyen Thi Viet T, Pham Thi H. Photoinitiated cationic polymerization of epoxides. Polym Int. 2001 Sep 1;50(9):986–97.
24. Park Y-J, Lim D-H, Kim H-J, Park D-S, Sung I-K. UV- and thermal-curing behaviors of dual-curable adhesives based on epoxy acrylate oligomers. Int J Adhes Adhes. 2009 Oct 1;29(7):710–7.
25. Park C-H, Lee S-W, Park J-W, Kim H-J. Preparation and characterization of dual curable adhesives containing epoxy and acrylate functionalities. React Funct Polym. 2013 Apr 1;73(4):641–6.
26. Kim Y-B, Park S-C, Kim H-K, Hong J-W. Dual-curable acrylic pressure-sensitive adhesives based on UV and thermal processes. Macromol Res. 2008 Feb 1;16(2):128–33.
27. Konuray O, Fernández-Francos X, Ramis X, Serra À. State of the Art in Dual-Curing Acrylate Systems. Polymers. 2018 Feb 12;10(2):178.
28. Fernández-Francos X, Konuray A-O, Belmonte A, Flor SD la, Serra À, Ramis X. Sequential curing of off-stoichiometric thiol–epoxy thermosets with a custom-tailored structure. Polym Chem. 2016;7(12):2280–90.
29. Belmonte A, Guzmán D, Fernández-Francos X, De la Flor S. Effect of the Network Structure and Programming Temperature on the Shape-Memory Response of Thiol-Epoxy "Click" Systems. Polymers. 2015 Oct 26;7(10):2146–64.
30. Mather BD, Viswanathan K, Miller KM, Long TE. Michael addition reactions in macromolecular design for emerging technologies. Prog Polym Sci. 2006 May;31(5):487–531.

31. Stohr A, Strohriegl P. Networks with a cholesteric structure from acrylate-vinyl ether hybrid monomers. Macromol Chem Phys. 1998 May 1;199(5):751–6.
32. Vansteenkiste S, Matthijs G, Schacht E, De Schrijver FC, Van Damme M, Vermeersch J. Preparation of Tailor-Made Multifunctional Propenyl Ethers by Radical Copolymerization of 2-(1-Propenyl)oxyethyl Methacrylate. Macromolecules. 1999 Jan 1;32(1):55–9.
33. Warburton CE, Rounds NA. Process for preparing photocured coatings. [Internet]. EP0335629 (A2), 1989 [cited 2017 Sep 1]. Available from: https://worldwide.espacenet.com/publicationDetails/biblio?FT=D&date=19891004&DB=EPODOC&locale=en_EP&CC=EP&NR=0335629A2&KC=A2&ND=4
34. El-ghayoury A, Boukaftane C, de Ruiter B, van der Linde R. Ultraviolet–ultraviolet dual-cure process based on acrylate oxetane monomers. J Polym Sci Part Polym Chem. 2003 Feb 15;41(4):469–75.
35. de Ruiter B, El-ghayoury A, Hofmeier H, Schubert US, Manea M. Two-step curing processes for coating application. Prog Org Coat. 2006 Feb 1;55(2):154–9.
36. Nair DP, Cramer NB, Gaipa JC, McBride MK, Matherly EM, McLeod RR, et al. Two-Stage Reactive Polymer Network Forming Systems. Adv Funct Mater. 2012 Apr 10;22(7):1502–10.
37. Nair DP, Cramer NB, McBride MK, Gaipa JC, Shandas R, Bowman CN. Enhanced two-stage reactive polymer network forming systems. Polymer. 2012 May 25;53(12):2429–34.
38. González G, Fernández-Francos X, Serra À, Sangermano M, Ramis X. Environmentally-friendly processing of thermosets by two-stage sequential aza-Michael addition and free-radical polymerization of amine–acrylate mixtures. Polym Chem. 2015;6(39):6987–97.
39. Retailleau M, Ibrahim A, Croutxé-Barghorn C, Allonas X. Towards two-step photopolymerization using aza-Michael click addition. Prog Org Coat. 2016 Nov 1;100:51–5.
40. Konuray AO, Fernández-Francos X, Serra À, Ramis X. Sequential curing of amine-acrylate-methacrylate mixtures based on selective aza-Michael addition followed by radical photopolymerization. Eur Polym J. 2016 Nov 1;84:256–67.
41. Retailleau M, Pierrel J, Ibrahim A, Croutxé-Barghorn C, Allonas X. Sequenced click chemistry and photopolymerization: a new approach toward semi-interpenetrating polymer networks. Polym Adv Technol. 2017 Apr 1;28(4):491–5.
42. Rubinstein M, Colby RH. Polymer physics. Oxford ; New York: Oxford University Press; 2003. 440 p.
43. Mooney M. A Theory of Large Elastic Deformation. J Appl Phys. 1940;11(9):582.
44. Rivlin RS. Large elastic deformations of isotropic materials IV. further developments of the general theory. Phil Trans R Soc Lond A. 1948 Oct 5;241(835):379–97.
45. Gumbrell SM, Mullins L, Rivlin RS. Departures of the elastic behaviour of rubbers in simple extension from the kinetic theory. Trans Faraday Soc. 1953 Jan 1;49(0):1495–505.
46. Rubinstein M, Panyukov S. Elasticity of Polymer Networks. Macromolecules. 2002 Aug;35(17):6670–86.
47. Edwards SF. The statistical mechanics of polymerized material. Proc Phys Soc. 1967;92(1):9.

48. Arruda EM, Boyce MC. A three-dimensional constitutive model for the large stretch behavior of rubber elastic materials. J Mech Phys Solids. 1993 Feb 1;41(2):389–412.
49. Gent AN. A New Constitutive Relation for Rubber. Rubber Chem Technol. 1996 Mar 1;69(1):59–61.
50. Griffith AA. The phenomena of rupture and flow in solids. Philos Trans R Soc Lond Ser Contain Pap Math Phys Character. 1921;221:163–98.
51. Ward IM, Sweeney J. Mechanical Properties of Solid Polymers: Third Edition [Internet]. Chichester, UK: John Wiley & Sons, Ltd; 2012 [cited 2016 Oct 12]. Available from: http://doi.wiley.com/10.1002/9781119967125
52. Irwin GR. The stress analysis of cracks. Res Corp Hellertown PA. 1973;
53. Creton C, Ciccotti M. Fracture and adhesion of soft materials: a review. Rep Prog Phys. 2016 Apr 1;79(4):046601.
54. Rice JR, others. A path independent integral and the approximate analysis of strain concentration by notches and cracks. In ASME; 1968 [cited 2017 Aug 25]. Available from: https://appliedmechanics.asmedigitalcollection.asme.org/pdfaccess.ashx?resourceid=4366906&pdfsource=13
55. Hui C-Y, A J, Bennison SJ, Londono JD. Crack blunting and the strength of soft elastic solids. Proc R Soc Lond Math Phys Eng Sci. 2003 Jun 8;459(2034):1489–516.
56. Rivlin RS, Thomas AG. Rupture of rubber. I. Characteristic energy for tearing. In: Collected Papers of RS Rivlin [Internet]. Springer; 1997 [cited 2017 Jan 6]. p. 2615–2642. Available from: http://link.springer.com/chapter/10.1007/978-1-4612-2416-7_180
57. Greensmith HW. Rupture of rubber. X. The change in stored energy on making a small cut in a test piece held in simple extension. J Appl Polym Sci. 1963 May 1;7(3):993–1002.
58. Wang S, Panyukov S, Rubinstein M, Craig SL. Quantitative Adjustment to the Molecular Energy Parameter in the Lake–Thomas Theory of Polymer Fracture Energy. Macromolecules. 2019 Apr 9;52(7):2772–7.
59. Mzabi S. Caractérisation et analyse des mécanismes de fracture en fatigue des élastomères chargés [Internet] [Thèse de doctorat]. [Paris]: Paris 6; 2010 [cited 2017 Apr 5]. Available from: http://www.theses.fr/2010PA066079
60. Lake GJ, Lindley PB. The mechanical fatigue limit for rubber. J Appl Polym Sci. 1965;9(4):1233–1251.
61. Ellul MD. Mechanical Fatigue. In: Gent AN, editor. Engineering with Rubber (Third Edition) [Internet]. Hanser; 2012 [cited 2017 Apr 3]. p. 159–203. Available from: http://www.sciencedirect.com/science/article/pii/B9783446427648500272
62. ISO 27727:2008 - Rubber, vulcanized - Measurement of fatigue crack growth rate [Internet]. Available from: http://sagaweb.afnor.org/fr-FR/sw/consultation/notice/1391842?recordfromsearch=True

63. Chen Q, Zhu L, Chen H, Yan H, Huang L, Yang J, et al. A Novel Design Strategy for Fully Physically Linked Double Network Hydrogels with Tough, Fatigue Resistant, and Self-Healing Properties. Adv Funct Mater. 2015 Mar 1;25(10):1598–607.
64. Haque MA, Kurokawa T, Kamita G, Gong JP. Lamellar Bilayers as Reversible Sacrificial Bonds To Toughen Hydrogel: Hysteresis, Self-Recovery, Fatigue Resistance, and Crack Blunting. Macromolecules. 2011 Nov 22;44(22):8916–24.
65. Ping Gong J. Why are double network hydrogels so tough? Soft Matter. 2010;6(12):2583–90.
66. Creton C. 50th Anniversary Perspective: Networks and Gels: Soft but Dynamic and Tough. Macromolecules. 2017 Nov 14;50(21):8297–316.
67. Zhao X. Multi-scale multi-mechanism design of tough hydrogels: Building dissipation into stretchy networks. Soft Matter. 2014;10(5):672–87.
68. Ahmed EM. Hydrogel: Preparation, characterization, and applications: A review. J Adv Res. 2015 Mar;6(2):105–21.
69. Nicolson PC, Vogt J. Soft contact lens polymers: an evolution. Biomaterials. 2001 Dec 15;22(24):3273–83.
70. Hoare TR, Kohane DS. Hydrogels in drug delivery: Progress and challenges. Polymer. 2008 Apr 15;49(8):1993–2007.
71. Kashyap N, Kumar N, Kumar MNVR. Hydrogels for pharmaceutical and biomedical applications. Crit Rev Ther Drug Carrier Syst. 2005;22(2):107–49.
72. Shibayama M. Structure-mechanical property relationship of tough hydrogels. Soft Matter. 2012;8(31):8030–8.
73. Sakai T, Matsunaga T, Yamamoto Y, Ito C, Yoshida R, Suzuki S, et al. Design and Fabrication of a High-Strength Hydrogel with Ideally Homogeneous Network Structure from Tetrahedron-like Macromonomers. Macromolecules. 2008 Jul 1;41(14):5379–84.
74. Matsunaga T, Sakai T, Akagi Y, Chung U, Shibayama M. Structure Characterization of Tetra-PEG Gel by Small-Angle Neutron Scattering. Macromolecules. 2009 Feb 24;42(4):1344–51.
75. Matsunaga T, Sakai T, Akagi Y, Chung U, Shibayama M. SANS and SLS Studies on Tetra-Arm PEG Gels in As-Prepared and Swollen States. Macromolecules. 2009 Aug 25;42(16):6245–52.
76. Sakai T, Akagi Y, Matsunaga T, Kurakazu M, Chung U, Shibayama M. Highly Elastic and Deformable Hydrogel Formed from Tetra-arm Polymers. Macromol Rapid Commun. 2010 Nov 15;31(22):1954–9.
77. Cui J, Lackey MA, Madkour AE, Saffer EM, Griffin DM, Bhatia SR, et al. Synthetically Simple, Highly Resilient Hydrogels. Biomacromolecules. 2012 Mar 12;13(3):584–8.
78. Okumura Y, Ito K. The Polyrotaxane Gel: A Topological Gel by Figure-of-Eight Cross-links. Adv Mater. 2001 Apr 1;13(7):485–7.
79. Ito K. Novel Cross-Linking Concept of Polymer Network: Synthesis, Structure, and Properties of Slide-Ring Gels with Freely Movable Junctions. Polym J. 2007 May 9;39(6):489–99.
80. Ito K. Slide-ring materials using topological supramolecular architecture. Curr Opin Solid State Mater Sci. 2010 Apr;14(2):28–34.

81. Akagi Y, Sakurai H, Gong JP, Chung U, Sakai T. Fracture energy of polymer gels with controlled network structures. J Chem Phys. 2013 Oct 11;139(14):144905.
82. Sakai T. Gelation mechanism and mechanical properties of Tetra-PEG gel. React Funct Polym. 2013 Jul 1;73(7):898–903.
83. Liu C, Kadono H, Mayumi K, Kato K, Yokoyama H, Ito K. Unusual Fracture Behavior of Slide-Ring Gels with Movable Cross-Links. ACS Macro Lett. 2017 Dec 19;6(12):1409–13.
84. Li J, Illeperuma WRK, Suo Z, Vlassak JJ. Hybrid hydrogels with extremely high stiffness and toughness. ACS Macro Lett. 2014;3(6):520–3.
85. Sun J-Y, Zhao X, Illeperuma WRK, Chaudhuri O, Oh KH, Mooney DJ, et al. Highly stretchable and tough hydrogels. Nature. 2012;489(7414):133–6.
86. Sun TL, Kurokawa T, Kuroda S, Ihsan AB, Akasaki T, Sato K, et al. Physical hydrogels composed of polyampholytes demonstrate high toughness and viscoelasticity. Nat Mater. 2013;12(10):932–7.
87. Zhao X, Huebsch N, Mooney DJ, Suo Z. Stress-relaxation behavior in gels with ionic and covalent crosslinks. J Appl Phys [Internet]. 2010;107(6). Available from: https://www.scopus.com/inward/record.uri?eid=2-s2.0-77950567347&partnerID=40&md5=572a2dbc6bfb28c99e18e1d34f0a7da7
88. Kersey FR, Loveless DM, Craig SL. A hybrid polymer gel with controlled rates of cross-link rupture and self-repair. J R Soc Interface. 2007 Apr 22;4(13):373–80.
89. Hu X, Vatankhah-Varnoosfaderani M, Zhou J, Li Q, Sheiko SS. Weak Hydrogen Bonding Enables Hard, Strong, Tough, and Elastic Hydrogels. Adv Mater. 2015;27(43):6899–905.
90. Abdurrahmanoglu S, Can V, Okay O. Design of high-toughness polyacrylamide hydrogels by hydrophobic modification. Polymer. 2009;50(23):5449–55.
91. Miquelard-Garnier G, Demoures S, Creton C, Hourdet D. Synthesis and Rheological Behavior of New Hydrophobically Modified Hydrogels with Tunable Properties. Macromolecules. 2006 Nov 1;39(23):8128–39.
92. Carlsson L, Rose S, Hourdet D, Marcellan A. Nano-hybrid self-crosslinked PDMA/silica hydrogels. Soft Matter. 2010;6(15):3619–31.
93. Haraguchi K. Synthesis and properties of soft nanocomposite materials with novel organic/inorganic network structures. Polym J. 2011;43(3):223–41.
94. Haraguchi K, Takehisa T, Fan S. Effects of Clay Content on the Properties of Nanocomposite Hydrogels Composed of Poly(N-isopropylacrylamide) and Clay. Macromolecules. 2002 Dec 1;35(27):10162–71.
95. Liu Y, Zhu M, Liu X, Zhang W, Sun B, Chen Y, et al. High clay content nanocomposite hydrogels with surprising mechanical strength and interesting deswelling kinetics. Polymer. 2006;47(1):1–5.
96. Liu R, Liang S, Tang X-Z, Yan D, Li X, Yu Z-Z. Tough and highly stretchable graphene oxide/polyacrylamide nanocomposite hydrogels. J Mater Chem. 2012;22(28):14160–7.

97. Peppas NA, Merrill EW. Poly(vinyl alcohol) hydrogels: Reinforcement of radiation-crosslinked networks by crystallization. J Polym Sci Polym Chem Ed. 1976 Feb 1;14(2):441–57.

98. Peppas NA, Merrill EW. Development of semicrystalline poly(vinyl alcohol) hydrogels for biomedical applications. J Biomed Mater Res. 1977 May 1;11(3):423–34.

99. Stauffer SR, Peppast NA. Poly(vinyl alcohol) hydrogels prepared by freezing-thawing cyclic processing. Polymer. 1992 Sep 1;33(18):3932–6.

100. Huang T, Xu HG, Jiao KX, Zhu LP, Brown HR, Wang HL. A Novel Hydrogel with High Mechanical Strength: A Macromolecular Microsphere Composite Hydrogel. Adv Mater. 2007 Jun 18;19(12):1622–6.

101. E. Seitz M, Martina D, Baumberger T, R. Krishnan V, Hui C-Y, R. Shull K. Fracture and large strain behavior of self-assembled triblock copolymer gels. Soft Matter. 2009;5(2):447–56.

102. Gent AN, Schultz J. Effect of Wetting Liquids on the Strength of Adhesion of Viscoelastic Material. J Adhes. 1972 Mar;3(4):281–94.

103. Gent AN, Lai S-M, Nah C, Wang C. Viscoelastic Effects in Cutting and Tearing Rubber. Rubber Chem Technol. 1994 Sep 1;67(4):610–8.

104. Gent AN. Adhesion and Strength of Viscoelastic Solids. Is There a Relationship between Adhesion and Bulk Properties? Langmuir. 1996 Jan 1;12(19):4492–6.

105. Gotoh H, Liu C, Imran AB, Hara M, Seki T, Mayumi K, et al. Optically transparent, high-toughness elastomer using a polyrotaxane cross-linker as a molecular pulley. Sci Adv. 2018 Oct 1;4(10):eaat7629.

106. Zhao J, Mayumi K, Creton C, Narita T. Rheological properties of tough hydrogels based on an associating polymer with permanent and transient crosslinks: Effects of crosslinking density. J Rheol. 2017 Nov 1;61(6):1371–83.

107. Liu M, Guo J, Hui C-Y, Creton C, Narita T, Zehnder A. Time-temperature equivalence in a PVA dual cross-link self-healing hydrogel. J Rheol. 2018 Jul 1;62(4):991–1000.

108. D'Amico F, Carbone G, Foglia MM, Galietti U. Moving cracks in viscoelastic materials: Temperature and energy-release-rate measurements. Eng Fract Mech. 2013 Jan 1;98:315–25.

109. Carbone G, Persson BNJ. Hot Cracks in Rubber: Origin of the Giant Toughness of Rubberlike Materials. Phys Rev Lett. 2005 Sep 8;95(11):114301.

110. Chazeau L, Gauthier C, Chenal JM. Mechanical Properties of Rubber Nanocomposites: How, Why … and Then? In: Rubber Nanocomposites [Internet]. Wiley-Blackwell; 2010 [cited 2018 Oct 15]. p. 291–330. Available from: https://onlinelibrary.wiley.com/doi/abs/10.1002/9780470823477.ch12

111. Edwards DC. Polymer-filler interactions in rubber reinforcement. J Mater Sci. 1990 Oct;25(10):4175–85.

112. Bhowmick AK, Neogi C, Basu SP. Threshold tear strength of carbon black filled rubber vulcanizates. J Appl Polym Sci. 1990 Jan 1;41(5-6):917–28.

113. Payne AR, Whittaker RE. Low Strain Dynamic Properties of Filled Rubbers. Rubber Chem Technol. 1971 May 1;44(2):440–78.

114. Payne AR. The dynamic properties of carbon black-loaded natural rubber vulcanizates. Part I. J Appl Polym Sci. 1962;6(19):57–63.

115. Holt WL. Behavior of Rubber under Repeated Stresses. Rubber Chem Technol. 1932 Mar;5(1):79–89.

116. Mullins L. Effect of Stretching on the Properties of Rubber. Rubber Chem Technol. 1948 Jun 1;21(2):281–300.

117. Mullins L, Tobin NR. Stress softening in rubber vulcanizates. Part I. Use of a strain amplification factor to describe the elastic behavior of filler-reinforced vulcanized rubber. J Appl Polym Sci. 1965 Sep;9(9):2993–3009.

118. Diani J, Fayolle B, Gilormini P. A review on the Mullins effect. Eur Polym J. 2009 Mar 1;45(3):601–12.

119. Pu Z, Mark JE, Jethmalani JM, Ford WT. Effects of Dispersion and Aggregation of Silica in the Reinforcement of Poly(methyl acrylate) Elastomers. Chem Mater. 1997 Nov 1;9(11):2442–7.

120. Bréchet Y, Cavaillé J-Y, Chabert E, Chazeau L, Dendievel R, Flandin L, et al. Polymer Based Nanocomposites: Effect of Filler-Filler and Filler-Matrix Interactions. Adv Eng Mater. 2001;3(8):571–7.

121. Ramier J, Chazeau L, Gauthier C, Stelandre L, Guy L, Peuvrel-Disdier E. In situ SALS and volume variation measurements during deformation of treated silica filled SBR. J Mater Sci. 2007 Oct 1;42(19):8130–8.

122. Dutta NK, Choudhury NR, Haidar B, Vidal A, Donnet JB, Delmotte L, et al. High resolution solid-state n.m.r. investigation of the filler-rubber interaction: 1. High speed 1H magic-angle spinning n.m.r. spectroscopy in carbon black filled styrene-butadiene rubber. Polymer. 1994 Sep;35(20):4293–9.

123. Berriot J, Montes H, Lequeux F, Long D, Sotta P. Evidence for the Shift of the Glass Transition near the Particles in Silica-Filled Elastomers. Macromolecules. 2002 Dec 1;35(26):9756–62.

124. Montes H, Lequeux F, Berriot J. Influence of the Glass Transition Temperature Gradient on the Nonlinear Viscoelastic Behavior in Reinforced Elastomers. Macromolecules. 2003 Oct 1;36(21):8107–18.

125. Qian S, Huang J, Guo W, Wu C. Investigation of Carbon Black Network in Natural Rubber with Different Bound Rubber Contents. J Macromol Sci Part B. 2007 Apr;46(3):453–66.

126. Zhang L, Brostowitz NR, Cavicchi KA, Weiss RA. Perspective: Ionomer Research and Applications. Macromol React Eng. 2014 Feb 1;8(2):81–99.

127. Kirkmeyer BP, Weiss RA, Winey KI. Spherical and vesicular ionic aggregates in Zn-neutralized sulfonated polystyrene ionomers. J Polym Sci Part B Polym Phys. 2001;39(5):477–83.

128. Shabbir A, Huang Q, Chen Q, H. Colby R, J. Alvarez N, Hassager O. Brittle fracture in associative polymers: the case of ionomer melts. Soft Matter. 2016;12(36):7606–12.

129. Li C-H, Wang C, Keplinger C, Zuo J-L, Jin L, Sun Y, et al. A highly stretchable autonomous self-healing elastomer. Nat Chem. 2016 Jun;8(6):618–24.

130. Wu J, Cai L-H, Weitz DA. Tough Self-Healing Elastomers by Molecular Enforced Integration of Covalent and Reversible Networks. Adv Mater. 2017;29(38):1702616.

131. Cordier P, Tournilhac F, Soulié-Ziakovic C, Leibler L. Self-healing and thermoreversible rubber from supramolecular assembly. Nature. 2008 Feb;451(7181):977–80.

132. Montarnal D, Capelot M, Tournilhac F, Leibler L. Silica-Like Malleable Materials from Permanent Organic Networks. Science. 2011 Nov 18;334(6058):965–8.

133. Mark JE. The effect of strain-induced crystallization on the ultimate properties of an elastomeric polymer network. Polym Eng Sci. 1979;19(6):409–13.

134. Gent AN, Zhang L-Q. Strain-Induced Crystallization and Strength of Rubber. Rubber Chem Technol. 2002 Nov 1;75(5):923–34.

135. Le Gac PY, Broudin M, Roux G, Verdu J, Davies P, Fayolle B. Role of strain induced crystallization and oxidative crosslinking in fracture properties of rubbers. Polymer. 2014 May 13;55(10):2535–42.

136. Gong J p., Katsuyama Y, Kurokawa T, Osada Y. Double-Network Hydrogels with Extremely High Mechanical Strength. Adv Mater. 2003 Jul 17;15(14):1155–8.

137. Na Y-H, Kurokawa T, Katsuyama Y, Tsukeshiba H, Gong JP, Osada Y, et al. Structural characteristics of double network gels with extremely high mechanical strength. Macromolecules. 2004;37(14):5370–4.

138. Tanaka Y, Kuwabara R, Na Y-H, Kurokawa T, Gong JP, Osada Y. Determination of Fracture Energy of High Strength Double Network Hydrogels. J Phys Chem B. 2005 Jun 1;109(23):11559–62.

139. Tsukeshiba H, Huang M, Na Y-H, Kurokawa T, Kuwabara R, Tanaka Y, et al. Effect of polymer entanglement on the toughening of double network hydrogels. J Phys Chem B. 2005;109(34):16304–9.

140. Na Y-H, Tanaka Y, Kawauchi Y, Furukawa H, Sumiyoshi T, Gong JP, et al. Necking phenomenon of double-network gels. Macromolecules. 2006;39(14):4641–5.

141. Webber RE, Creton C, Brown HR, Gong JP. Large strain hysteresis and mullins effect of tough double-network hydrogels. Macromolecules. 2007;40(8):2919–27.

142. Tanaka Y. A local damage model for anomalous high toughness of double-network gels. EPL Europhys Lett. 2007;78(5):56005.

143. Brown HR. A Model of the Fracture of Double Network Gels. Macromolecules. 2007 May;40(10):3815–8.

144. Tanaka Y, Kawauchi Y, Kurokawa T, Furukawa H, Okajima T, Gong JP. Localized yielding around crack tips of double-network gels. Macromol Rapid Commun. 2008;29(18):1514–20.

145. Yu QM, Tanaka Y, Furukawa H, Kurokawa T, Gong JP. Direct observation of damage zone around crack tips in double-network gels. Macromolecules. 2009;42(12):3852–5.

146. Tominaga T, Tirumala VR, Lin EK, Gong JP, Furukawa H, Osada Y, et al. The molecular origin of enhanced toughness in double-network hydrogels: A neutron scattering study. Polymer. 2007;48(26):7449–54.

147. Tominaga T, Tirumala VR, Lee S, Lin EK, Gong JP, Wu W-L. Thermodynamic interactions in double-network hydrogels. J Phys Chem B. 2008;112(13):3903–9.

148. Tirumala VR, Tominaga T, Lee S, Butler PD, Lin EK, Gong JP, et al. Molecular model for toughening in double-network hydrogels. J Phys Chem B. 2008;112(27):8024–31.

149. Nakajima T, Furukawa H, Tanaka Y, Kurokawa T, Osada Y, Gong JP. True chemical structure of double network hydrogels. Macromolecules. 2009;42(6):2184–9.

150. Gong JP. Why are double network hydrogels so tough? Soft Matter. 2010;6(12):2583–90.

151. Nakajima T, Kurokawa T, Ahmed S, Wu W, Gong JP. Characterization of internal fracture process of double network hydrogels under uniaxial elongation. Soft Matter. 2013 Jan 16;9(6):1955–66.

152. Matsuda T, Nakajima T, Fukuda Y, Hong W, Sakai T, Kurokawa T, et al. Yielding Criteria of Double Network Hydrogels. Macromolecules. 2016 Mar 8;49(5):1865–72.

153. Mai T-T, Matsuda T, Nakajima T, Gong JP, Urayama K. Distinctive Characteristics of Internal Fracture in Tough Double Network Hydrogels Revealed by Various Modes of Stretching. Macromolecules. 2018 Jul 24;51(14):5245–57.

154. Mai T-T, Matsuda T, Nakajima T, Ping Gong J, Urayama K. Damage cross-effect and anisotropy in tough double network hydrogels revealed by biaxial stretching. Soft Matter [Internet]. 2019 [cited 2019 Apr 19]; Available from: https://pubs.rsc.org/en/content/articlelanding/2019/sm/c9sm00409b

155. Zhang W, Liu X, Wang J, Tang J, Hu J, Lu T, et al. Fatigue of double-network hydrogels. Eng Fract Mech. 2018 Jan 1;187:74–93.

156. Zhang E, Bai R, Morelle XP, Suo Z. Fatigue fracture of nearly elastic hydrogels. Soft Matter. 2018 May 9;14(18):3563–71.

157. Bai R, Yang Q, Tang J, Morelle XP, Vlassak J, Suo Z. Fatigue fracture of tough hydrogels. Extreme Mech Lett. 2017 Sep;15:91–6.

158. Milner PE, Parkes M, Puetzer JL, Chapman R, Stevens MM, Cann P, et al. A low friction, biphasic and boundary lubricating hydrogel for cartilage replacement. Acta Biomater. 2018 Jan 1;65:102–11.

159. Matsuda T, Kawakami R, Namba R, Nakajima T, Gong JP. Mechanoresponsive self-growing hydrogels inspired by muscle training. Science. 2019 Feb 1;363(6426):504–8.

160. Takahashi R, Shimano K, Okazaki H, Kurokawa T, Nakajima T, Nonoyama T, et al. Tough Particle-Based Double Network Hydrogels for Functional Solid Surface Coatings. Adv Mater Interfaces. 2018;5(23):1801018.

161. Ducrot E. Innovative tough elastomers: Designed sacrificial bonds in multiple networks [PhD thesis]. [Paris]: Université Pierre et Marie Curie; 2013.

162. Ducrot E, Montes H, Creton C. Structure of Tough Multiple Network Elastomers by Small Angle Neutron Scattering. Macromolecules. 2015;48(21):7945–52.

163. Ducrot E, Chen Y, Bulters M, Sijbesma RP, Creton C. Toughening elastomers with sacrificial bonds and watching them break. Science. 2014;344(6180):186–9.

164. Millereau P. Large Strain and Fracture of Multiple Network Elastomers [PhD thesis]. [Paris]: Université Pierre et Marie Curie; 2017.

165. Chen Y. Quantitative mapping of stress in soft materials by mechanochemistry [PhD thesis]. [Paris]: PSL Research University; 2018.

166. Li M, Zhang Q, Zhou Y-N, Zhu S. Let spiropyran help polymers feel force! Prog Polym Sci. 2018 Apr;79:26–39.

167. Millereau P, Ducrot E, Clough JM, Wiseman ME, Brown HR, Sijbesma RP, et al. Mechanics of elastomeric molecular composites. Proc Natl Acad Sci. 2018 Aug 28;201807750.

168. Aylsworth JW. Plastic composition. [Internet]. US1111284 A, 1914 [cited 2017 Aug 30]. Available from: http://www.google.com/patents/US1111284

169. Sperling LH, Hu R. Interpenetrating Polymer Networks. In: Utracki LA, Wilkie CA, editors. Polymer Blends Handbook [Internet]. Dordrecht: Springer Netherlands; 2014 [cited 2016 Oct 25]. p. 677–724. Available from: http://link.springer.com/10.1007/978-94-007-6064-6_8

170. Roland CM. Unconventional rubber networks: Circumventing the compromise between stiffness and strength. Rubber Chem Technol. 2013;86(3):351–66.

171. Andrews RD, Tobolsky AV, Hanson EE. The Theory of Permanent Set at Elevated Temperatures in Natural and Synthetic Rubber Vulcanizates. J Appl Phys. 1946;17(5):352.

172. Charlesby A, Arnim E von. Crosslinking of oriented rubber. J Polym Sci. 1957 Jul 1;25(109):151–8.

173. Berry JP, Scanlan J, Watson WF. Cross-link formation in stretched rubber networks. Trans Faraday Soc. 1956;52:1137–1151.

174. Flory PJ. Elasticity of polymer networks cross-linked in states of strain. Trans Faraday Soc. 1960 Jan 1;56(0):722–43.

175. Baxandall LG, Edwards SF. Deformation-dependent properties of polymer networks constructed by addition of crosslinks under strain. Macromolecules. 1988 Jun 1;21(6):1763–72.

176. Smith KJ, Ciferri A, Hermans JJ. Anisotropic elasticity of composite molecular networks formed from non-gaussian chains. J Polym Sci A. 1964 Mar 1;2(3):1025–41.

177. Yanai HS. Two Network Model for Vulcanizates Crosslinked under Strain. Rubber Chem Technol. 1967 Sep;40(4):1060–70.

178. Jr KJS, Gaylord RJ. Non-gaussian elasticity of composite and interpenetrating networks. J Polym Sci Part -2 Polym Phys. 1972 Feb 1;10(2):283–93.

179. Meissner B, Matějka L. Langevin-elasticity-theory-based description of the tensile properties of double network rubbers. Polymer. 2003 Jul;44(16):4611–7.

180. Aprem AS, Joseph K, Thomas S. Studies on double networks in natural rubber vulcanizates. J Appl Polym Sci. 2004 Jan 15;91(2):1068–76.

181. Kaang S, Gong D, Nah C. Some physical characteristics of double-networked natural rubber. J Appl Polym Sci. 1997 Aug 1;65(5):917–24.

182. Santangelo PG, Roland CM. The Mechanical Behavior of Double Network Elastomers. Rubber Chem Technol. 1994 May 1;67(2):359–65.

183. Petrova SB, Priss LS. Effect of deformation during crosslinking on elastic properties of rubbers. Polym Sci USSR. 1983 Jan;25(1):204–8.

184. Greene A, Smith KJ, Ciferri A. Elastic properties of networks formed from oriented chain molecules. Part 2.—Composite networks. Trans Faraday Soc. 1965;61:2772–2783.

185. Greene A, Ciferri A. Elastic properties of networks formed from oriented chain molecules. Kolloid-Z Z Für Polym. 1962 Nov 1;186(1):1–15.

186. Santangelo PG, Roland CM. Failure Properties of Natural Rubber Double Networks. Rubber Chem Technol. 1995 Mar 1;68(1):124–31.

187. Kaang S, Nah C. Fatigue crack growth of double-networked natural rubber. Polymer. 1998;39(11):2209–2214.

188. Roland CM, Warzel ML. Orientation Effects in Rubber Double Networks. Rubber Chem Technol. 1990 May 1;63(2):285–97.

189. Mott PH, Roland CM. Mechanical and Optical Behavior of Double Network Rubbers. Macromolecules. 2000 May;33(11):4132–7.

190. Rottach DR, Curro JG, Budzien J, Grest GS, Svaneborg C, Everaers R. Permanent Set of Cross-Linking Networks: Comparison of Theory with Molecular Dynamics Simulations. Macromolecules. 2006 Aug 1;39(16):5521–30.

191. Rottach DR, Curro JG, Budzien J, Grest GS, Svaneborg C, Everaers R. Molecular Dynamics Simulations of Polymer Networks Undergoing Sequential Cross-Linking and Scission Reactions. Macromolecules. 2007 Jan 1;40(1):131–9.

192. Kramer O, Carpenter RL, Ty V, Ferry JD. Entanglement Networks of 1,2-Polybutadiene Cross-Linked in States of Strain. I. Cross-Linking at 0 °. 1974;7(1):6.

193. Kramer O, Ferry JD. Entanglement Networks of 1,2-Polybutadiene Cross-Linked in States of Strain. II. Application of the Mooney-Rivlin Equation to Networks Cross-Linked at O°. Macromolecules. 1975 Jan 1;8(1):87–9.

194. Batsberg W, Hvidt S, Kramer O. Swelling and elastic anisotropies of an amorphous elastomer crosslinked in the strained state. 1,2-polybutadiene. J Polym Sci Polym Lett Ed. 1982;20(6):341–6.

195. Singh NK, Lesser AJ. Mechanical and thermo-mechanical studies of double networks based on thermoplastic elastomers. J Polym Sci Part B Polym Phys. 2010 Apr 1;48(7):778–89.

196. Singh NK, Lesser AJ. A physical and mechanical study of prestressed competitive double network thermoplastic elastomers. Macromolecules. 2011;44(6):1480–90.

197. Katashima T, Chung U, Sakai T. Mechanical properties of doubly crosslinked gels. Polym J [Internet]. 2019 May 22 [cited 2019 May 29]; Available from: http://www.nature.com/articles/s41428-019-0203-6

198. Lu T, Wang J, Yang R, Wang TJ. A constitutive model for soft materials incorporating viscoelasticity and Mullins effect. J Appl Mech [Internet]. 2016 Nov 8 [cited 2016 Nov 15]; Available from: http://appliedmechanics.asmedigitalcollection.asme.org/article.aspx?doi=10.1115/1.4035180

199. Bacca M, Creton C, McMeeking RM. A model for the Mullins effect in multi-network elastomers. J Appl Mech [Internet]. 2017 Sep 13 [cited 2017 Sep 19]; Available from: http://appliedmechanics.asmedigitalcollection.asme.org/article.aspx?doi=10.1115/1.4037881

200. Wang X, Hong W. Pseudo-elasticity of a double network gel. Soft Matter. 2011;7(18):8576–81.

201. Zhao X. A theory for large deformation and damage of interpenetrating polymer networks. J Mech Phys Solids. 2012;60(2):319–32.

202. Vernerey FJ, Long R, Brighenti R. A statistically-based continuum theory for polymers with transient networks. J Mech Phys Solids. 2017 Oct 1;107:1–20.

203. Vernerey FJ. Transient response of nonlinear polymer networks: A kinetic theory. J Mech Phys Solids. 2018 Jun 1;115:230–47.

204. Vernerey FJ, Brighenti R, Long R, Shen T. Statistical Damage Mechanics of Polymer Networks. Macromolecules. 2018 Sep 11;51(17):6609–22.

205. Lavoie SR, Millereau P, Creton C, Long R, Tang T. A continuum model for progressive damage in tough multinetwork elastomers. J Mech Phys Solids. 2019 Apr;125:523–49.

206. Slootman J. Quantitative detection of damage in soft materials using mechano-fluorescence [PhD thesis]. [Paris]: PSL Research University; 2019.

207. Munch E, Pelletier JM, Sixou B, Vigier G. Molecular mobility of crosslinked elastomers stretched above Tg. Polymer. 2006 May 3;47(10):3477–85.

208. Green DW, Winandy JE, Kretschmann DE. Mechanical properties of wood. Wood Handb Wood Eng Mater Madison WI USDA For Serv For Prod Lab 1999 Gen Tech Rep FPL GTR-113 Pages 41-445. 1999;113.

209. Miller RB. Structure of wood. Wood Handb Wood Eng Mater Madison WI USDA For Serv For Prod Lab 1999 Gen Tech Rep FPL GTR-113 Pages 21-24. 1999;113.

210. Polymer Composites: Macroscale and Microscale. In: Mechanical Properties of Solid Polymers [Internet]. Chichester, UK: John Wiley & Sons, Ltd; 2012 [cited 2018 Nov 26]. p. 227–59. Available from: http://doi.wiley.com/10.1002/9781119967125.ch9

211. Wang Q, Dai J, Li W, Wei Z, Jiang J. The effects of CNT alignment on electrical conductivity and mechanical properties of SWNT/epoxy nanocomposites. Compos Sci Technol. 2008 Jun 1;68(7):1644–8.

212. Hamed GR. Anisotropy induced during compression molding of rubber. J Appl Polym Sci. 1982 Oct;27(10):4081–3.

213. Blow CM, Demirli HB, Southwart DW. Anisotropy in Molded Nitrile Rubber. Rubber Chem Technol. 1975 May 1;48(2):236–45.

214. Machado G, Chagnon G, Favier D. Induced anisotropy by the Mullins effect in filled silicone rubber. Mech Mater. 2012 Jul;50:70–80.

215. Hanson DE, Hawley M, Houlton R, Chitanvis K, Rae P, Orler EB, et al. Stress softening experiments in silica-filled polydimethylsiloxane provide insight into a mechanism for the Mullins effect. Polymer. 2005 Nov;46(24):10989–95.

216. Arruda EM, Boyce MC, Quintus-Bosz H. Effects of initial anisotropy on the finite strain deformation behavior of glassy polymers. Int J Plast. 1993 Jan 1;9(7):783–811.

217. Arruda EM, Boyce MC. Evolution of plastic anisotropy in amorphous polymers during finite straining. Int J Plast. 1993 Jan 1;9(6):697–720.

218. Holzapfel G. Biomechanics of soft tissue. In: The HANDBOOK OF MATERIALS BEHAVIOR MODELS. Academic Press; 2001.

219. Sano K, Ishida Y, Aida T. Synthesis of Anisotropic Hydrogels and Their Applications. Angew Chem Int Ed. 2017 Oct 16;57(10):2532–43.

220. Haque MdA, Kamita G, Kurokawa T, Tsujii K, Gong JP. Unidirectional Alignment of Lamellar Bilayer in Hydrogel: One-Dimensional Swelling, Anisotropic Modulus, and Stress/Strain Tunable Structural Color. Adv Mater. 2010 Sep 13;22(45):5110–4.

221. Lu Q, Bai S, Ding Z, Guo H, Shao Z, Zhu H, et al. Hydrogel Assembly with Hierarchical Alignment by Balancing Electrostatic Forces. Adv Mater Interfaces. 2016 Feb 8;3(8):1500687.

222. Wu L, Ohtani M, Takata M, Saeki A, Seki S, Ishida Y, et al. Magnetically Induced Anisotropic Orientation of Graphene Oxide Locked by in Situ Hydrogelation. ACS Nano. 2014 May 27;8(5):4640–9.

223. Chau M, De France KJ, Kopera B, Machado VR, Rosenfeldt S, Reyes L, et al. Composite Hydrogels with Tunable Anisotropic Morphologies and Mechanical Properties. Chem Mater. 2016 May 24;28(10):3406–15.

224. Zhu J, Wang J, Liu Q, Liu Y, Wang L, He C, et al. Anisotropic tough poly(2-hydroxyethyl methacrylate) hydrogels fabricated by directional freezing redox polymerization. J Mater Chem B. 2013;1(7):978–86.

225. Chen M, Zhu J, Qi G, He C, Wang H. Anisotropic hydrogels fabricated with directional freezing and radiation-induced polymerization and crosslinking method. Mater Lett. 2012 Dec 15;89:104–7.

226. Wu ZL, Kurokawa T, Sawada D, Hu J, Furukawa H, Gong JP. Anisotropic hydrogel from complexation-driven reorientation of semirigid polyanion at Ca2+ diffusion flux front. Macromolecules. 2011;44(9):3535–41.

227. Choi S, Kim J. Designed fabrication of super-stiff, anisotropic hybrid hydrogels via linear remodeling of polymer networks and subsequent crosslinking. J Mater Chem B. 2015;3(8):1479–83.

228. Lin P, Zhang T, Wang X, Yu B, Zhou F. Freezing Molecular Orientation under Stretch for High Mechanical Strength but Anisotropic Hydrogels. Small. 2016;4386–92.

229. Mredha MdTI, Guo YZ, Nonoyama T, Nakajima T, Kurokawa T, Gong JP. A Facile Method to Fabricate Anisotropic Hydrogels with Perfectly Aligned Hierarchical Fibrous Structures. Adv Mater. 2018 Jan 17;30(9):1704937.

230. Lodge AS. The isotropy of Gaussian molecular networks and the stress-birefringence relations for rubberlike materials cross-linked in stressed states. Kolloid-Z. 1960 Jul 1;171(1):46–51.

231. Lendlein A, Kelch S. Shape-Memory Polymers. Angew Chem Int Ed. 2002 Jun 17;41(12):2034–57.

232. Zhao Q, Qi HJ, Xie T. Recent progress in shape memory polymer: New behavior, enabling materials, and mechanistic understanding. Prog Polym Sci. 2015 Oct 1;49:79–120.

233. Luo X, Mather PT. Triple-Shape Polymeric Composites (TSPCs). Adv Funct Mater. 2010 Aug 23;20(16):2649–56.

234. Beblo R, Weiland LM. Strain induced anisotropic properties of shape memory polymer. Smart Mater Struct. 2008;17(5):055021.

235. Berg GJ, McBride MK, Wang C, Bowman CN. New directions in the chemistry of shape memory polymers. Polymer. 2014 Nov 5;55(23):5849–72.

236. Warner M, Terentjev EM. Liquid crystal elastomers [Internet]. Oxford: Clarendon Press; 2007 [cited 2017 Sep 4]. Available from: http://site.ebrary.com/id/10271647

237. Saed MO, Torbati AH, Nair DP, Yakacki CM. Synthesis of Programmable Main-chain Liquid-crystalline Elastomers Using a Two-stage Thiol-acrylate Reaction. JoVE J Vis Exp. 2016 Jan 19;(107):e53546–e53546.

238. Ware TH, McConney ME, Wie JJ, Tondiglia VP, White TJ. Voxelated liquid crystal elastomers. Science. 2015 Feb 27;347(6225):982–4.

239. O'Halloran A, O'Malley F, McHugh P. A review on dielectric elastomer actuators, technology, applications, and challenges. J Appl Phys. 2008;104(7):071101.

240. Ni N, Zhang L. Dielectric Elastomer Sensors. Elastomers [Internet]. 2017 Aug 30 [cited 2018 Nov 30]; Available from: https://www.intechopen.com/books/elastomers/dielectric-elastomer-sensors

241. Brochu P, Pei Q. Advances in Dielectric Elastomers for Actuators and Artificial Muscles. Macromol Rapid Commun. 2010 Jan 4;31(1):10–36.

242. Pelrine R, Kornbluh R, Pei Q, Joseph J. High-Speed Electrically Actuated Elastomers with Strain Greater Than 100%. Science. 2000 Feb 4;287(5454):836–9.

243. Choi HR, Jung K, Chuc NH, Jung M, Koo I, Koo J, et al. Effects of prestrain on behavior of dielectric elastomer actuator. In: Bar-Cohen Y, editor. San Diego, CA; 2005 [cited 2018 Nov

30]. p. 283. Available from: http://proceedings.spiedigitallibrary.org/proceeding.aspx?doi=10.1117/12.599363

244. Kofod G. The static actuation of dielectric elastomer actuators: how does pre-stretch improve actuation? J Phys Appl Phys. 2008;41(21):215405.

245. Zhao X, Suo Z. Theory of Dielectric Elastomers Capable of Giant Deformation of Actuation. Phys Rev Lett. 2010 Apr 30;104(17):178302.

246. Suo Z. Theory of dielectric elastomers. Acta Mech Solida Sin. 2010 Dec 1;23(6):549–78.

247. Ha SM, Yuan W, Pei Q, Pelrine R, Stanford S. Interpenetrating Polymer Networks for High-Performance Electroelastomer Artificial Muscles. Adv Mater. 2006 Apr 4;18(7):887–91.

248. Ha SM, Yuan W, Pei Q, Pelrine R, Stanford S. Interpenetrating networks of elastomers exhibiting 300% electrically-induced area strain. Smart Mater Struct. 2007 Apr 1;16(2):S280–7.

249. Suo Z, Zhu J. Dielectric elastomers of interpenetrating networks. Appl Phys Lett. 2009 Dec 7;95(23):232909.

250. Ducrot E, Creton C. Characterizing Large Strain Elasticity of Brittle Elastomeric Networks by Embedding Them in a Soft Extensible Matrix. Adv Funct Mater. 2016;26(15):2482–92.

251. Flory PJ, Rehner J. Statistical Mechanics of Cross-Linked Polymer Networks II. Swelling. J Chem Phys. 1943;11(11):521.

252. Flory PJ. Network Structure and the Elastic Properties of Vulcanized Rubber. Chem Rev. 1944 Aug 1;35(1):51–75.

253. Gee G. The interaction between rubber and liquids. X. Some new experimental tests of a statistical thermodynamic theory of rubber-liquid systems. Trans Faraday Soc. 1946;42:B033–44.

254. Treloar LRG. The swelling of cross-linked amorphous polymers under strain. Trans Faraday Soc. 1950;46:783–789.

255. Treloar LRG. The equilibrium swelling of cross-linked amorphous polymers. In: Proceedings of the Royal Society of London A: Mathematical, Physical and Engineering Sciences [Internet]. The Royal Society; 1950 [cited 2016 Nov 14]. p. 176–183. Available from: http://rspa.royalsocietypublishing.org/content/200/1061/176.short

256. Urayama K. Network Topology–Mechanical Properties Relationships of Model Elastomers. Polym J. 2008 Aug;40(8):669–78.

Chapter 2

Design and preliminary study of two effective dual-curing systems

Table of contents

1. Introduction 89
1.1. Overview of the requirements specifications 89
1.2. Presentation of the thermal system 89
1.3. Presentation of the UV system 90
1.4. Outline 91
2. Generalities about chemistry and material preparation 93
2.1. Chemicals and formulation 93
2.1.1. Chemicals 93
2.1.2. Formulations 93
2.2. Materials synthesis 94
2.2.1. Initial network synthesis 94
2.2.2. Thermal system second curing 95
2.2.3. UV system second curing 95
2.3. Characterization methods 96
2.3.1. Equilibrium Swelling 96
2.3.2. Dynamic Mechanical Analysis (DMA) 96
2.3.3. Tensile tests 97
3. Study of the thermal system 101
3.1. A kinetic study of the system 101
3.2. Variation of the initial formulation 106
3.2.1. Effect on small strain mechanical properties 106
3.2.2. Effect on the uniaxial tensile response 110
3.2.3. Effect on swelling ratio 111
3.3. Partial conclusion and identification of a working point formulation 112
4. Study of the UV system 115
4.1. Effect of crosslinker content 115
4.2. Effect of initiator content 116
4.2.1. On the initial network polymerization 116
4.2.2. On the second curing process 117
4.3. Effect of allyl acrylate content 117
4.4. The issue of sample-to-sample variability 121

5. Conclusions 125
6. References 127

1. Introduction

1.1. Overview of the requirements specifications

As stated in the introduction, the aim of this PhD is to prepare double network elastomers with a prestretched filler network. From the knowledge that has been developed in the field of multiple network elastomers, such a material is expected to display anisotropic properties at large strains. These properties are interesting to study, but require to find the adequate chemistry. Namely, we need a system that enables us to perform the crosslinking of the filler network in two steps. First an initial network with low crosslinking density needs to be prepared. This network should then be stretched and crosslinked further in the stretched state. The addition of crosslinks should make the material stiffer and prevent it from returning to its original state.

What is needed is therefore a so-called "dual-curing system". The ideal system would possess the following characteristics:

- The initial network should be as loosely crosslinked as possible, in order to get a significant asymmetry in crosslinking density and thus a significant final prestretching.
- The final filler network should be crosslinked enough to get prestretching, but not too much so that the material swells enough to be employed in a multiple network architecture.
- Before the second curing, the single-cured network should be stable. In other words, the triggering of the second curing reaction should be on demand in order to avoid any ageing phenomenon.

Among the different chemistries that have been tried, two successful systems have been studied in more details. The first one uses a second curing reaction that is activated by temperature while the second one uses a second curing that is activated by UV light.

1.2. Presentation of the thermal system

The thermal system involves the use of two comonomers and one catalyst. This strategy is inspired by an existing method published in the literature in the field of adhesives [1]. The main monomer is copolymerized with acrylic acid (AA) and glycidyl methacrylate (GMA) in order to incorporate glycidyl and carboxylic acid functions in the network structure. These functions are then reacted together by a condensation reaction catalyzed by an amine base, which is triethylamine here (NEt3). The equation of the reaction may be written as follows:

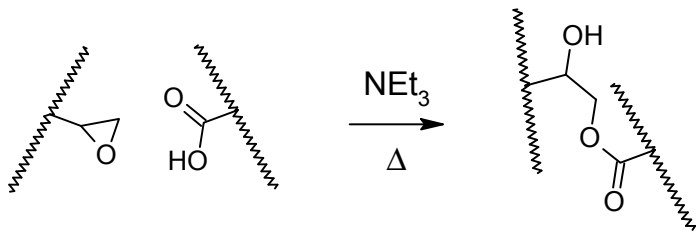

Since the second curing reaction requires heat, the crosslinking density of the first step should be mainly controlled by the amount of initial crosslinker molecules. This advantage of an a priori better control of the intermediate network properties comes at the expense of a more complex chemical system, since two comonomers and a catalyst need to be used.

1.3. Presentation of the UV system

The UV system uses a single comonomer from the acrylate family, allyl acrylate (ALA, see Figure 1). The basic idea is to copolymerize it with a standard crosslinked network formulation, and then use the remaining poorly reactive functions to create additional crosslinks in a second activation step.

Use of allyl acrylate as a comonomer is motivated by three reasons. First, it is commercially available and fairly inexpensive which avoids custom-made synthesis. Second, use of a monomer from the acrylate family avoids problems of copolymerization kinetics and helps ensuring random incorporation. Third, dual-curing systems in the literature often use differences in reactivities to separate the two crosslinking steps, as illustrated in Chapter 1. In this specific system however, the separability of the two steps is not ensured since allyl groups are susceptible to free radical polymerization (although with a much lower rate than acrylates).

The envisioned procedure for the dual-curing system is as follows (Figure 2):

- In a first step, a standard network formulation is used with the addition of a few molar percents of allyl acrylate. A first low-power UV irradiation is performed to prepare the initial network without reacting too much of the allyl groups.
- The crosslinked network is dried to remove most of unreacted species and then swollen in a bath containing a good solvent (acetone) and a radical photoinitiator. Once equilibrium swelling is reached, the swollen gel is dried again to remove the solvent, hopefully retaining most of the photoinitiator
- The second curing step is then performed by irradiating the now dry activated network with UV at high power in nitrogen atmosphere.

Although this second curing process is slightly more time consuming due to the need of an infiltration step, the simplicity of the chemical design should give materials that are easier to analyze.

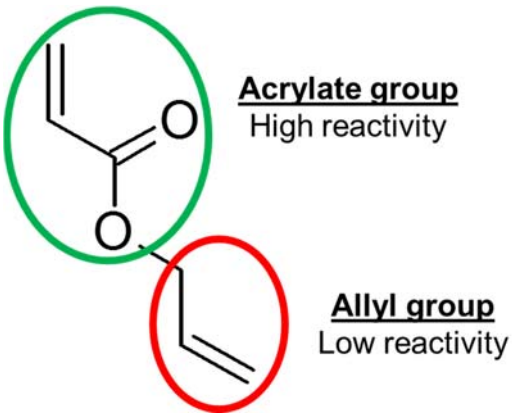

Figure 1: chemical structure of allyl acrylate. The molecule has two reactive double-bonds, one being much more reactive than the other one.

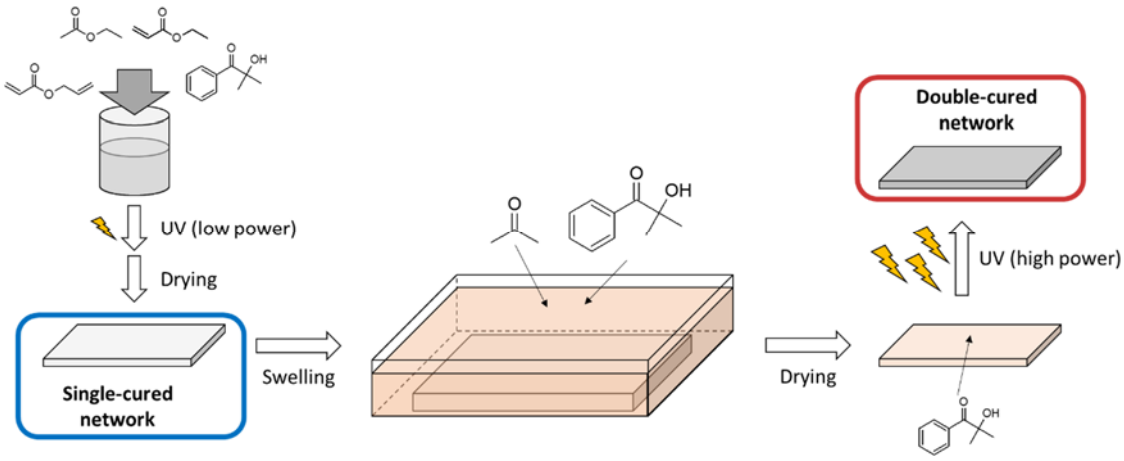

Figure 2: schematic representation of the dual-curing process. The single-cured network is obtained by polymerizing the initial mixture at low UV power. The material is then infiltrated with UV initiator and cured a second time at large UV lower.

1.4. Outline

The present chapter focuses on the design and study of two dual-curing systems independently from prestretching and multiple network reinforcement. After an explanation of the materials and methods that have been used throughout the project, the thermal system is first investigated in details. Notably, the working parameters are identified in terms of heating time and formulation. Then, the UV system is studied in the same way. By the end of the chapter, two optimum working points are identified and used in the following chapters.

2. Generalities about chemistry and material preparation

2.1. Chemicals and formulation

2.1.1. Chemicals

All the materials of this PhD project are synthesized in the laboratory from commercial chemicals. Table 1 gives basic information about the monomers. All liquid monomers except allyl acrylate (ALA) are purified by elution through an alumina column before use. ALA is used without prior purification. Table 2 gives information about the solvents and other chemicals. All of them are used without prior purification.

Nitrogen is bubbled into liquids to be used in the glovebox for at least 15 minutes before being introduced in N_2 atmosphere to remove dissolved oxygen. For large volumes (>100mL), this bubbling is extended to 30 minutes at least and is assisted with magnetic agitation.

2.1.2. Formulations

A basic elastomer formulation comprises a main monomer and some additives (initiator, crosslinker, comonomers, etc.). Throughout the manuscript, formulations are presented in tables. Depending on the compound, quantities may be expressed with different percentages:

- In case of volume percentage (noted v%), the percentage is given with respect to the total volume (which is roughly the volume of monomer plus solvent)

Abbrev.	Chemical name	Molecular formula	Purity	Origin	CAS
MA	Methyl acrylate	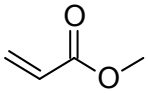	99%	Aldrich	96-33-3
EA	Ethyl acrylate	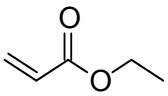	99%	Aldrich	140-88-5
AA	Acrylic acid	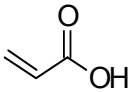	≥99%	Merck	79-10-7
GMA	Glycidyl methacrylate	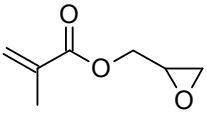	97%	Aldrich	106-91-2
BDA	1,4-Butanediol diacrylate	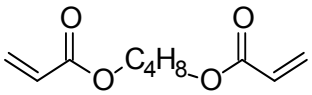	90% (tech)	Aldrich	1070-70-8
ALA	Ally acrylate	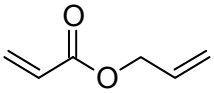	90% (tech)	Alfa Aesar	999-55-3

Abbrev.	Chemical name	Molecular formula	Purity	Origin	CAS
AcOEt	Ethyl acetate	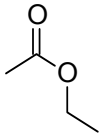	99%	Sigma-Aldrich	141-78-6
/	Acetone		≥99.8%	Carlo Erba	67-64-1
NEt3	Triethylamine	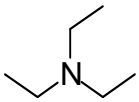	≥99.5%	Sigma-Aldrich	121-44-8
HMP	2-Hydroxy-2-methylpropiophenone	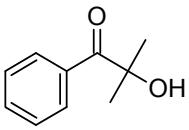	97%	Aldrich	7473-98-5

Table 2: information about solvents, initiators and catalysts used in this work

- In case of molar percentage (m% or mol%), the percentage is given with respect to the molar quantity of the main monomer
- In case of mass/weight percentage (noted w%), the percentage is given with respect to the mass of the main monomer

The table below gives a fictive example of formulation table. For the sake of simplicity, lines in gray colour are omitted in the rest of the manuscript.

Compound	A	B	C	D
Role	Monomer	Solvent	Comonomer	…
Volume	10 mL	10 mL	65 µL	/
Mass	6 g	/	/	0.03 g
Moles	50 mmol	/	0.5 mmol	/
Quantity	/	50 v%	1 m%	0.5 w%

2.2. Materials synthesis

2.2.1. Initial network synthesis

The initial network is synthesized by UV-initiated free radical polymerization in an MBraun Unilab glovebox under nitrogen atmosphere. Solutions are prepared from purified monomers (see 2.1.1) stored in the glovebox freezer before use (except for acrylic acid which is stored at room temperature in the glovebox). Reactive mixtures are placed in a home-made mold, as depicted in Figure 3. Two glass slides are tightened between two Dural frames and separated by four Dural spacers of identical thickness (1 mm) and a Teflon tube seal. Glass slides are covered with a thin PET sheet (54 µm thickness) stuck with adhesive tape to ease unmolding and avoid surface defects.

Films are irradiated on both sides (using a set of mirrors) with a Vilbert Lourmat lamp, model VL-215.L, centered on the 365nm wavelength and covered with several thick PET sheets to reduce

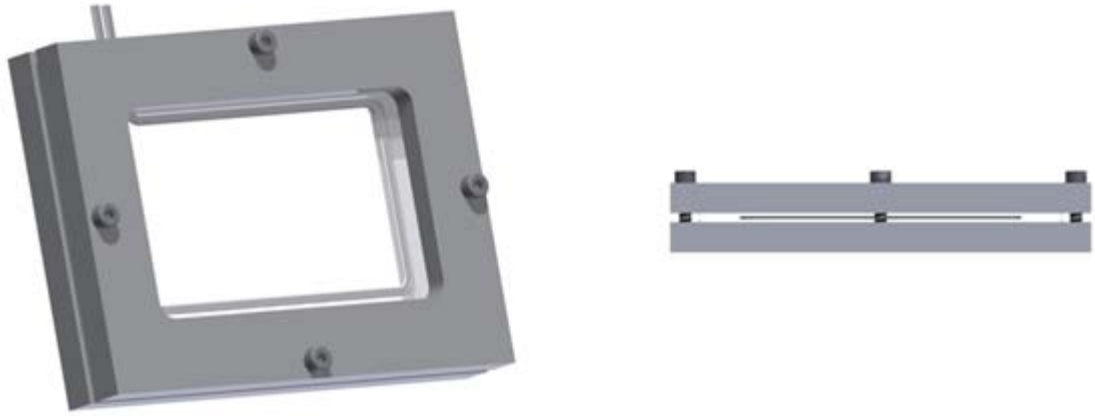

Figure 3: home-made molds used for UV polymerizations (image from Ducrot's PhD thesis)

light intensity. The UV power is checked regularly using a radiometer VLX-3W from Vilbert Lourmat. For network synthesis, a low UV power is used ($5 - 10\ \mu W/cm^2$) for 2h, which corresponds to a UV dose of about 50 mJ/cm^2. This low intensity polymerization is inspired by Gong's original procedure [2] and aims to ensure a low concentration of radicals and better homogeneity in the samples.

After UV irradiation, films are dried to remove unreacted monomers and solvent. Drying is performed at room temperature in vacuum for at least 6h and less than 16h. After drying, samples are stored in the dark at -18°C until later use to avoid undesired second curing reaction as much as possible.

2.2.2. Thermal system second curing

The thermally activated second curing is done using a XF020 France Etuves vacuum oven in air conditions. Heating is performed in two stages: first uncontrolled heating up to a set temperature of 120°C and then controlled heating at 0.5°C/min up to 150°C. Note that after the first stage the temperature overshoots and reaches a temperature between 130 and 140°C. The final temperature is then maintained for 2h. Overall, the heating process lasts approximately 2h40.

After completion of the second curing, the oven is flushed using a vacuum pump and refilled with fresh air several times to avoid air contamination when the mold is removed.

2.2.3. UV system second curing

For the UV system, irradiation is preceded by an infiltration step during which the UV initiator (HMP) is incorporated in the network. The basic idea behind this infiltration process is to incorporate UV initiator in the mesh of the network. It relies on the large difference between the vapor pressure of acetone (184 mmHg at 20°C) and HMP (0.008 mmHg at 25°C). It is therefore expected that almost all the initiator absorbed during the swelling phase remains in the material after drying.

Initial network samples are taken from the freezer and placed for 2h in a swelling bath. The bath typically contains about 170mL of acetone and 1 w% of HMP (weight percent with respect to the mass of acetone). The bath is wrapped in aluminum foil to avoid undesired activation of HMP by ambient UV light. After 2h, the highly swollen networks are taken out of the bath, weighed and then dried under vacuum for 6 to 8h to evacuate most of the solvent. Swelling ratio Q_{w} is estimated by dividing the swollen mass by the initial mass. This is highly variable even for samples of same composition but usually ranges between 6 and 8. By using reasonable values for the ALA content in the material (same as formulation, i.e. around 1%) and the swelling ratio (the average value for all samples, i.e. 6.6), one can estimate that the absorbed quantity of HMP is approximatively the same as the quantity of allyl acrylate in the starting material.

Irradiation is then performed in the glovebox using the same UV lamp as for the initial synthesis. PET filters are removed in order to increase the UV power, which reaches 0.4mW/cm^2 at most. Irradiation lasts 2h and the samples are left in nitrogen atmosphere overnight after the reaction to ensure complete conversion. A slight yellowing of the samples is observed after the second curing.

2.3. Characterization methods

2.3.1. Equilibrium Swelling

Equilibrium swelling experiments are performed by cutting small pieces of networks (about 0.5×1 cm^2) using scissors. Samples are placed in glass vials filled with ethyl acrylate (at least 5mL). Swollen samples are regularly taken out of the vials using tweezers, quickly and gently pressed against absorbing paper to remove the excess of liquid, and placed in a tared closed vial to measure the mass.

Although some uncertainty is due to the removal of excess liquid, the precision of the measurement may be estimated knowing the uncertainty of each mass measurement (about 1mg). The relative uncertainty on the measurement of mass swelling ratio is thus 3% at most.

2.3.2. Dynamic Mechanical Analysis (DMA)

The measurement of viscoelastic properties is done with a Q800 Dynamic Mechanical Analyzer from Thermal Analysis. A 5 mm wide strip of material is cut or punched and placed on a tensile clamp in the DMA.

The basic principle of DMA is represented in Figure 4. A sinusoidal deformation is applied on the sample and the resulting dynamic force is measured. The dynamic force is normalized by the cross-section and by the deformation to give the complex modulus. This modulus may then be separated in an in-phase component (the storage modulus E') and an out-of-phase component (the loss modulus E''). The ratio between the two is the loss tangent $\tan(\delta) = E''/E'$.

To be thorough, a tensile static force is also applied in order to avoid buckling. This static force should not be too large so that the sample stays in its linear regime. When the samples experience large changes of stiffness (for example during glass transition), it becomes challenging to set a

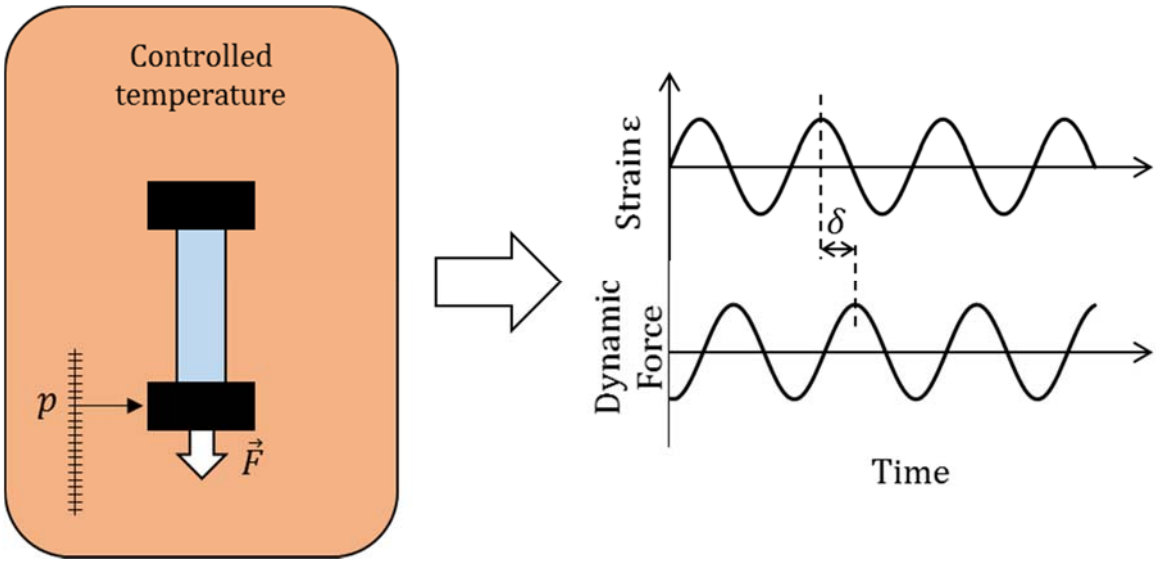

Figure 4: schematic representation of the working principle of DMA. p represents the position of the mobile clamp, $\vec{F}$ is the total force that is applied.

static force that works for the entire test. To circumvent this, the static force may be defined as a ratio of the dynamic force. It therefore evolves when the material softens or hardens. This ratio is called "forcetrack", and the manufacturer suggests values between 120 and 150%.

In the rest of the manuscript, the parameters used for DMA characterization are specified using a table as in the example below:

Parameter	Frequency	Strain	Static force	Forcetrack	Heating rate
Value	1 Hz	0.1%	0.05N	125%	5°C/min

2.3.3. Tensile tests

All the experiments are performed on an Instron tensile tester, model 5565 or 5590, equipped with a 100N load cell, a video extensometer and a temperature controlled chamber. Measurement errors for force and deformation are 0.5% at most. Home-made pneumatic clamps are used to hold the samples as previously described [3] (see Figure 5). The chamber enables tests at temperatures between 20 and 100°C with a precision of 2°C. A fan at low speed is used to help homogenize the temperature in the chamber.

Tests are performed on dumbbell samples cut using a punch. Two white marks are placed about 1 cm apart on the sample using a white paint marker. Gauge length is 20 mm, width is 4 mm and thickness depends on the sample in the range 0.5-2 mm. The crosshead is moved at a constant speed of either 100 or 500 µm/sec. Deformation is measured using the video extensometer and previously mentioned white marks. A crosshead speed of 100 µm/sec corresponds to a strain rate of 0.4%/sec while 500 µm/sec corresponds to 2%/sec.

Raw data from the test includes force F, crosshead displacement and stretch ratio $\lambda = L/L_0$ where L is the distance between the two marks during the test and L_0 is the initial value of L. From these

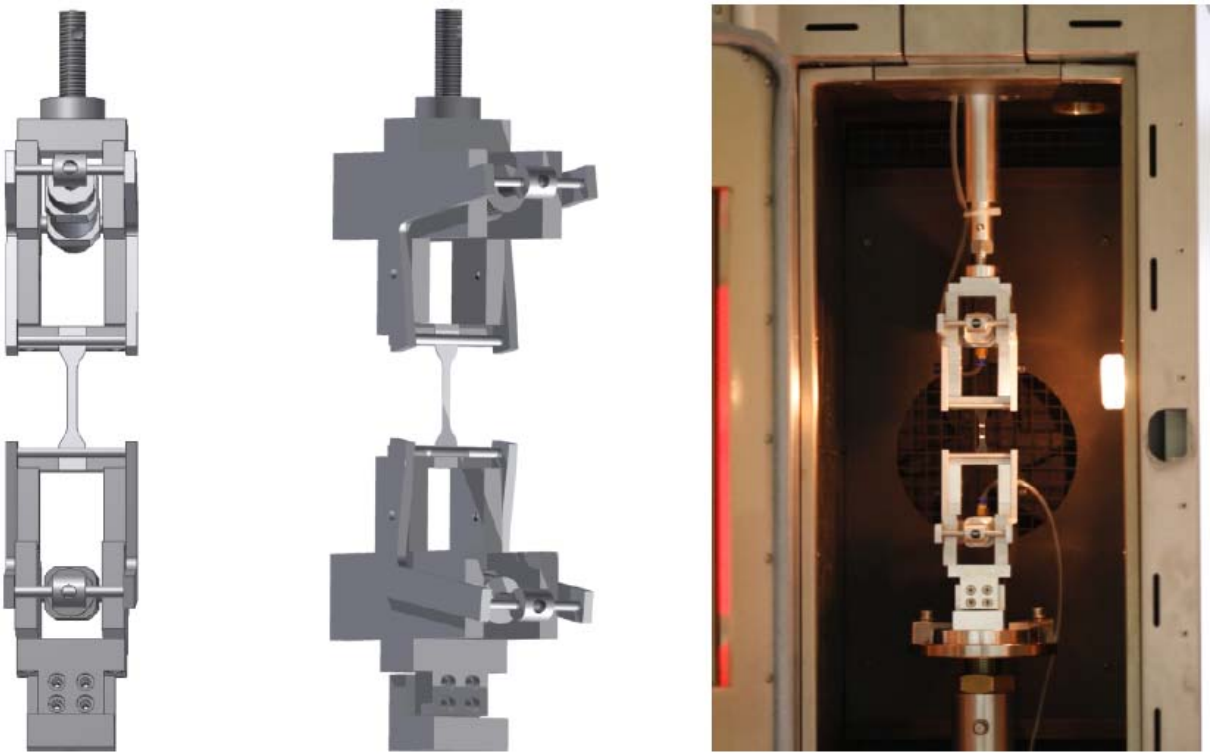

Figure 5: pneumatic clamps used in this study. Left: face view. Middle: lateral view. Right: picture of the clamps once in the climatic chamber. Images from Ducrot's PhD thesis.

data, the nominal stress is calculated, making sure the points corresponding to pre-load are removed from the force vs deformation curve:

$$\sigma_N = F/w_0 h_0 \qquad \text{Eq. 1}$$

The Young's modulus is measured by fitting the region between 0 and 5-8% deformation on the σ_N versus $\epsilon = \lambda - 1$ curve using an affine fit.

For very extensible networks, the maximum extensibility cannot be measured directly using the extensometer data. The range of detection of the extensometer being limited, deformations larger than typically 400% cannot be measured. To circumvent this limitation, deformation data is computed from the crosshead position. First, the relative change in crosshead position is calculated:

$$\gamma_{\text{crosshead}}(t) = \frac{p(t) - p_0}{p_0} \qquad \text{Eq. 2}$$

where $p(t)$ the instantaneous position of the crosshead and p_0 its initial position. Then, the crosshead deformation is computed using the following formula:

$$\epsilon_{\text{crosshead}}(t) = \frac{a_{\text{extenso}}}{a_{\text{crosshead}}} \gamma_{\text{crosshead}}(t) \qquad \text{Eq. 3}$$

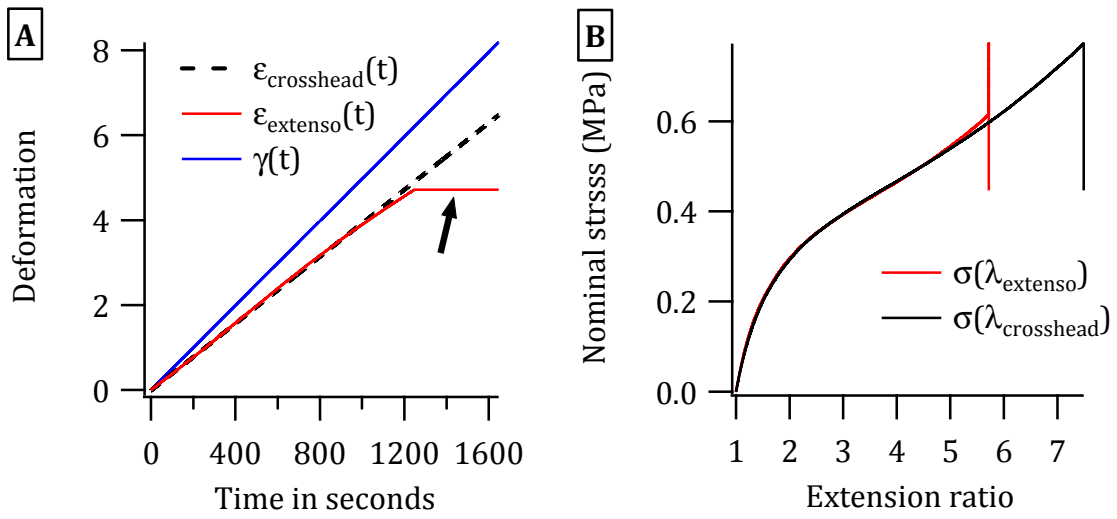

Figure 6: calculation of the crosshead deformation when the extensometer switches off because of the too large deformation. A) illustration of the crosshead deformation calculation process. The horizontal line on the red curves (pointed by the black arrow) shows the inability of the extensometer to track deformation above 400%. B) result of the deformation calculation process. The red curve uses the extension ratio taken from the extensometer directly. The black curve uses the extension ratio calculated from the crosshead position.

where a_{extenso} is the slope of the $\epsilon_{\text{extenso}}(t)$ curve and $a_{\text{crosshead}}$ is the slope of the $\gamma_{\text{crosshead}}(t)$ curve.

Figure 6 shows an example where the extensometer does not follow the deformation throughout the test and the calculation of the crosshead deformation. In the manuscript, $\lambda_{\text{crosshead}}$ is used whenever curves with deformation larger than 400% are presented. λ_{extenso} is used for all cases that require precision of the stretch ratio, like the measurement of modulus or extensibility for fracture tests for instance. In other words, $\lambda_{\text{crosshead}}$ will only be used for qualitative comparison between samples.

3.Study of the thermal system

3.1. A kinetic study of the system

The basic idea of this first study is to bring the initial single-cured network at a given temperature and observe how the second curing step proceeds. DMA is a tool of choice for this since it enables one to follow the buildup of stiffness.

The initial network is prepared using the following formulation:

Compound	MA	AA	GMA	BDA	HMP	NEt3
Role	Monomer	Comonomer	Comonomer	Crosslinker	UV initiator	Catalyst
Quantity	/	1.5 mol%	1.5 mol%	0.01 mol%	0.01 mol%	1 mol%

Samples are cut and tested in DMA using the following set of parameters:

Parameter	Frequency	Strain	Static force	Forcetrack	Heating rate
Value	1 Hz	0.1%	0.01N	125%	10°C/min

The temperature profiles are shown in Figure 7. Due to the high heating rate the profiles show some accidents here and there. The plateau temperatures are however reached shortly after the beginning of the tests, between 7 and 16 minutes depending on the temperature. In the rest of the study, the heating stage is omitted and only the variation of mechanical properties at the plateau temperature is considered.

Storage and loss moduli (E' and E'' respectively) are followed as a function of time at the plateau temperature. Results are presented in Figure 8 and show that **at all temperatures the storage modulus at 1Hz increases strongly with time**. The effect of the curing temperature follows that of a classical thermally-activated process, i.e. the reaction is faster when the temperature is higher. The second curing process seems to be particularly effective since the modulus increases significantly from 0.5 MPa to more than 2 MPa. The decrease in the loss tangent in Figure 8-B is consistent with a significant increase in crosslinking density. An increase in $\tan(\delta)$ is observed at very large times (especially at 80°C), which could be due either to an experimental artifact (slippage) or to oxidation/degradation of the material (since the experiment is carried out in ambient conditions).

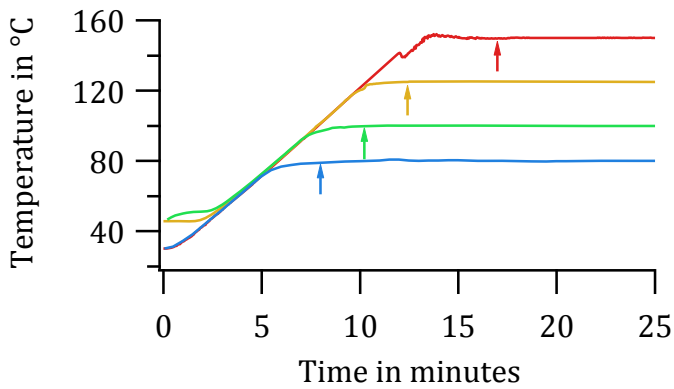

Figure 7: temperature profiles for the 4 temperatures tested in the kinetic study. Heating is fairly fast (10°C/min) hence artefacts are visible on the temperature curves. Arrows represent the time at which the temperature is considered as constant.

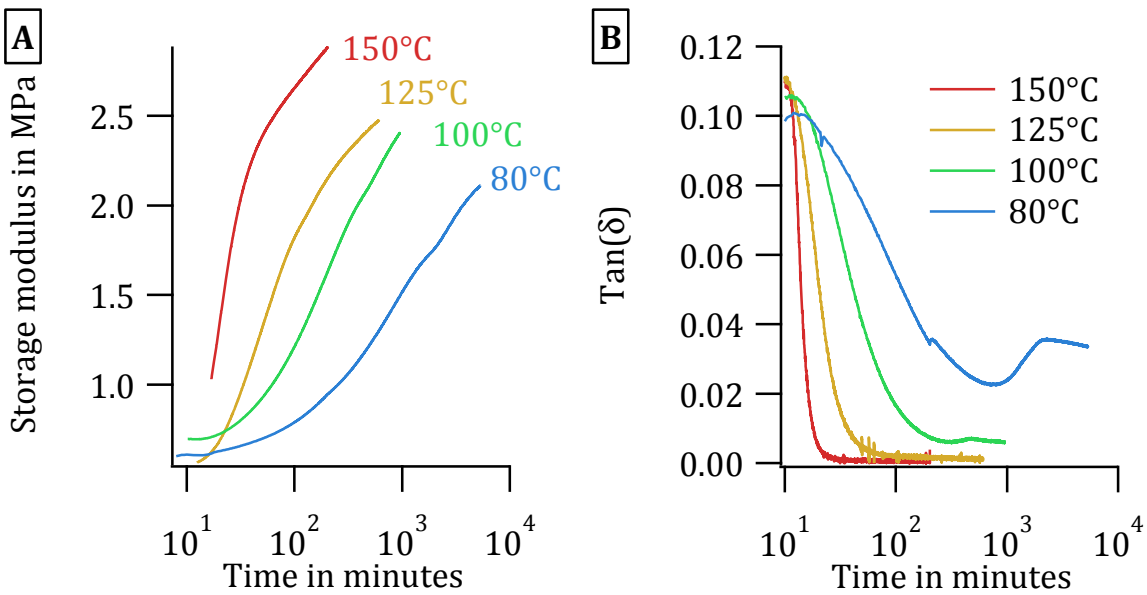

Figure 8: measurement of the variation of storage and loss moduli at various temperatures. Heating stage has been omitted from the curves. A) variation of the storage modulus B) variation of the loss tangent, i.e. the ratio of E'' over E'.

This simple experiment is a tool to understand how the second curing reaction proceeds. Qualitatively, the reaction is effective, but what about the quantitative aspect of the reaction? To evaluate this, a simple kinetic model is built. The reaction may be written in a simplified way as follows:

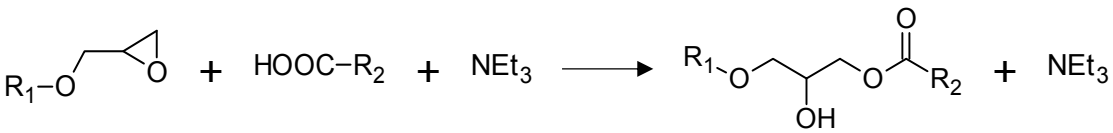

The reaction rate v may thus be written in a general way as follows:

$$v = -\frac{d[\text{glycidyl}]}{dt} = k[\text{glycidyl}]^{\alpha}[\text{COOH}]^{\beta}[\text{NEt}_3]^{\gamma} \qquad \text{Eq. 4}$$

with α, β and γ the partial orders of reaction and k the rate constant.

The consumption of glycidyl and carboxylic groups mainly leads to crosslinks, hence to an increase in storage modulus and decrease in $\tan(\delta)$. Assuming that all reactions are intermolecular, there is therefore a direct proportionality between the increase in storage modulus and the decrease in concentration of glycidyl groups:

$$E'(t) - E'(t=0) \propto [\text{glycidyl}]_t - [\text{glycidyl}]_{t=0} \qquad \text{Eq. 5}$$

The intermolecular assumption is not very strong since levels of GMA and AA that are used are low. The probability for the reacting glycidyl and acid units to be located on the same chain is thus very low.

In first approximation, concentration of NEt3 may be considered constant since it is a catalyst. Besides, GMA and AA concentrations are identical in the formulation hence are assumed to be identical in the network too. This leads to the following simplified kinetic law:

$$v = k_{\text{app}}[\text{glycidyl}]^n \qquad \text{Eq. 6}$$

where $n = \alpha + \beta$ is a global order of reaction.

Two possible situations are considered for the value of n.

- If $n = 1$ then the concentration of glycidyl groups has a decreasing exponential functional form. The storage modulus may then be modelled with the following expression:

$$E'(t) = E'_\infty + (E'_0 - E'_\infty)\exp\left[-k_{\text{app}}(t - t_0)\right] \qquad \text{Eq. 7}$$

- If $n = 2$ then the concentration of glycidyl groups follows an inverse relationship with time:

$$E'(t) = E'_\infty - \frac{1}{\frac{1}{E'_\infty - E'_0} + k_{\text{app}}(t - t_0)} \qquad \text{Eq. 8}$$

In both Eq. 7 and Eq. 8 E'_0 is the value of storage modulus for $t = t_0$ at the beginning of the plateau modulus and E'_∞ is the asymptotic value of E' for $t \to \infty$.

These two models are confronted to experiments by fitting the curves of Figure 8. Experimental data is used to fix the values of t_0 and E'_0 whereas E'_∞ and k_{app} are adjusted using a least-square regression. Results are shown in Figure 9 and suggest that **the model with $n = 2$ fits best the experimental data**. For all four temperatures, the coefficient of determination is larger when the second order model is used (on average, $R^2 = 0.977$ for $n = 1$ and $R^2 = 0.997$ for $n = 2$). Nevertheless, neither the qualitative observation nor the value of the coefficient of determination can be considered as a proof that the global order of the reaction is two, especially since the range of explored time is rather limited. In particular, the value of the final modulus is only extrapolated and is not actually reached during the test.

The literature is actually not unanimous about the order of this reaction. Authors studying the kinetics of similar systems report either a first global order [4–6], a second global order [7–9] or even intermediate values [10,11]. Matějka and Dušek have attempted to unify these results by demonstrating that the order with respect to acid actually depends on the amount and efficiency of the catalyst [10]. They report that the partial order ranges from 0 when the acid is used in excess to 1 when the amine catalyst is in excess. This however does not really match our observations since in this formulation the amine catalyst is not used in excess. In practice however, the idea behind the study of the kinetics of the reaction is merely to determine experimental conditions that suit our materials and application. The model with $n = 2$ is therefore used from now on.

Numerical values of the fitted parameters are given in Table 3. As a side note, the values of k_{app} for the exponential model (data not shown) are of the same order of magnitude as the values of

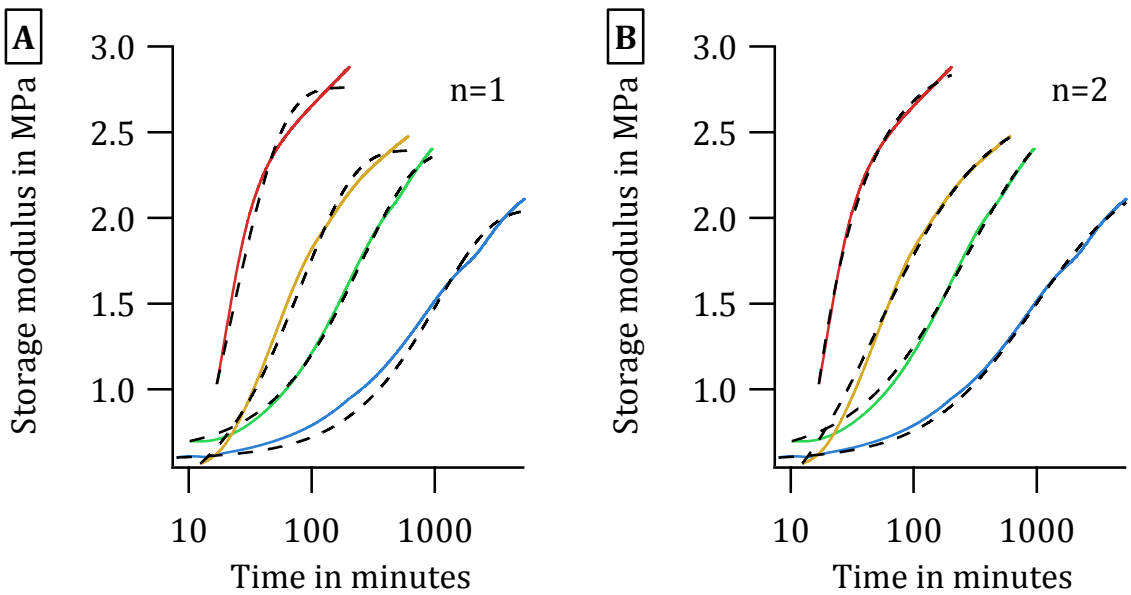

Figure 9: comparison of DMA experimental data with simple kinetic models. Colored plain lines are experimental data reproduced from Figure 8, dashed lines are fits from the model. A) Model with global order $n = 1$ using Eq. 7. B) Model with global order $n = 2$ using Eq. 8.

Table 3. The precise knowledge of the reaction order does not seem to be required to quantify the way the reaction proceeds with temperature. Fitted values from Table 3 may be used in an Arrhenius model in order to extract the rate dependence with temperature:

$$k_{\text{app}} = A \exp(-E_a/RT) \qquad \text{Eq. 9}$$

where A is an exponential prefactor, E_a is the activation energy of the reaction, R is the perfect gas constant and T is the absolute temperature. In Figure 10, **the Arrhenian plot confirms the thermally-activated aspect of the second curing reaction. A linear regression returns a value for the activation energy of** $E_a = 71 \pm 19$ kJ/mol with a 95% confidence interval. This is in complete agreement with values from the literature since the screening of several publications on similar systems yields an average value of 73kJ/mol with standard deviation of 10kJ/mol [4–12].

Now that the temperature dependence of our reaction is quantified, the kinetic law may be used to predict the extent of reaction for specific conditions of heating time and temperature. The extent of reaction $\chi_T(t)$ for a given temperature T and a heating time t is defined as follows:

T (°C)	E'_∞ (MPa)	$10^4\ k_{\text{app}}$ (MPa^{-1} min^{-1})
80	2.4	6.10
100	2.9	17.1
125	2.7	73.7
150	3.0	342

Table 3: numerical values of the fit parameters for the model of global order $n = 2$. t_0 and E'_0 are fixed to experimental values so that the first points of the fitted and experimental curves match. Graphic result of the fit is shown in Figure 9-B.

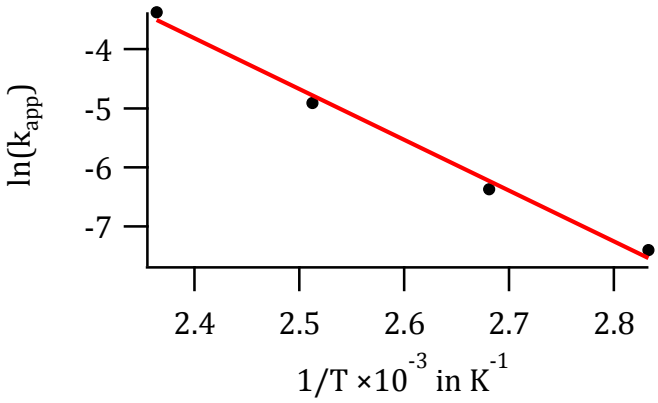

Figure 10: Arrhenius plot using fitted parameters from Table 3. The red line is a linear fit ($y = a + bx$) that gives $a = 16.816 \pm 5.99$ and $b = 8591 \pm 2301$ (the plus or minus being 95% confidence interval)

$$\chi_T(t) = \frac{E'(t) - E'_0}{E'_\infty - E'_0} \qquad \text{Eq. 10}$$

Using Eq. 8, $\chi(t)$ may be rewritten as follows:

$$\chi_T(t) = 1 - \frac{1}{1 + \Delta E'_{\max} k_{\text{app}}(t - t_0)} \qquad \text{Eq. 11}$$

where $\Delta E'_{\max}$ is the maximum increase of storage modulus that is due to the second curing reaction. To evaluate the latter, we calculate the modulus of a hypothetic network that would only be crosslinked by the reaction of GMA and AA units. In the initial network, the average number of EA units between two reactive units may be estimated as:

$$N_{\text{GMA/AA}} = \frac{1}{x_{\text{GMA}}} = \frac{1}{x_{\text{AA}}} \qquad \text{Eq. 12}$$

where x_i is the molar fraction of component i in the initial formulation. In our case, $x_{\text{GMA}} = x_{\text{AA}} = 1.5\%$ so $N_{\text{GMA/AA}} = 67$. The corresponding Young modulus may then be estimated using the equation:

$$E = \frac{3\rho RT}{\mathcal{M}_0 N} \qquad \text{Eq. 13}$$

With ρ the density of the polymer and $\mathcal{M}_0$ the molar mass of the monomer. This gives a result of 1.4 MPa in our case at 25°C ($\rho = 1.11$ g/cm³ [13] and $\mathcal{M}_0 = 86$ g/mol). This value may then be used as $\Delta E'_{\max}$ to estimate $\chi_T(t)$ at various times and temperatures, as in Figure 11. From these predictions, it seems fairly obvious that **the temperature needs to be relatively high in order to get high conversion**. In the reference that was used to inspire this system, authors heated their samples for 1h at 150°C [1], which according to our study would ensure about 70% conversion in our system. At only 30°C less, such a conversion would require more than 4 hours.

Based on this kinetic study, **a temperature of 150°C and a heating time of two hours are chosen** for the rest of the manuscript. This should be enough to ensure high conversion (>80%) of glycidyl and acid groups. These conditions are nevertheless quite harsh and may raise some issues and limitation in the preparation of prestretched structures.

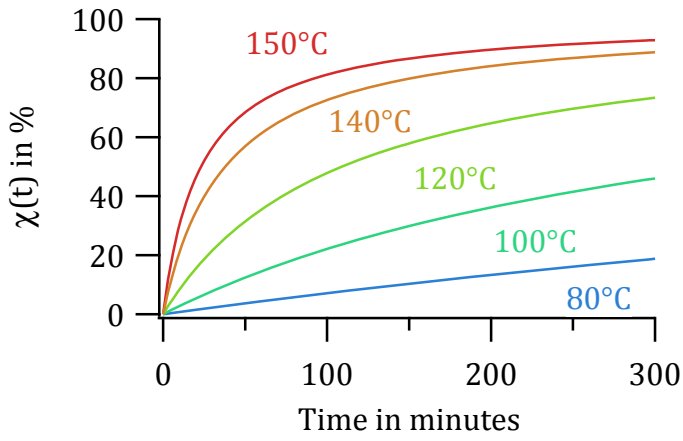

Figure 11: prediction of the extent of reaction at different heating times and for different temperatures using the kinetic model detailed above and fitted values of parameters based on experimental data.

3.2. Variation of the initial formulation

Different networks have been prepared with formulations detailed in the table below in order to probe the effect of the initial formulation on the mechanical properties of the single and dual-cured networks.

Compound	MA	AcOEt	AA	GMA	BDA	HMP	NEt3
MA_0.1/1.0	/	50 v%	1.0 m%	1.0 m%	0.1 m%	0.1 m%	1 m%
MA_0.2/0.5	/	50 v%	0.5 m%	0.5 m%	0.2 m%	0.1 m%	1 m%
MA_0.2/1.0	/	50 v%	1.0 m%	1.0 m%	0.2 m%	0.1 m%	1 m%
MA_0.2/1.5	/	50 v%	1.5 m%	1.5 m%	0.2 m%	0.1 m%	1 m%
MA_0.2/2.0	/	50 v%	2.0 m%	2.0 m%	0.2 m%	0.1 m%	1 m%
MA_0.3/1.0	/	50 v%	1.0 m%	1.0 m%	0.3 m%	0.1 m%	1 m%

The main difference with samples from the previous section is the presence of 50 vol% solvent. The generic sample name for the thermal system is MA_Y/Z with Y the amount of BDA (crosslinker) and Z the amount of GMA and AA. The latter are kept identical to remain in stoechiometric conditions.

3.2.1. Effect on small strain mechanical properties

First characterizations are performed by DMA in order to evaluate the influence of formulation on the small strain mechanical properties. The experiment is performed in three successive steps: first heating from -50°C to 100°C, then cooling back to -50°C and finally heating up again to 100°C.

Parameter	Frequency	Strain	Static force	Forcetrack	Heating rate
Value	1 Hz	0.1%	0.01N (0.1 N)	125% (150%)	5°C/min

For static force and forcetrack, values of 0.01 N and 125% are used for all samples except for MA_0.2/0.5 and MA_0.2/1.0 after heating where bracketed values are used (0.1N and 150%).

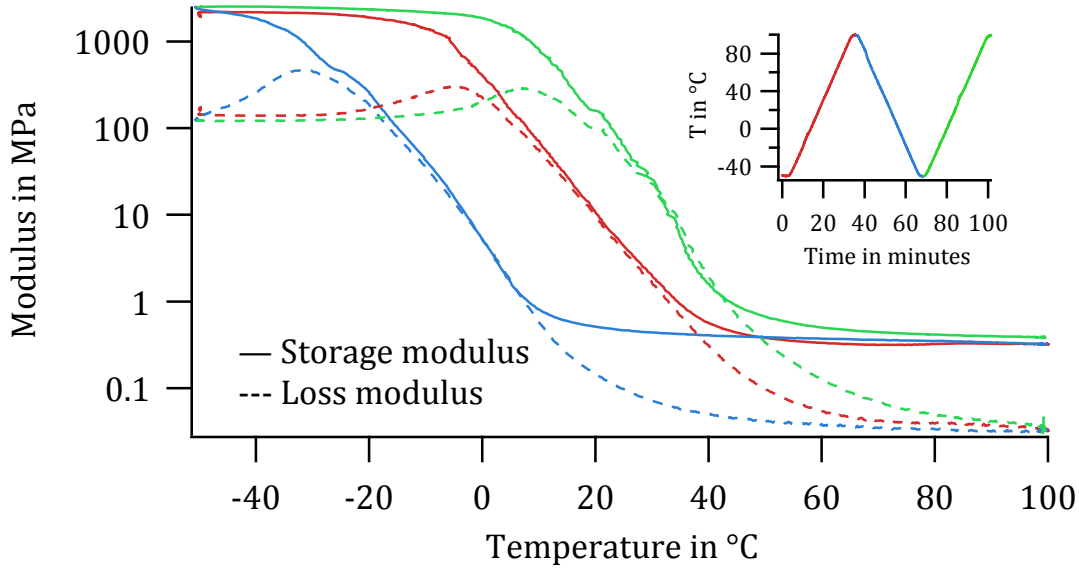

Figure 12: example of a DMA analysis on a single-cured network. Three ramps of temperature are perfromed, as shown in the insert. Plain lines are storage moduli and dashed lines are loss moduli. Each color is a temperature ramp.

An example of the viscoelastic spectrum is given Figure 12 for the sample MA_0.2/1.5. The viscoelastic profile that is obtained is typical from a viscoelastic crosslinked network: a sharp decrease in modulus is seen at the glass transition temperature, and loss modulus is below storage modulus on the entire range of temperature. A large hysteresis is visible when comparing the curves for the first heating and for the cooling: this may be explained by the fairly high heating rate that is used (5°C/min). Due to the non-instantaneous thermal conductivity, curves are shifted toward the right when heating and toward the left when cooling.

This however does not explain why curves for the first and second heating do not superimpose. This suggests that something happens in the material during the first heating phase. This increase in glass transition temperature could be due to the second curing reaction, although the maximum temperature of the heating cycle is quite low (100°C). This explanation is consistent with the slight increase in rubbery modulus at high temperatures (from 0.32 to 0.41 MPa on the example from Figure 12). An alternative explanation would involve the presence of polar components in the network structure, such as carboxylic acid groups from the AA units. The latter may tend to form clusters when the material is heated up. This would change the mobility of the neighboring network strands and thus increase the glass transition temperature.

In order to compare the different formulations, the almost constant region from the first heating stages between 70°C and 90°C are compared at a reference temperature. In practice, the storage modulus between these two temperatures is multiplied by T_0/T where T_0 is the reference temperature (25°C) and T is the actual temperature. This renormalization is used to take into account the expected linear dependence of modulus on temperature, as predicted by rubber elasticity. The normalized values are then averaged to give an average rubbery plateau modulus at 60°C.

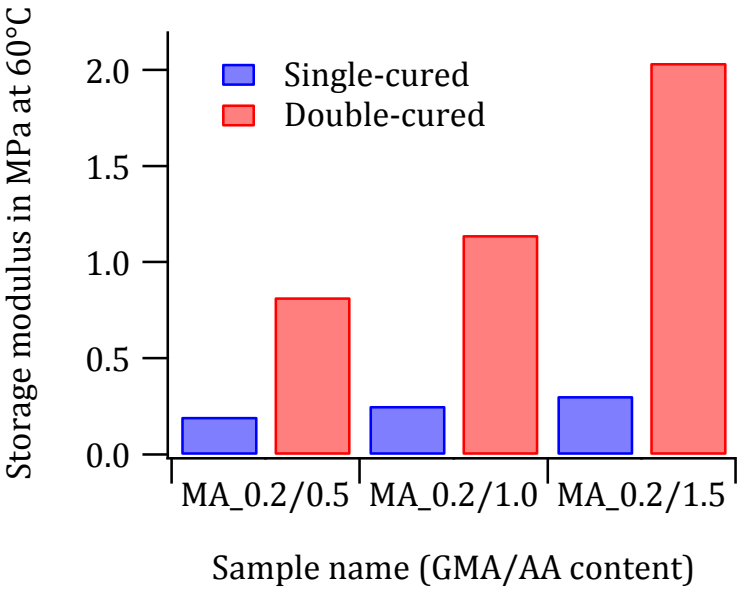

Figure 13: effect of GMA/AA content on the rubbery plateau value of the storage modulus. Values before (in blue) and after (in red) second curing are compared.

Figure 13 shows the comparison between samples with constant BDA content and increasing GMA/AA content. The first striking observation is that **the dual-curing mechanism is very effective and stiffness strongly increases after the second curing stage**. One would also expect to observe a constant modulus before the second curing (since the amount of initial crosslinker is the same) and an increasing modulus after second curing. This is effectively what is observed, the dual-cured modulus strongly depends on the amount of GMA/AA. Note that there is a slight increase in single-cured modulus with GMA/AA concentration. One possible explanation would be that there is some degree of reaction between GMA and AA occurring before the second curing step. This would be consistent with the kinetics of the reaction (roughly a second order) which predicts an increase in the initial rate of reaction with the initial concentration of reactants. Another plausible explanation is that the addition of GMA and AA in the reactive medium could influence the polymerization reaction because of the high polarity of acrylic acid. This could influence the way BDA is incorporated in the initial network structure, and thus influence the value of storage modulus in the single-cured state.

The effect of BDA content is shown in Figure 14. Trends are much harder to interpret this time. First, there seems to be a large variability in the modulus after the second curing although the amount of GMA/AA is the same in the three formulations. More surprisingly, the modulus before the second curing clearly decreases when the amount of BDA increases. This is the exactly the opposite of the expected behavior, since BDA is supposed to be the only crosslinker in the initial single-cured network. In simpler systems with only BDA used as crosslinker, the modulus follows a clear linear tendency when the quantity of BDA is increased from 1.45 to 5.81 mol% [14]. Once again, the details of the polymerization reaction could be different in the three formulations tested in Figure 14. In particular, the amount of extractible has not been measured and could be sensibly different between the three samples given the low levels of BDA that are used.

Beside the trends with respect to crosslinker concentrations, the most surprising feature from Figure 13 and Figure 14 is the **mismatch between the actual increases in modulus and expectations based on the levels of crosslinkers used in formulations**. The modulus in a simple elastomer network should scale linearly with the density of crosslinker molecules, which

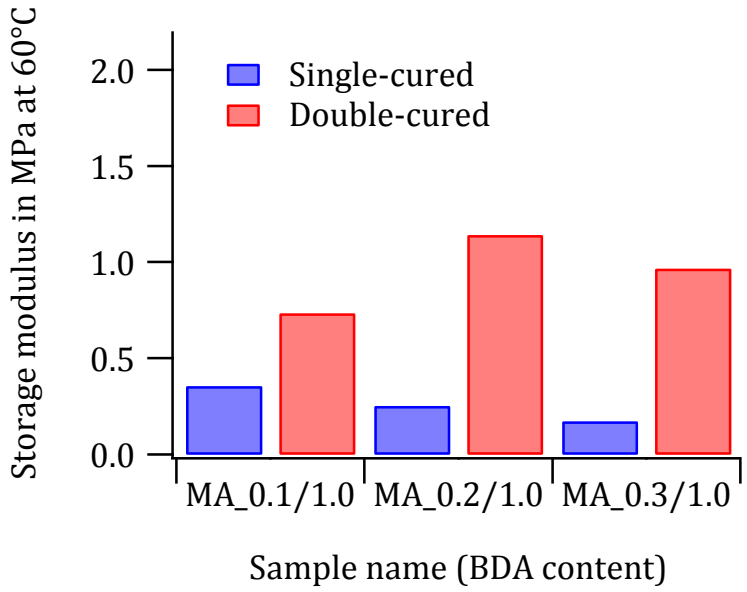

Figure 14: effect of BDA content on the rubbery plateau value of the storage modulus. Values before (in blue) and after (in red) second curing are compared.

in turn should scale with the concentration of crosslinker (assuming that the crosslinkers incorporate completely and statistically in the network). Since BDA is a bifunctional crosslinker, the modulus before the second curing should scale with $2x_{\mathrm{BDA}}$ where x_{BDA} is the molar concentration of BDA. After the second curing, the reaction between glycidyl and acid units adds crosslinks. The increase in modulus ΔE should thus scale with $x_{\mathrm{GMA}} = x_{\mathrm{AA}}$ (without the factor 2 since this time the crosslinker molecules are monofunctional and connect to each other). The increase in modulus can therefore be predicted as follows using only concentrations from the formulations:

$$\frac{E_{\mathrm{after}}}{E_{\mathrm{before}}} = 1 + \frac{\Delta E}{E_{\mathrm{before}}} = 1 + \frac{x_{\mathrm{GMA}}}{2\,x_{\mathrm{BDA}}} \qquad \text{Eq. 14}$$

Figure 15 compares graphically the experimental increase in stiffness with the predictions from Eq. 14. For all samples the markers are far from the unit line, meaning that **the formulation cannot be used as an indicator of the actual level of crosslinking in the samples**. In most cases though, the actual increase in crosslinking density seems to be higher than the expectation.

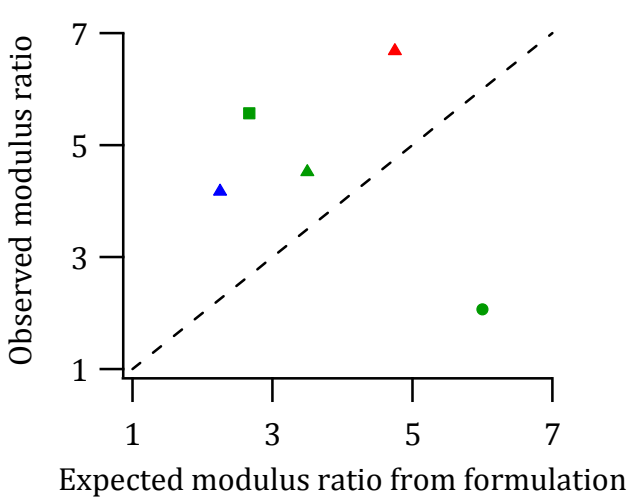

Figure 15: comparison of measured increase in stiffness during second curing with the expectation from the formulation (BDA versus GMA/AA level). Legend is given in the top right table: the color of the marker changes with GMA/AA level, while the shape changes with BDA content. Unit line is shown in dashed line.

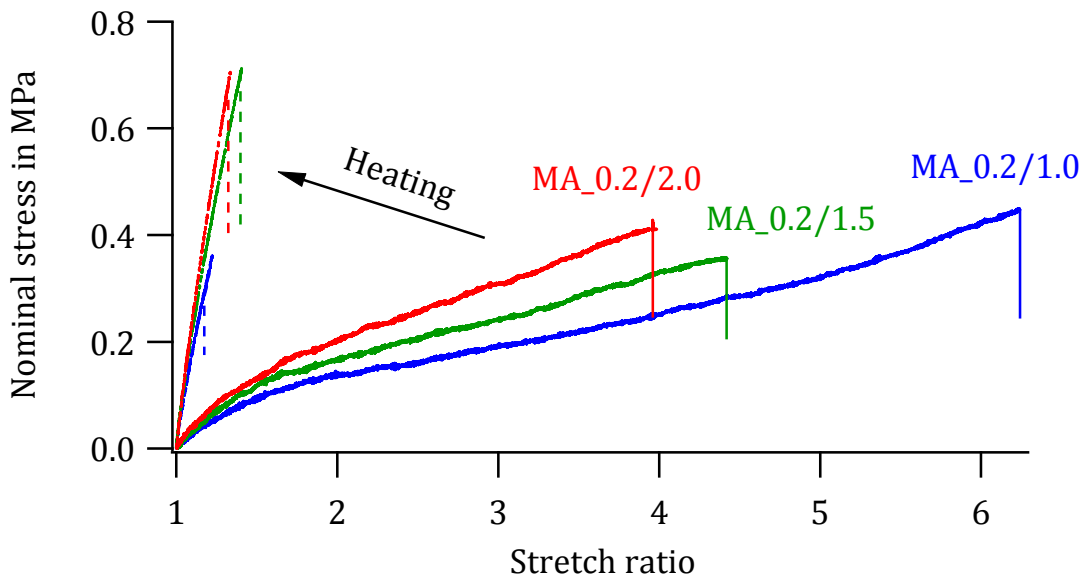

Figure 16: tensile test performed at 60°C and 100 µm/secon samples with increasing amounts of GMA/AA and same amount of BDA. Plain curves are samples before heating and dotted lines are samples after heating. Samples were testes at 60°C. Note that the curve for MA_0.2/1.0 after heating shows a premature failure that is probably due to a defect on the edge of the material.

In other words, the second curing reaction is more effective than expected and the increase in crosslinking density is larger than what the formulation indicates.

3.2.2. Effect on the uniaxial tensile response

In order to further characterize the materials, samples with similar formulations have been tested in uniaxial traction at 100 µm/sec and 60°C. Stress strain curves are presented in Figure 16 and numerical values of modulus and maximum extensibility are given in Table 4. **Tensile tests confirm the efficiency of the dual curing system** since heating induces a strong increase in modulus as well as a strong decrease in maximum extensibility. The same trends as before are observed in uniaxial traction: when the level of GMA/AA is increased, the modulus of the single-cured network increases weakly, and the modulus of the dual-cured sample increases steeply. The slight increase in modulus before the second curing is accompanied by a decrease in maximum extensibility, which goes in the direction of a larger effective crosslinking density when there is more second-curing comonomers.

Since two samples are common between the DMA experiment and the tensile test (MA_0.2/1.0 and MA_0.2/1.5), the corresponding moduli may be compared. Values are very close to each other before the second curing, with only 7% of difference at most. By contrast, values after the second curing are much higher in uniaxial traction than in DMA (68% and 23% larger for MA_0.2/1.0 and MA_0.2/1.5 respectively). The difference is too large to be due to viscoelasticity, since the value of the measured tan(δ) at 1 Hz at 60°C is 0.3 at most and the test in uniaxial traction is performed very slowly (0.4%/sec). Although samples tested in DMA and uniaxial traction have been prepared with the same formulation and same procedure, they have nevertheless been prepared in two separate batches and therefore the details of the second curing procedure might differ

Sample	Before heating		After heating	
	Modulus (MPa)	Extensibility (%)	Modulus (MPa)	Extensibility (%)
MA_0.2/1.0	0.27	387.7	1.92	(22.2)
MA_0.2/1.5	0.30	341.7	2.51	40.6
MA_0.2/2.0	0.47	293.1	2.63	33.6

Table 4: numerical values extracted from the tensile tests presented in Figure 16. Sample MA_0.2/1.0 after heating broke prematurely therefore maximum extensibility value is underestimated and presented in brackets.

slightly. For instance, the applied ramp of temperature is probably different. The thermal system is thus intrinsically variable, and comparisons between different batches of material should be considered with caution.

All in all, mechanical tests performed on samples with various levels of GMA and AA generally confirm the expected trends. **The final modulus of the filler network is primarily determined by the amount of second crosslinkers**. It appears however that the final modulus cannot easily be predicted from the formulation, which means that the second curing reaction may be more efficient than expected. As a result, it is important to test several formulations to find out which one is actually compatible with the double network strategy aimed in this study.

3.2.3. Effect on swelling ratio

Swelling ratio is a very important parameter to control in order to prepare double networks. The synthesis of the matrix network requires to swell the filler network in a bath of monomer. The level of swelling determines the degree of isotropic prestretching of the filler network chains, which determines the toughening effect of the double network structure according to previous studies [14–16].

Dual-cured samples are thus placed in vials containing ethyl acrylate stabilized with 10-20 ppm MEHQ. Samples are weighed regularly to track the increase in mass with time. The mass swelling ratio is then calculated as follows:

$$Q_{mass} = \frac{m_{swollen}}{m_{initial}} \qquad \text{Eq. 15}$$

Results of swelling ratio measurement are shown in Figure 17. A first observation is that **the swelling ratio reaches its equilibrium value within experimental error margin in 2 hours**. This means that the original protocol for the preparation of double networks [14] is fully applicable and that the kinetics of swelling should not be an issue for the preparation of dual-cure double networks. Comparison of values of equilibrium swelling ratios shows a very clear trend with the amount of GMA and AA. The larger the GMA/AA content, and the lower the equilibrium swelling ratio. This is in complete agreement with previous observations on mechanical properties, stiffer materials being associated to lower swelling ratios. This confirms that the amount of GMA/AA in the formulation is a major lever to control the final average mass between crosslinks. When the BDA content is varied however, the change in equilibrium swelling ratio is

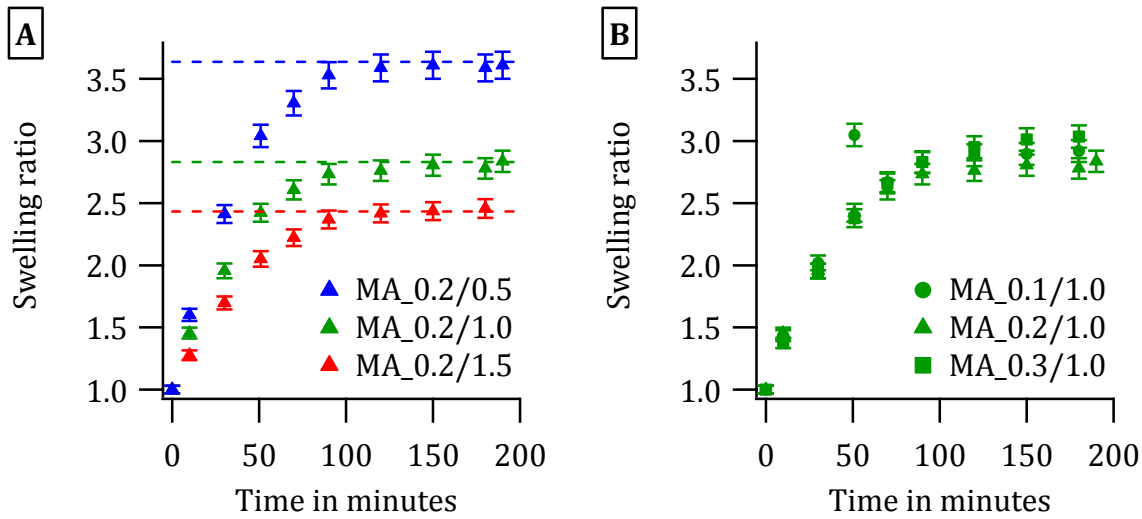

Figure 17: mass swelling ratio after second curing in ethyl acrylate. Different formulations are compared with either increasing amount of GMA/AA (A) or BDA (B). Dashed lines are equilibrium values after 3 days. Error bars are 3% of displayed values. The isolated circle in the right figure is an outlier probably due to unremoved excess liquid on the surface of the sample during weighing.

very narrow. This is once again in agreement with previous DMA results where no clear effect of BDA content could be identified on dual-cured networks.

Finally, one can calculate the estimated polymer fractions in the swollen system using equilibrium values of swelling ratios (the polymer fraction is simply the inverse of mass swelling ratio). Table 5 shows the numerical values, which corresponds to the filler network fraction that would be obtained in double networks if the matrix network was polymerized (and assuming there would be no evaporation during the process). It appears that polymer fractions values are fairly high compared to previous networks used for double network structures. In comparison, the double network from Ducrot et al. shows the best mechanical reinforcement ($EA_{0.5}MA$) with a first network mass fraction of about 20% [14]. In Millereau et al., networks exhibit a "double network effect" when the filler content is roughly below 30% [16]. Therefore, **the only usable formulation for double network structures is probably MA_0.2/0.5**. Future investigations should thus focus around this working point, since higher values for GMA and AA result in networks that do not swell enough to expect a clear double network effect.

3.3. Partial conclusion and identification of a working point formulation

This preliminary study on unprestretched filler networks confirms that the strategy of using the condensation reaction of GMA and AA catalyzed with NEt_3 is an effective dual-curing system. It indeed yields materials that are compatible with the multiple network toughening strategy, provided the right formulation is chosen. A kinetic model shows that the reaction should be completed within 2 hours at 150°C. Although these conditions are quite extreme for acrylic elastomers, they ensure a large conversion of the second curing reaction and a significant increase in modulus. Tensile tests, dynamic mechanical analysis and swelling ratio measurements show

Sample	$Q_{mass,eq}$	ϕ_{mass}
MA_0.2/0.5	3.6	28%
MA_0.2/1.0	2.8	35%
MA_0.2/1.5	2.4	41%
MA_0.1/1.0	2.9	34%
MA_0.3/1.0	3.1	33%

Table 5: values of equilibrium swelling ratios and polymer mass fractions for various formulations.

that the amount of GMA and AA in the formulation is the primary lever to tune the properties of the filler network. As expected, increasing the concentration of GMA and AA results in a decrease in swelling ratio and an increase in stiffness.

All in all, the best candidate for a future double network preparation is the formulation based on 0.5 mol% GMA and AA, 0.2 mol% BDA, 0.1 mol% HMP and 1 mol% NEt_3. This formulation yields networks that swell enough to possibly observe double network effects, and with a significant increase in modulus and decrease in maximum extensibility. Formulations with higher GMA/AA contents may nevertheless be used to increase the final stiffness of the material and see the effects on prestretching.

4.Study of the UV system

For the UV system, the initial network is prepared using the generic formulation presented in the table below.

Compound	EA	AcOEt	BDA	HMP	ALA
Role	Monomer	Solvent	Crosslinker	Initiator	Comonomer
Quantity	/	50 v%	0-0.2 m%	0.01-0.1 m%	1-3 m%

The quality of the initial synthesis is assessed by calculating the ratio between the final mass of the dry material and the maximum theoretical mass given by the formulation:

$$\eta = \frac{\text{mass of the dry sample}}{m_{\text{EA}} + m_{\text{BDA}} + m_{\text{HMP}} + m_{\text{ALA}}} \approx \frac{\text{mass of the dry sample}}{m_{\text{EA}} + m_{\text{ALA}}} \qquad \text{Eq. 16}$$

For simplicity this parameter is called "yield" although it is not rigorously the yield of the polymerization reaction (an estimation of the actual yield should take into account the evaporation of the monomer over the 2h irradiation period).

In this part, the impact of formulation is studied in a way similar to that of the thermal system.

4.1. Effect of crosslinker content

First, samples with same ALA and HMP contents (3% and 0.1% respectively) are compared in uniaxial tension at 500 µm/sec (see Figure 18). **The second curing is associated to a significant increase in modulus and decrease in strain at break**, which is entirely consistent with the addition of many crosslinks with the reaction of allyl groups together. Besides, dual-cured samples show almost no difference with the amount of BDA in formulation. This is consistent with the fact

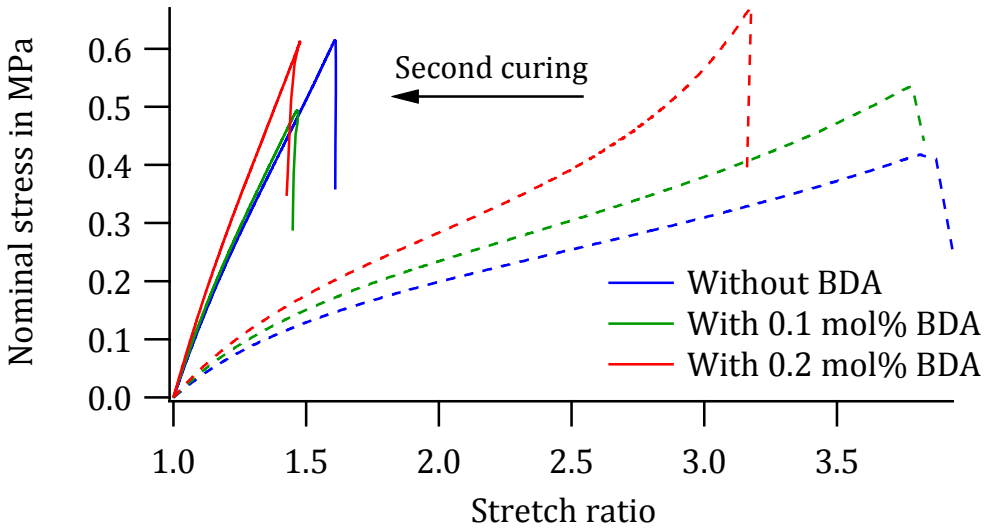

Figure 18: tensile test at 500µm/sec on samples that differ by their concentration in BDA. Dotted lines are single-cured samples, plain lines are dual-cured samples. HMP and ALA contents are similar for the three sets of samples (respectively 0.1% and 3%)

that after the second curing reaction, crosslinks due to BDA are in large minority compared to the ones due to ALA. The stiffness of the samples before and after the second curing is also consistent with the levels of BDA that are used, the more BDA is used and the stiffer the sample.

This first comparison shows that the synthetic method is fairly reliable in the sense that the mechanical properties agree with the formulations that are used. More interestingly, it shows that samples without BDA can be prepared and dual-cured. This means that some of the ALA groups react on both sides in the first step, giving crosslinked materials even if no diacrylate crosslinker is used.

According to the requirements defined in 1.1, as many crosslinks as possible should be added in the second step of the dual-cure system in order to ensure as large a prestretching as possible. This means that the softer the material in the beginning the better. Therefore, formulations without BDA are of practical interest. As a result, **all following formulations omit BDA and only use ALA as both first-stage and second-stage crosslinker**.

4.2. Effect of initiator content

4.2.1. On the initial network polymerization

As previously explained, reacting ALA on both sides in the initial synthesis gives the possibility to reduce the initial amount of crosslinks by using no BDA in the initial formulation. In this subpart, we envision to further soften the initial networks by reducing the amount of initiator. Since initial crosslinks are due to the reaction of some allyl groups, maybe reducing the amount of initiator could reduce the amount of bireacted groups.

Starting from a formulation with no BDA, 2 mol% ALA and 0.1 mol% HMP, the quantity of HMP is reduced down to 0.01 mol% and the change in mechanical properties is followed (see Figure 19). As expected, lower initiator concentrations are associated with lower moduli and larger extensibilities. After the second curing, mechanical responses are essentially the same which is consistent with the fact that the same amount of ALA is used for the three samples.

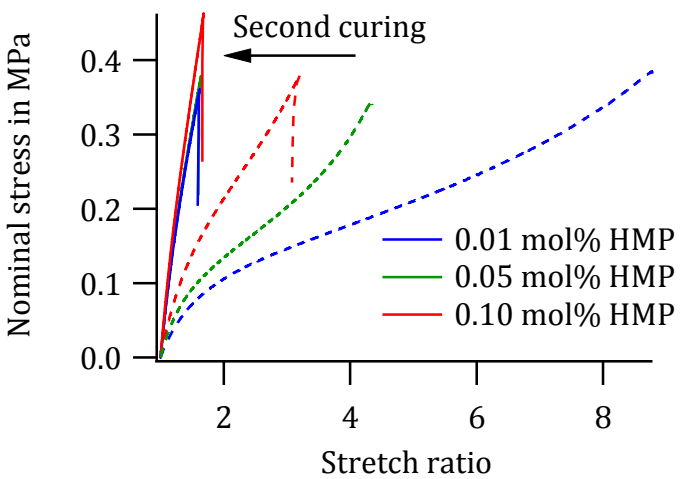

Figure 19: tensile test response at 0.5 mm/s of samples with 2 mol% ALA and various amounts of ALA, before and after second curing, in dotted and plain lines respectively.

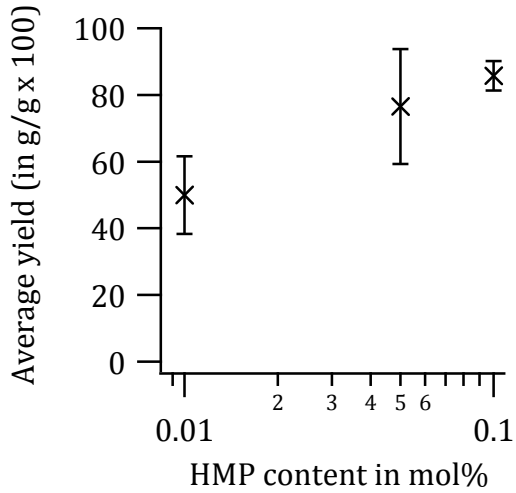

Figure 20: average estimated yield of the polymerization reactions with 2 mol% ALA and various amounts of HMP. Error bars are the standard deviations of the various synthesis performed with identical formulations.

The average yield of the polymerization reaction is plotted in Figure 20. It seems clear that **lowering the initiator concentrations results in a significant decrease in reaction yield**. Consequently, less material will be available for further mechanical testing and less control may be expected on the actual composition of the samples. For these reasons, HMP concentration will be fixed at 0.1 mol% in the rest of the chapter.

4.2.2. On the second curing process

Until now, the infiltration of the UV initiator prior to the second UV irradiation step has been presented as neutral for the properties of the network. It turns out that this is only an approximation, as presented in Figure 21. In this experiment, the shape of the stress-strain curve of a sample with a standard formulation (no BDA, 0.1 mol% HMP and 3 mol% ALA) is followed throughout the second curing process.

The infiltration step is associated to a small but finite increase in modulus (going from 0.38 to 0.45 MPa). Also, the shape of the curve close to the fracture point changes, with an increase of stress that is more pronounced for the infiltrated sample. This feature is even more visible when the reduced (or Mooney) stress is plotted, as in the insert of Figure 21. Strain-hardening is thus much more pronounced after infiltration.

These differences could be due to a beginning of reaction before irradiation. Swelling by acetone significantly increases the mobility of the chains in the network which eases the reaction between residual reacting groups. Besides, UV initiator molecules are reactive and can be triggered by UV light from the environment. The moderate increase in modulus however ensures that the reaction has not significantly changed the average properties of the material. In particular, the increase in stiffness and decrease in strain at break are still much more pronounced after UV irradiation.

4.3. Effect of allyl acrylate content

We now study formulations with no BDA, 0.1 mol% HMP and ALA contents from 1 to 2 mol%. The average yield of the reaction is given in Figure 22 and shows no significant difference when the concentration of comonomer is changed. Results of uniaxial traction are shown in Figure 23.

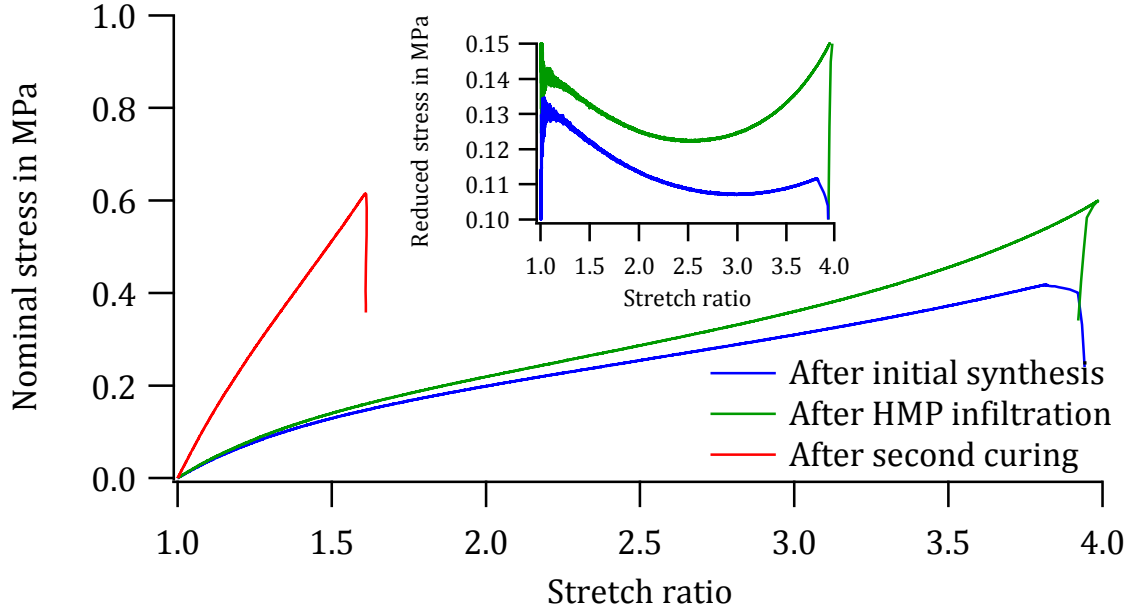

Figure 21: tensile tests at 500 µm on a sample containing no BDA, 3 mol% ALA, 0.1 mol% HMP at various stages of the dual-cure process. The blue curve is the sample after initial synthesis, green curve is after initiator infiltration and drying, red curve is after

All double-cured samples are in full agreement with the behavior expected from their formulation: the higher the ALA concentration, the higher the modulus and the lower the maximum extensibility. Singly-cured samples have tensile responses that are more scattered. Except for the 1 mol% that is notably softer, all samples have more or less the same stress-strain curve. Possibly the content in comonomer is not the right lever to tune the properties of the material in between the first and second-curing steps. It also indicates that the extent of reaction of allyl groups in the first stage cannot easily be controlled. The rigidity of the sample after the initial synthesis is thus expected to be somewhat variable.

In order to further analyze the data, values of Young's moduli E (i.e. slope at small strain) are measured and converted into number of monomers between crosslinks using the basic laws of rubber elasticity (see chapter 1):

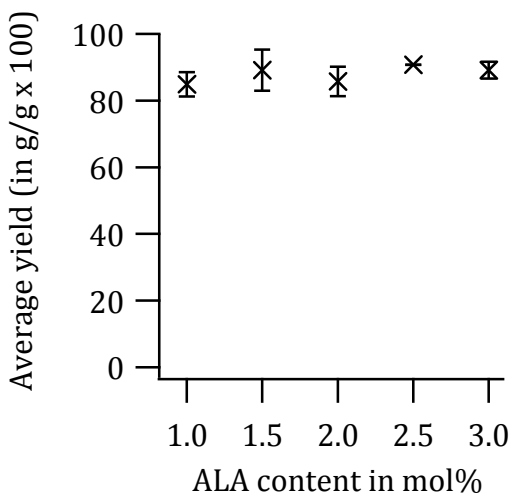

Figure 22: average estimated yield of the polymerization reactions with 0.1 mol% HMP and various amounts of ALA. Error bars are standard deviations. 2.5 mol% ALA was tested only once thus no error bar could be associated.

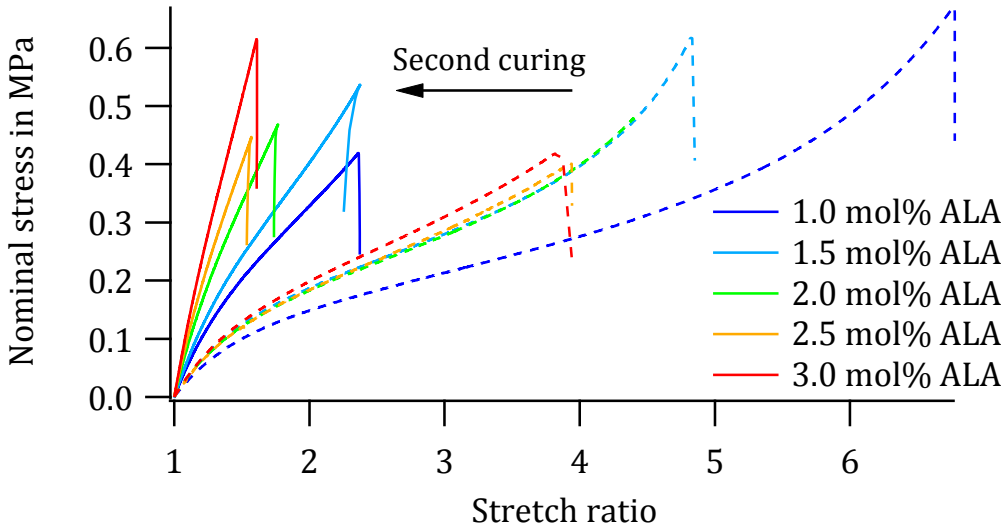

Figure 23: tensile tests at 0.5mm/s on samples with 0.1 mol% HMP and various ALA contents. Dotted and plain lines are single and dual-cured samples respectively.

$$N_x = \frac{3\rho_{\mathrm{PEA}}RT}{\mathcal{M}_0 E} \qquad \text{Eq. 17}$$

where ρ_{PEA} is the density of poly(ethyl acrylate) (1.11 g/cm³ [13]), RT is the perfect gas constant times the absolute temperature (298K) and $\mathcal{M}_0$ is the molar mass of ethyl acrylate (100.12 g/mol).

Defining ξ as the amount of bifunctional crosslinkers that have reacted and given an elastically active crosslink, ξ and N_x may be linked fairly straightforwardly with $N_x = 1/2\xi$. Note that ξ is then expressed in mol% with respect to the amount of monomer. Using Eq. 17, one can thus estimate the values of ξ before and after the second curing step from the measurement of Young moduli:

$$\xi = \frac{E\mathcal{M}_0}{6\rho_{\mathrm{PEA}}RT} \qquad \text{Eq. 18}$$

ξ may then be compared to the amount of crosslinker used in the formulation, yielding the parameter Ξ:

$$\Xi = \frac{\xi}{x_{\mathrm{ALA,\ from\ formulation}}} \qquad \text{Eq. 19}$$

Ξ may be interpreted as the efficiency of the crosslinker. In other words, a fraction Ξ of all crosslinkers initially in the formulation eventually leads to an elastically active crosslink.

Table 6 gives the values of ξ and Ξ parameters for samples tested in Figure 23. **Before the second curing, ξ is almost constant around 0.2%**. This indicates that the formulation does not have a large influence on the properties of the single-cured material. This result is not really surprising, the crosslinking reaction is believed to be limited by the amount of initiator rather than by the quantity of crosslinker that is used in the first stage. Remember that in between the first and

ALA content	Before second curing			After second curing		
	E (MPa)	ξ (mol%)	Ξ (%)	E (MPa)	ξ (mol%)	Ξ (%)
1.0%	0.31	0.19%	19%	0.56	0.34%	34%
1.5%	0.37	0.23%	15%	0.65	0.39%	26%
2.0%	0.35	0.21%	11%	0.89	0.54%	27%
2.5%	0.32	0.19%	7.7%	1.05	0.64%	26%
3.0%	0.38	0.23%	7.7%	1.31	0.79%	26%

Table 6: estimation of the fraction of reacted ALA at each stage of the dual-curing process for increasing amounts of ALA in formulation. E is the Young modulus measured from tensile tests of Figure 23, ξ is the fraction of ALA comonomers that have reacted and given an elastically active crosslink. Ξ is the ratio between ξ and the amount of ALA used in the formulation and may be interpreted as the efficiency of the crosslinker.

second curing steps the free radical reaction is purposely stopped while there are some allyl groups remaining.

After the second curing, the increase in modulus is associated to an increase in ξ. The efficiency of the crosslinker Ξ ultimately reaches levels around 30%. For comparison purposes, the same analysis is performed using data from Etienne Ducrot's PhD [3] (see Table 7). Samples have been prepared with the same procedure, extractibles are reported to be less than 2w% thus ensuring complete conversion. Formulation table is as follows:

Compound	EA	Toluene	BDA	HMP
Role	Monomer	Solvent	Crosslinker	Initiator
Quantity	/	50 v%	1.45-5.81 m%	1.16 m%

Table 7 shows values of Ξ very similar to our system, with maximum values of crosslinker efficiencies close to 30%. In other words, less than one third of the initial crosslinker molecules actually gives an elastic strand in the final material. These low values of crosslinker efficiencies may appear surprising. However, in free radical polymerization, most of crosslinking molecules are incorporated in the initial stages of the reaction, mostly giving intramolecular crosslinks that are not elastically active [17]. Besides, large crosslinking densities may be linked to mobility issues during polymerization which would explain the decrease in Ξ values for large amounts of crosslinker.

Last but not least, we compare the reduced stresses σ_{red} of dual-cured samples with different ALA contents in Figure 24. As a reminder, reduced stress is the ratio between the nominal stress and $\lambda - 1/\lambda^2$ and should give a constant value for samples that are in full agreement with the affine

BDA content	E (MPa)	ξ (mol%)	Ξ (%)
1.45%	0.8	0.49%	34%
2.81%	1.2	0.73%	26%
5.81%	2.3	1.40%	24%

Table 7: ξ and Ξ parameters for samples from Ducrot's PhD thesis. Young moduli measurements originate from tensile tests performed at 0.5mm/s

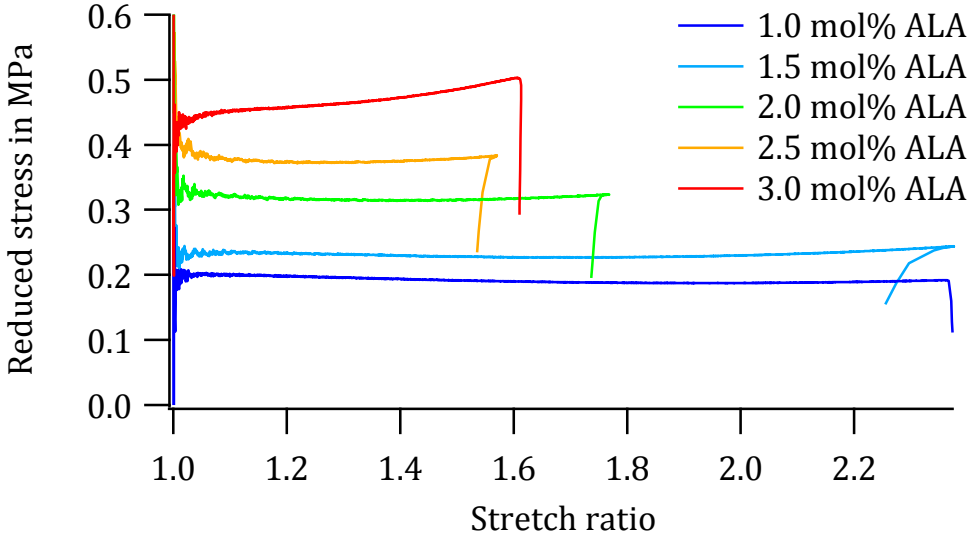

Figure 24: comparison of the shape of reduced stress curves for dual-cured samples with various amounts of ALA. The red curve (3 mol% ALA) features a visibly positive slope that is not expected from a classical affine behavior. Noise at very small strain is an artefact due to the division by zero.

model of rubber elasticity. In the case where entanglements cannot be neglected, $\sigma_{\mathrm{red}}(\lambda)$ becomes a decreasing function at small values of λ. At large deformations, the limit of extensibility of the chains may lead to an increase in reduced stress that is due to a strain-hardening phenomenon. In Figure 24, samples with ALA contents of 1 to 2.5% show a classical behavior of well-crosslinked and weakly entangled elastomers: reduced stress is almost constant, slightly decreasing and show an upturn at stretch ratios close to failure. The 3% curve however is strikingly different and increases at all values of λ. This unusual behavior may be due to the presence of a significant amount of very short chains that are close to their maximum extensibilities even when no strain is applied. Remember that no prestretching is applied here, thus this change cannot be due to an effect of molecular orientation. This implies that **dual-curing is not neutral in terms of network heterogeneity**. In other words, performing the crosslinking in two steps probably makes the material more heterogeneous and incorporates some short chains in the network architecture.

Now that the effect of formulation has been investigated, the next section will focus on the repeatability of the synthesis. Although a variability from sample to sample is neither unexpected nor crippling for the use of the UV system as dual-curing system, it is important to measure it in order to know whether the previously performed mechanical characterizations are indeed representative of networks with similar formulations or not.

4.4. The issue of sample-to-sample variability

In practice, it is not practically possible to do a tensile test on each sample before the second curing. The amount of material that is obtained at the end of the initial synthesis is not large and most of the material must be kept to perform the prestretching and double network synthesis that is presented in the following chapters. Some information may however be obtained from the measurement of the swelling ratio in acetone during the infiltration stage. Figure 25 shows the

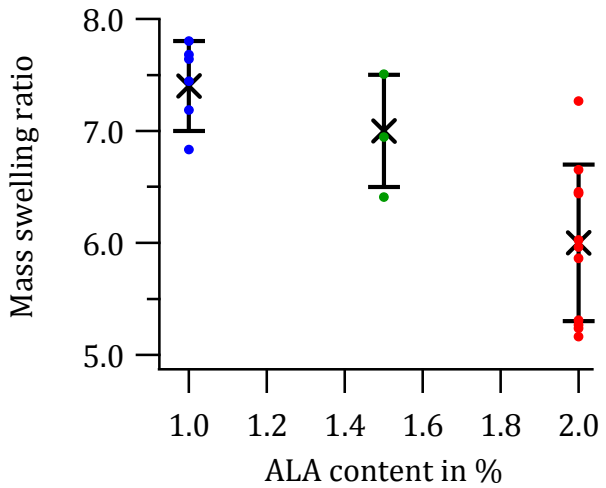

Figure 25: recap of mass swelling ratio measurements for various samples containing no BDA, 0.1 mol% HMP and 1-2 mol% ALA. Circles are experimental data points, the cross gives the average value for each formulation and the error bar represents one standard deviation.

values of swelling ratios for 20 samples with ALA contents ranging from 1 to 2 mol%. The first striking observation is the **large variability of swelling ratios, even at a given formulation**. There is nevertheless a global trend, the higher the ALA content and the lower the swelling ratio.

For a simple elastomeric network, swelling is the result of the competition between osmotic pressure that tends to stretch the chains and elasticity that opposes it. It should therefore be possible to use the measured values of swelling ratios to estimate the crosslinking density in the samples before the second curing [18]. To this intent, we define ϕ_{vol} the polymer volume fraction (i.e. the inverse of the volume swelling ratio), n_{solv} the number of moles of solvent molecules that come into the network and $\mathcal{v}_{\text{solv}}$ the molar volume of the solvent (equal to 47.74 cm³/mol for acetone). ϕ_{vol} and n_{solv} are linked by the equation

$$\frac{1}{\phi_{\text{vol}}} = 1 + \frac{n_{\text{solv}}\mathcal{v}_{\text{solv}}}{V_{\text{sample}}} \qquad \text{Eq. 20}$$

where V_{sample} is the unswollen volume of the sample.

On the one hand, the change in free energy due to the mixing of polymer and solvent is given by Flory-Rehner's equation [19]:

$$\Delta G_{\text{mix}} = RT\left[\ln(1-\phi_{\text{vol}}) + \phi_{\text{vol}} + \chi\phi_{\text{vol}}^2\right] \qquad \text{Eq. 21}$$

where χ is the Flory parameter that describes the energetic interactions between the polymer and the solvent. This parameter is tabulated for several polymer-solvent systems but can also be estimated from values of solubility parameters [13]:

$$\chi = 0.34 + \frac{\mathcal{v}_{\text{solv}}}{RT}\left(\delta_{\text{polymer}} - \delta_{\text{solvent}}\right)^2 \qquad \text{Eq. 22}$$

Solubility parameters values of 19.0 [20] for poly(ethyl acrylate) and 20.3 [13] for acetone yield a χ value of 0.39 at 25°C.

On the other hand, the change in elastic energy due to swelling may be written as follows:

$$W = \frac{1}{6} E V_{\text{sample}} \left(\lambda_x^2 + \lambda_y^2 + \lambda_z^2 - 3\right) = \frac{1}{2} E V_0 \left(\phi_{\text{vol}}^{-2/3} - 1\right) \qquad \text{Eq. 23}$$

with E the Young modulus and λ_i the stretch ratio due to swelling in direction i. Isotropic swelling ensures $\lambda_x = \lambda_y = \lambda_z = \phi_{\text{vol}}^{-1/3}$. The change in free energy due to elasticity may therefore be calculated by deriving W with respect to n_{solv}:

$$\Delta G_{\text{el}} = \frac{\partial W}{\partial n_{\text{solv}}} = \frac{\rho R T \mathcal{v}_{\text{solv}}}{\mathcal{M}_0 \text{N}} \phi_{\text{vol}}^{1/3} \qquad \text{Eq. 24}$$

where ρ is the polymer density, $\mathcal{M}_0$ the molar mass of the monomer and N the number of monomer per elastic strand.

Equilibrium swelling is achieved when both changes in free energy compensate. The equilibrium polymer fraction ϕ_{vol} is therefore given by the equation:

$$\Delta G_{\text{tot}} = \Delta G_{\text{mix}} + \Delta \text{G}_{\text{el}} = RT \left[\ln(1 - \phi_{\text{vol}}) + \phi + \chi \phi_{\text{vol}}^2 + \frac{\rho \mathcal{v}_{\text{solv}}}{\mathcal{M}_0 \text{N}} \phi_{\text{vol}}^{1/3}\right] = 0 \qquad \text{Eq. 25}$$

This equation may be solved to obtain calculated values of Young modulus based on the measurement of swelling ratios:

$$\text{E} = -\frac{3RT}{\mathcal{v}_{\text{solv}}} \left(\frac{\ln(1 - \phi_{\text{vol}}) + \phi_{\text{vol}} + \chi \phi_{\text{vol}}^2}{\phi_{\text{vol}}^{1/3}}\right) \qquad \text{Eq. 26}$$

Calculated values of E are given in Table 8 for the three tested levels of ALA and compared to Young's moduli measured by uniaxial tensile test in Figure 26. **The agreement between the two methods is overall satisfactory**, except maybe for the 2.0 mol% content. It has to be remembered that only one sample was tested in tensile tests while swelling ratio measurements reveal a large variability in sample composition.

To sum up, although the UV system shows a large variability from sample to sample, the use of swelling ratio gives a way to estimate the modulus in the intermediate stage between the first and second curing step.

ALA content	Q_w (g/g)	ϕ_{vol} (in vol%)	E (MPa)
1.0%	7.4 ± 0.4	9.9 ± 0.5	0.31 ± 0.03
1.5%	7.0 ± 0.5	10.7 ± 0.9	0.36 ± 0.06
2.0%	6.0 ± 0.7	12.6 ± 1.5	0.51 ± 0.12

Table 8: measurement of average values of swelling ratios for three different ALA contents, and calculation of corresponding moduli based on Flory-Rehner theory of swelling.

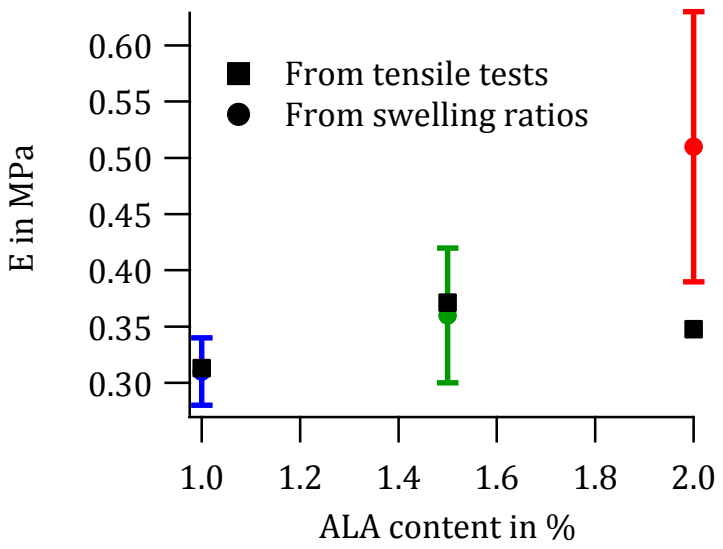

Figure 26: comparison of modulus values for three different ALA contents from tensile tests (via a fit a low strain) and from swelling ratio measurements (using Flory-Rehner's theory). Values from swelling are averaged values and error bars give one standard deviation.

5.Conclusions

As a first step toward double network structures using a permanently uniaxially prestretched filler network, the synthesis of two dual-curing systems has been developed. In both cases, an initial network is first prepared by UV polymerization using a formulation made of an acrylic monomer, an initiator and several additives. A second curing reaction is then activated using an external stimulus and monitored by studying the changes in elastic modulus.

The first system that has been studied involves the use of two comonomers (acrylic acid and glycidyl methacrylate) and a catalyst (triethylamine) used in one-pot. The resulting singly-cured networks are soft and extensible and can be stiffened by heating and triggering the condensation reaction of acid and glycidyl units copolymerized in the polymer backbone. An isostrain iso-thermal DMA experiment has been performed and confronted to a simple kinetic model. The model that suits the most our experimental data is a second-order model with an activation energy of 70 kJ/mol. Using this model, optimal second curing conditions have been defined (2h heating at 150°C).In these formulations, the parameter that is the easiest to play with is the quantity of second curing comonomers. Swelling experiments and measurements of the mechanical properties give an optimal formulation that should be compatible with the preparation of tough dual-cured double networks. With this formulation, the Young's modulus of the network typically increases from 0.20 to 0.82 MPa.

The second system that has been studied uses a much simpler formulation with only one comonomer (allyl acrylate). This comonomer bears two functional groups with different reactivities, which gives the possibility of performing curing in two steps. In order to make sure that all allyl groups react in the second step, the irradiation is performed with a much larger UV dose and is preceded by an infiltration of initiator. Use of BDA in the initial formulation has been found to be unnecessary and the decrease of HMP concentration has been found to be detrimental for the yield of the initial polymerization reaction. The main parameter that has been used to tune the mechanical properties of the filler network is the level of ALA in the initial formulation. Contrary to the thermal system, trends in terms of mechanical properties are in much better agreement with the expectations based on the formulation. Depending on the formulation, the singly-cured network shows a modulus ranging from 0.56 to 0.89 MPa, and the doubly-cured network from 0.86 to 1.5 MPa.

All in all, rational working formulations and second curing conditions have been determined to make isotropic networks for the two dual-curing systems under study. The properties of the unprestretched dual-cured filler networks are consistent with a potential use in a double network structure. Before addressing the double network materials, the next chapter focuses on the prestretching step more specifically and aims to predict the effect of a second curing carried out in the stretched state on the properties of the dual-cured filler network.

6.References

1. Park C-H, Lee S-W, Park J-W, Kim H-J. Preparation and characterization of dual curable adhesives containing epoxy and acrylate functionalities. React Funct Polym. 2013 Apr 1;73(4):641–6.

2. Gong J p., Katsuyama Y, Kurokawa T, Osada Y. Double-Network Hydrogels with Extremely High Mechanical Strength. Adv Mater. 2003 Jul 17;15(14):1155–8.

3. Ducrot E. Innovative tough elastomers: Designed sacrificial bonds in multiple networks [PhD thesis]. [Paris]: Université Pierre et Marie Curie; 2013.

4. Hamedani GH, Ebrahimi M, Ghaffarian SR. Synthesis and Kinetics Study of Vinyl Ester Resin in the Presence of Triethylamine. Iran Polym J. 2006;15(11):871–8.

5. Pal N, Srivastava A, Agrawal S, Rai JSP. KINETICS AND MECHANISM OF ESTERIFICATION OF MONOEPOXIES. Mater Manuf Process. 2005 Mar 16;20(2):317–27.

6. Srivastava A, Pal N, Agarwal S, Rai JSP. Kinetics and mechanism of esterification of epoxy resin with methacrylic acid in the presence of tertiary amines. Adv Polym Technol. 2005 Mar 1;24(1):1–13.

7. Wu S, Soucek MD. Kinetic modelling of crosslinking reactions for cycloaliphatic epoxides with hydroxyl- and carboxyl-functionalized acrylic copolymers: 1. pH and temperature effects. Polymer. 1998 Nov 1;39(23):5747–59.

8. Tanaka Y. Catalytic effects of substituted pyridines and quinolines on the reaction of phenyl glycidyl ether and benzoic acid. J Org Chem. 1967 Aug;32(8):2405–9.

9. Kakiuchi H, Tanaka Y. Study of Epoxy Compounds. VII. [1,2] Base-Catalyzed Reaction of Substituted Phenyl Glycidyl Ethers with Benzoic Acid. J Org Chem. 1966 May;31(5):1559–64.

10. Matějka L, Dušek K. Specific features of the kinetics of addition esterification of epoxide with the carboxyl group. Polym Bull. 1986;15(3):215–221.

11. Fiala V, Lidařík M. Reaction of glycidyl benzoate with acid in the presence of tertiary amines as the catalyst. Angew Makromol Chem. 1970 Jun 24;12(1):157–65.

12. Srivastava A, Agrawal S, Rai JSP. Kinetics of esterification of cycloaliphatic epoxies with methacrylic acid. J Appl Polym Sci. 2002 Dec 20;86(13):3197–204.

13. Mark JE. Physical properties of polymers handbook [Internet]. Vol. 1076. Springer; 2007 [cited 2016 Oct 28]. Available from: http://link.springer.com/content/pdf/10.1007/978-0-387-69002-5.pdf

14. Ducrot E, Chen Y, Bulters M, Sijbesma RP, Creton C. Toughening elastomers with sacrificial bonds and watching them break. Science. 2014;344(6180):186–9.

15. Ducrot E, Creton C. Characterizing Large Strain Elasticity of Brittle Elastomeric Networks by Embedding Them in a Soft Extensible Matrix. Adv Funct Mater. 2016;26(15):2482–92.

16. Millereau P, Ducrot E, Clough JM, Wiseman ME, Brown HR, Sijbesma RP, et al. Mechanics of elastomeric molecular composites. Proc Natl Acad Sci. 2018 Aug 28;201807750.

17. Hernández-Ortiz JC, Vivaldo-Lima E. Crosslinking. In: Handbook of Polymer Synthesis, Characterization, and Processing [Internet]. John Wiley & Sons, Inc.; 2013. p. 187–204. Available from: http://dx.doi.org/10.1002/9781118480793.ch9

18. Treloar LRG. The physics of rubber elasticity /: by L.R.G. Treloar. 3rd ed. Oxford : New York: Clarendon Press ; Oxford University Press; 2005. 310 p. (Oxford classic texts in the physical sciences).

19. Flory PJ, Rehner J. Statistical Mechanics of Cross-Linked Polymer Networks II. Swelling. J Chem Phys. 1943;11(11):521.

20. Barton AM. Handbook of Poylmer-Liquid Interaction Parameters and Solubility Parameters. Routledge; 2018. 794 p.

Chapter 3

Application of the dual-cure systems to the preparation of prestretched filler networks

Table of contents

1. Introduction 133
2. Preparation process 135
2.1. Initial network formulations 135
2.2. Prestretching and second curing 135
2.3. Problems encountered during the thermal second curing 135
3. Preparation of prestretched samples and measurement of prestretching 139
3.1. Presentation of the results 139
3.1.1. Measurement of final prestretching 139
3.1.2. Extent of prestretching 140
3.2. Comparison to Flory's model 140
3.2.1. Modelling the behavior of dual-cured networks 141
3.2.2. Comparison to experimental results 148
3.3. Additional mechanical characterization for the thermal system 152
4. Prospective: what to expect in a double network structure? 155
4.1. Description of the approach 155
4.2. Derivation of the model 156
4.2.1. General framework 156
4.2.2. Unprestretched case ($\Lambda^*=1$) 157
4.2.3. Prestretched case ($\Lambda^*\neq1$) 157
4.2.4. Application using experimental values 159
5. Conclusions 163
6. References 165

1.Introduction

In the previous chapter, two dual-curing systems have been designed and studied. The two systems differ by their chemistry and activation mode (temperature for the first one, UV light for the second one). They however both yield dual-cured filler networks with mechanical properties that are compatible with their use in a multiple network structure.

In order to incorporate a dose of anisotropy in a multiple network architecture, these dual-cured networks need to be stretched and dual-cured in the stretched state. This step was initially believed to be fairly trivial but turned out to be challenging and imposed some practical constraints. In a first part, the preparation of prestretched filler networks with its experimental issues is detailed.

Eventually, the dual-curing is indeed performed on stretched samples which results in materials that have a permanent uniaxial elongation. This situation has already been described in the literature and is the focus of several models and theories. In a second part, the prestretching is then measured and analyzed for both dual-curing systems. A model is used to predict values of final prestretching and is compared to the actual experimental data.

In a last part, a theoretical digression is proposed. Since the prestretched filler networks are to be used in multiple network structures as filler networks [1], it is interesting to put on paper the relevant physical parameters that are going to influence the behavior of these networks at large strains. Starting from Flory's network at small strain, an extension to large strains is proposed. This extended model gives an insight of what can be expected when the filler networks are incorporated in double network structure.

2. Preparation process

Information about chemicals, preparation and characterization processes have already been given in chapter 2.

2.1. Initial network formulations

For the thermal system, the generic formulation is as follows:

Compound	MA	AcOEt	AA	GMA	BDA	HMP	NEt3
Quantity	/	50 v%	0.5-1.5 m%	0.5-1.5 m%	0.2 m%	0.1 m%	1 m%

For the UV system, the generic formulation is as follows:

Compound	EA	AcOEt	BDA	HMP	ALA
Role	Monomer	Solvent	Crosslinker	Initiator	Comonomer
Quantity	/	50 v%	0 %	0.1 m%	1-2 m%

2.2. Prestretching and second curing

After the initial synthesis (and HMP infiltration step for the UV system), the initial network is cut in two parts. The first part is uniaxially extended to a stretch ratio of λ_{clamp} while the second one is left without manual prestretching. Both samples are dual-cured together by using the procedures described in the previous chapter. After unloading, the prestretched sample shows a permanent stretch ratio λ^* while the unprestretched one shows almost no change in dimensions. Figure 1 shows a schematic representation of the second curing process and illustrates the definition of the two stretch ratios that characterize the second curing process λ_{clamp} and λ^*.

The changes in dimensions are measured by printing dots on the surface of the materials and measuring the distance between them throughout the process. Measurement of distances is done by taking a picture of the sample along with a ruler and analyzing the image using the software ImageJ.

2.3. Problems encountered during the thermal second curing

As already stated in the previous chapter, heating for 2 hours at 150°C is pretty intense for acrylic elastomers. Beside the potential problem of thermal degradation, the material loses all kind of viscoelastic dissipation mechanisms this far away from its T_g. As a result, **the materials become very brittle and subject to the propagation of defects due to cutting when stretched and heated at the same time**. An example of this is shown in Figure 2, samples systematically break in the middle and no permanent prestretching is obtained after the second curing. Note that the

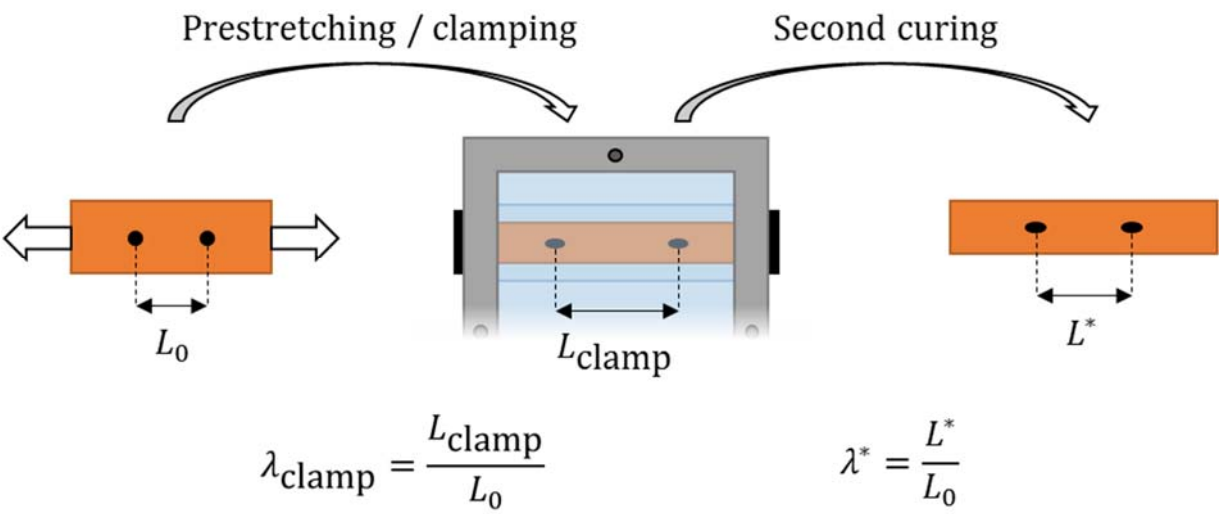

Figure 1: schematic representation of the dual-curing process in prestretched conditions and definition of relevant length scales.

failure does not initiate from the clamps, meaning that the problem cannot be solved by optimizing the clamping conditions.

The solution that has been found is to place the prestretched sample between two clean glass slides and apply pressure on the top slide. The idea behind this is to promote some adhesion between the stretched sample and the stiff glass slide in order to redistribute stress and avoid stress concentration around the side defects. A similar device has been used for the UV system in order to anticipate any problem of crack propagation, although for this system the second curing is performed at room temperature (see Figure 3). The use of glass slides works fairly well for clamped stretch ratios up to 3 approximatively. Up to this stretch ratio, the second curing proceeds without any visible problem, and permanently prestretched networks are obtained at the end of the process. Above $\lambda_{clamp} = 3$, the material usually breaks between the glass slides giving a very characteristic pattern shown in Figure 4.

This original fracture pattern has been investigated a little bit further using the thermal system. A sample with formulation MA_0.2/1.5 has been synthesized and prepared for second curing (see definition of sample notation in chapter 2). A video camera has been used along with a thermocouple to visualize the failure process. Heating stage is performed as usual on a clamped

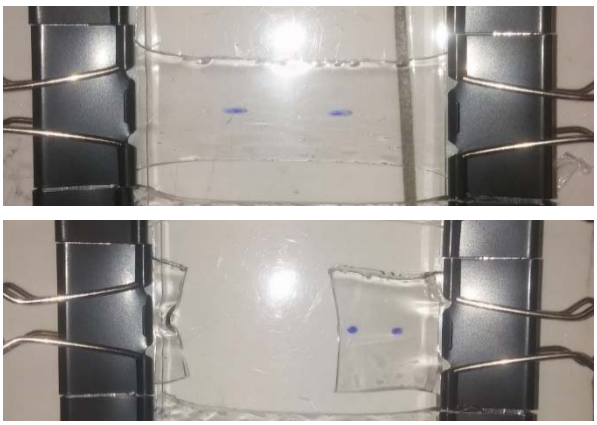

Figure 2: pictures of samples during the second curing process. Because of heating, the material becomes very brittle and side defects easily propagate into cracks. Top: picture of a sample before second-curing. Bottom: picture of a sample after second curing.

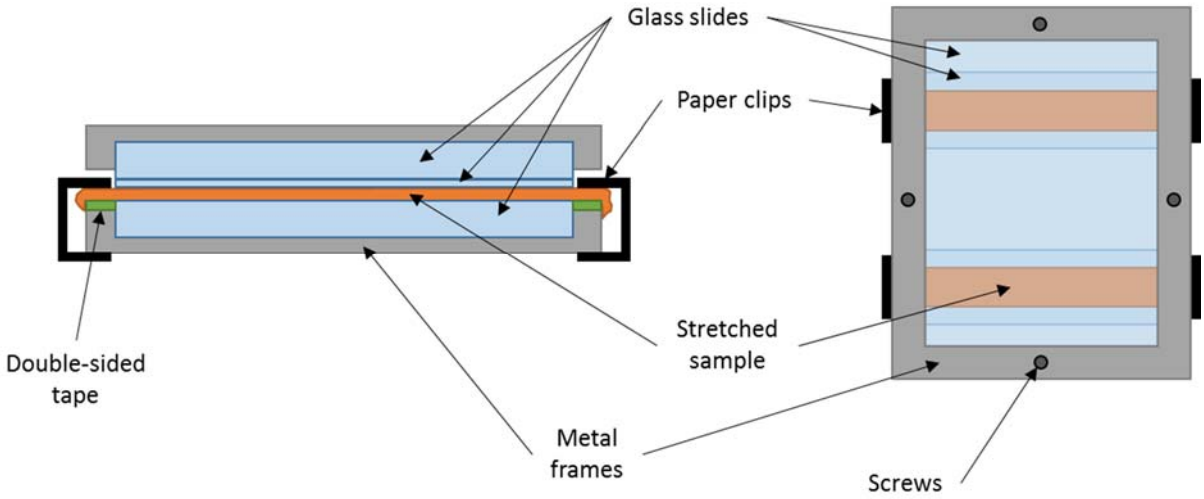

Figure 3: illustration of the device used for the dual-curing of the UV system. The device used with the thermal system is identical except that pressure on the top glass slides is applied using paper clips.

sample with $\lambda_{\text{clamp}} = 3.84$. Video frames of the moment when the sample fails are shown in Figure 5. A first useful information is that the sample actually fails around 90°C, while the sample heats up. Fracture is therefore not a direct result of the second curing reaction, since the latter mainly happens at higher temperature. Second, the failure process occurs from the edges, and propagates rapidly.

What happens is probably that the adhesion is not uniform and that some areas on the edge of the sample do not adhere well to the glass slide. Once a crack propagates from here, the sample detaches from the glass slide locally. The adhesion force is then not strong enough to keep the fractured sample in place so it slips back to its original length. The slippage could be circumvented by applying a larger pressure, and as a matter of fact this is done with the UV system where pressure is applied with screws instead of paper clips. With the device from Figure 3, even when the material breaks during second curing it stays in place. However, the sample rarely breaks only in one place, and even so it is often close to the middle of the sample so that the remaining parts cannot really be used as prestretched filler network. Therefore, for practical reasons, prestretching is normally limited to clamped stretched ratios below 3. Some rare points have been obtained above this limit, but they could not be reproduced.

Figure 4: Example of a constrained sample stretched to a large stretch ratio. Top: sample before second curing. Bottom: sample after second curing. In this specific example, the sample is MA_0.2/2.0 and clamped stretch ratio is about 3.5.

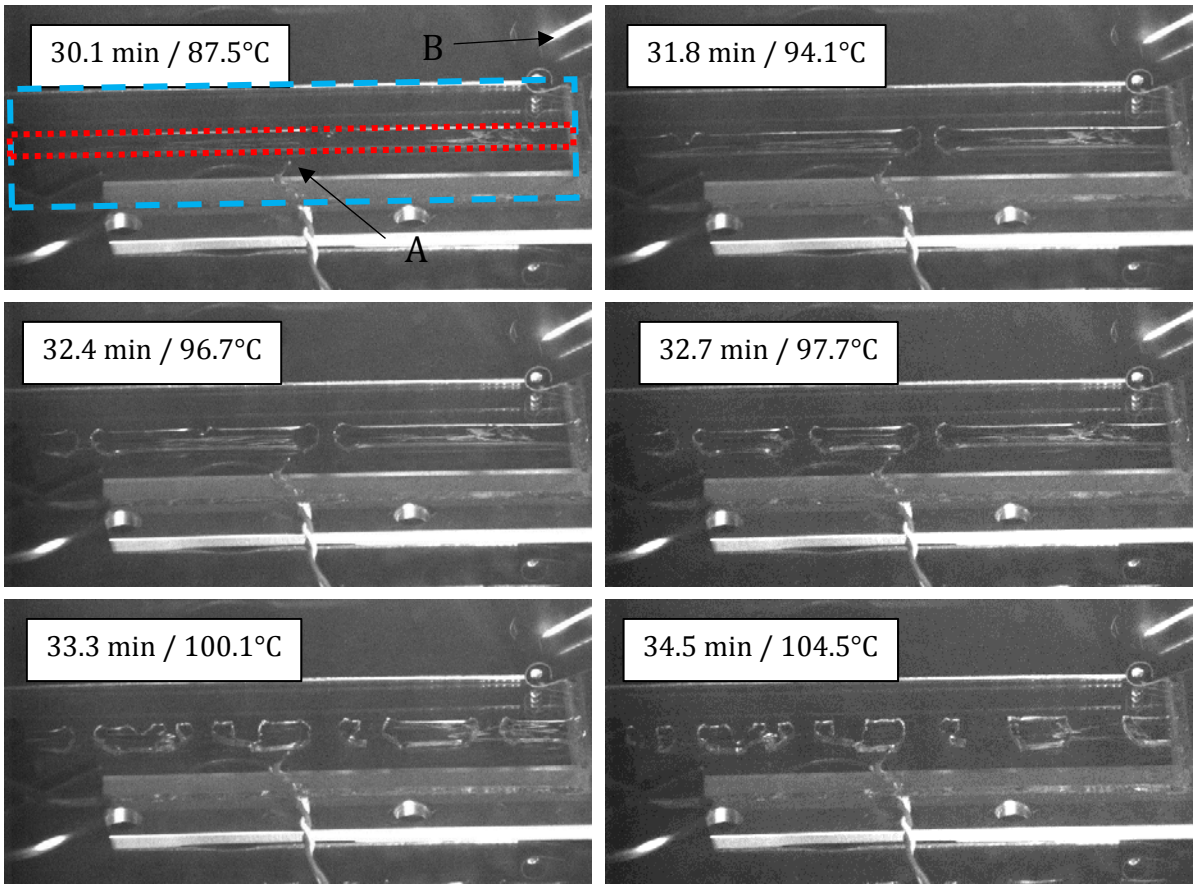

Figure 5: pictures taken during the heating phase in order to capture the moment when the overstretched sample fails. Time and temperature (measured with a thermocouple) are given for each picture. On the first picture, blue dahsed rectangle shows the edges of the top glass slide. Red dotted rectangle shows the edges of the stretched sample. A is the tip of the thermocouple (where the temperature is actually measured) and B is the paper clip to keep the sample compressed.

The other problem faced during the second curing is a **visible and significant change of colour**, as exemplified in Figure 4. Dual-cured samples using the thermal system are clearly yellow/brownish while single-cured samples are perfectly transparent. The UV system yields samples that are slightly yellow, but the colour is much less pronounced.

In the case of the thermal system, this phenomenon is probably due to the oxidation of the amine catalyst. The latter has been reported to yield brown coloured products in the industrial literature [2]. Another explanation is the possible oxidation of the crosslink formed by the reaction of glycidyl and acid units. In epoxy resins, the formations of carbonyl units in the chain has been reported to be the origin of yellowing [3]. For the UV system, oxidation should not occur since the second curing step is performed in the glovebox (and hence in inert atmosphere). Colour might come from the excessive degradation of initiator by UV light.

Despite its obvious character, this coloration problem has not been tackled. Regardless of its origin (amine or HMP degradation, chain oxidation, etc.), the color change should not affect the architecture of the network since it is probably not associated to chain scission. Moreover, the color does not seem to have any effect on the matrix network polymerization. In particular, extractibles and swelling stretch ratios have been found to be coherent with data collected on traditional double network elastomers.

3. Preparation of prestretched samples and measurement of prestretching

3.1. Presentation of the results

3.1.1. Measurement of final prestretching

First the results of the thermal system are presented. Values of λ_{clamp} and λ^* are compared for samples of two different compositions in Figure 6. λ^* **seems to increase with** λ_{clamp}, which is intuitive since the second crosslinking step links the preoriented chains together. When the structure relaxes, the final prestretch ratio λ^* is obviously smaller than λ_{clamp} and should increase with it. The more surprising fact is that this increase occurs in an almost-linear way.

More surprisingly, **the formulation does not seem to have a very high impact on the final stretch ratio**. In Figure 6, the two sets of markers follow the same trends whereas the level of GMA and AA for the second set is three times higher than in the first set. Care must however be taken with this comparison since the ranges of explored λ_{clamp} are not exactly the same for the two formulations.

Figure 7 shows the same graph as Figure 6 but for the UV system. Three different formulations are compared, varying the amount of ALA in the initial synthesis. The first striking observation is that **experimental data points are more scattered than in the thermal system case**. In particular, the formulation with 1.5 mol% ALA does not seem to follow a clear trend. For the two other trends however, it seems that for a given λ_{clamp} the final prestretching λ^* is higher when the level of ALA is higher.

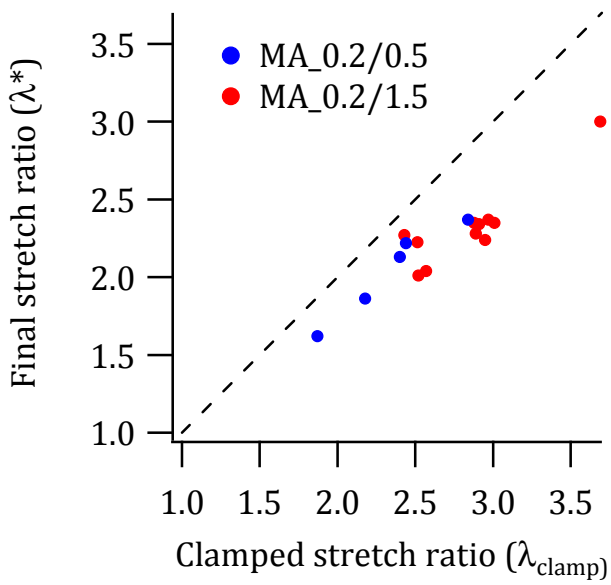

Figure 6: comparison of final stretch ratios for networks made from two different formulations and at various levels of clamped stretch ratio. Red points correspond to MA_0.2/1.5 and blue points correspond to MA_0.2/0.5. Dashed line is the unit line. Each data point corresponds to one tested sample.

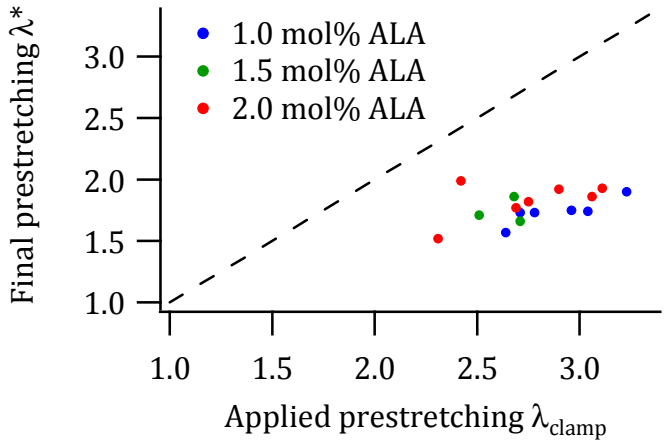

Figure 7: relationship between final and clamped stretch ratios for samples with different ALA contents that are dual-cured in the stretched state. Each data point corresponds to one tested sample.

The slope of the $\lambda^*(\lambda_{\text{clamp}})$ curve is actually visibly smaller in Figure 7 than in Figure 6, which indicates that in the UV case the final prestretching depends much less on the clamped stretch ratio than in the thermal case.

3.1.2. Extent of prestretching

The other immediate comparison that can be made with the thermal system is that the final degree of prestretching λ^* seems to be larger for the thermal system than for the UV system. A way to quantify this, is to calculate for both systems the extent of prestretching defined as follows:

$$\mathcal{P} = \frac{\lambda^* - 1}{\lambda_{\text{clamp}} - 1} \qquad \text{Eq. 1}$$

$\mathcal{P}$ may be seen as the orientation that is retained by the second curing process. It reaches 1 if the material does not retract after second curing and 0 if the material completely goes back to its original shape. Results are shown in Figure 8 and confrms the qualitative observations made earlier. The thermal system returns values of $\mathcal{P}$ that are significantly larger than the UV system. Also, The formulation does not really seem to impact the extent of prestretching. In the UV system however, a slight positive trend may be identified in the UV system, although the variability of the system alrealy identified in the previous parts induces large error bars.

3.2. Comparison to Flory's model

As already stated in the introduction, the preparation and study of permanently prestretched elastomers is not something new and has been extensively studied in the literature. The main theoretical framework is based on Flory's assumption of network superposition, and is recalled and compared to experimental data in this part.

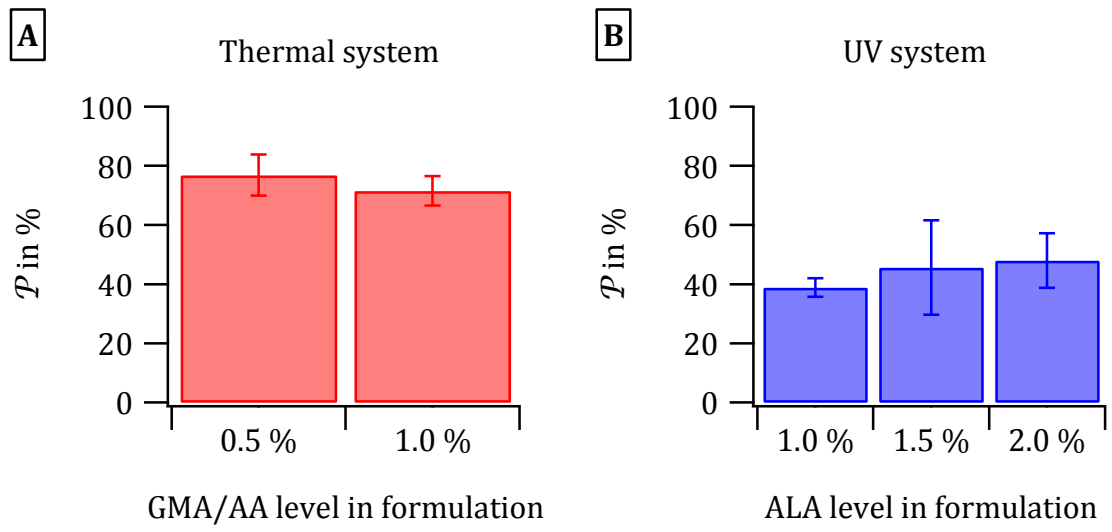

Figure 8: comparison of the extent of prestretching $\mathcal{P}$ for the two systems at different formulation levels. A) thermal system, B) UV system. Presented values are averages values and error bars are confidence intervals at 95%

3.2.1. Modelling the behavior of dual-cured networks

Basics of the model

As a reminder from chapter 1, the fundamental assumption behind Flory's model is that the addition of crosslinks during the second curing reaction is equivalent to superimposing another (virtual) network to the initial (real) network [4,5]. This additional network has a different crosslinking density and more importantly a different state of reference since it is at rest in the stretched state. Therefore, when the dual-cured network is unclamped, the initial network wants to go toward its reference position while the virtual network enters compression. The final equilibrium state is eventually reached when forces compensate. The stress that results of an additional stretch from this equilibrium position is then modelled as the superposition of the contribution of the first and second networks. The total crosslinking density is thus indeed the one of the dual-cured material.

In order to fix notations, ν_1 is the initial crosslinking density of the single-cured network. The Young modulus in the single-cured stage is $E_{\text{single-cured}} = 3\nu_1 kT$ in the frame of rubber elasticity. ν_2 is the crosslinking density that is added by the second curing step, so that the final modulus is $E_{\text{dual-cured}} = 3(\nu_1 + \nu_2)kT$. The clamped stretch ratio at the beginning of the dual-curing process is called λ_{clamp} and the final stretch ratio is noted λ^*. From this dual-cured state, an arbitrary deformation is applied and characterized by the three stretch ratios λ_x, λ_y and λ_z. The prestretched direction is arbitrary taken as the x-direction. The dual-curing system and network superposition principle from Flory's model are schematically represented in Figure 9. The additional $(\lambda_x, \lambda_y, \lambda_z)$ are applied taking the "dual-cured" situation as a reference position (last picture on the right in the red square).

The main assumption of Flory's model is that the two populations of crosslinks may be added linearly to obtain the change in free energy of the dual-cured network. Defining W as the strain

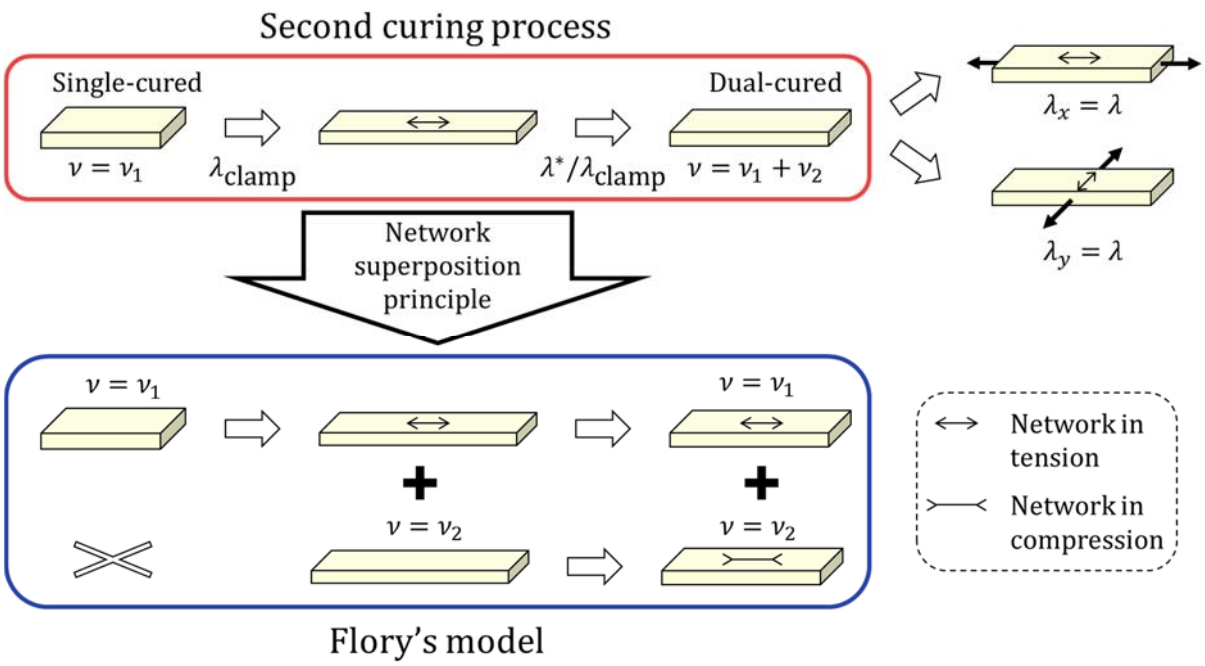

Figure 9: recapitulative schematics of the dual-curing process and network superposition principle from Flory's model. The dual-curing process is represented in the red square. After dual-curing (on the right of the red square), the material may be deformed either in the longitudinal direction (top case) or in the transverse direction (bottom case). The network superposition principle is illustrated in the blue square. The dual-curing process is modelled as the superposition of the initial network with crosslinking density ν_1 and a second virtual network with crosslinking density ν_2 that is added and at rest in the stretched situation. In the end, at equilibrium, the initial network is in traction while the virtual one is in compression. Double arrows represent the stretch state of the network: in traction when arrows point outward and in compression when arrows point inward.

energy density function, the network superposition principle gives the change in free energy when the dual-cured network is stretched from its original initial unclamped reference position:

$$W(\lambda_x, \lambda_y, \lambda_z) = W_1\left(\lambda_x\lambda^*, \frac{\lambda_y}{\sqrt{\lambda^*}}, \frac{\lambda_z}{\sqrt{\lambda^*}}\right) + W_2\left(\frac{\lambda_x\lambda^*}{\lambda_{\text{clamp}}}, \lambda_y\sqrt{\frac{\lambda_{\text{clamp}}}{\lambda^*}}, \lambda_z\sqrt{\frac{\lambda_{\text{clamp}}}{\lambda^*}}\right) \qquad \text{Eq. 2}$$

where W_i is the strain energy density associated to the network i. Eq. 2 is the superposition of a first network prestretched by a factor λ^* in the x-direction and a second network compressed by a factor $\lambda^*/\lambda_{\text{clamp}}$ in the x-direction.

Let us first consider a uniaxial tensile test performed in the prestretched direction. In this case, symmetry and volume conservation ensures $\lambda_y = \lambda_z = 1/\sqrt{\lambda_x} = 1/\sqrt{\lambda}$. Eq. 2 therefore becomes:

$$W^{\parallel}(\lambda) = W_1\left(\lambda\lambda^*, \frac{1}{\sqrt{\lambda\lambda^*}}, \frac{1}{\sqrt{\lambda\lambda^*}}\right) + W_2\left(\frac{\lambda\lambda^*}{\lambda_{\text{clamp}}}, \sqrt{\frac{\lambda_{\text{clamp}}}{\lambda\lambda^*}}, \sqrt{\frac{\lambda_{\text{clamp}}}{\lambda\lambda^*}}\right) \qquad \text{Eq. 3}$$

In the transverse direction, the stretch λ is no longer applied in the same direction as the prestretching. Eq. 2 thus becomes

$$W^{\perp}(\lambda) = W_1\left(\frac{\lambda^*}{\sqrt{\lambda}}, \frac{\lambda}{\sqrt{\lambda^*}}, \frac{1}{\sqrt{\lambda\lambda^*}}\right) + W_2\left(\frac{\lambda^*}{\lambda_{\text{clamp}}\sqrt{\lambda}}, \lambda\sqrt{\frac{\lambda_{\text{clamp}}}{\lambda^*}}, \sqrt{\frac{\lambda_{\text{clamp}}}{\lambda\lambda^*}}\right) \quad \text{Eq. 4}$$

The stresses that correspond to the additional stretch λ may then be calculated by differentiating W with respect to λ. Note that up to this point, the model works with any constitutive law for W.

Case of Gaussian chains [6,7]

A simple Neo-Hookean law is first chosen for W, which corresponds to the assumption of Gaussian chains in the network:

$$W_i(\lambda_x, \lambda_y, \lambda_z) = \frac{\nu_i kT}{2}\left(\lambda_x^2 + \lambda_y^2 + \lambda_z^2 - 3\right) \quad \text{Eq. 5}$$

which gives after differentiation in the longitudinal direction:

$$\sigma^{\parallel}(\lambda) = \nu_1 kT\left(\lambda\lambda^{*2} - \frac{1}{\lambda^2\lambda^*}\right) + \nu_2 kT\left(\frac{\lambda\lambda^{*2}}{\lambda_{\text{clamp}}^2} - \frac{\lambda_{\text{clamp}}}{\lambda^2\lambda^*}\right) \quad \text{Eq. 6}$$

and in the transverse direction:

$$\sigma^{\perp}(\lambda) = \nu_1 kT\left[\frac{\lambda}{\lambda^*} - \frac{1}{2\lambda^2}\left(\lambda^{*2} - \frac{1}{\lambda^*}\right)\right] + \nu_2 kT\left[\frac{\lambda\lambda_{\text{clamp}}}{\lambda^*} - \frac{1}{2\lambda^2}\left(\frac{\lambda^{*2}}{\lambda_{\text{clamp}}^2} - \frac{\lambda_{\text{clamp}}}{\lambda^*}\right)\right] \quad \text{Eq. 7}$$

From either Eq. 6 or Eq. 7 the relationship between λ_{clamp} and λ^* may be calculated by taking $\lambda = 1$ (since λ is the stretch ratio applied with respect to the equilibrium situation of the dual-cured network). This gives a first relationship:

$$\nu_1\left(\lambda^{*2} - \frac{1}{\lambda^*}\right) + \nu_2\left(\frac{\lambda^{*2}}{\lambda_{\text{clamp}}^2} - \frac{\lambda_{\text{clamp}}}{\lambda^*}\right) = 0 \quad \text{Eq. 8}$$

that can be further simplified to obtain an expression for λ^* in the case of Gaussian chains:

$$\lambda_{\text{Gauss}}^* = \left(\frac{\lambda_{\text{clamp}}^2 + (\nu_2/\nu_1)\lambda_{\text{clamp}}^3}{\lambda_{\text{clamp}}^2 + (\nu_2/\nu_1)}\right)^{1/3} \quad \text{Eq. 9}$$

This equation basically states that **the final degree of prestretching is primarily controlled by the crosslinking asymmetry between the first and the second steps and increases with the clamped stretch ratio**. When only very few additional crosslinks are added (i.e. $\nu_2 \ll \nu_1$), λ_{Gauss}^* takes the minimum possible value of 1, meaning that the elastomer goes back to its initial position entirely. If on the opposite the crosslinking density increases a lot during second curing (i.e. $\nu_2 \gg \nu_1$), then λ_{Gauss}^* goes toward λ_{clamp}. In between these two extreme cases, a fraction of the clamped stretch ratio is retained after the second curing, and this fraction increases with the ratio of crosslinking densities.

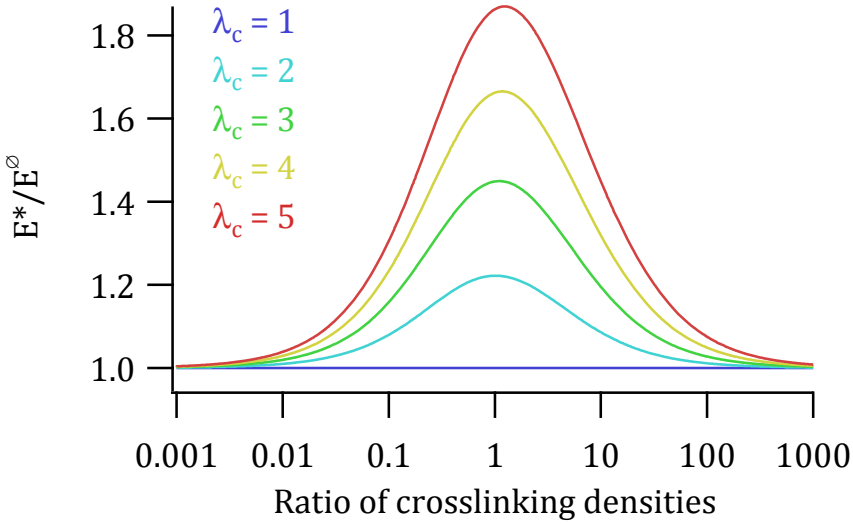

Figure 10: plot of Eq. 11 over a large range of crosslinking density ratio for 5 different levels of clamped stretch ratio.

Very importantly, one can show that $\sigma^{\parallel}(\lambda) = \sigma^{\perp}(\lambda)$ by rearranging the equations. The easiest way to do so is to calculate the difference and use Eq. 8 to reduce it to zero. This means that dual-cured networks based on Gaussian chains are intrinsically isotropic so that no directional effect may be expected. This result is fairly counter-intuitive, one would expect an effect from prestretching on the stress. This is due to the fact that Gaussian chains are considered as infinitely deformable which is obviously not true in reality.

Finally, one can calculate the stiffness of the dual-cured network by calculating the limit of $\partial\sigma/\partial\lambda$ when λ tends toward one. This gives:

$$E^{\parallel}_{\text{Gauss}} = E^{\perp}_{\text{Gauss}} = 3\text{kT}\left(\frac{\nu_1}{\lambda^*_{\text{Gauss}}} + \frac{\nu_2\lambda_{\text{clamp}}}{\lambda^*_{\text{Gauss}}}\right) \qquad \text{Eq. 10}$$

which can be compared to the modulus of an unprestretched dual-cured network $E^{\emptyset} = 3(\nu_1 + \nu_2)kT$, yielding:

$$\frac{E^{\parallel}_{\text{Gauss}}}{E^{\emptyset}} = \left(\frac{\nu_1}{\nu_1 + \nu_2}\right)\frac{1}{\lambda^*_{\text{Gauss}}} + \left(\frac{\nu_2}{\nu_1 + \nu_2}\right)\frac{\lambda_{\text{clamp}}}{\lambda^*_{\text{Gauss}}} \qquad \text{Eq. 11}$$

Eq. 11 shows that $E^{\parallel}_{\text{Gauss}}$ is always larger or equal to $E^{\emptyset}$. In the frame of Flory's model and assuming Gaussian chains, there is therefore a stiffening effect of prestretching. Remember that this result originates from the very basic laws of rubber elasticity, and in particular does not involve any finite extensibility effect. The increase in modulus is therefore only the result of a topological constraint due to the fact that the two populations of crosslinks are stretched from a position that is not their reference state.

In order to better understand this equation, a numerical application is shown in Figure 10. The increase in stiffness from Eq. 11 is calculated over a large range of crosslinking density ratio and for increasing values of clamped stretch ratio. It illustrates that **the prestretched material appears significantly stiffer provided the clamped stretch ratio is large and the ratio of crosslinking densities is around unity**. In other words, the two populations of crosslinks need to be balanced to observe this stiffening effect. The physical explanation for the latter condition is

that the increase in stiffness results from the competition between the two populations of crosslinks. If the asymmetry in crosslinking is too large, then the overall material properties are either entirely controlled by the first curing reaction (if $\nu_2 \ll \nu_1$, then $E^{\parallel}/E^{\emptyset} \approx 1/\lambda^* \approx 1$) or by the second (if $\nu_1 \ll \nu_2$, then $E^{\parallel}/E^{\emptyset} \approx \lambda_c/\lambda^* \approx 1$).

Case of non-Gaussian chains [8–12]

Use of a Gaussian law for the strain energy density gives an isotropic prediction for the stress of the dual-cured network. Anisotropy therefore results from deviations from the Gaussian behavior. A possible deviation that has been studied in the literature is the presence of a softening at small strain. This type of behavior is fairly well captured by the Mooney-Rivlin expression of W:

$$W_i(\lambda_x, \lambda_y, \lambda_z) = \alpha_i(\lambda_x^2 + \lambda_y^2 + \lambda_z^2 - 3) + \beta_i(\lambda_x^2\lambda_y^2 + \lambda_y^2\lambda_z^2 + \lambda_x^2\lambda_z^2) \qquad \text{Eq. 12}$$

In the equation above, parameters usually referred to as C_1 and C_2 have been renamed α and β to avoid the accumulation of subscripts. Such a model predicts a slight anisotropic behavior, and the difference in modulus is given by the following equation:

$$E^{\parallel}_{\text{NG-MR}} - E^{\perp}_{\text{NG-MR}} = \beta_2\left(\lambda^2_{\text{clamp}} - \frac{1}{\lambda_{\text{clamp}}}\right) - \beta_1\left(\lambda^*_{\text{Gauss}} - \frac{1}{{\lambda^*_{\text{Gauss}}}^2}\right) \qquad \text{Eq. 13}$$

with λ^*_{Gauss} the expression from Eq. 9 where the ratio ν_2/ν_1 has been replaced by α_2/α_1. Qualitatively, this model therefore predicts that the magnitude and sign of anisotropy depends on the relative contribution of β_1 and β_2. Basically, the more the material softens at small strains, and the larger the final stiffness anisotropy. However, these two parameters β_1 and β_2 do not bear any intrinsic physical meaning. The interpretation of this model is thus a sensitive task and the link to experiment is made difficult by the fact that β_2 cannot be measured since it corresponds to the added crosslinks only.

An alternative non-Gaussian model that can be used involves a serial expansion of the Langevin's function to take into account finite extensibility effects. This approach is particularly relevant in our case since we envision to use the prestretched networks as filler networks in double network elastomers. Having a closer look to the combined effects of prestretching and finite extensibility is therefore a useful piece of information.

The mathematical formalism of this model is much heavier than the previous ones, so that only the main results are given here. The interested reader may find the derivation and equations for all the parameters in the corresponding reference [9].

In addition to the crosslinking density of each network ν_i, the number of repetitive units per network strand N_i is also taken into account. These two parameters may be linked together using the following equation:

$$\nu_i = \frac{\rho \mathcal{N}_A}{\mathcal{M}_0 N_i} \qquad \text{Eq. 14}$$

where ρ is the polymer density (that may be found in handbooks [13]), $\mathcal{N}_A$ is Avogadro's number and $\mathcal{M}_0$ is the molar mass of a repetitive unit. Eventually, using this model, the relationship between the final stretch ratio and the clamped stretch ratio becomes:

$$\lambda^*_{\text{NG-Langevin}} = \lambda^*_{\text{Gauss}} \left[1 + \frac{\delta}{{\lambda^*_{\text{Gauss}}}^2 \left(\nu_1 + \nu_2 / \lambda^2_{\text{clamp}} \right)} \right] \qquad \text{Eq. 15}$$

where δ is a complicated function of ν_1, ν_2, N_1, N_2, λ_{clamp} and λ^*_{Gauss}. This expression be seen as a first-order correction from the Gaussian case.

By using the very same reasoning as in the Gaussian case, the stresses in the longitudinal and transverse directions may be calculated (equations not shown). Once again, an anisotropic behavior is predicted and an expression for the difference of modulus may be derived. The anisotropy may be represented by an anisotropy factor which increases when the relative difference in stiffness between the two principle directions increases:

$$\Delta_{\text{anisotropy}} = 2 \frac{E^{\parallel}_{\text{NG-MR}} - E^{\perp}_{\text{NG-MR}}}{E^{\parallel}_{\text{NG-MR}} + E^{\perp}_{\text{NG-MR}}} \qquad \text{Eq. 16}$$

Simulation using experimental values

In order to get a qualitative intuition of what the model predicts, we use the experimental values from the previous chapter as input parameters for the model. We take the specific example of a network dual-cured using the thermal system with an initial formulation MA_0.5/1.5. The values of modulus before and after second curing are taken from the DMA characterization of chapter 2. The input and ouput parameters of the models are summarized in Table 1. Immediately, it appears that **the numerical values of λ^*_{Gauss} and $\lambda^*_{\text{NG-Langevin}}$ (in bold characters in Table 1) are very close from each others**. In other words, far from the maximum extensibility of the material, the correction of the permanent stretch ratio due to the effect of finite extensibility is very weak.

The stresses in the longitudinal and transverse directions are calculated and compared in Figure 11. The stress-strain curve corresponding to the isotropic Gaussian case is added for comparison. Once again, the effect of finite extensibility in the small strain regime appears to be quite small,

Measured and tabulated parameters			Calculated parameters	
Parameter	Value	Source	Parameter	Value
$E_{\text{single-cured}}$	0.30 MPa	DMA (see chapter 2)	$\nu_1/\mathcal{N}_A$	36.7 mol/m³
$E_{\text{dual-cured}}$	2.04 MPa		N_1	352
λ_{clamp}	2.89	See 3.1.1	$\nu_2/\mathcal{N}_A$	208 mol/m³
λ^*	2.28		N_2	62
ρ	1.11 g/cm³	[13]	$\boldsymbol{\lambda^*_{\text{Gauss}}}$	**2.18031**
$\mathcal{M}_0$	86 g/mol		$\boldsymbol{\lambda^*_{\text{NG-Langevin}}}$	**2.18038**

Table 1: recap of the various parameters used and calculated by the non-Gaussian model based on an approached expression of the Langevin's function.

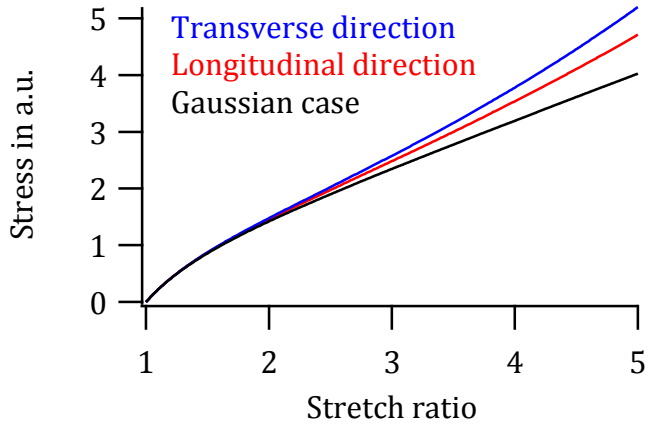

Figure 11: comparison of the predicted stress in the two directions using a non-Gaussian model based on an approached form of the Langevin's function. Stress is given in arbitrary units. Black curve is the stress corresponding to the isotropic Gaussian case with the same set of parameters.

the curves overall follow the same trend and are almost indistinguishable. In the large strain regime, levels of stress are higher when maximum extensibility is taken into account. With this specific set of parameters, the transverse direction is predicted to be slightly stiffer than the longitudinal direction in the large strain regime. The calculation of the anisotropy factor gives a value of -0.87%, which means that the stiffness is predicted to be very slightly larger in the transverse direction.

Interpretation and physical relevance of the model

Even though the extensive use of this specific theoretical model is not necessarily useful in the frame of an experimental study as ours, it still gives some trends and physical interpretations that are useful for the rest of the project.

First and foremost, the modelled modulus anisotropy results from the orientation of the chains is in all cases predicted to be weak and only a first order correction of the isotropic Gaussian case. If there is a directionality effect due to the prestretching, it can only be expected to be visible in the large strain regime.

The fact that the effect of prestretching is not very important may appear surprising given the relatively large change in geometrical dimensions of prestretched materials. Using the numerical values from Table 1, the prestretched material is extended by a factor 2.28 in the longitudinal direction and compressed by a factor 0.66 in the transverse direction (because of Poisson's effect). Assuming the network has a given fixed extensibility, there should therefore be a ratio of 2.28/0.66=3.45 between the maximum possible stretch ratio in the longitudinal direction and in the transverse direction. Yet, the upturn of stress occurs at similar stretch ratios in both directions (see Figure 11). How to explain this? Worse, how to explain that strain-hardening may occur first in the transverse direction?

The answer to this question lies in the assumption of the superposition of the two networks strain energies. Each population of crosslinks is modelled as a network with a given number of repetitive units, hence a given maximum extensibility that is basically linked to the contour length of a network strand. The initial network (i.e. the initial population of crosslinks) is of course extended in the prestretched direction, but it also has a larger maximum extensibility since the crosslinking density is low in the single-cured stage. On the contrary, the second population of crosslinks is dense so even if it is not as stretched in the longitudinal direction it may reach its maximum

extensibility before the initial network. Moreover, the recoil from the clamped state to the equilibrium prestretched state induces a compression of the second population of crosslinks in the longitudinal direction, hence a traction in the transverse direction. The second population of crosslinks is therefore less extensible *and* extended in the transverse direction. This explains why some specific sets of parameters give a stress larger in the transverse direction than in the longitudinal direction.

To conclude, the apparent paradox that comes from the study of the change in geometrical dimensions vanishes when one realizes that **the two populations of crosslinks have neither the same density nor the same stretch state in both directions**. There is an equilibrium in the dual-cured system between the loose and prestretched initial population of crosslinks and the less prestretched and less extensible second population of crosslinks. The final response of the prestretched dual-cure network is therefore the result of a balance between all the parameters of the preparation process. These parameters are all linked together, so that increasing one of them may affect all the others and radically change the mechanical signature of the material.

3.2.2. Comparison to experimental results

Now that Flory's model has been stated and explained, it is now confronted to our experimental data for both the thermal and the UV system. Since the case of non-Gaussian chains is merely a correction and does not fundamentally change the predictions of the model, the simple Gaussian version of the model is used.

Thermal system

In order to calculate λ^*_{Gauss} using Eq. 9 we need a numerical value for the crosslinking density ratio ν_2/ν_1. Values of Young's moduli measured by DMA in chapter 2 are used for this purpose[1]. Figure 12 compares the measurements of λ^* with predictions from Flory's model. With materials made from the formulation MA_0.2/0.5 (Figure 12-A), **the prediction based on the values of Young's moduli to obtain ν_2/ν_1 clearly underestimates the value of final prestretching**. All data points are above the model line. The agreement with the model is slightly better with the formulation MA_0.2/1.5 Figure 12-B although once again data points are clearly above the model line. As a general trend, **the measured values indicate that the actual crosslinking asymmetry seen by the system is larger than what is measured by DMA**. This may be due to the contribution of entanglements to the modulus of the singly-cured network. Since DMA does not permit to isolate the contribution of crosslinks only, the estimated value of ν_1 may be overestimated. This may in turn underestimate the ratio ν_2/ν_1 and thus the predicted value of λ^*.

[1] Note that a discrepancy has been pointed out in chapter 2 between the results obtained by DMA and by tensile tests for the thermal system. This mismatch has been attributed to a batch-to-batch variability and it may therefore appear surprising to use a single-value measurement to calculate the ν_2/ν_1 ratios. This is however believed to give the right order of magnitude, although absolute values of ν_2/ν_1 could differ from what is presented here.

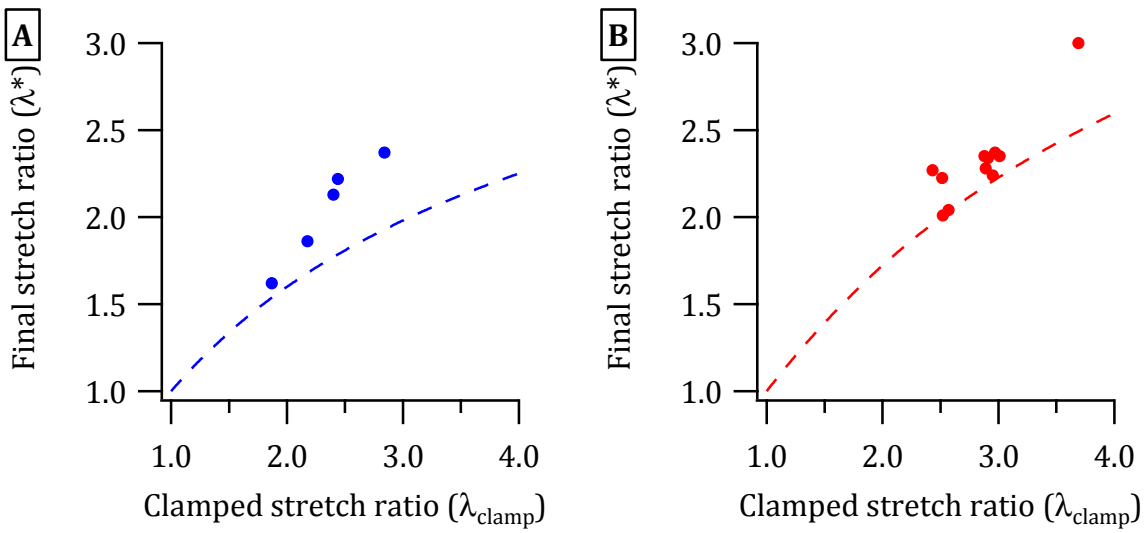

Figure 12: comparison of results with Flory's model for the thermal system. Dots are experimental data points and dashed lines are predictions from the model. A) Formulation MA_0.2/0.5. B) Formulation MA_0.2/1.5. Each data point corresponds to one tested sample.

Note the the presence of entanglements also affect the value of ν_2, but since the value of the modulus is higher the magnitude of the correction would be lower.

The observation is confirmed by the study of the extent of prestretching presented in Figure 13. For the two formulations the actual extent of prestretching is larger than what could be expected from the measured values of stiffness. There is a slightly better agreement with the model for the formulation with the higher level of GMA/AA, but predictions are still too low. Note that when studying the dependence of $\mathcal{P}$ with λ_{clamp} our data show significant scatter and do not seem to show a clear trend whereas a negative slope is expected with the model.

As shown in the previous chapter, the thermal system is characterized by a mechanical response that cannot be predicted directly from the amounts of crosslinkers used in the formulation. Also, the presence of polar groups in the initial stage probably results in partial clustering of acid groups during the heating of the second curing step. The structure of the thermally dual-cured network is thus probably more complex than the ideal case of a homogeneously crosslinked network, and the measurement of average quantities such a Young's modulus is probably not really

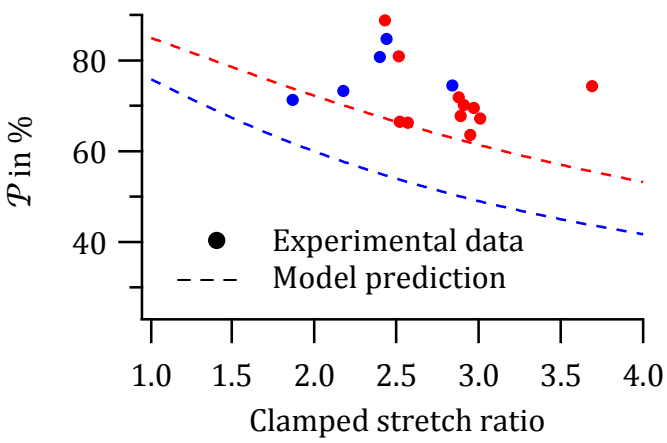

Figure 13: comparison of experimental extents of prestretching with predictions from Flory's model using experimental stiffnesses measured by DMA. Each data point corresponds to one tested sample. Blue and red points are for the MA_0.2/0.5 and MA_0.2/1.5 formulations respectively.

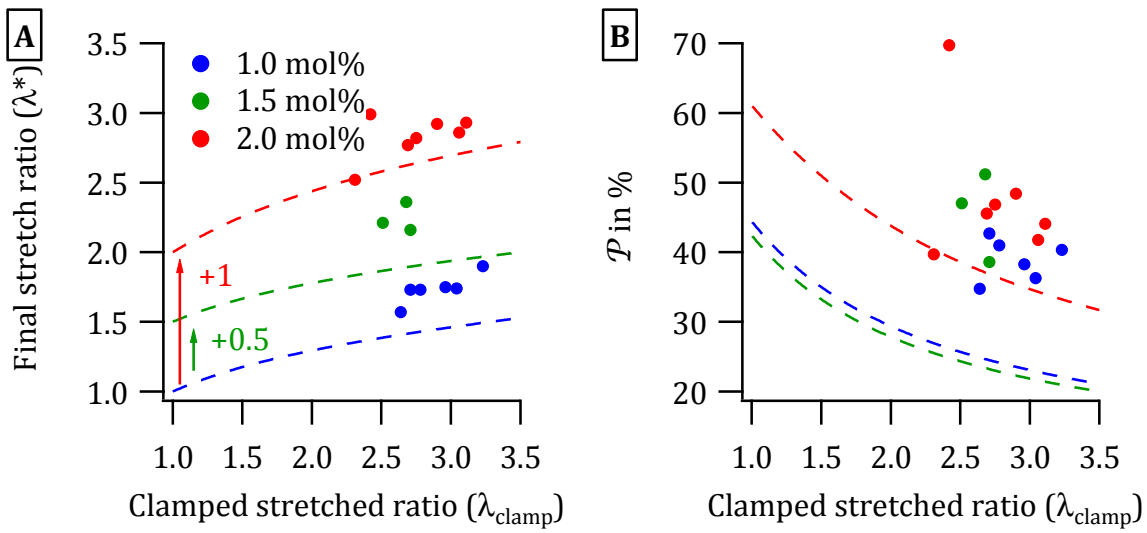

Figure 14: comparison of experimental data with Flory's model for the UV system. Dots are experimental data points and dashed lines are predictions from the model. A) comparison to final stretch ratio predictions. B) compairson to extent of prestretching. In subfigure A, Formulations with 1.5 and 2.0 mol% have been shifted upward by 0.5 and 1 respectively. Each data point corresponds to one tested sample.

representative of the architecture of the dual-cured filler network. Here, the use of average quantities directly measured by DMA fail to catch the prestretching of the dual-cured system.

UV system

As in the thermal system, predictions of λ^* and $\mathcal{P}$ are made using values of Young moduli measured by uniaxial traction in the previous chapter. Predictions are compared with experimental values in Figure 14 for the three formulations tested. Note that formulations have been graphically split using vertical offsets, for readability.

The prediction of λ^* is compared to experimental data in Figure 14-A and shows very poor agreement. **For the three formulations tested, the predictions of λ^* are clearly lower than the experimental values**. Here again, the fact that predictions based on the measured values of Young moduli are off is not really surprising. In the previous chapter, we have shown that the UV system bears a large variability. The main manifestation of this is the large variability in the observed values of swelling ratios during the HMP infiltration step. The network structure in the single-cured stage is thus not very well defined and may vary quite significantly from sample to sample. Here, we have used single values of Young's moduli based on particular samples that have been assumed to be representative of their formulation groups. This hypothesis is thus very likely to be wrong.

As a confirmation of the discrepancy between Flory's model and experimental data, the predicted extent of prestretching $\mathcal{P}$ is compared to experiment in Figure 14-B. Experimental values of average values of $\mathcal{P}$ overall increase slightly with the amount of ALA in the formulation, although there is scatter in the data points. Predictions however do not follow this observation, since predictions of $\mathcal{P}$ for the 1.0 mol% formulation is slightly higher than for the 1.5 mol% formulation, and much lower than for the 2.0 mol% formulation. Not only the prediction does not match the experimental data points, but it also does not match the trend that is observed between the

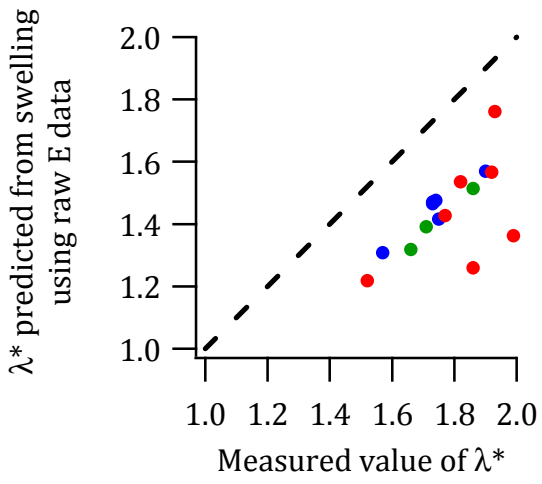

Figure 15: comparison of predicted values of λ^* with experimental data. Predictions are based on ν_1 values extracted from Young's moduli obtained from swelling ratios using Flory-Rehner's theory. Dashed line is the unit line. Colors represent the different levels of ALA in formulation (blue is 1.0 mol%, green is 1.5 mol% and red is 2.0 mol%). Each data point corresponds to one tested sample.

different formulations. Once again, this confirms that the use of a single value of $E_{\text{single-cured}}$ to build predictions is probably erroneous.

Attempts to reduce and explain the error in the UV system

In order to take the sample to sample variability of the UV system into account, one may try to use the calculated values of modulus from swelling ratio measurements to make new predictions. The measurement of the equilibrium swelling ratio after the HMP infiltration step is carried out for each sample and can be used to obtain a value of $E_{\text{single-cured}}$ for each network (assuming that χ is known between the solvent and the polymer). In turn, the modulus can be used to estimate ν_1 in Flory's model (see chapter 2) for each sample. For ν_2, the value of modulus measured by uniaxial traction may be used. The use of the traction modulus for $E_{\text{dual-cured}}$ is justified by the fact that the final crosslinking density is expected to be reproducible, since it only depends on the amount of ALA units incorporated in the initial stage. In other words, the unpredictable amount of bireacted ALA units in the intermediate stage induces some variability, but the latter vanishes when all ALA units have reacted after the second UV irradiation.

In the end, one prediction of λ^* is obtained for each sample, as opposed to the previous section where one single prediction was obtained for each formulation. Comparison of predictions with experimental data is given in Figure 15. The large distance between data points and unit line shows that the quality of the quantitative prediction is still poor. However trends in experimental data are clearer. **The variability from sample to sample in the single-cured stage reduces scatter but is not the only origin of the error of Flory's model**. Interestingly, most data points in Figure 15 lie at the same distance to the unit line regardless of the formulation. This means that there is a systematic error with Flory's model that does not depend on formulation and prevents correct predictions of λ^* to be built.

Once again, a possible source of error is the presence of trapped entanglements in the singly-cured network which would overestimate the measured value of ν_1. Also, the error of Flory's model may originate from the fact that the structure of the dual-cured network is probably far from the perfect homogeneously crosslinked case. In particular, with the UV system, the second crosslink step comes from the combination of pendent double bonds. These bonds may combine in the first stage (which gives the initial crosslinks) or in the second step after UV irradiation and second

curing. In both cases, the reaction of allyl groups may induce some strong heterogeneities in the network structure:

- In the first curing step, the reaction of allyl groups is actually a copolymerization with acrylate functions. Kinetic issues may therefore arise and induce a non-random incorporation of allyl groups in the network structure. The initial crosslinks may therefore be partially clustered, or at least not-uniformly located along the polymer backbone.
- In the second curing step, allyl groups react together after UV initiation. The reaction is actually a free radical polymerization of allyl groups. One could therefore imagine in principle that several allyl groups react in chain thus creating very rigid nods or multifunctional crosslinks. There are however three major differences with a standard polymerization reaction that relativizes such a scenario: 1) allyl groups are not very reactive toward radical polymerization, 2) allyl groups are diluted among poly(ethyl acrylate) chains, and 3) the reaction proceeds in a solid matrix and not in a solution which means that the mobility of the reacting units is low. For these reasons, the second curing reaction probably does not add much heterogeneity to the situation

Therefore, the network structure in the dual-cured stage is far from being ideal. The Gaussian assumption in Flory's model is most probably the major source of error for the prediction of final prestretching.

3.3. Additional mechanical characterization for the thermal system

Before moving to the next part, an additional characterization has been carried out on a prestretched dual-cured network using the thermal system. The idea is to investigate whether prestretching has a visible effect on the tensile response of the material before incorporating it in a double network structure. A sample of formulation MA_0.2/1.5 is used with $\lambda_{\text{clamp}} = 2.89$. After the second curing, a residual stretch ratio of $\lambda^* = 2.28$ is observed. As usual, an unprestertched sample from the same initial material is dual-cured at the same time for comparison. Both samples are then tested in uniaxial extension at 100 µm/sec at 60°C (see Figure 16). Note that these experimental conditions correspond and corresponds to the simulations of section 3.2.1.

The three tensile curves are very close to each other, with **no significant effect due to prestretching and no clear difference between the prestretched and transverse directions**. Taking a closer look at numerical values of Young moduli, it seems that there is no real stiffening effect of prestretching in these conditions, since the average prestretched modulus is equal to the modulus of the unprestretched network. Yet, simulation from Figure 10 predicts a difference of 20% for the prestretched network, which should be measurable here. The longitudinal direction of the prestretched network is also slightly stiffer than the transverse direction. This is in qualitative agreement with predictions from Flory's model when a non-Gaussian model is used (see Figure 11). Overall, the differences in modulus are very limited and the three samples tested return similar traction curves. It can therefore be concluded that prestretching does not significantly change the tensile response of this dual-cured filler network at small strains.

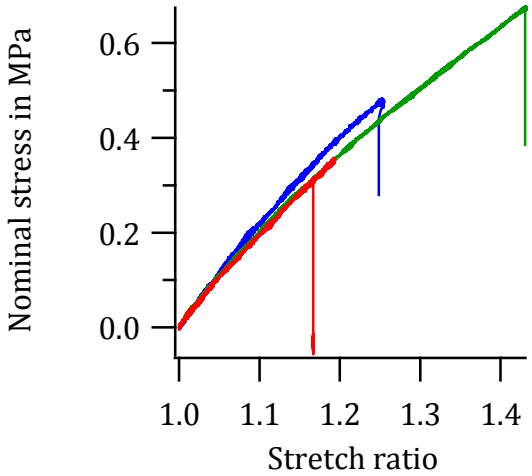

Sub-sample	E in MPa	ϵ_{max} in %
Longitudinal	2.1	19.3
Transverse	2.3	25.5
Unprestretched	2.2	43.3

Figure 16: tensile test at 100 µm/sec on a permanently prestretched filler network with formulation MA_0.2/1.5. Clamped stretch ratio is 2.89 and final stretch ratio is 2.28. Values of Young Moduli and maximum extensibilities are given in the table above. Red, blue and green curves correspond to longitudinal, transverse and unprestretched subsamples respectively.

Although the values of moduli are very close, there seem to be a larger difference in Figure 16 in terms of maximum extensibility. The sample tested in the longitudinal direction breaks at stretch ratios smaller than in the transverse direction, which in turn breaks at extensions smaller than the unprestretched sample. This could indicate that our materials could exhibit differences in the large strain regime if they were tougher. This information should however be considered with caution, since crack initiation in unnotched tensile tests is purely random and not necessarily representative of the actual maximum extensibility of the material.

4. Prospective: what to expect in a double network structure?

Now that experimental results of filler networks have been reviewed and compared to Flory's model, it becomes interesting to put things into perspective and to anticipate on the following step. In the rest of the project, the prestretched filler networks are swollen and incorporated in a double network structure. Such a process is likely to enhance the non-linear large strain effects of the filler network. As a result, we try here to establish a physical model to develop an intuition of what these effects could give on the mechanical response of prestretched double networks.

4.1. Description of the approach

Comparison of experimental results with Flory's model show that it does not predict accurately the values of prestretching that are observed after dual curing. Predictions are systematically below experimental values, which indicates that there is a contribution to prestretching that is not taken into account in the Gaussian version of the model. In order to model the behavior of double networks, one could therefore imagine using a more realistic version of Flory's model, for instance using one of the non-Gaussian expressions of strain energy given in 3.2.1. This gives expressions that are mathematically much more complex and therefore difficult to handle. Meanwhile, these models still rely on a mean-field approach consisting in summing the contributions of all the chains. This approach neglects the connectivity and the percolation of the least extensible chains, which makes it intrinsically limited, as already stated in the first chapter. Knowing that such an approach is necessarily limited, we therefore choose to base our model on a physically-based model that has the advantage of being mathematically simple while containing the same main physical ingredients as more complicated models.

The pragmatic approach presented here is based on a fundamental experimental observation. Namely, double networks based on isotropic filler networks strain-harden when the filler network reaches its maximum extensibility [1]. This maximum extensibility may be estimated theoretically taking into account the limit of extensibility of the filler network strands. One may therefore try to predict the stretch ratio at which the double network structure should strain-harden considering all the deformations processes that have been applied on the filler network (stretching, swelling, etc.). This should give an extension of Flory's model that predicts only the position of strain-hardening in the double network structure, by opposition to a more complete and much more complex version of the model that would model the entire stress-strain curve.

First, the equations of this extended Flory's model are derived and will then be calculated numerically using the values corresponding to a prestretched filler network prepared with the thermal system.

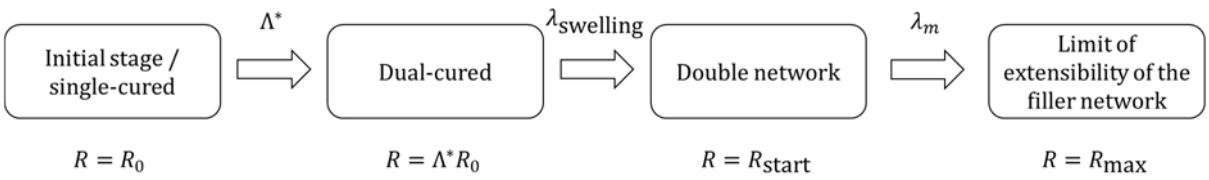

Figure 17: diagram representing the life cycle of a network strand. Boxes represent the different stages, from the initial synthesis of the network to the final stretch ratio applied during a traction test on the double network. The symbols above the arrows are the stretch ratios associated to each step. Below each box, the symbol corresponding to the size of a network strand is recalled.

4.2. Derivation of the model

4.2.1. General framework

We use here the same fundamental hypothesis as in Flory's model, which is the superposition of a virtual network to the initial network when second curing is performed. In the dual-cured filler network, there are thus two population of crosslinks with two different volume densities ν_1 and ν_2. Each crosslinking density may be estimated from the knowledge of the Young's moduli before and after second curing (see 3.2.1).

The basic idea of the modelling is now to follow the deformation state of a network strand throughout its life, from the initial network to the double network in traction when the strand reaches its maximum size. The lifecycle of a network strand may be represented as in the diagram from Figure 17, which defines the notations that are used thereafter.

In the initial stage and in the absence of prestretching, the typical end-to-end distance of a single-cured network strand may be calculated assuming the population of chains is Gaussian for the two populations of crosslinks. This gives an initial size R_0 that basically depends on the crosslinking density. From this initial size, the network strands are first deformed by the prestretching, inducing a stretch ratio Λ^*. Then, an isotropic swelling stretch ratio $\lambda_{\text{swelling}}$ is applied to obtain the double network reference state. The latter is associated to a network strand size R_{start} that can be written as follows:

$$R_{\text{start}} = \Lambda^* \, \lambda_{\text{swelling}} \, R_0 \qquad \text{Eq. 17}$$

From this reference state, a tensile test is applied either in the longitudinal (λ_x) or in the transverse (λ_y) direction. This brings the network strands to their maximum size R_{max}. Defining λ_m as the maximum stretch ratio during the final tensile test, one may write:

$$\lambda_m = \frac{R_{\text{max}}}{R_{\text{start}}} = \frac{R_{\text{max}}}{R_0 \, \Lambda^* \, \lambda_{\text{swelling}}} \qquad \text{Eq. 18}$$

The goal is now to obtain expressions for R_{max}, R_0 and Λ^* first when there is no prestretching, and then when a prestretching is applied during the second curing stage.

4.2.2. Unprestretched case ($\Lambda^*=1$)

When there is no applied prestretching during the second curing process, the two populations of crosslinks have the same reference state and are therefore undistinguishable. The second-curing process only adds crosslinks, increasing the crosslinking density from ν_1 to $\nu_1+\nu_2$. The crosslinking density ν is linked to the average number of repetitive units between crosslinks N_{mono} and to the Young modulus, as already stated in 3.2.1. The initial size of the filler network strands may therefore be linked to the Young modulus of the dual-cured network $E_{\text{dual-cured}}$ via the equation:

$$R_{0,\,\text{unprestretched}} = \sqrt{C_\infty . 2N_{\text{mono}}^{\text{unprestretched}}}\, l_{\text{C-C}} = \sqrt{C_\infty . 2\left(\frac{3\rho RT}{\mathcal{M}_0 E_{\text{dual-cured}}}\right)}\, l_{\text{C-C}} \qquad \text{Eq. 19}$$

where C_∞ is the characteristic ratio of the polymer (7.91 for PMA and 9.76 for PEA [13]), $N_{\text{mono}}^{\text{unprestretched}}$ is the number of repetitive units between crosslinks in the unprestretched case (the factor 2 originates from the conversion from a number of repeat units to a number of carbon-carbon bonds), $l_{\text{C-C}}$ is the length of a carbon-carbon bond and ρ is the polymer density (1.11 for PMA and 1.13 for PEA [13]).

Using a chain model with fixed valence angle (see chapter 1), the maximum size of a network strand may be calculated:

$$\text{R}_{\text{max}} = \cos\left(\frac{\theta}{2}\right) . 2N_{\text{mono}}^{\text{unprestretched}} . l_{\text{C-C}} = \cos\left(\frac{\theta}{2}\right) . 2\left(\frac{3\rho RT}{\mathcal{M}_0 E_{\text{dual-cured}}}\right) . l_{\text{C-C}} \qquad \text{Eq. 20}$$

The combination of these two equations with the expression giving R_{start} with respect to R_0 (Eq. 17) gives the following expression for the maximum stretch ratio:

$$\lambda_m^{\text{unprestretched}} = \frac{\cos(\theta/2)}{\lambda_{\text{swelling}}}\sqrt{\frac{2N_{\text{mono}}^{\text{unprestretched}}}{C_\infty}} = \frac{\cos(\theta/2)}{\lambda_{\text{swelling}}}\sqrt{\frac{6\rho RT}{C_\infty \mathcal{M}_0 E_{\text{dual-cured}}}} \qquad \text{Eq. 21}$$

4.2.3. Prestretched case ($\Lambda^*\neq1$)

When a prestretching is applied, the situation becomes more complex since the two populations of crosslinks are not equivalent any longer and do not have the same reference state. As a result, the number of repetitive units differs between the two populations of crosslinks:

$$N_{\text{mono}}^{\text{1st generation}} = \frac{3\rho RT}{\mathcal{M}_0 E_{\text{single-cured}}} \qquad \text{Eq. 22}$$

and

$$N_{\text{mono}}^{\text{2nd generation}} = \frac{3\rho RT}{\mathcal{M}_0\left(E_{\text{dual-cured}} - E_{\text{single-cured}}\right)} \qquad \text{Eq. 23}$$

Therefore, the values of initial size R_0 and maximum size $R_{\max}$ now depend on the population of crosslinks. Eventually, one gets two distinct expressions for the maximum stretch ratio:

$$\lambda_m^{\text{1st generation}} = \frac{\cos(\theta/2)}{\Lambda^* \lambda_{\text{swelling}}} \sqrt{\frac{6\rho RT}{C_\infty \mathcal{M}_0 E_{\text{single-cured}}}} \qquad \text{Eq. 24}$$

and

$$\lambda_m^{\text{2nd generation}} = \frac{\cos(\theta/2)}{\Lambda^* \lambda_{\text{swelling}}} \sqrt{\frac{6\rho RT}{C_\infty \mathcal{M}_0 \left(E_{\text{dual-cured}} - E_{\text{single-cured}}\right)}} \qquad \text{Eq. 25}$$

The other difference with the unprestretched case is the presence of the factor Λ^* in the denominator of λ_m. Since it represents the effect of prestretching, Λ^* is obviously linked to λ_{clamp} and λ^*. The equation linking them is however not the same for the two populations of crosslinks, and not the same depending on the direction, as illustrated in Figure 18. The latter shows a schematic representation of the stretch state for the two populations of crosslinks (in blue and red for the first and second generations of network strands respectively) throughout the second curing process.

In the dual-cured stage and in the longitudinal direction, the initial network is in traction by a factor λ^*. On the contrary, the second network is in compression by a factor $\lambda^*/\lambda_{\text{clamp}}$ in the longitudinal direction, since it is at rest in the intermediate clamped stage. In the transverse direction, because of Poisson's effect, it is the opposite: the initial network is in compression and the second one is in traction.

The equations linking Λ^* to λ_{clamp} and λ^* are given in Table 2 in all four cases. Note that these equations along with Eq. 17 implicitely assume that directions are independent from each other beside Poisson's effect. Any cross-directional effect is therefore neglected.

Eventually, the combination of Eq. 24 and Eq. 25 with the equations from Table 2 gives four predictions for the maximum stretch ratio, one per population of crosslinks and one per direction. The final step of the reasoning is to keep only the smallest value between the two crosslinking densities, since only the least extensible population of network strands will contribute to the observed strain hardening.

To sum up, this extended version of Flory's model uses the same basic assumption, which is the separation of the dual-cured network in two separate populations of crosslinks. While the standard version of Flory's model calculates the global strain energy density assuming a linear superposition, we merely use this separation to calculate values of maximum extensibilities for

	First generation	Second generation
Longitudinal direction	$\Lambda^* = \lambda^*$	$\Lambda^* = \lambda_{\text{clamp}}/\lambda^*$
Transverse direction	$\Lambda^* = 1/\sqrt{\lambda^*}$	$\Lambda^* = \sqrt{\lambda^*/\lambda_{\text{clamp}}}$

Table 2: recap of equations linking the global prestretching ratio with the actual clamped and permanent stretch ratio in the longitudinal direction, for each direction and each generation of network strand.

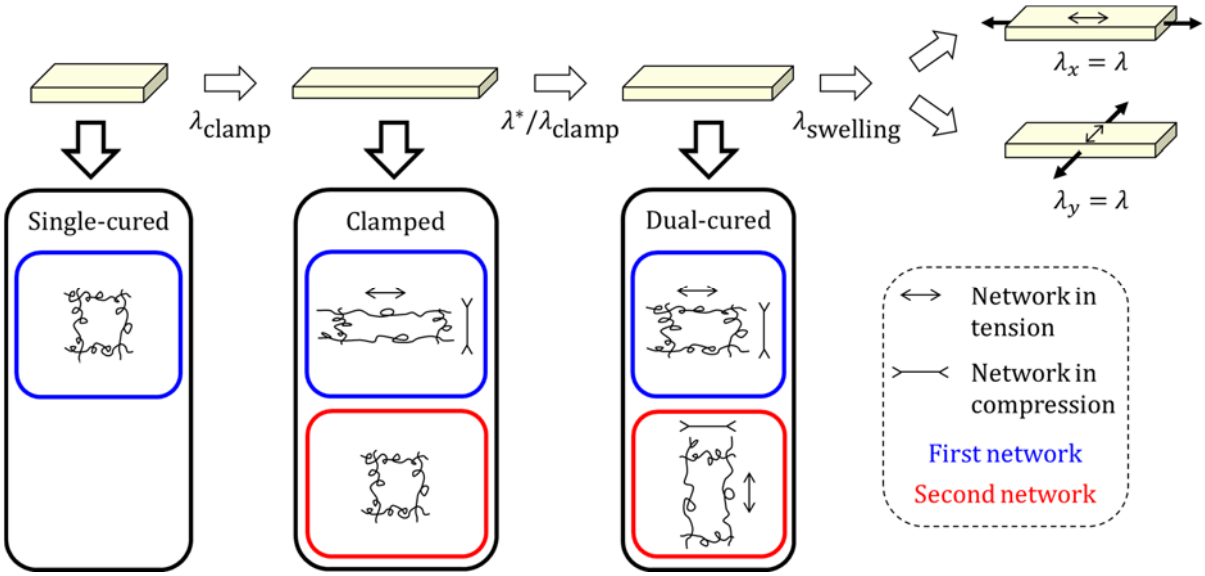

Figure 18: illustration of the effect of prestretching on the two network population. Top line represents the preparation and testing process of the prestretched double networks, from the initial single-cured stage to the final uniaxial testing stage in either the longitudinal or the transverse direction. For each stage a schematic of the two networks is given, with the stretch state represented by a double arrow in each direction.

the two populations of crosslinks, and for each direction. In the initial Flory's model, all chains are considered to contribute equally to the mechanical behavior of the system, while in our extension of the model we implicitly assume that the mechanical response in large strain is dominated by the least extensible chains in the network. This obviously simplifies the model and probably makes it less accurate, but it keeps the main physical ingredients and makes it much easier to handle and compare to experimental values.

4.2.4. Application using experimental values

As an illustration, the numerical values that have been used previously in 3.2.1 (see Table 1) are incorporated in the previous equations. As a reminder, these values also correspond to the material tested in uniaxial traction in section 3.3. A value of 1.50 is used for $\lambda_{\text{swelling}}$, which is the order of magnitude that is typically observed for standard double networks.

The resulting numerical values are given in Table 3. The first four lines give parameters that are calculated from the values of Young's moduli measured by DMA. By looking at the calculated values of $\lambda_{\max} = R_{\max}/R_0$, one sees that **the two populations of crosslinks have widely different maximum extensibilities**. As expected from the values of Young's moduli, the network corresponding to the initial population of crosslinks is much more extensible than the second one. This is the case here because the crosslinking asymmetry is fairly strong, with a 7-fold increase in modulus during the second curing.

The rest of the table gives numerical values for the global prestretching factor Λ^* and final predictions of λ_m. They show that we can indeed expect differences in maximum extensibilities in the three cases. With this specific set of parameters, the longitudinal direction is expected to be the most extensible and the transverse one is expected to be the least extensible. This matches the simulations from Figure 11 that have been established using a non-Gaussian version of Flory's

Parameter	Direction	Prediction		
		First generation	Second generation	Both generations
E in MPa	/	0.30	1.73	2.04
$\nu/\mathcal{N}_A$ in mol/m³	/	37	208	245
N_{mono}	/	352	62	53
$\lambda_{\max} = R_{\max}/R_0$	/	7.70	3.23	2.98
Λ^*	Longitudinal	2.28	0.79	/
	Transverse	0.66	1.13	/
	Unprestretched	/	/	1
λ_{m}	Longitudinal	**2.25**	(2.73)	/
	Transverse	(7.75)	**1.91**	/
	Unprestretched	/	/	**1.99**

Table 3: Illustration of the proposed extension of Flory's model using experimental values from a prestretched filler network based on the thermal system. The four first lines are parameters directly extracted from the measurement of Young moduli by DMA. The final predictions of λ_m are in bold characters, the ones that are left aside are between brackets.

model. Our extension of Flory's model therefore gives predictions of maximum extensibility that are consistent with a more rigorous mathematical model. It however has the advantage of a light mathematical form, which enables direct comparison to experiments.

The numerical application of this extended version of Flory's model also illustrates a seemingly counterintuitive aspect of prestretching. Despite the large difference in terms of crosslinking density and maximum extensibility of network strands, the final anisotropy at large strains is expected to be fairly moderate. Here, the predicted maximum stretch ratios differ by only 35% between the two directions, despite the large increase of modulus during second curing and large extent of prestretching at the end of the dual-curing process. **A large permanent stretch ratio is therefore not necessarily linked to a large difference in maximum extensibility**.

As already explained, this apparent discrepancy comes from the fact that prestretching does not apply on the two populations of crosslinks the same way. Even if the initial population of crosslinks is stretched a lot in the longitudinal direction, its associated crosslinking density is low and hence it is very extensible. The resulting maximum stretch ratio is therefore comparable to the one in the transverse direction, which corresponds to the maximum extensibility of the second less extensible generation of crosslinks.

To sum up, the direct application of this extension of Flory's model to the case of double networks gives us two physical intuitions that are compared to experimental data in the next chapter:

- The maximum extensibility of the prestretched filler network is not expected to be very anisotropic, but **a slight directional effect is still expected**.

- **The magnitude of this anisotropy at large strain may be calculated** using an extension of Flory's model. The latter gives results that agree qualitatively with more complete versions of Flory's model that use non-Gaussian expressions for the strain energy density.

5.Conclusions

In this chapter, the previously identified conditions for an efficient second curing have been applied to prepare elastomers that are permanently prestretched in one direction.

As a first obvious and immediate conclusion, the preparation of prestretched networks has turned out to be a delicate task, and unexpected challenges have been faced. The initial idea was to simply stretch the initial loosely crosslinked network and subject it to the second curing conditions. This however ignored the fact that the initial material could not sustain high clamped stretch ratios for extended periods of time and/or high temperatures without breaking, despite its large extensibility at room temperature. After some optimization, a solution has been found and clamped stretch ratios up to 3 have been used. Using this apparatus, permanently prestretched filler networks have been prepared with a permanent elongation λ^* that basically increases with the clamped stretch ratio λ_{clamp}.

The rest of the chapter has been devoted to the presentation, extension and application of Flory's model. This conceptual framework models the behavior of dual-cured network. It assumes that the second curing step is equivalent to the superposition of a virtual network to the initial network. This additional network is at rest in the clamped position and has a different crosslinking density, so that the equilibrium position of the prestretched dual-cured network may be predicted by balancing the forces of the first initial and second virtual networks.

Comparison of Flory's model to our prestretching data shows however major quantitative discrepancies, both for the thermal and the UV system. Even when the sample to sample variability is taken into account, the predictions based on the Gaussian version of Flory's model systematically underestimate the observed values of final stretch ratio. This has been interpreted as the result of the possible presence of trapped entanglements in the initial singly-cured network structure, and as an indication that the architecture of the dual-cured networks is probably not simple and fairly heterogeneous. Note that one could in theory correct the measured values of Young modulus to take into account the presence of entanglements. However, the very likely presence of defects and dangling chains makes it a sensitive task.

Refinements of Flory's model have been presented and take into account the non-Gaussian behavior of the chains, but their heavy mathematical framework and the fact that they do not have much added value with respect to a simple mean-field approach plead against their use in our case. Instead, we propose in this chapter an empirical extension of Flory's model based on the theoretical prediction of the limit of extensibility of the two populations of chains. This model qualitatively agrees with non-Gaussian complete versions of Flory's model and will be compared to experimental data in the rest of the project.

Despite the inability of Flory's model to predict the final stretch ratios of our material, the prestretched filler networks that have been obtained may and will be incorporated in double network structures in the next chapter.

6. References

1. Millereau P, Ducrot E, Clough JM, Wiseman ME, Brown HR, Sijbesma RP, et al. Mechanics of elastomeric molecular composites. Proc Natl Acad Sci. 2018 Aug 28;201807750.

2. Su W-Y, Posey ML, Weeme MP ter. Color stabilization of amines [Internet]. US7169268B2, 2007 [cited 2019 Sep 17]. Available from: https://patents.google.com/patent/US7169268B2/en

3. Krauklis AE, Echtermeyer AT. Mechanism of Yellowing: Carbonyl Formation during Hygrothermal Aging in a Common Amine Epoxy. Polymers. 2018 Sep;10(9):1017.

4. Berry JP, Scanlan J, Watson WF. Cross-link formation in stretched rubber networks. Trans Faraday Soc. 1956;52:1137–1151.

5. Flory PJ. Elasticity of polymer networks cross-linked in states of strain. Trans Faraday Soc. 1960 Jan 1;56(0):722–43.

6. Lodge AS. The isotropy of Gaussian molecular networks and the stress-birefringence relations for rubberlike materials cross-linked in stressed states. Kolloid-Z. 1960 Jul 1;171(1):46–51.

7. Charlesby A, Arnim E von. Crosslinking of oriented rubber. J Polym Sci. 1957 Jul 1;25(109):151–8.

8. Smith KJ, Ciferri A, Hermans JJ. Anisotropic elasticity of composite molecular networks formed from non-gaussian chains. J Polym Sci A. 1964 Mar 1;2(3):1025–41.

9. Greene A, Smith KJ, Ciferri A. Elastic properties of networks formed from oriented chain molecules. Part 2.—Composite networks. Trans Faraday Soc. 1965;61:2772–2783.

10. Yanai HS. Two Network Model for Vulcanizates Crosslinked under Strain. Rubber Chem Technol. 1967 Sep;40(4):1060–70.

11. Jr KJS, Gaylord RJ. Non-gaussian elasticity of composite and interpenetrating networks. J Polym Sci Part -2 Polym Phys. 1972 Feb 1;10(2):283–93.

12. Smith KJ, Gaylord RJ. On the Anisotropy of Composite Networks. Macromolecules. 1975 Jan;8(1):89–89.

13. Mark JE. Physical properties of polymers handbook [Internet]. Vol. 1076. Springer; 2007 [cited 2016 Oct 28]. Available from: http://link.springer.com/content/pdf/10.1007/978-0-387-69002-5.pdf

Chapter 4

Incorporation of prestretched filler networks into double network structures

Table of contents

1. Introduction ... 171
2. Preparation process and additional characterization tools ... 173
2.1. Filler networks ... 173
2.2. Preparation of double networks ... 173
2.3. Step-cyclic tests ... 174
2.3.1. Description of the test ... 174
2.3.2. Extraction of the cyclic test envelope ... 174
2.3.3. Study of strain-hardening using Gent's model ... 174
2.4. Fracture tests ... 176
2.4.1. Principle of the measurement of fracture energy ... 176
2.4.2. Specific procedure ... 177
2.4.3. Determination of error margin ... 178
3. Study of two examples of prestretched DN ... 181
3.1. Relative changes in dimensions ... 181
3.2. Mechanical characterization ... 183
3.2.1. Global comparison of the two systems ... 183
3.2.2. Observation of the small strain regimes ... 184
3.2.3. Observation of the large strain regime ... 186
3.3. Toward a more detailed characterization? ... 186
3.3.1. Comparison of the thermal system to Flory's model ... 187
3.3.2. The reproducibility issue of the thermal system ... 189
3.3.3. Cyclic testing of the UV system ... 190
3.4. Partial conclusion ... 193
4. Systematic study of the UV system ... 195
4.1. Identification of typical trends and odd ones ... 195
4.2. Study of unprestretched double network samples ... 196
4.2.1. Overall presentation and study of small strain regime ... 196
4.2.2. Large strain behavior and strain-hardening phenomenon ... 198
4.3. Study of prestretched DN using envelope curves ... 201
4.3.1. Identification of common trends within each formulation group ... 201
4.3.2. Study of the small strain regime – Flory's model ... 203

4.3.3. Large strain behavior and strain-hardening 205
4.4. Exploitation of the entire cyclic test 207
4.4.1. Study of large strain behavior and strain-hardening 207
4.4.2. Study of damage in terms of mechanical hysteresis 211
4.4.3. Comparison with Mullins Effect in filled rubbers 218
4.5. Suggested physical picture 222
4.5.1. Dual-curing means two populations of chains 224
4.5.2. The origin of damage in cyclic loading 226
4.5.3. The effect of prestretching and formulation 227
4.5.4. Summary 230
5. Influence of damage on mechanical properties for the UV system 231
5.1. Study of viscoelastic properties 231
5.1.1. Study of undamaged materials 231
5.1.2. Study of damaged samples 233
5.2. Study of fracture properties 234
5.2.1. Fracture study of virgin samples 234
5.2.2. Effect of damage on fracture resistance 235
6. Conclusions 239
7. References 241

1. Introduction

In the previous chapters, two dual-curing systems have been developed and used to prepare elastomers that are permanently and uniaxially prestretched. Although the amount of prestretching is not easily predictable from the materials properties and processing conditions, the visible change in dimensions indicate that the network strands should be at least partly oriented. This alignment should have some visible consequences on the large strain response of the materials.

In order to study this large strain behavior, it is necessary to toughen the dual-cured networks. Dual-cured networks are pretty stiff, so that when they are deformed they fail at fairly low extension ratios. This is because of the presence of defects in the network structure and the absence of dissipation mechanism, which induces brittle failure of the material below 50% extension.

In this chapter, the isotropic and uniaxially prestretched dual-cured networks are therefore incorporated in a double network architecture. The latter consists in embedding the stiff network into a soft and extensible matrix by swelling the elastomer and polymerizing the matrix network in situ. As a result of this specific macroarchitecture, there is an additional isotropic prestretching that applies on the dual-cured network because of the presence of the incompressible matrix. Additionally, a dissipation mechanism by bond breakage becomes active and delays the onset of fracture. The double networks should therefore exhibit a tough mechanical response with stresses and strains at break much larger than the filler networks alone.

This strategy is now used with uniaxially prestretched dual-cured network. Using the multiple network architecture, we expect to highlight the effect of this directional anisotropy in prestretching on the mechanical response of the material. As a matter of fact, permanently prestretched double networks are obtained in this chapter, using either the thermal or the UV systems. Both systems share some similar characteristics but also show some major differences, one of them being that the UV system is much more reproducible and more adapted to a systematic study.

This systematic study is the focus of the second half of this chapter. The idea is to compare several samples of each formulation in order to identify common trends. The study of the materials response to cyclic loading gives us some clues on a hypothetic molecular structure that could explain the mechanical response of prestretched double networks.

Despite the variability due to the chemical systems that are used, the study of prestretched double networks give some interesting insights on the details of the second curing reactions. The resulting materials have interesting and original properties, particularly at large strains.

2.Preparation process and additional characterization tools

2.1. Filler networks

The preparation and second curing of filler networks has already been detailed in the previous chapters.

For the thermal system, the generic formulation is as follows:

Compound	MA	AcOEt	AA	GMA	BDA	HMP	NEt3
Quantity	/	50 v%	0.5 m%	0.5 m%	0.2 m%	0.1 m%	1 m%

For the UV system, the generic formulation is as follows:

Compound	EA	AcOEt	BDA	HMP	ALA
Quantity	/	50 v%	0 %	0.1 m%	1-2 m%

As in the previous chapter, the second curing reaction is performed on two samples at the same time, one that is prestretched at a clamped stretch ratio λ_{clamp} and one that is left at rest. Eventually, the prestretched dual-cured sample shows a residual extension λ^* while the other one shows almost no change in dimensions. Note that the two subsamples originate from the same initial network.

2.2. Preparation of double networks

The two dual-cured filler networks are then incorporated in double network structures by swelling and polymerization (see Figure 1). The method is strictly identical to the one reported earlier [1]. Essentially, the filler network is swollen in the glovebox in a bath of the following formulation:

Compound	EA	BDA	HMP
Role	Monomer	Crosslinker	UV initiator
Quantity	/	0.01 mol%	0.01 mol%

After 2h swelling, the swollen gel is placed between two sheets of PET (54µ µm thickness) and two glass slides. The sample is then irradiated on both sides at 5-10µW/cm^2 for 2h. Drying for 12h at least in vacuum yields the multiple network elastomer. In all cases, mass losses during drying are low (about 2% at most), indicating that the matrix networks are well-polymerized.

For efficiency reasons, two samples are sometimes prepared at the same time. In this case, the volume of the swelling bath is increased and samples are placed next to each other between the glass slides to ensure uniform UV irradiation.

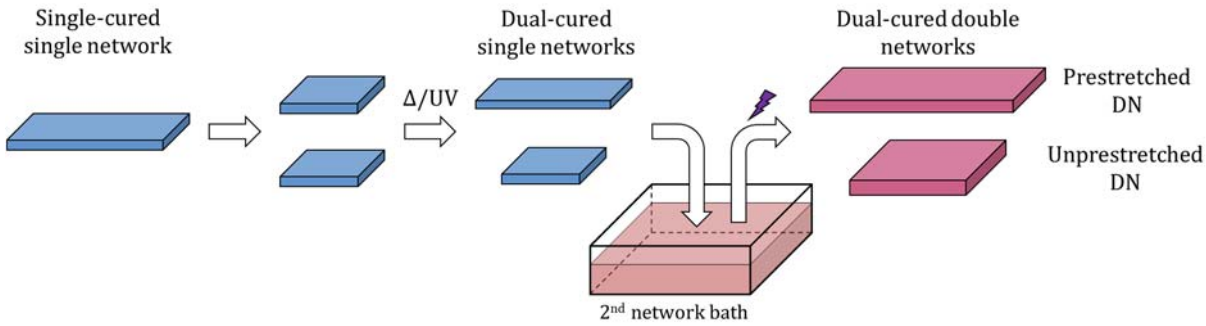

Figure 1: schematic representation of double networks preparation process. From the same initial single-cured network, two double networks are prepared, one that is prestretched and one that is not.

2.3. Step-cyclic tests

2.3.1. Description of the test

In addition to unidirectional tensile tests already described in chapter 2, DN samples of the UV system are tested in step-cyclic tensile test. The shape of samples and the equipments are similar to unidirectional tensile tests (see chapter 2). The major difference is that stretch is applied with a specific loading sequence. Specifically, 3 cycles are performed at each level of stretch, as shown in the example of Figure 2. The maximum applied stretch ratio λ_{step} is increased step-by-step until the sample breaks. The loading speed is constant during the test. Unloading phases are stopped once the force reaches the arbitrary level of 0.05 N to prevent any buckling of the sample

2.3.2. Extraction of the cyclic test envelope

Due to the small amount of material available for mechanical testing, most UV-based DN samples have only been tested in step-cyclic tests. In order to mimic the unidirectional tensile test, the envelope of cyclic tensile tests is extracted using a moving maximum algorithm. The latter starts by measuring the maximum stretch ratio of the cyclic test, defined as $\lambda_{\text{max, test}}$. The overall stress curve is then scanned from $\lambda = 1$ to $\lambda = \lambda_{\text{max, test}}$ by steps of $(\lambda_{\text{max, test}} - 1)/999$. For each interval of stretch ratio that is scanned, only the largest value of nominal stress in retained. The 1000th data point of the envelope is finally defined as the maximum stress of the overall test.

Comparison of cyclic test envelopes with unidirectional tensile tests is shown later in the manuscript. It proves that the procedure may be used to accurately mimic the results of a unidirectional tensile test using only the results of a step-cyclic test.

2.3.3. Study of strain-hardening using Gent's model

Fitting model

Gent's model [2] is phenomenological and models the strain-hardening functional form using an inverse relationship:

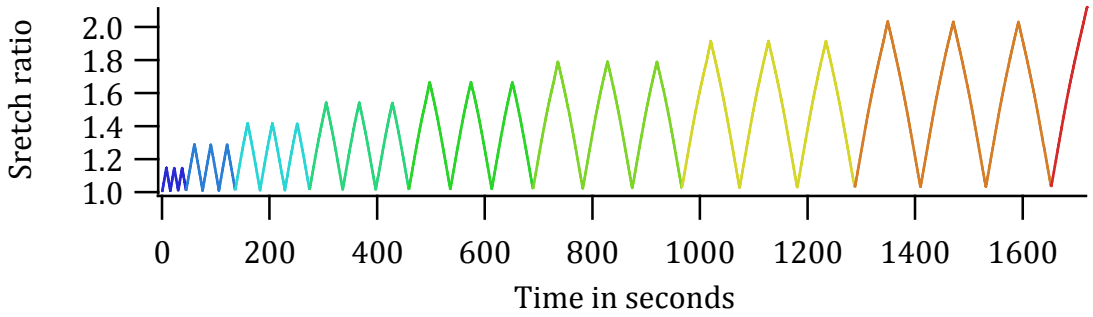

Figure 2: example of a stypical stretch profile used for a cyclic test.

$$\sigma_{\mathrm{N}} = G\left(\lambda - \frac{1}{\lambda^2}\right)\left(\frac{1}{1 - J_1/J_{\mathrm{m}}}\right) \qquad \text{Eq. 1}$$

where G is the shear modulus, $J_1 = \lambda^2 + 2/\lambda - 3$ is the first strain invariant (minus 3) and J_{m} is an adjustable parameter that sets the largest possible value of J_1. This relationship works fine provided strain-softening at small strain is moderate. In addition, experimental data need to show a pronounced strain-hardening to have enough data points for the fit of J_m. When either of the two conditions is not fulfilled, the fit returns absurd values for J_m.

Our experimental data sometimes show softening at low strain, especially for the last steps of the cyclic tests, probably because of the presence of a permanent set. In order to catch this behavior, a modified version of Eq. 1 is used by combining it to Mooney-Rivlin's model. This modification gives a stretch dependence to the shear modulus:

$$\sigma_{\mathrm{nom}} = \left(C_1 + \frac{C_2}{\lambda}\right)\left(\lambda - \frac{1}{\lambda^2}\right)\left(\frac{1}{1 - J_1/J_{\mathrm{m}}}\right) \qquad \text{Eq. 2}$$

where C_1 and C_2 are adjustable parameters whose sum is the shear modulus at zero strain.

More specifically, the following version of the equation is used to fit our data in order to take into account the finite stretch ratio $\lambda_{\mathrm{initial}}$ and nominal stress $\sigma_{\mathrm{initial}}$ at the beginning of each cycle (remember that the end of each cycle is defined by a residual force of 0.05N):

$$\sigma_{\mathrm{nom}} = \sigma_{\mathrm{initial}} + \left(C_1 + \frac{C_2}{\lambda\lambda_{\mathrm{initial}}}\right)\left(\lambda - \frac{1}{(\lambda\lambda_{\mathrm{initial}})^2}\right)\left(\frac{1}{1 - \frac{(\lambda\lambda_{\mathrm{initial}})^2 + 2/\lambda\lambda_{\mathrm{initial}} - 3}{J_{\mathrm{m}}}}\right) \qquad \text{Eq. 3}$$

Note that $\sigma_{\mathrm{initial}}$ and $\lambda_{\mathrm{initial}}$ are not fitting parameters but constants that are set to actual experimental values for each fit.

Fitting procedure

For each step of the cyclic tests, only the third unloading cycles are fitted. The raw experimental data looks like the left graph of Figure 3.

First, the very last cycle of the test is fitted using Eq. 3, with the restriction that J_{m} must be larger than $1.01 \times J_{1,\,\mathrm{max,\,test}}$ where $J_{1,\,\mathrm{max,\,test}}$ is the value of J_1 at $\lambda_{\mathrm{max,\,test}}$ the largest stretch ratio of the cyclic test. This restriction is arbitrary and used merely to avoid numerical divergences.

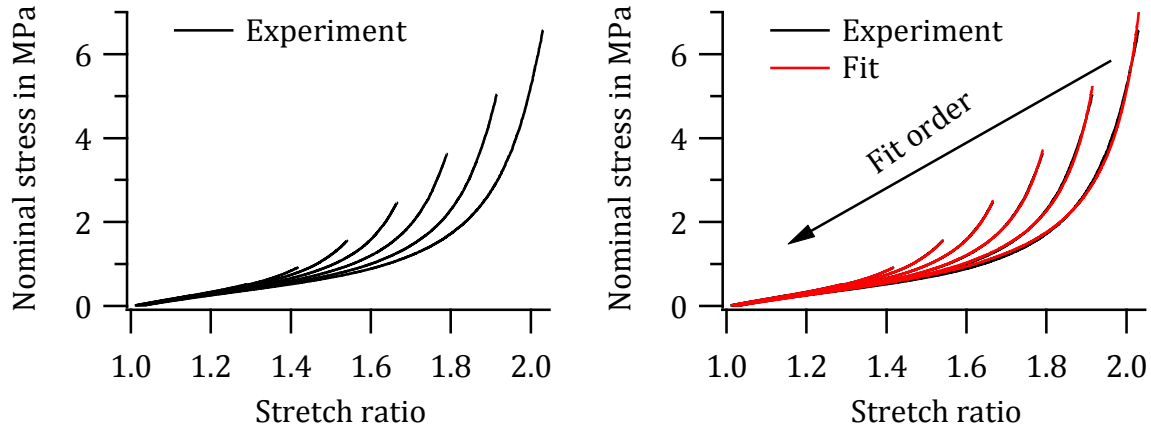

Figure 3: example of fitting experimental cyclic test data using Gent's model. Left: raw experimental data. Right: experimental data with fitted curves superimposed. Fits are performed from the last cycle to the first one.

At this stage, the last step of the test is fitted which gives a maximum value for the J_{m} parameter. The previous cycle is then fitted. This time, the fitted value of J_{m} is restricted to the interval ranging from $1.01 \times J_{1,\,\mathrm{max,\,step}}$ for the lower bound to the previously fitted value of J_m for the upper bound. In other words, the value of J_m is forced to decrease throughout the fitting procedure, which means that J_m is an increasing function of the maximum stretch ratio of each step λ_{step}. This procedure is based on the fundamental assumption that the maximum extensibility of the network can only increase when the material is damaged. Therefore, the value of J_{m} at step n is an upper bound for step $n-1$.

Previous steps are treated this way sequentially so that values of J_{m} are obtained for all steps. Note that the first steps also return values for J_{m} although there is no visible strain hardening on the curves. These values are only obtained thanks to the fitting procedure that starts from the last cycle and fits the cyclic test backwards. They may be seen as hypothetic values of maximum extensibility that would be observed if the material was stretched further without damaging.

Finally, these values of J_{m} are converted into values of λ_{m} by numerically solving the defining equation of J_{m}.

2.4. Fracture tests

2.4.1. Principle of the measurement of fracture energy

For reasons that are specified later, the study of the fracture properties have only been performed on samples based on the UV dual-curing system. In order to determine the fracture energy Γ, a notched sample is stretched in a unidirectional tensile test and Greensmith's approximation [3] is used:

$$\Gamma = \frac{6\,c\,W(\lambda_{\mathrm{prop}})}{\sqrt{\lambda_{\mathrm{prop}}}} \qquad \text{Eq. 4}$$

where c is the initial crack length, λ_{prop} is the stretch ratio at which the crack propagates in the notched sample and $W(\lambda_{\text{prop}})$ is the value of the strain energy density when the crack propagates.

Tested samples are strips of material of 5 mm width and are cut with a punch. The length of the strip is roughly 20 mm. The initial notch is made in the width direction with a razor blade. On average, the initial crack length is about 0.8 mm. The actual size of the notch is measured using an image of the sample and the software ImageJ. The notched sample is then clamped and stretched at a constant speed (500 µm/sec) until the crack propagates.

2.4.2. Specific procedure

A specific fracture study focusing on the influence of previous damage on the fracture energy is carried out, which requires an adaptation of the measurement procedure. Two strips of material are cut from each double network sample. The first strip is tested directly in the single-edge notch test configuration at 500 µm/sec, as described in section 2.4.1. This virgin sample gives a first value of fracture energy Γ_{virgin}.

The other unnoteched strip of material is stretched up to a certain stretch ratio at 500 µm/sec and is then unloaded at the same speed. The stress-strain curve features a mechanical hysteresis. The level of stretch ratio that is applied during this conditioning cycle depends on the the level of ALA in the formulation. Levels of applied stretched are as follows:

ALA content in formulation	1.0 mol%	1.5 mol%	2.0 mol%
Max applied λ	80%	115%	150%

After unloading, a notch is made and the fracture energy is estimated on this damaged sample, still at 500 µm/sec. This new fracture energy Γ_{damaged} is the fracture energy of the damaged sample.

In the determination of the fracture energy using Eq. 4 the value of W should be calculated by integrating the stress-strain curve of an unnotched sample of similar dimensions and from the same material. Here, the stress-strain curve used for the calculation of W is not the same for the virgin and for the damaged sample:

- For the virgin material, the loading curve of the conditioning cycle is normally used. When this cycle is not available, a unidirectional tensile test is used. When only a cyclic test has been performed, the envelope of the test is used.
- For the damaged sample, the unloading curve of the conditioning cycle is normally used. When this cycle is not complete (for instance when the sample broke before the end of unloading), the unloading curve of a cycle from the step-cyclic test is used. In this case, the cycle with the maximum stretch ratio closest to the applied stretch in the conditioning cycle is used. In last resort, a unidirectional tensile test curve is used (and in this case, the resulting integral is slightly overestimated). The latter case has only been used for one sample (one of the transverse subsamples at 2.0 mol% ALA)

Figure 4 shows an example calculation of Γ, with on the left a superposition of the stress-strain curves of the notched samples as well as the conditioning cycle. On the right, the numerical

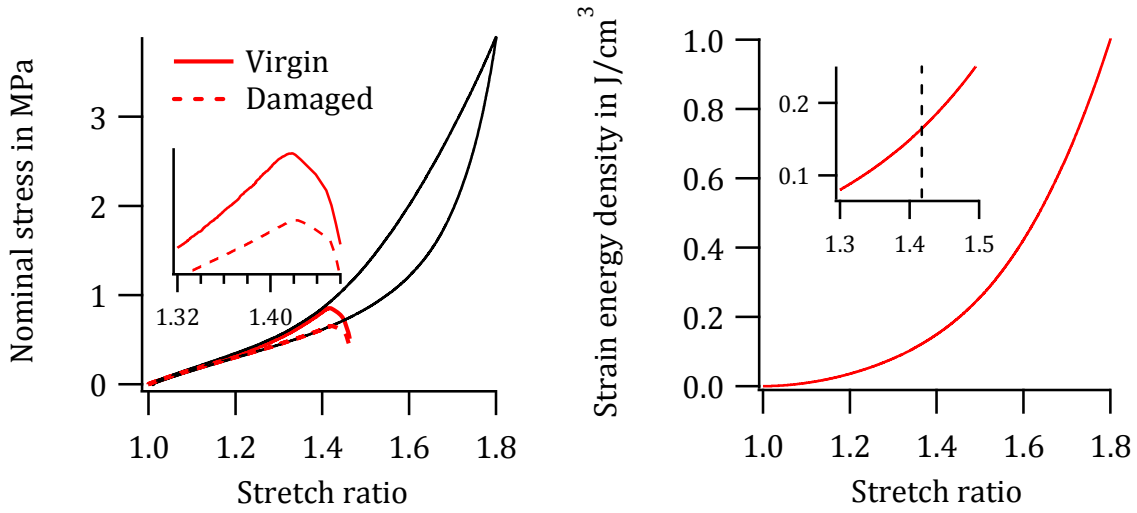

Figure 4: example of a calculation of fracture energy on a sample using the conditioning cycle. Left: conditioning cycle (in black) with the stress-strain curves of virgin and damaged notched samples (plain and dashed lines respectively). Insert is a close up of the notched curves around the propagation point. Right: Integral of the loading curve of the conditioning cycle for the calculation of Γ_{virgin}. Insert is a close up in the area of the propagating stretch ratio of the notched virgin sample.

integration of the unnotched sample loading curve is given. The different parameters necessary for the estimation of Γ with Eq. 4 are first calculated. By image analysis, the crack length is estimated at 0.62 ± 0.08 mm. Using the graph from Figure 4-A, the stretch ratio at which the crack propagates is estimated at 1.42 ± 0.02. The corresponding value of $W(\lambda_{prop})$ is then read on Figure 4-B. This yields a raw value of 509 J/cm^2 for Γ_{virgin}.

2.4.3. Determination of error margin

To estimate the uncertainty associated to the measurement of Γ, Eq. 4 is first differentiated. After calculation, this yields:

$$\frac{d\Gamma}{\Gamma} = \left(\frac{dc}{c}\right) + \left[\frac{\sigma(\lambda_{prop})}{W(\lambda_{prop})} - \frac{1}{2\lambda_{prop}}\right] d\lambda_{prop} \qquad \text{Eq. 5}$$

The two sources of errors (on λ_{prop} and on c) are assumed to be independent, which gives after normalization:

$$\frac{\Delta\Gamma}{\Gamma} = \sqrt{\left(\frac{\Delta c}{c}\right)^2 + \left(\frac{\sigma(\lambda_{prop})}{W(\lambda_{prop})} - \frac{1}{2\lambda_{prop}}\right)^2 (\Delta\lambda_{prop})^2} \qquad \text{Eq. 6}$$

If we consider the curves from Figure 4 as a representative example, a numerical application of Eq. 6 gives a relative error of about 15%.

This value may appear quite high, but it has to be compared to the variability between samples of similar formulations, the latter being also quite high. In slightly more rigorous terms, the measurement of Γ for a given formulation may be written as

$$\Gamma = \bar{\Gamma} + \sigma^2 + \sigma_{\text{mes}}^2 \qquad \text{Eq. 7}$$

where $\bar{\Gamma}$ is the average value of the fracture energy (the one we try to estimate for each formulation group), σ^2 is the variance due to the variability between samples of similar formulations and σ_{mes}^2 is the variance due to the error of measurement.

One can estimate the overall variance $\sigma_{\text{tot}}^2 = \sigma^2 + \sigma_{\text{mes}}^2$ by calculating an estimate of the variance with the experimental values for a given formulation. Obviously, the overall variance should be larger than the variance associated with the measurement. In practice, it is assumed that $\sigma_{\text{tot}}^2 > \sigma_{\text{mes}}^2$ so that the estimated variance may be used safely to construct a confidence interval and present values for fracture energies (using a Student's law and a risk of 5%). Throughout the study, this hypothesis has not been refuted when using a chi square statistical test with a risk of 5%. In other words, the observed variance measured using the square distance to the average of data points of each formulation is consistent with the error of measurement associated to Γ.

All in all, one should keep in mind that the real limiting factor for the presentation of clean and reliable data in fracture tests is the number of samples tested. Unfortunately, in our case, the cost of material is very high in terms of preparation time, and therefore only a limited number of samples could be tested. This explains why very large confidence intervals are presented thereafter.

3. Study of two examples of prestretched DN

The preparation and mechanical characterization of two example materials is first presented. The first one is made using a prestretched filler network using the thermal system with the formulation MA_0.2/0.5. The second one uses the UV system with a formulation containing 2.0 mol% ALA. Despite the differences in terms of chemistry, stiffness and prestretching, the two materials share some interesting characteristics that are now detailed.

3.1. Relative changes in dimensions

The preparation of the prestretched double networks starts with a swelling step followed by the UV polymerization of the matrix network. Changes in dimensions and masses are followed throughout the process in the three dimensions. Only the relative dimensional changes are shown here, mass increase being entirely consistent with it.

Data is shown in Table 1 for the thermal system and Table 2 for the UV system[1]. Clamped stretched ratios λ_{clamp} are fairly similar in both cases, but **the final prestretching λ^* is larger for the thermal system**. As stated in the previous chapter, the extent of prestretching is linked to the crosslinking asymmetry during second curing: the larger the increase in stiffness and the larger the final prestretching for a given clamped stretch ratio. This in indeed the case here: according to the mechanical characterizations from chapter 2, the modulus should increase from 0.20 to 0.82 MPa for the thermal system and from 0.35 to 0.89 MPa in the UV case. The crosslinking asymmetry is therefore larger with the thermal system, which explains why the final prestretching is larger for this system. The fact that the two systems swell the same is also consistent with the similar Young's moduli of the dual-cured filler networks.

For both UV and thermal systems, **prestretched and unprestretched samples swell more or less isotropically**, with a difference in swelling stretch ratio of only a few percents at most between the two directions. In other words, the prestretching is too small to influence the way the sample swells. This may appear counterintuitive but is consistent with the fact that asymmetry is only expected in case of strong deviation from Gaussian behavior. Here, deformation is moderate during swelling and prestretching is not very high.

Another important observation is that **the extent of swelling is not significantly affected by the presence of prestretching**. The average swelling stretch ratio is larger in the unprestretched sample, but only by a few percents. This indicates that the average crosslinking density of the filler networks is probably approximately the same with and without prestretching. In other words, the

[1] Note that thicknesses of dual-cured samples are small (less than 1 mm) so that measurement with a caliper bears a larger relative error compared to the two other dimensions.

Thermal system

Sample	Direction	Preparation stage			Swelling stretch ratio ($\lambda_{\text{swelling}}$)
		After clamping	After second curing	After second polymeriz.	
Prestretched	Length	$\lambda_{\text{clamp}} = 2.84$	$\lambda^* = 2.37$	3.56	1.50
	Width	[0.59]	[0.65]	[0.99]	1.53
	Thickness	[0.59]	[0.65]	[0.98]	1.51
Unprestretched	Length	1	1	1.54	1.54
	Width	1	1	1.57	1.57
	Thickness	1	1	1.48	1.48

Table 1: evolution of relative geometrical dimensions during the preparation process of double networks prepared from dual-cured samples using the thermal system. Bracketed values are calculated assuming volume conservation during second curing. Swelling ratio is calculated from the change of dimensions between first and double networks. Note that measurement error is larger in the thickness direction because of the smaller size of the sample in this direction.

extent of the second curing reaction does not really seem to be affected by prestretching. The fact that prestretched samples swell a little bit less than the unprestretched ones is also consistent with expectations based on Flory's model. Prestretching is supposed to induce a slight increase in stiffness, and therefore it is not suprising that the swelling stretch ratio is slightly lower when prestretching is applied.

In both cases, measured values of swelling ratio are similar to what has been observed before in multiple network elastomers. Using Millereau's classification of mechanical behaviors in multiple network families [1,4], these values of $\lambda_{\text{swelling}}$ sould correspond to a "type 2" multiple network reinforcement. The expected mechanical signature for these samples is a strain-hardening with no visible softening. This of course is only true if prestretching does not influence the toughening mechanism of standard double network elastomers.

UV system

Sample	Direction	Preparation stage			Swelling stretch ratio ($\lambda_{\text{swelling}}$)
		After clamping	After second curing	After second polymeriz.	
Prestretched	Length	$\lambda_{\text{clamp}} = 2.69$	$\lambda^* = 1.77$	2.67	1.51
	Width	[0.61]	[0.75]	[1.14]	1.51
	Thickness	[0.61]	[0.75]	[1.15]	1.53
Unprestretched	Length	1	1	1.53	1.53
	Width	1	1	1.53	1.53
	Thickness	1	1	1.57	1.57

Table 2: evolution of relative geometrical dimensions during the preparation process of double networks prepared from dual-cured samples using the UV system. Conventions about calculated values are identical to Table 1.

Finally, despite the isotropic swelling that is observed, it is worth pointing out that prestretched samples show a very pronounced "geometrical anisotropy", in the sense that the overall relative change of dimensions is much larger in the longitudinal direction than in the transverse direction. Chains should therefore be (at least partly) oriented, which should have a visible effect on the mechanical properties of the material.

3.2. Mechanical characterization

Samples are first characterized by uniaxial traction and results are presented in Figure 5 for the thermal system and in Figure 6 for the UV system. The measured values of Young's Moduli are presented in Table 3. Tests are performed at similar temperature differences from the glass transition temperature (60°C for the PMA-based thermal system, room temperature for the PEA-based UV system) but at different strain rates (100 µm/sec for the thermal system, 500 µm/sec for the UV one). Since the two families of materials are only weakly viscoelastic at these testing temperatures, the difference in strain rate is not believed to be very important and comparison between the two systems is believed to remain relevant.

3.2.1. Global comparison of the two systems

First and foremost, the same kind of mechanical response is obtained for all samples. **A slight softening at small strain is observed, followed by a significant strain hardening at larger strains**. This response is typical from tough double networks [1,5]. A first immediate conclusion is therefore that the toughening mechanism of multiple networks is efficient despite the presence of a residual prestretching.

Another direct comparison shows that **the double networks prepared with the UV system exhibit overall larger stresses and strain-hardenings located at smaller stretch ratios on average**. In conventional double networks, this feature is typically linked to a difference in filler network crosslink density. This is probably not the case here for three reasons:

- First, as stated in chapter 2, the measured Young's moduli of unprestretched filler networks with the same formulations are very close to each other. The thermal unprestretched dual-cured filler network has a modulus of 0.82 MPa (measured by DMA) while the UV one has a modulus of 0.89 MPa (measured by uniaxial traction).
- Second, the values of swelling equilibrium and hence the values of isotropic stretch ratios $\lambda_{\text{swelling}}$ are very similar between the two systems, as shown by the comparison of Table 1 and Table 2.
- Third and last, the modulus of the unprestretched double networks are very close to each other between the two families of materials(see Table 3).

For all these reasons, there should not be a significant difference in terms of average crosslinking density between the thermal and UV dual-cured filler networks. The difference in strain hardening behavior cannot be explained either by the difference of monomer chemical nature. The maximum extensibility of the filler network typically scales with $\sqrt{\mathcal{M}_x/C_\infty}$ (see chapter 3) where $\mathcal{M}_x$ is the molar mass of a network strand and is therefore proportional to the monomer molar mass $\mathcal{M}_0$. A

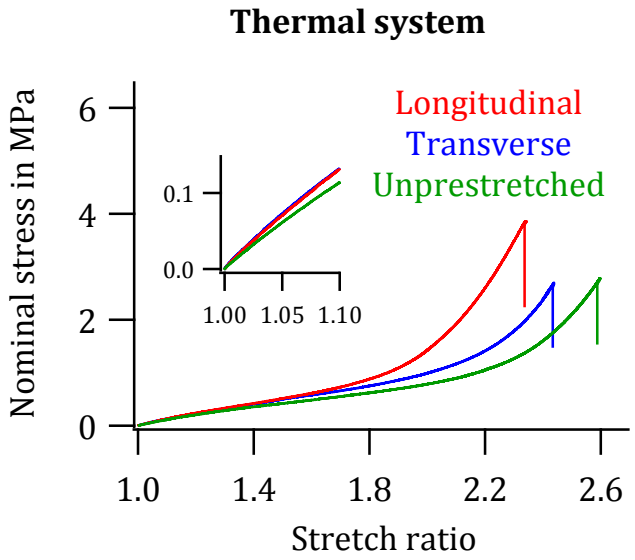

Figure 5: mechanical characterization of double networks based on the thermal system. All samples originate from the same initial network. "Longitudinal" and "transverse" curves correspond to the prestretched sample, in the respective directions. "Unprestretched" curve corresponds to the unprestretched dual-cured double network. The insert shows a zoom at small strains. Samples are tested at 60°C and 100 µm/sec.

numerical application using values of PMA and PEA and assuming the same number of repeat units between crosslinks gives an expected difference in maximum extensibiity of a few percents. This is well below the actual differences observed here between Figure 5 and Figure 6.

Instead, the difference between the stresses at large strains of the two systems might originate from more subtle differences in the networks architectures. Heterogeneity for instance could play an important role, maybe because of the hypothetic presence of clusters of crosslinks in the thermal networks. The amount of transfer reactions between the filler and matrix networks may also play a role.

3.2.2. Observation of the small strain regimes

From the results of Table 3, the modulus of the prestretched DN is on average 32% larger than the unprestretched one for the UV system and 19% larger for the thermal one. In the two systems, **the unprestretched double networks appear to be significantly softer than the prestretched ones, regardless of the direction**. The stiffening effect of prestretching is however more pronounced in the UV system.

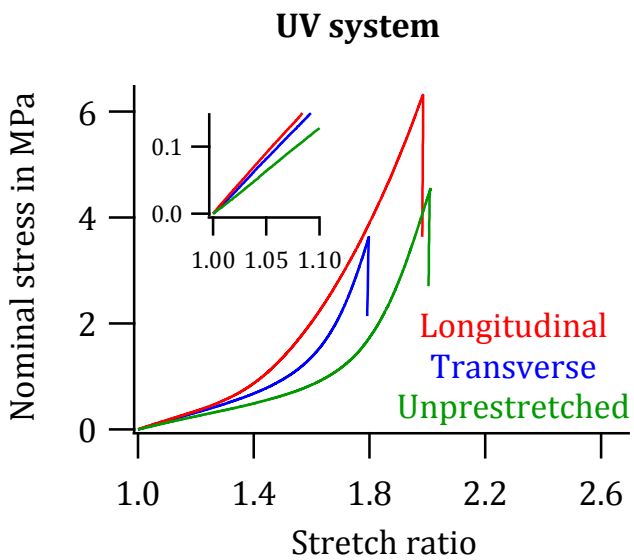

Figure 6: mechanical characterization of double networks based on the UV system. All samples originate from the same initial network. Legend and axis scales are identical to Figure 5. The insert shows a zoom at small strains. Samples are tested at room temperature and 500 µm/sec.

Type of sample	Direction	Young modulus (MPa)	
		Thermal system	UV system
Prestretched DN	Longitudinal	1.50	1.78
	Transverse	1.51	1.66
Unprestretched	Any	1.26	1.30

Table 3: comparison of the Young moduli of prestretched and unprestretched double networks prepared using the thermal or the UV system.

Based on the knowledge of traditional double networks [6] and since the fraction of filler network is approximately the same for the two systems (swelling stretch ratios are almost identical), the modulus of the double networks is certainly directly linked to the modulus of the filler networks. Therefore, differences between the two series of double networks in the small strain regime should be due to differences between the filler networks. Since the swelling stretch ratios are roughly similar between the prestretched and unprestretched networks, the difference in double network modulus probably does not come from differences in filler network average crosslinking density. Instead, it might originate from the increase in modulus due to prestretching that is predicted by Flory's model. The latter model predicts that the modulus of a prestretched dual-cured network should be larger than the modulus of an unprestretched network with identical crosslinking density, which is consistent with the observation made on prestretched and unprestretched DN regardless of the second-curing system.

The magnitude of this stiffening effect is also expected to increase when the crosslinking asymmetry is not very pronounced (see chapter 3). This may explain the difference in terms of stiffening due to prestretching between the UV and thermal systems. Based on the results from chapter 2, the stiffness of an unprestretched dual-cured network of same formulation as here increases by a factor 7 for the thermal system during the second curing. This increase is only by a factor of 3 for the UV system. This means that the increase in crosslinking density during the second curing is more pronounced for the thermal system than for the UV one, and so is the crosslinking asymmetry between the two populations of crosslinks. One therefore expects a larger increase in modulus because of prestretching in double networks with the UV system than with the thermal one, which is exactly what is observed here.

The study of the small strain regime also reveals another difference between the two systems. When the values of the Young's moduli are compared between the longitudinal and the transverse directions, **the modulus seems to be perfectly isotropic for the thermal system**. On the other hand, **the longitudinal direction is slightly but visibly stiffer than the transverse one in the UV system**. This directional difference is small (about 7%) but visible on the stress-strain response at small strains (see insert of Figure 6). Once again, this difference in stiffness does not correlate with the observed swelling ratios since in both cases the values of $\lambda_{\text{swelling}}$ are roughly the same in the longitudinal and transverse directions. This additional longitudinal stiffness may be due to the presence of short chains in the UV-based filler network structure. These chains would be stretched isotropically by the matrix network, and anisotropically in the longitudinal

direction by the effect of permanent stretch ratio. As a result, these short chains could be close to their maximum extensibility, and especially in the longitudinal direction. When the prestretched DN is stretched in this direction, these short chains could therefore increase the observed value of stress, and hence increase the value of modulus that is measured in range of 0 to 8% deformation. Remember that the presence of short chains in the network structure has already been hypothesized in chapter 2 from the shape of unprestretched dual-cured tensile responses.

To sum up, the study of the small strain response of these two example materials shows that prestretched double networks are stiffer than their unprestretched counterparts. This stiffening effect is qualitatively consistent with predictions based on Flory's model. The small strain response of the prestretched double networks is mostly isotropic, although a slight directional effect may be observed with the UV system specifically.

3.2.3. Observation of the large strain regime

In contrast with the fairly small differences observed in the small strain regime, the large strain responses show much bigger differences. First, for the two systems under study, **the onset of strain-hardening is located at smaller stretch ratios for the prestretched DN compared to the unprestretched ones**. This larger extensibility in the unprestretched case is also accompanied by a lower stress in the mid-strain region. This agrees well with the observed difference in Young's modulus, since stiffer materials are usually associated to shorter network strands and thus smaller maximum extensibility. This observation is substantiated later in the manuscript.

Another important observation may be done by comparing the prestretched double networks between the two systems. **In both cases, the longitudinal direction of the prestretched networks strain-hardens before the transverse direction**. The prestretched double networks that we have prepared are therefore anisotropic at large strains despite the apparent isotropy of the properties at small strains. This anisotropy is most probably due to the combined effect of prestretching and maximum extensibility of the filler network chains. As explained in chapter 3, prestretched dual-cured networks are supposed to remain isotropic as long as the network strands remain Gaussian. Anisotropy may arise at large strain when the strands get close to their maximum extensibility. In a double network structure, this is typically the case since the filler network chains are prestretched by the presence of the matrix network. The experimental observation of directional dependence of strain hardening in prestretched double networks therefore confirms our physical intuition based on the extension of Flory's model at large strains.

3.3. Toward a more detailed characterization?

Until now, only a direct comparison and overall observation of the two examples of prestretched double networks have been made. These first observations confirm that the toughening mechanism of double network elastomers is still active in prestretched materials and that their mechanical properties are globally isotropic at small strains but anisotropic at large strains. This directional effect is qualitatively attributed to the presence of prestretching.

These observations should now be substantiated with additional characterization and comparison to models.

3.3.1. Comparison of the thermal system to Flory's model

This subsection focuses specifically on the double networks prepared from a thermal filler network (i.e. tensile curves from Figure 5). The idea here is to use the extended version of Flory's model derived in chapter 3 to analyze the anisotropy in the prestretched double network elastomers.

Quantification of experimental results

The first step to understand the large strain response of our materials is to put numbers on it. As described in 2.3.3, this may be done by fitting the data with a combined version of Gent and Mooney-Rivlin's models:

$$\sigma_{\mathrm{N}} = \left(C_1 + \frac{C_2}{\lambda}\right)\left(\lambda - \frac{1}{\lambda^2}\right)\left(\frac{1}{1 - \frac{\lambda^2 + 2/\lambda - 1}{J_{\mathrm{m}}}}\right) \qquad \text{Eq. 8}$$

where C_1 and C_2 are two constants and J_{m} is the maximum allowed value of the first strain invariant minus 3. J_m corresponds to a certain maximum stretch ratio λ_m in the tensile direction, and the equation linking the two is $J_m = \lambda_m^2 + 2/\lambda_m - 3$.

This equation is used to fit the tensile curves from Figure 5 in order to extract values of J_m for the three samples tested. The result of the fits are shown in Figure 7. While the model agrees well with data for the transverse and unprestretched cases, the functional form is clearly not adequate for the longitudinal direction. A least square regression fails to catch the shape of the curve, especially at moderate strains and gives an unrealistic null value for C_2. This however does not really concerns the value that is measured for J_m since the position of the vertical asymptote of the curve after strain-hardening is unaffected by the lack of fit at intermediate strains. In other words, the fitted value for J_m is still believed to be meaningful even if the values of C_1 and C_2 are not.

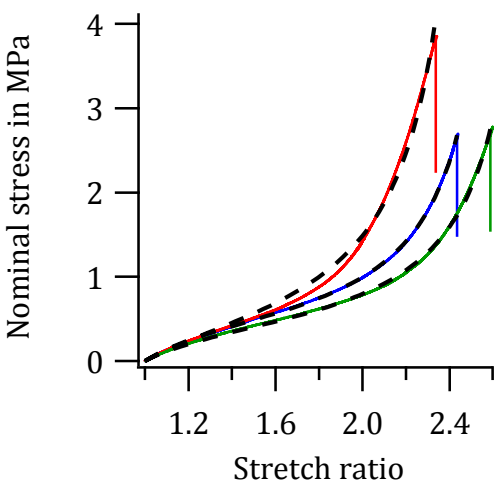

Sample	C_1 (MPa)	C_2 (MPa)	J_m
Longitudinal	0.46	0.00	4.39
Transverse	0.15	0.39	5.08
Unprestretched	0.16	0.27	5.87

Figure 7: fit of tensile curves from Figure 5 using modified Gent's model. Numerical values of fit parameters are given in the table above. Plain lines are experimental curves and dashed lines are results from the fit. The same color code is used for the curves: red = stretched sample in longitudinal direction, blue = stretched sample in transverse direction and green = unstretched sample.

Parameter	Direction	Prediction			Experiment
		First gen.	Second gen.	Both gen.	
E in MPa	/	0.20	0.62	0.82	/
$\nu/\mathcal{N}_A$ in mol/m³	/	23.6	74.9	98.5	/
N_{mono}	/	546	172	131	/
$\lambda_{\max} = R_{\max}/R_0$	/	9.6	5.4	4.7	/
Λ^*	Longitudinal	2.37	0.83	/	/
	Transverse	0.65	1.09	/	/
	Unprestretched	/	/	1	/
$\lambda_{\text{swelling}}$	Longitudinal	1.50	1.50	/	/
	Transverse	1.53	1.53	/	/
	Unprestretched	/	/	1.53	/
λ_{m}	Longitudinal	**2.7**	(4.3)	/	2.57
	Transverse	(9.7)	**3.2**	/	2.71
	Unprestretched	/	/	**3.1**	2.86

Table 4: calculation and comparison of the theoretical prediction for the maximum extensibility of the double network structure λ_{m} with experimental values obtained by fitting the tensile curves with a modified version of Gent's model. The actual predictions of λ_{m} are the smallest possible values (in bold characters), the other one is left aside (and put between brackets)

The next step is then to convert these fitted values of J_m into values of λ_m and to compare the latter with predictions from the extended version of Flory's model presented in chapter 3.

Prediction of λ_m using an extension of Flory's model

As in chapter 3, the results of DMA are used to calculate the crosslinking density ratio corresponding to the formulation that is used here for the filler network. The parameters and results of the extended Flory's model are presented in Table 4 along with the fitted valued of λ_m.

Comparison of experimental values with theoretical predictions shows a pretty good agreement. At least, the correct order of magnitude is predicted for the three samples within a margin of 20%. This margin is not that large considering the variability of the system as well as the relatively weak precision of the measurements. **The error is the most important in the transverse direction subsample**, which indicates that the behavior in this direction is not well captured by the model. Another clear discrepancy between model and experiment (that might be associated to the previous one) is that the order in which the samples strain-harden is not correctly predicted (longitudinal-transverse-unprestretched for the experiment versus longitudinal-unprestretched-transverse for the prediction). Both errors might be due to cross-directional effects. The assumption of separability of the two populations of crosslinks may not be correct in the transverse direction, although the underlying reasons why remain obscure.

The model however confirms the reason behind the apparent discrepancy between mechanical characterization and geometrical change of dimensions. Although the relative change in length is

much larger than the relative change in width, the final difference in terms of stretch ratio at which strain hardening is observed is only about 15%. In other words, the relative difference in size does not match the relative difference in filler network maximum extensibility between the two tested directions. Flory's model gives a qualitative explanation for this:

- In the longitudinal direction, the network strands that are more extensible (first generation) are stretched, while the less extensible ones (second generation) are compressed. The limiting extensibility is therefore due to the first generation of network strands even if the crosslinking density is low.
- In the transverse direction, the less extensible network strands (second generation) are weakly stretched while the ones from the first generation are compressed. The limiting extensibility is therefore due to the second generation of network strands.

As explained in chapter 3, prestretching has a compensating effect according to Flory's model. The visible difference in dimensions only accounts for the deformation of the initial population of crosslinks, yet it is the second one that induces strain-hardening in the transverse direction.

After this first encouraging comparison, the natural follow-up would be to compare the predictions of the model with more materials. For this reason, samples with similar formulations and experimental conditions have been prepared and have raised an unexpected and major issue with the thermal system.

3.3.2. The reproducibility issue of the thermal system

Unfortunately, attempts to reproduce the materials resulted in very different mechanical behaviors. Table 5 compares the experimental parameters between samples that use the same formulation as the example material, and Figure 8 compares their tensile curves. Note that the synthesis yield is the ratio between the actual mass of the initial single-cured network and the expected mass of the sample assuming all monomeric species have reacted (see chapter 2). E is the modulus of the double networks presented in Figure 8.

Figure 8 immediately shows that **all the replicate double networks are brittle, contrary to the reference sample** from Figure 5. There is no visible strain-hardening and the materials break at low extensions (less than 100% deformation). This is very surprising given the measured values of $\lambda_{\text{swelling}}$: with a filler fraction of this order of magnitude, reinforcement should be observed [1].

Sample	Initial yield	λ_{clamp}	λ^*	$\lambda_{\text{swelling}}$	E (in MPa)
Reference	61.2%	2.84	2.37	1.50	1.50
Replicate #1	66.7%	3.42	2.47	1.53	1.59
Replicate #2	62.4%	2.44	2.22	1.52	1.49
Replicate #3	58.4%	1.87	1.62	1.53	1.50
Replicate #4	66.6%	2.38	2.05	1.50	1.50

Table 5: Experimental parameters corresponding to samples from Figure 8.

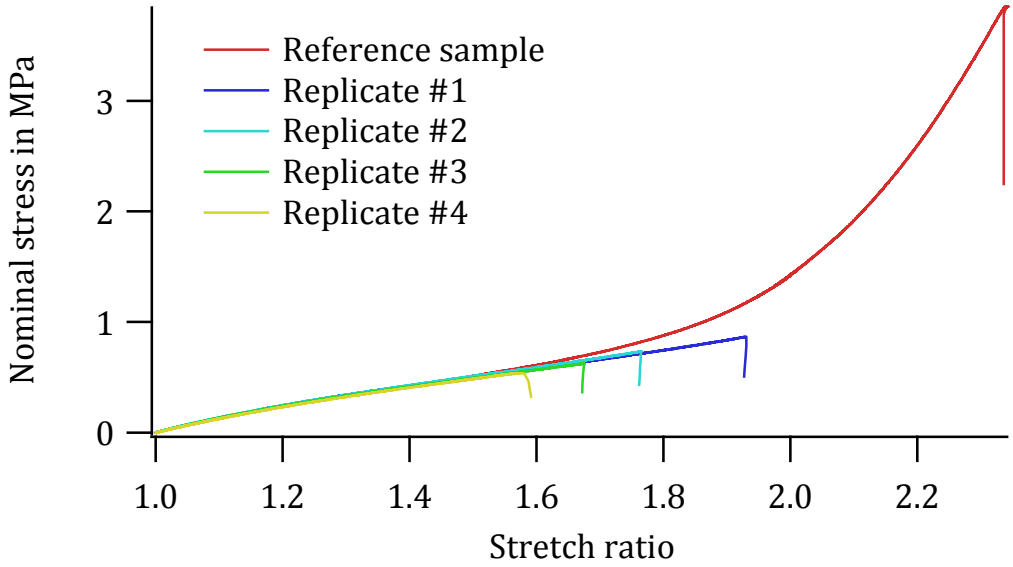

Figure 8: comparison of the example material shown in Figure 5 with replicates using the same formulation and same experimental conditions. All samples presented here are prestretched and tested in the longitudinal direction at 100 µm/sec.

The other puzzling fact is that the reference sample does not feature any extreme value for any of the experimental parameters presented in Table 5. Although there is a variability between samples, it is not possible to identify a critical parameter that could explain the difference between the reference sample and its replicates.

A few additional experiments have been conducted to identify the cause of the problem (infrared, extraction, liquid state NMR) but no conclusion could be drawn. So far, the origin of the difference between the reference and the replicate samples remains unknown. Because of this difficulty to reproduce the results, the thermal system is now set aside and the rest of the manuscript focuses on the UV system.

3.3.3. Cyclic testing of the UV system

When having a closer look at the tensile curves of the UV system in Figure 6, the shapes of the curves are not exactly the same between the longitudinal and the transverse direction. Strain-

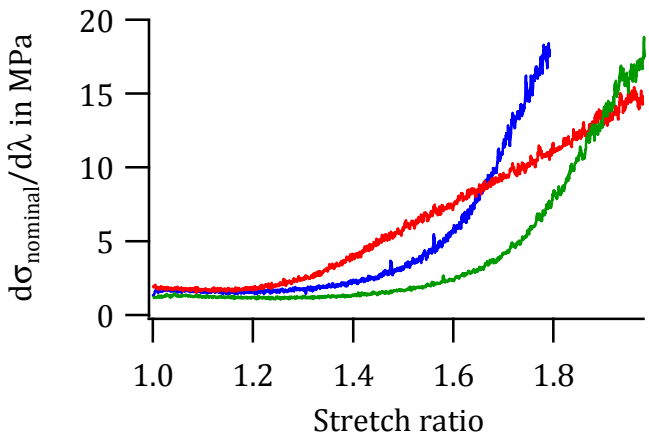

Figure 9: derivatives of the curves from Figure 6. The shapes of the curves are visibly different in the strain hardening region. Data were smoothed with a 10 points moving average filter for clarity (total number point is around 3000 points). Legend is identical to Figure 6.

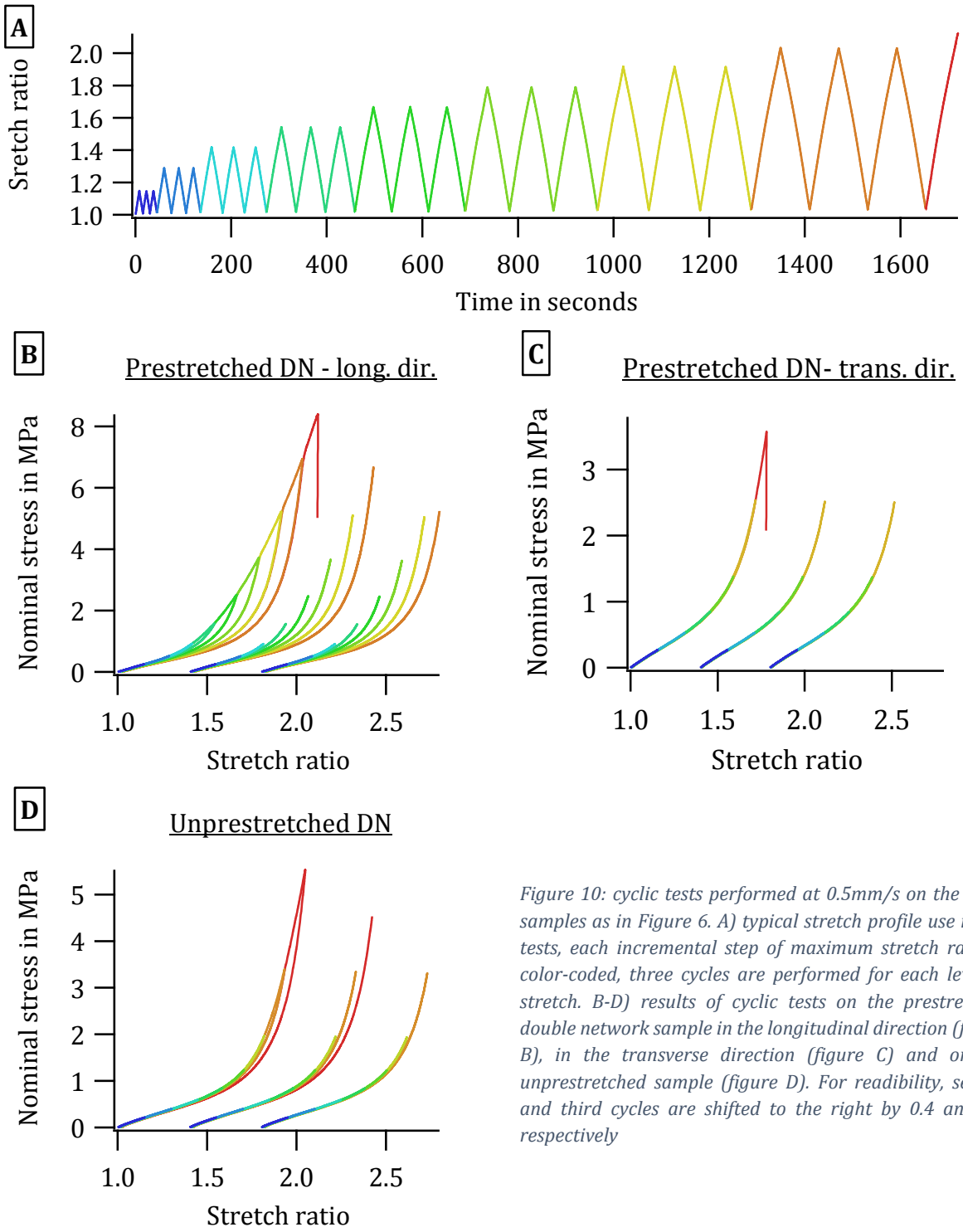

Figure 10: cyclic tests performed at 0.5mm/s on the same samples as in Figure 6. A) typical stretch profile use in the tests, each incremental step of maximum stretch ratio is color-coded, three cycles are performed for each level of stretch. B-D) results of cyclic tests on the prestretched double network sample in the longitudinal direction (figure B), in the transverse direction (figure C) and on the unprestretched sample (figure D). For readibility, second and third cycles are shifted to the right by 0.4 and 0.8 respectively

hardening seems to be more progressive in the longitudinal direction, and this difference seems to be specific to the UV system. To emphasize this observation, the derivatives of the stress vs stretch curves are shown for the UV system in Figure 9 and clearly show that **the slope of the stress-strain curve in the longitudinal direction increases less fast than in the two other cases**.

To investigate the origin of this difference, samples from the same three materials are tested in step-cyclic loading. Results are shown in Figure 10 and the loading history that is applied to the

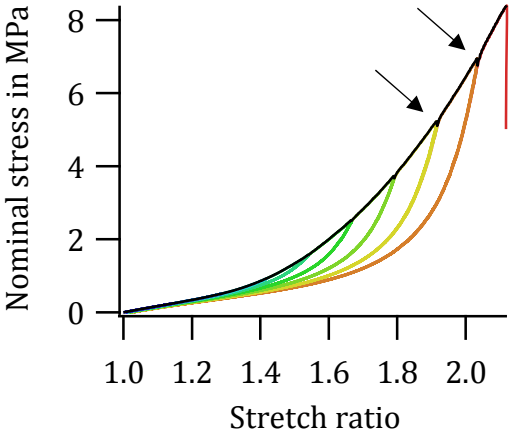

Figure 11: superposition of a typical cyclic test curve with its calculated envelope. The algorithm that is used returns a much simpler curve with only accidental artifacts (shown with arrows) due to the discontinuous increase in stretch.

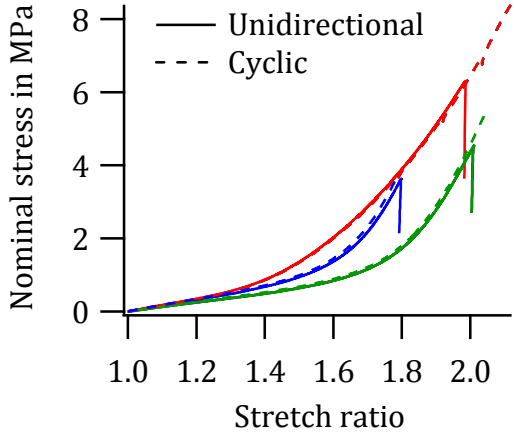

Figure 12: comparison of unidirectional tensile tests (from Figure 6) with calculated envelopes from cyclic loadings (from Figure 10).

samples is shown in sub-figure A. For each increment of stretch, three cycles are performed to account for the potential viscoelasticity of the material. Sub-figures B to D gives the results of the tests for the longitudinal direction (B), the transverse direction (C) and the unprestretched case (D). For readability, the second and third cycles are shifted toward the right by 0.4 and 0.8 respectively.

The results of the unprestretched double network in sub-figure D are first reviewed. **The unprestretched subsample does not show any trace of mechanical hysteresis until the very end of the tensile test**, close to the fracture point. Then, a stress drop is observed during the unloading of the first cycle of the last step. Subsequent cycles follow the unloading curve until the material breaks. Note that the residual deformation is very low throughout the test and only reaches 2.4% at the end of the test. Besides, second and third cycles show virtually no hysteresis loop, which indicates that the material is mainly elastic and only very weakly viscoelastic. Overall, this type of behavior is very typical of classical double network elastomers, and has already been reported before, notably in Ducrot and Millereau PhD works [1,5]. Sub-figure C shows a very similar behavior, although this time **the prestretched sample in the transverse direction breaks before showing any kind of mechanical hysteresis**.

As could be expected from the tensile test results, **the behavior of the prestretched sample is very different in the longitudinal direction**. The beginning of the test proceeds as before, with an almost perfect superposition of the curves, meaning that there is no permanent damage and almost no viscoelastic dissipation. When the material starts to strain-harden (around λ=1.4), the material exhibits massive decrease in stress with large hysteresis loops. This goes on as the material is stretched further until the breakage point. Very notably, damage is only observed in the first cycle of each incremental stretch. Subsequent cycles follow the unloading curves of the first cycles of each step. This goes in favor of breakage of covalent bonds in the system, and more specifically of the most prestretched filler network chains. This type of behavior is commonly observed in multiple network elastomers when the swelling stretch ratio is large and the fraction

of filler network is low. In previous works, this mechanical hysteresis has been attributed to the breakage of covalent bonds in the filler network [5].

In light of these results, cyclic testing seems to be a relevant test to perform on our materials in order to get as much information as possible while using as little material as possible. The test however returns a massive amount of data that is less convenient to handle than a simple unidirectional tensile test. To simplify the data, the envelope of the cyclic stress-strain curve is extracted (see procedure in 2.3.2). As shown in Figure 11, **the envelope is correctly calculated by the algorithm** and shows only occasional accidents due to the non-monotonic increase of stretch. In Figure 12 the envelopes are compared to the actual unidirectional tensile tests. The curves clearly superimpose which proves that cyclic loadings can be used to extract the traditional tensile response of our materials, even when damage is observed in the cyclic test. Only cyclic tests are thus exploited from now on and the envelopes are used to mimic the unidirectional responses of the materials.

3.4. Partial conclusion

Up to this point, the successful preparation of permanently prestretched double networks elastomers has been shown. Using the prestretched filler networks prepared in the previous chapter, swollen gels are obtained and UV-polymerized to give double network elastomers. The latter can be tested in two directions, the longitudinal/prestretched one and the transverse one. These two directions are compared with an unprestretched double network whose filler network has also been dual-cured and comes from the same initial network. This material serves as a comparative reference in order to highlight the specific effect of prestretching on the material tensile response.

Two example materials have been studied in details, one using the thermal dual-curing system and one using the UV system. Regardless of the dual-curing system that is used, the prestretched double network elastomers share the same four properties:

- They are tough, as indicated by the strong increase in stress at large strains (strain-hardening). This mechanical response is typical from standard double network elastomers, which proves that the presence of prestretching does not impair the toughening mechanism at stake.
- They are stiffer than the reference unprestretched double networks. This is consistent with the fact that prestretching is predicted to have a stiffening effect on dual-cured filler networks by Flory's model.
- They are mainly isotropic at small strain. This indicates that the prestretching that is applied is too small to really change the statistics of the chains in the absence of stretch. At rest, the filler network strands are still Gaussian.
- They are visibly anisotropic at large strain. More precisely, the strain-hardening (which corresponds to the limit of extensibility of the filler network in a double network elastomer) occurs at different stretch ratios depending on the direction that is tested.

Despite these common features, the two systems are not strictly identical. In particular, despite showing similar swelling stretch ratios, the double networks prepared with the UV system show larger stresses than the thermal system. Also, the UV system shows a more progressive strain-hardening in the longitudinal direction. This specific difference has been studied by step-cyclic loading and correlates with a massive damage phenomenon. The latter translates into visible stress softening at intermediate and large strains, and looks like a Mullins' effect.

We have also attempted to reproduce the results of the thermal system using replicates with identical formulations and similar preparation parameters. All these copy materials are surprisingly brittle with no visible strain-hardening. Despite its promising results, the thermal system is therefore not suitable for a systematic study of a permanently prestretched double network structure.

Therefore, the rest of the chapter now focuses on the UV system and on a systematic study of the resulting double network elastomers.

4.Systematic study of the UV system

4.1. Identification of typical trends and odd ones

The previous section features an example of prestretched double network elastomer based on the UV dual-curing system. This example is now compared with other materials with various levels of ALA contents in order to identify trends.

For all the rest of this chapter, three ALA contents are studied. All in all, 11 samples are being compared:

ALA content in formulation	1.0 mol %	1.5 mol%	2.0 mol%
Number of samples	4	3	4

Each sample gives two double networks (one prestretched and one unprestretched). Three separate sub-samples are tested in step-cyclic tests (one for the unprestretched sample and one per direction for the prestretched sample).

For consistency, a unique graphic code is used for all plots (see Table 6). The type of line or symbol that is used represents the quantity of ALA in the initial formulation (1.0, 1.5 or 2.0 mol%). The color of the lines or symbols represents the type of sub-sample tested for each sample (red and blue for the prestretched DN in the longitudinal and transverse directions respectively, and green for the unprestretched DN).

First, all the envelope curves are compared in Figure 13. An average behavior may be identified in each formulation group, despite the variability of the parameters of the dual-curing process. A very important point is that **all samples show a visible strain-hardening**: despite the obvious variability of the chemical system, **all samples are tough**. This is therefore a fundamental difference with the thermal system, which makes this UV system much more reliable and suitable for further studies.

It shall be pointed out however that **some samples (one per formulation) visibly differ from the rest of their formulation groups**, probably because of the variability of the chemistry. This difference may typically be seen in the position of strain-hardening in the longitudinal direction. Sometimes it is also visible on other measurable mechanical quantities (modulus, strain/stress at

		1.0 mol% ALA	1.5 mol% ALA	2.0 mol% ALA
Prestretched DN	Longitudinal direction	▲ or ·····	■ or ----	● or ——
	Transverse direction	▲ or ·····	■ or ----	● or ——
Unprestretched DN	Any direction	▲ or ·····	■ or ----	● or ——

Table 6: color code that is used for all the rest of the chapter. The shape of the symbol or line represents the formulation (amount of ALA in the initial network), the color represents the type of sub-sample tested.

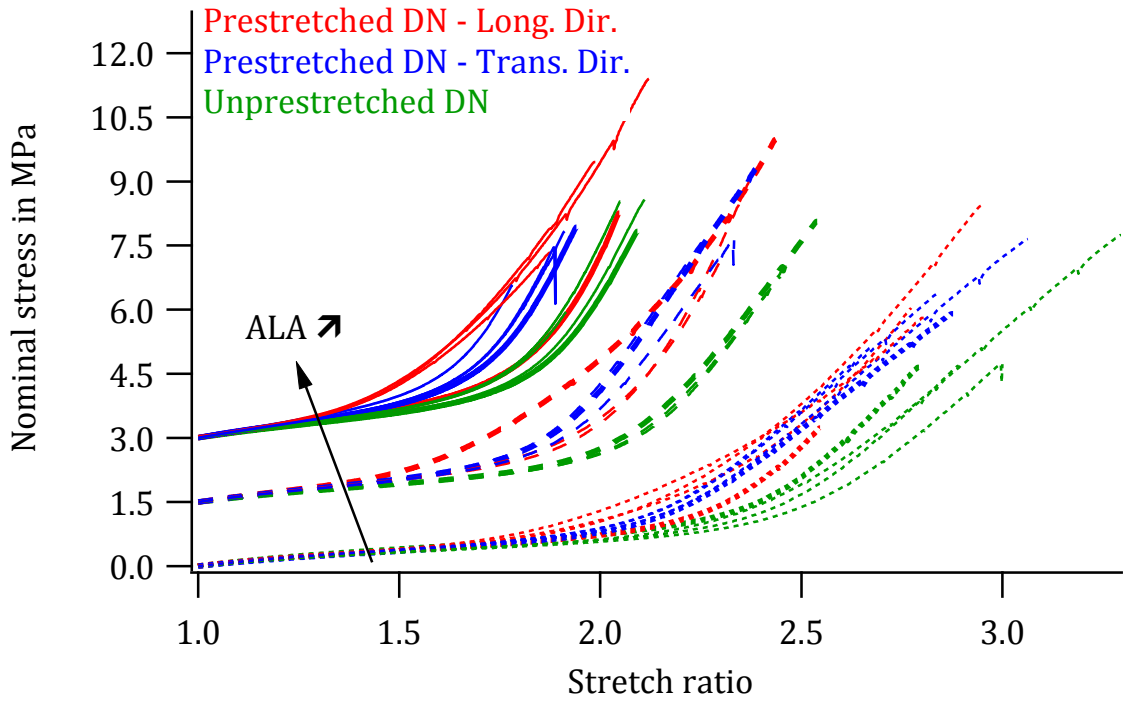

Figure 13: cumulated graph of all cyclic test envelopes for the 11 samples tested. Each sample corresponds to three sub-samples and thus three curves, one per color. The type of line gives the ALA content (1.0, 1.5 or 2.0 mol%). Some samples visibly differ from the average behavior of their formulation group and are highlighted in thicker lines.

break) but not always. A closer look at the various parameters of the preparation process (initial yield, infiltration swelling ratio, prestretching and swelling stretch ratios) does not reveal any significant difference with these samples (data not shown).

Due to the very small number of samples tested, it is impossible to simply rule these samples out. Therefore, the samples are still presented on the different graphs, but with thicker lines and/or open symbols in order to identify them from the other ones. Calculations of average quantities however neglects them and considers them as outliers.

4.2. Study of unprestretched double network samples

This first section only focuses on the unprestreched sample for each formulation group (i.e. all the green curves) in order to avoid comparing all the samples at the same time straight away.

4.2.1. Overall presentation and study of small strain regime

Cyclic test envelopes obtained from the cyclic tests are first compared in Figure 14. These samples have been prepared by dual-curing the initial network without any prestretching. These materials should be similar to traditional double networks, in the sense that the prestretching of the filler network chains only originates from the swelling due to the matrix network polymerization. The only differences comes from the way the filler network has been crosslinked (in two steps here, versus one simultaneous step for traditional DN)

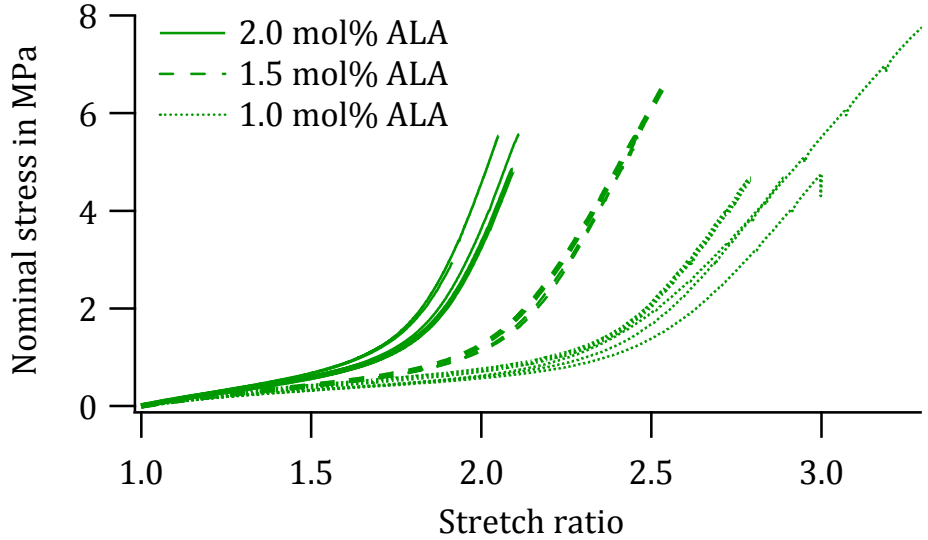

Figure 14: envelopes of cyclic tests performed at 0.5 mm/s on unprestretched DN samples. The type of line gives the amount of ALA in the initial formulation. Thicker lines are samples which show visible differences with the average trends in Figure 13.

Immediately, we see that **the level of ALA in the formulation has a strong impact on the properties of the material at large strain**, since the three groups of curves are well separated. Inside each formulation group, there is not so much variability from sample to sample.

The modulus of all the unprestretched samples is measured by fitting the beginning of the stress-stretch curves with a straight line. Results are given in Figure 15 and clearly show that **the modulus of the double networks increases with the amount of ALA**. This result is not surprising since the properties of the multiple network structures mainly depend on the properties of the filler networks, and in particular on their crosslinking density. A similar result has already been reported by Etienne Ducrot in his PhD manuscript [6]. When the crosslinker content is varied in poly(methyl acrylate) filler networks, the modulus of the PMA-PEA double network elastomer increases almost linearly with the modulus of the filler networks. The same trend may be found here: for each formulation, the average value of the Young modulus is calculated along with a Student's law confidence interval at 95%. This is done to enable safe comparison between the formulations despite the different and small size of the population tested. The result is plotted with respect to the Young modulus of the filler networks, measured

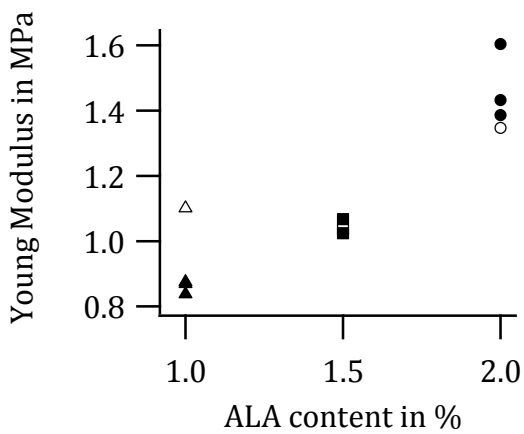

Figure 15: study of Young modulus of unprestretched double network samples with three different levels of ALA. Open symbols are samples that visibly differs from the average trends of their formulation groups. These values are excluded in the calculation of average values.

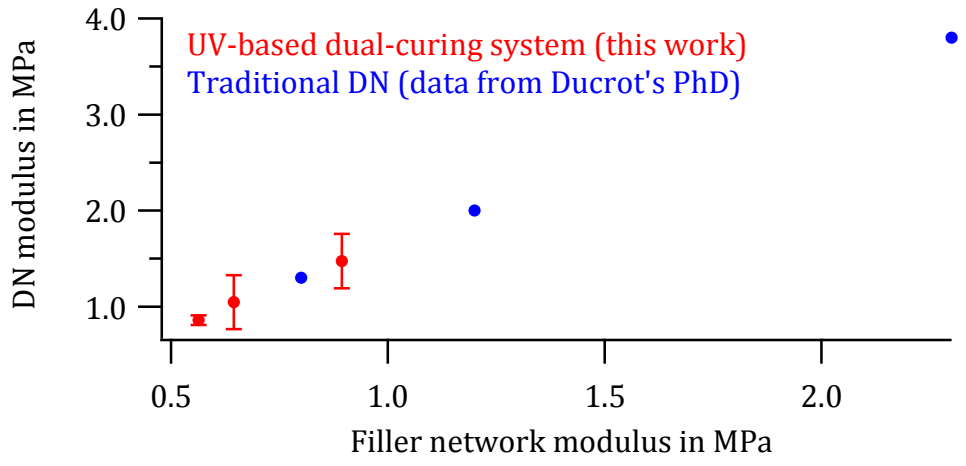

Figure 16: study of the relationship between the modulus of unprestretched double networks with the modulus of the associated filler network. Data from the present daul-curing system (in red) is compared with data from Ducrot's PhD on DN samples with a PEA filler network and a PMA matrix network tested at 60°C. For dual-cured samples, error bars are confidence intervals at 95%.

by uniaxial traction on one sample per formulation (see chapter 2) in Figure 16. Despite the obvious difference in terms of processing route, **our unprestretched double networks are fairly similar to classical double network elastomers in small strains and follow the same linear trend**. Note that our double networks are overall softer than Etienne Ducrot's ones.

4.2.2. Large strain behavior and strain-hardening phenomenon

As already stated, Figure 14 clearly shows three well-separated groups of curves, one for each ALA concentration. The effect of crosslinker concentration on the properties of traditional double network elastomers at large strain has already been studied [6] and our materials follow the same trend. When the filler network is more crosslinked, its maximum extensibility decreases and the strain hardening in the double network occurs at lower strains. A way to analyze further the stress strain curves is thus to rescale the stretch ratio by considering the deformation of the filler network alone. In standard double network elastomers, when samples coming from the same filler network are compared, the stress-stretch curves collapse into a single master curve with a single position for the onset of strain-hardening [1].

The stretch ratio of our tensile experiments is therefore multiplied by the swelling stretch ratio as measured by the average change of dimensions after matrix network polymarization. The result of this rescaling is plotted in Figure 17 and shows once again three well defined batches of curves, one for each formulation. This confirms that **the difference in strain-hardening position primarly comes from differences in maximum extensibility of filler networks**. The fact that the three batches of curves do not collapse into a single curve also proves that the difference in strain-hardening position cannot be explained by a difference in swelling stretch ratio. Filler networks prepared with a lower ALA content are softer and swell more, but this additional swelling stretch ratio is not large enough to compensate the difference in maximum extensibility between the different crosslinker concentrations.

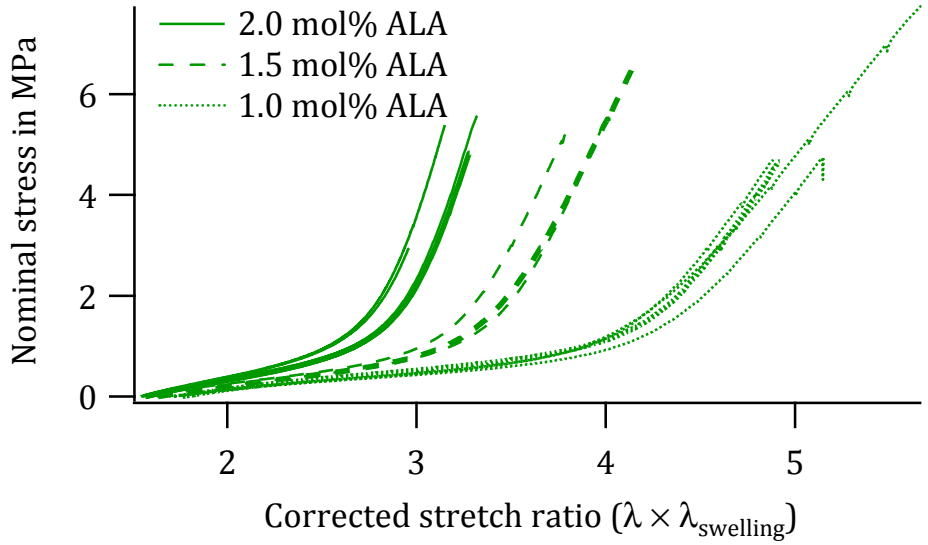

Figure 17: rescaling of curves from Figure 15 by taking into account the stretch due to swelling. This is equivalent to plotting the nominal stress with respect to the extension of the filler network. Thicker lines are anomalous samples identified from Figure 13.

As a last refinement to this analysis, we now compare the observed positions of strain-hardening with predictions based on the extended Flory's model (see chapter 3). Since the filler network is only dual-cured but not prestretched, the two populations of crosslinks are undistinguishable, which gives the following prediction for the maximum extensibility of filler network chains:

$$\lambda_m^{\text{unprestretched}} = \frac{\cos(\theta/2)}{\lambda_{\text{swelling}}} \sqrt{\frac{6\rho RT}{C_\infty \mathcal{M}_0 E_{\text{dual-cured}}}} \qquad \text{Eq. 9}$$

A value of $\lambda_m^{\text{unprestretched}}$ can thus be predicted for sample, and the stretch ratio of each tensile test may then be renormalized by this value to give the parameter φ:

$$\varphi = \frac{\lambda}{\lambda_m} \qquad \text{Eq. 10}$$

Under affine assumption, φ is the average ratio of the length of a network strand over its maximum length. This parameters gives a way to compare visually the experiment with the prediction of the model. If the material follows the behavior of the average strand, strain hardening should be located around $\varphi \approx 1$. This is typically the case in traditional double network elastomers, as illustrated in Figure 18 which uses data from Ducrot's PhD (using a PEA filler network, a PMA matrix network and tests at 60°C) [6,7]. For the three formulations presented, he finds that the vertical line at $\varphi = 1$ corresponds to the asymptotic behavior of the tensile curves. Note that although the materials strain-harden and break well before the vertical line, their asymptotic behavior is still in agreement with this average strand model.

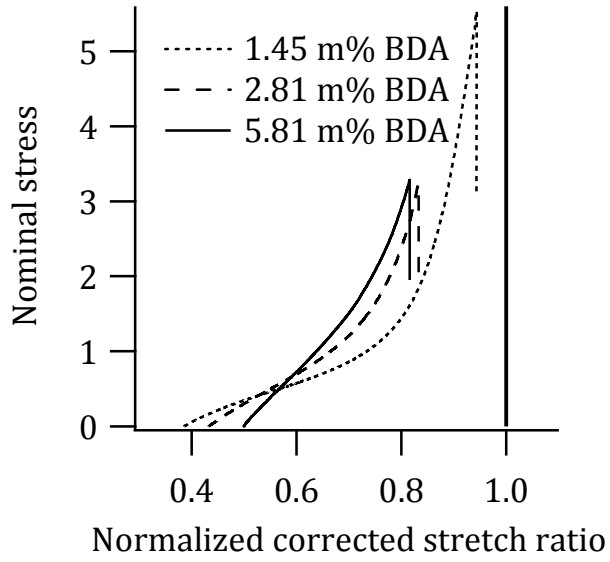

mol% BDA	$\lambda_{swelling}$	λ_m
1.45	1.7	4.4
2.81	1.6	3.7
5.81	1.3	2.6

Figure 18: comparison of Ducrot's results on traditional double network elastomers with predictions based on the maximum extensibility of the filler network strands, as estimated by the measurement of the Young's modulus.

For our dual-cured materials, the result of this renormalization is shown in Figure 19. Qualitatively, the curves look like the ones corresponding to traditional DN (Figure 18). In particular, in formulations with high crosslinker content (1.5 and 2.0 mol%), the onset of strain-hardening is located around $\varphi = 0.7$. The positions of the vertical asymptotes of the curves do not match the prediction of $\varphi = 1$ (contrary to traditional double networks from Figure 18) but the error remains acceptable. For the 1.0 mol% ALA however, the prediction is clearly off and one of the tested materials even exceeds this theoretical limit.

Despite some qualitative agreement, the average strand model fails to catch the precise limit of extensibility of the filler network. In other words, the maximum extensibility of the filler network strands differs from the predicted extensibility based on the measurement of the Young's modulus of the isolated filler network at small strains. This disagreement between the

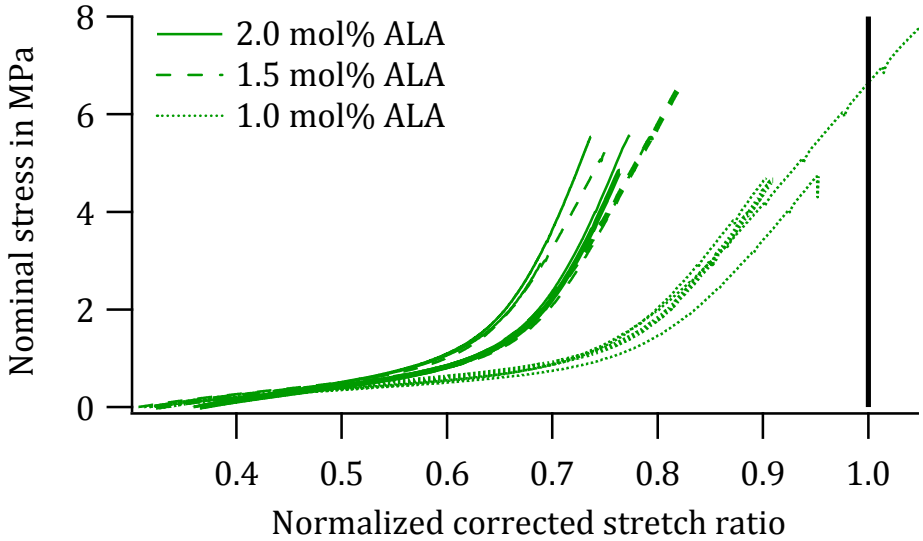

Figure 19: rescalling of the curves from Figure 17 by renormalizing the x-axis by the predicted maximum extensbility of a filler network strand. The vertical line at the abscisse 1 corresponds to $\lambda = \lambda_{max}$.

model and the experiment is not very surprising for two reasons. First, the chemistry that we use probably yields networks that are heterogeneous. The study of average quantities such as Young modulus is thus probably not very representative of the actual structure of the material. In particular, low levels of ALA are probably associated to larger extents of heterogeneity, which could explain why the model is so wrong for this formulation specifically. Second, the model that we use is very crude and assumes that only crosslinks limit the maximum extensibility of network strands. In particular, entanglements are completely neglected which may partly explain the overestimation of λ_m.

4.3. Study of prestretched DN using envelope curves

Now that the behavior of unprestretched DN has been reviewed and compared to traditional double network elastomers, the rest of this section focuses on both prestretched and unprestretched double networks and comparison between them.

4.3.1. Identification of common trends within each formulation group

First, the family of samples prepared with 1 mol% ALA is analyzed (Figure 20). **The three sets of curves are relatively homogeneous**. All subsamples give a similar response in the small strain regime, as the superimposition of the curves at small values of stretch ratios demonstrates. In the large strain regime, two groups may be distinguished: on the one hand, the prestretched samples (in red and blue) that strain-harden at smaller stretch ratios, and on the other hand the unprestretched samples (in green). Within the group of prestretched double networks, the curves are almost superimposed after the onset of strain-hardening. This shows that there is no clear directionality effect at this level of ALA concentration. The only visible difference might be a more progressive strain hardening in the longitudinal direction but it is not obvious.

In the 1.5 mol% ALA family (Figure 21), the observations are somewhat similar. **Prestretched samples behave almost isotropically both in the small and large strain regimes**.

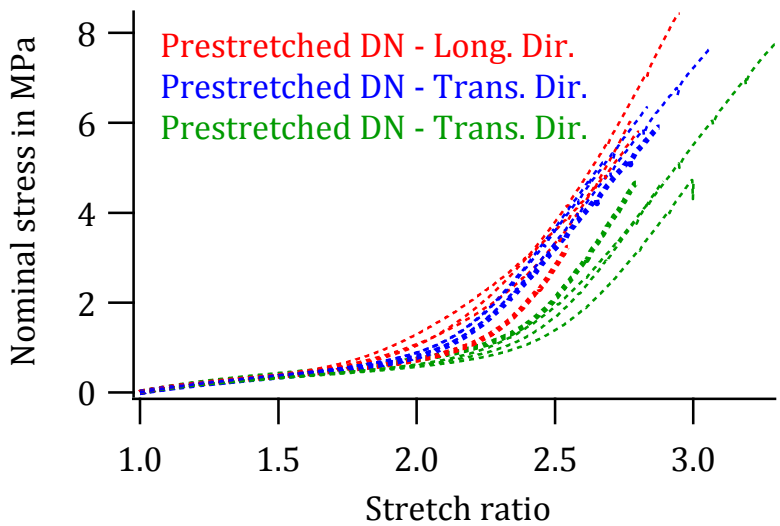

Figure 20: summary graph of all double network samples tested with the formulation containing 1 mol% ALA. Thicker lines come from the same samples and show an anomalous behavior in the longitudinal direction. Test speed is 500 µm/sec.

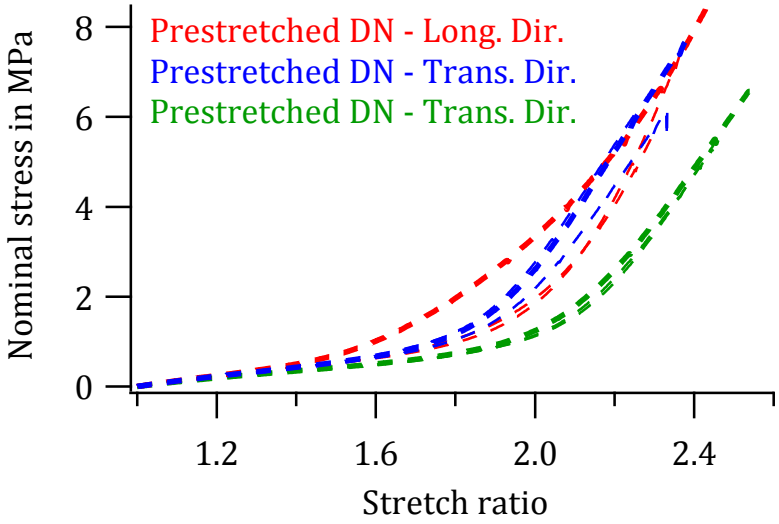

Figure 21: double network samples prepared with 1.5 moL% ALA. Thicker lines are from the same samples and show a different behavior in the longitudinal direction. Test speed is 500 µm/sec.

Prestretched samples are once again slightly stiffer and less extensible than the unprestretched ones.

Figure 22 shows the family with the largest amount of ALA tested (2 mol%). Once again, the unprestretched networks are softer and more extensible, but this time there is a **much clearer direction-dependent behavior in the large strain regime**. The onset of strain-hardening is located at deformations around 20% smaller in the longitudinal direction than in the transverse direction. The shape of the curves is also different and less steep in the longitudinal direction compared to the transverse one. Results are consistent with the previously mentioned example from section 3.3.3.

Some common features therefore arise from the comparison of the three levels of ALA. First, unprestretched samples seem to be systematically softer and more extensible than the prestretched ones. Second, the behavior of prestretched samples seem to be isotropic at small strains. Third, use of large levels of ALA seem to result in anisotropy at large strain. These trends are now studied in more details, starting with a more precise analysis of the small-strain regime.

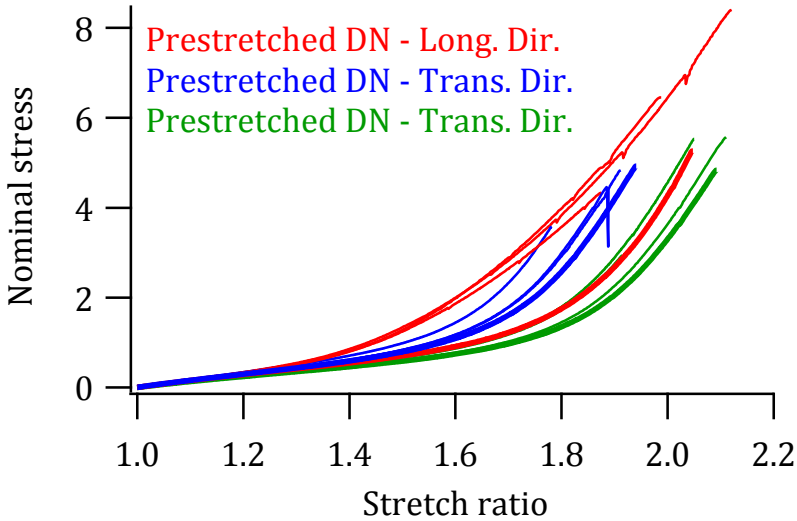

Figure 22: double network samples prepared with 2.0 mol% ALA. Thicker lines are from the same samples and show a different behavior in the longitudinal direction. Test speed is 500 µm/sec.

Sub-sample	Direction	1.0 mol%	1.5 mol% ALA	2.0 mol% ALA
Prestretched DN	Longitudinal	1.0 ± 0.1 MPa	1.3 ± 0.3 MPa	1.7 ± 0.2 MPa
	Transverse	1.0 ± 0.1 MPa	1.23 ± 0.01 MPa	1.7 ± 0.4 MPa
Unprestretched DN		0.9 ± 0.1 MPa	1.1 ± 0.3 MPa	1.5 ± 0.3 MPa
$E_{\text{prestretched}}/E_{\text{unprestretched}}$		1.2 ± 0.1	1.2 ± 0.2	1.1 ± 0.1

Table 7: recap of average values of Young's moduli for prestretched and unprestretched DN samples with various ALA contents. The three first lines of numbers give the values of average moduli in MPa with plus or minus the 95% confidence interval. The last line gives the average values of the ratio of prestretched modulus over unprestretched modulus with plus or minus one standard deviation. The unprestretched modulus is taken as the average value between the longitudinal and transverse directions.

4.3.2. Study of the small strain regime – Flory's model

As in section 4.2, values of Young moduli are fitted from the small strain response of the materials. Average values of Young's moduli with their 95% confidence intervals are given in Table 7. These numerical results confirm the average trend observed on the example material from section 3: **prestretched double network show an isotropic modulus and are stiffer than their unprestretched counterparts**. If the isotropy of the modulus may be explained by the relatively low values of prestretching (chains are thus still Gaussian in small strains), some elaboration is required to explain the difference in stiffness.

In traditional double networks as well as in the unprestretched dual-cured DN from section 4.2, the stiffness of the double network depends on two main parameters: the stiffness of the filler network, and the swelling stretch ratio. Here, swelling stretch ratios measured in the second polymerization step are on average only 2% larger in the unprestretched case compared to the prestretched case. The fractions of filler network are thus similar as well as the efficiency of the second curing reaction. Therefore, the difference in DN modulus should originate from a difference in filler network modulus.

It has also to be kept in mind that the prestretched and unprestretched samples come from the same single-cured network, which rules out the possibility of having a different initial synthesis yield or different single-cured network crosslinking density. This leaves only the possibility of having a direct effect of prestretching on the stiffness of the dual-cured filler network.

The link between prestretching and stiffness in filler networks may be accounted for using the independent network model, or Flory's model of dual-cured networks (see chapter 3). Using a Gaussian chain model, prestretching is predicted to stiffen the dual-cured filler network compared to a single-cured network with identical crosslinking density. Mathematically, the ratio between the prestretched (E^*) and unprestretched ($E^{\emptyset}$) Young moduli may be written as follows:

$$\frac{E^*}{E^{\emptyset}} = \left(\frac{\nu_1}{\nu_1 + \nu_2}\right)\frac{1}{\lambda^*} + \left(\frac{\nu_2}{\nu_1 + \nu_2}\right)\frac{\lambda_{\text{clamp}}}{\lambda^*} \qquad \text{Eq. 11}$$

where ν_1 is the initial crosslinking density, ν_2 is the crosslinking density added during the second curing, λ_{clamp} is the stretch ratio in clamped position and λ^* is the final prestretching. The

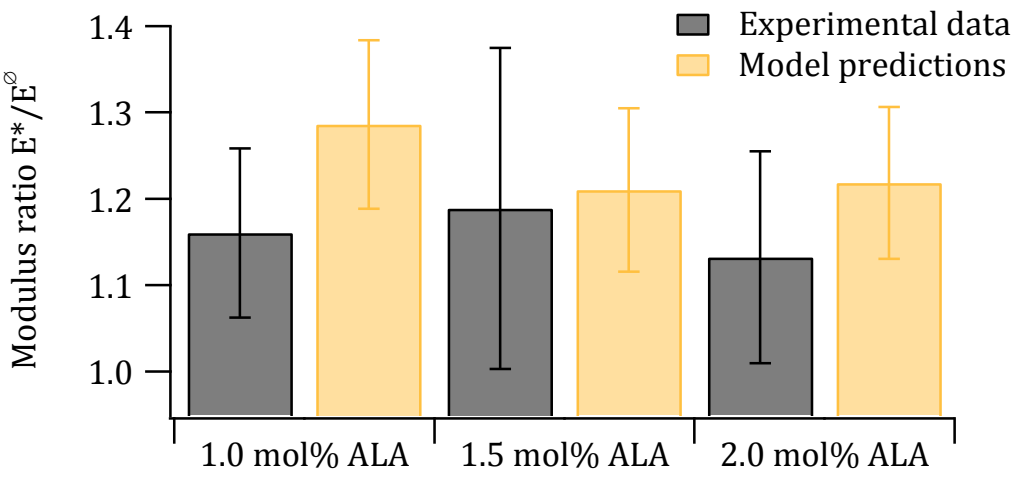

Figure 23: comparison of experimental data on double networks with prediction on the filler network from Flory's model based on the measurement of λ_c and λ^* during sample second curings. Average values are represented, error bars represent confidence intervals at 95%.

stiffening is therefore maximal when the clamped stretched ratio is high and when the ratio ν_2/ν_1 is around unity.

In the present case, according to the tensile results from chapter 2, the modulus increases only by approximatively a factor 2 in the UV system. With clamped stretch ratios of 2 to 3, the observed ratio of around 1.2 is qualitatively consistent with a numerical application of Eq. 11. Quantitatively speaking, Flory's model may be used to estimate the ratio ν_2/ν_1 for each filler network, using the numerical values of λ_c and λ^* and the inverted form of Flory's equation linking them together:

$$\lambda^* = \left(\frac{\lambda_{\text{clamp}}^2 + \left(\frac{\nu_2}{\nu_1}\right) \lambda_{\text{clamp}}^3}{\lambda_{\text{clamp}}^2 + \left(\frac{\nu_2}{\nu_1}\right)} \right)^{1/3} \qquad \text{Eq. 12}$$

This calculation gives the expected ratio of prestretched to unprestretched filler network Young's moduli, based on the measurement of prestretching. This ratio may be compared to the ratio observed on double networks, assuming that the modulus of the double network remains proportional to the modulus of the filler network (as shown in unprestretched DN in section 4.2.1)

The comparison of predicted and measured $E^*/E^{\emptyset}$ ratios are reported in the bar plot of Figure 23 with 95% confidence intervals. **The predictions from the model clearly give the right order of magnitude for the modulus ratio** (although systematically overestimated). The observed enhancement in stiffness of the prestretched double networks may thus be at least partly attributed to a direct effect of prestretching.

It is important to realize that this effect is purely physical and comes from the statistical description of rubber elasticity at moderate deformations. This is not a consequence of the limit of extensibility of the chains, this aspect being completely neglected in the Gaussian version of Flory's model and not measurable on double networks in the small strain regime (since the chains are too far from their limit of extensibility).

4.3.3. Large strain behavior and strain-hardening

Now that the behavior at small strains has been explained, the large strain behavior and more specifically the position of the onset of strain-hardening are studied.

Correction due to swelling

Data is first rescaled by plotting the stress curves taking swelling into account. Nominal stress is plotted against the product $\lambda \times \lambda_{\text{swelling}}$ in Figure 24. This is equivalent to studying the evolution of stress with respect to the stretch ratio of the filler network alone, taking into account the fact that the test starts while it is already prestretched by swelling. Comparison of the three formulation groups reveals that **the larger the ALA content and the smaller the overall stretch ratio at which the strain-hardening is observed**. This observation holds regardless of prestretching or not and regardless of the direction for prestretched samples. The overall maximum extensibility of the double network structure is thus primarily dictated by the amount of ALA in the initial formulation. That is, the amount of ALA is the main parameter that controls the maximum extensibility of the filler network, and hence the position of the onset of strain hardening in double network structures. Among each formulation group however, differences remain because of the presence of prestretching and possible directional effect. The next step is therefore to compare data with the extended Flory's model presented in chapter 3 in order to take prestretching into account.

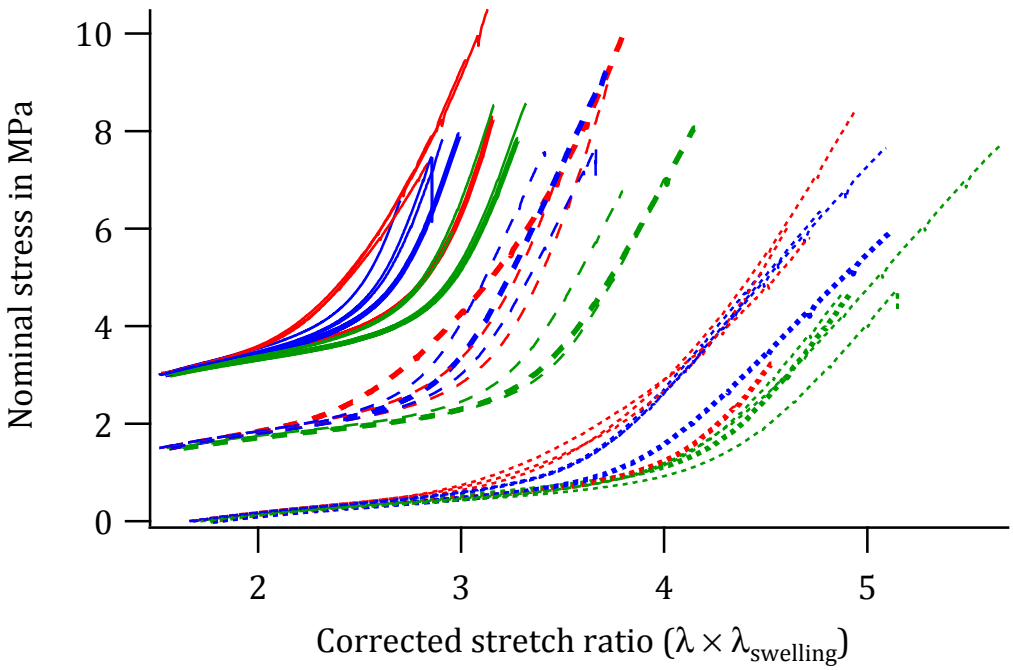

Figure 24: rescaling of the curves from all double network samples with the ALA system by taking into account the stretch ratio due to the swelling by the matrix network in the multiple network structure. The batches of curves for the 1 and 1.5 mol% formulations are shifted upward by a factor 1.5 and 3 respectively. Red and blue curves are the longitudinal and transverse directions of the prestretched samples. Green curves are for the unprestretched samples.

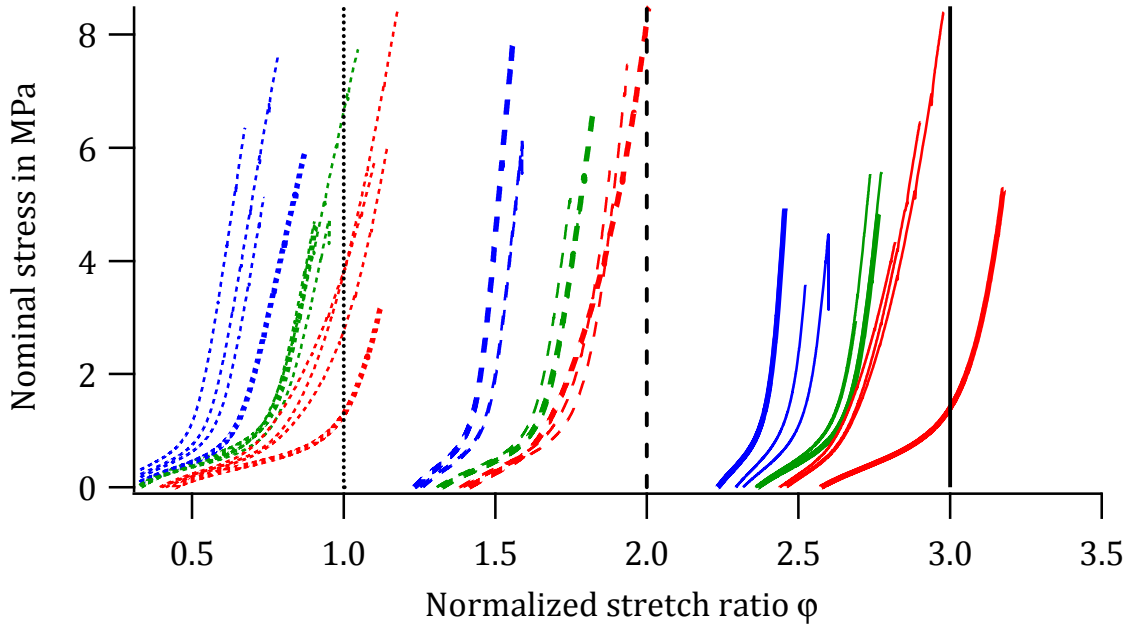

Figure 25: comparison of experimental results to a model predicting the position of the onset of strain-hardening by plotting the envelopes of cyclic tests with respect to a normalized parameter φ defined in Eq. 13. Thick lines are anomalous samples identified at the beginning of the section. Data for 1.5 and 2.0 mol% ALA have been shifted toward the right by 1 and 2 unities respectively. Vertical lines are the expected location of filler network maximum extensibility according to the model. Red and blue curves are the longitudinal and transverse directions of the prestretched samples. Green curves are for the unprestretched samples.

Comparison to the extended Flory's model

The extension of Flory's model presented in chapter 3 gives a prediction of the stretch ratio at which the filler network reaches its maximum extensibility λ_m for each sample and each direction. To establish this prediction, the modulus measured from the swelling ratio is used for $E_{\text{single-cured}}$ and the modulus measured from mechanical testing is used for $E_{\text{dual-cured}}$. As in the previous section, we define φ the stretch ratio divided by the predicted maximum extensibility of the filler network strands:

$$\varphi = \lambda/\lambda_{\text{m}} \qquad \text{Eq. 13}$$

Envelope curves are replotted in Figure 25 with respect to φ in order to illustrate the distance between the actual strain-hardening location and the prediction of our model. Said differently, this graph shows how strain-hardening is positioned with respect to the stretch ratio at which the filler network is predicted to reach its maximum extensibility ($\varphi = 1$).

In the three formulation groups, the trends are more of less the same. First, in the longitudinal direction, the vertical line corresponds to the vertical asymptote of strain-hardening in the 1.5 and 2.0 mol% formulation groups. At 1.0 mol%, it corresponds to the middle of the strain-hardening regime, probably because the heterogeneity at this level of ALA is larger. **The maximum extensibility of the prestretched double networks in the longitudinal thus seems to be relatively well described by our model**, even if numerical values are probably erroneous.

However, **the model very clearly overestimates the maximum extensibility of the samples in the transverse direction specifically**. This is especially true at large ALA levels where some samples break at only 50% of the predicted filler network maximum extensibility. The fairly simple model we use thus cannot completely explain the mechanical behavior of prestretched double network elastomers, possibly because several very crude assumptions are made. In particular, coupling between the two networks (via entanglements or crosslinks) are completely neglected although they most probably have a huge impact on the mechanical properties. The model we use assumes that all directions are completely independent from each other apart from Poisson's effect, and that the two populations of crosslinks are completely independent from each other. A last major limitation of the model is that is considers that the maximum extensibility of each population of network strands may be estimated from the knowledge of average values such as the Young modulus. This ignores the fact that only the less extensible chains are responsible for the apparent strain-hardening, and that these chains may not be representative of the population of network strands.

The extended Flory's model may therefore only be used to get a physical picture of what happens in the material at large strains. Although the unprestretched and longitudinal subsamples are correctly described, the transverse directions remains inaccessible to the model. The assumptions behind the model are probably too strong to make it reliable and predictable for all situations.

4.4. Exploitation of the entire cyclic test

Until now, only the envelopes of cyclic curves have been reviewed. Yet, as illustrated with the example material in section 3.3.3, cyclic loadings give more insights on the details of the large strain response of our materials. In particular, the breakage of bonds and the resulting damage in the materials with the evolution of the applied deformation may be studied.

4.4.1. Study of large strain behavior and strain-hardening

As seen previously, one of the main features in the large strain behavior is the presence of a pronounced strain-hardening. When cyclic loading is performed, a strain hardening is observed at each cycle. It becomes interesting to study its evolution when the maximum applied deformation is increased.

Evolution of strain-hardening on the example material

For all samples, three cycles are performed at each increasing level of maximum deformation. Damage always occurs only at the first cycle (when it occurs), so that the third cycle may be used to analyze the stable behavior of the damaged material, at a certain level of extension. Using the procedure described in 2.3.3, the third cycles of each step are fitted with a modified version of Gent's model. This treatment yields a parameter J_m that relates to the stretch ratio at which the stress goes to infinity after strain-hardening. This parameter is directly linked to the maximum extensibility of the material, which in our case is linked to the maximum extensibility of the filler network.

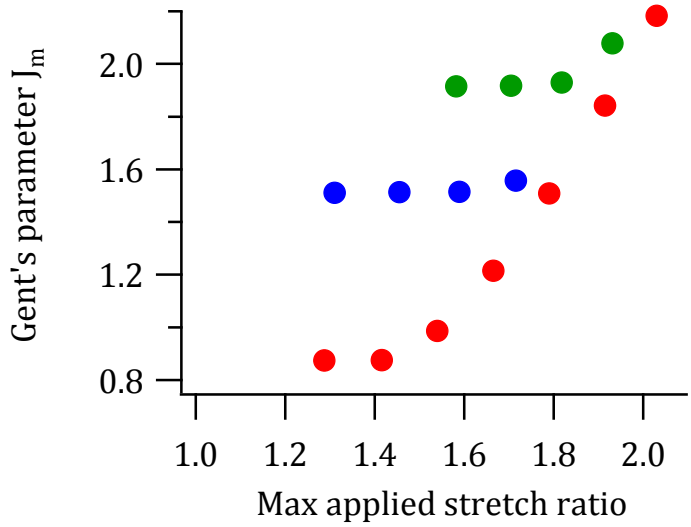

Figure 26: treatment of cyclic tests from section 3 in order to extract Gent's parameter at each step of the cyclic test. Red and blue dots are for the longitudinal and transverse directions of the prestretched DN respectively. Green dots are for the unprestretched DN. Data points for the first cycles are not shown because strain-hardening is not visible on the tensile curves so that fitted coefficients are meaningless.

In order to illustrate this, the example material from section 3.3.3 is used again and processed to get values of J_m at each level of stretch (see Figure 26). **At low levels of maximum stretch, J_m is almost constant**. This constant value may be interpreted as the maximum extensibility of the virgin filler network, before any damage occurs. Some care should however be taken with this interpretation because of the way the results are treated. As a reminder from section 2.3.3, J_m parameters are fitted from the last to the first cycle, and for each decreasing step the fitted value of J_m is not allowed to increase. In other words, it is assumed that the maximum extensibility can only increase with damage. **At larger levels of stretch, J_m increases in a roughly linear way**. This may be attributed to damage in the filler network: when the material is deformed above a certain threshold extension, some chains are broken and the observed network extensibility increases.

The results from the example of Figure 26 correlate well with the observed cyclic tests behavior from Figure 10. Transverse direction and unprestretched samples show no visible mechanical hysteresis (and thus no damage) in Figure 10 and conversely have an almost constant value of J_m in Figure 26 except for stretch values close to the failure point. The longitudinal direction on the contrary shows a different behavior with increasing damage as the material is further stretched. This may be interpreted as the sign that there is some heterogeneity in the material. The increase in maximum extensibility is most probably linked to the breakage of short chains in the material that are numerous enough to have an impact on the mechanical properties, but not too numerous so that they can break randomly in the material. The details of this physical picture are substantiated later in the manuscript.

Comparison of all samples

Now that an illustrative example has been covered, the entire population of tested samples are processed and presented in Figure 27. For clarity, formulation groups have been separated from each other using a horizontal offset (no vertical offset is applied). Except for the transverse and unprestretched samples at 2 moL% ALA, **all samples show the same general behavior, namely a plateau at low stretch until the beginning of damage and then an almost linear increase**

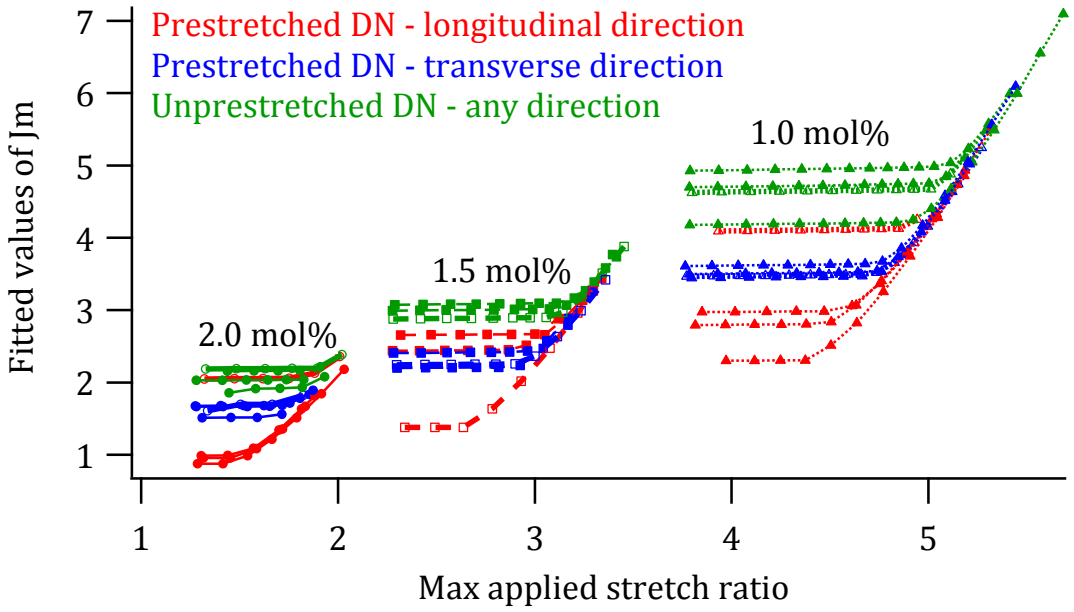

Figure 27: evolution of Gent's parameters with maximum applied stretch ratio for all double network samples tested in cyclic loading. Data for the 1.5 mol% and 1.0 mol% formulations have been shifted toward the right by 1 and 2.5 respectively. Thicker lines/open symbols are anomalous samples identified previously.

of J_m with stretch. According to the explanation above, this is interpreted as a sign of a wide distribution network strand sizes.

When the ALA content is decreased, all curves are shifted upward regardless of the type of subsample. **The overall extensibility of the materials therefore increase when ALA content decreases**. As expected, the overall level of J_m seems to be primarily dictated by the amount of crosslinker in the formulation.

The directionality effect is also confirmed for the 2% formulation: the values of J_m are clearly smaller for the red curves than for the blue ones. Conversely, the curves for the prestretched samples at 1.5 mol% ALA are close to each other, which confirms the absence of clear anisotropy. **On the 1 mol% group, a clear directionality effect is visible**. This effect is more visible with this data representation than when observing the envelope curves shown in Figure 20. The red and blue curves are fairly well-superimposed, with only a slightly lower position of strain-hardening for the longitudinal direction. This may be explained by the fact that when only the envelope of the curves is used, the effect of short chains is visible only in a very narrow range of stretch ratio. They indeed need to be stretched enough to trigger strain-hardening, but not too much otherwise they break and are not elastically active any longer. When the full cyclic test is used, their effect is much easier to visualize.

From the values of J_m, the corresponding values of λ_m may be derived and plotted against the maximum applied stretch ratio, as in Figure 28. Note there is a diagonal shift for readability and unit line is represented by a dashed line. Once again, the same general behavior is observed: **first the limiting value of lambda is almost constant, and then it increases linearly**. The constant value is noted $\lambda_{m,\,virgin}$ and is interpreted as the maximum extensibility of the virgin material.

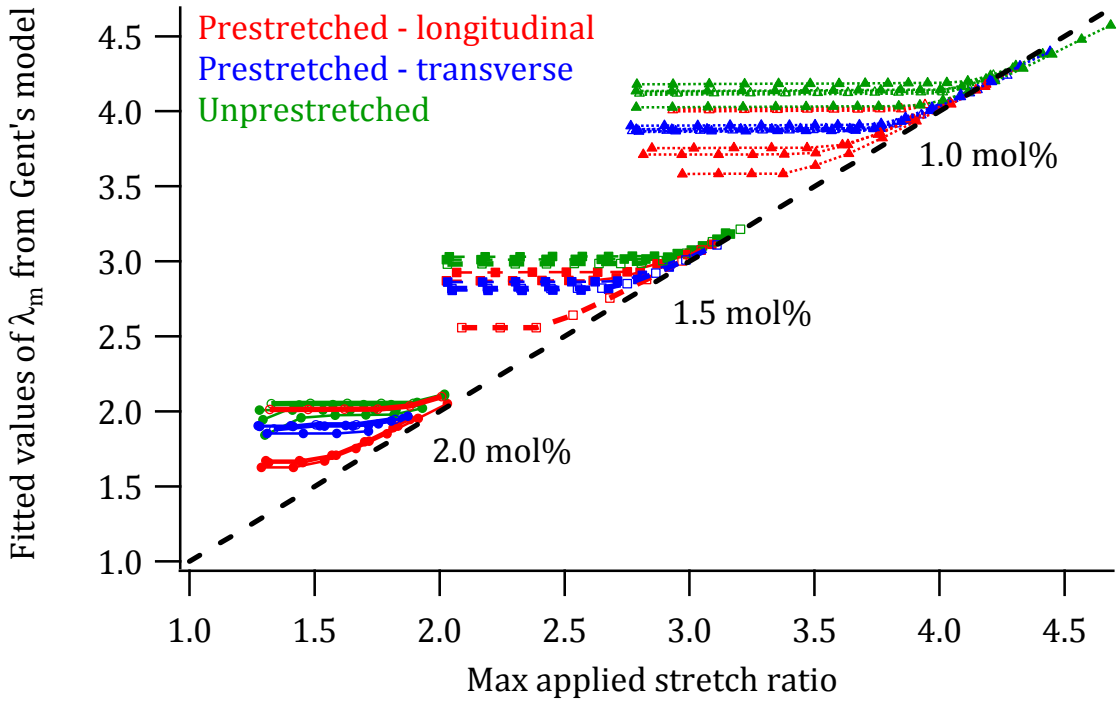

Figure 28: fitted values of λ_m using Gent's model for all samples tested by cyclic loading. Dotted line is the unit line. Results for 1.5 mol% and 1.0 mol% have been shifted diagonally by 0.75 and 1.5 on each axis. Thicker lines/open symbols are anomalous samples identified previously.

Interestingly, **the end of the plateau of λ_m seems to correspond to the unit line**, i.e. the moment when the maximum applied stretch ratio reaches $\lambda_{m,\,virgin}$. After this point, the fitted value of λ_m follows the unit line. Said differently, once the material is deformed at a stretch $\lambda_{step} > \lambda_{m,\,virgin}$, all chains with maximum extensibility smaller than λ_{step} are broken and the new observed maximum extensibility of the network becomes λ_{step}. Deformation and damage act as homogenizers of network strand length distribution and remove network strands that are much smaller than the average network strand length.

These considerations about the presence of short chains in the filler network structure explain why the extended Flory's model is unable to catch the overall behavior of our materials. The model involves the prediction of the maximum extensibility of the filler network strands based on the measurement of average properties such as the Young modulus. Yet, the mechanical response of the material at large strain typically depends on extreme parameters (such as the maximum extensibility of the shortest chains), not average ones.

One of the visible aspects of damage in the large strain regime is therefore an increase in the maximum extensibility of the material that is attributed to the breakage of the shortest chains in the network structure. The other aspect that is studied in the next part is the large mechanical hysteresis that is associated to the first cycles of each step.

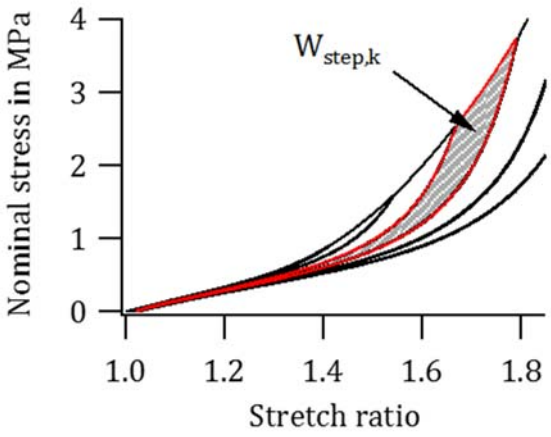

Figure 29: measurement of total dissipated energy by calculating the area of the first cycle hysteresis loop. The contribution of bond breakage only is then calculated by substracting the area from the third cycle.

4.4.2. Study of damage in terms of mechanical hysteresis

Calculation and application on an example material

As stated before, damage during cyclic loading is linked to the breakage of short chains in the materials. Accordingly, the stress decreases steeply when the material is unloaded and the stress-strain curves features a visible hysteresis loop (see Figure 29). The area of this loop is the energy that has been dissipated during the cycle. Mathematically, for each step k:

$$W_{\text{step,k}} = \int_{\lambda_{\text{res, k-1}}}^{\lambda_{\text{step,k}}} \sigma_{N,\,\text{loading}}\, d\lambda - \int_{\lambda_{\text{res, k}}}^{\lambda_{\text{step,k}}} \sigma_{N,\,\text{unloading}}\, d\lambda \qquad \text{Eq. 14}$$

where $W_{\text{step, k}}$ is the total amount of energy dissipated during cycle k, $\lambda_{\text{res, k}}$ is the residual stretch after step k (permanent set) and $\lambda_{\text{step, k}}$ is the maximum applied stretch ratio during step k. Being defined this way, W_{step} includes all sources of energy dissipation. In order to isolate permanent damage (i.e. bond breakage), the area of the hysteresis loop of the third cycle of each step is calculated. This integral represents the contribution from viscoelasticity and other sources of reversible damage. It is hence subtracted from W_{step} to give the permanently dissipated energy U_{step}:

$$\text{U}_{\text{step}} = W_{\text{step}}[\text{first cycle}] - W_{\text{step}}[\text{third cycle}] \qquad \text{Eq. 15}$$

As expected from the shape of the curves (very low permanent set, almost perfect superposition of loading and unloading after the first cycle), this correction is very weak and does not significantly changes the value of dissipated energy.

As an illustrating example, the procedure is applied first on the example from section 3.3.3 in Figure 30. Once again with this material, a clear directional effect is visible. The amount of energy dissipated by damage is much larger in the longitudinal direction than in the transverse direction. The unprestretched sample shows some signs of damage as well, but only toward the end of the test, close to the fracture point. These observations are perfectly consistent with the analysis of strain-hardening from the previous section.

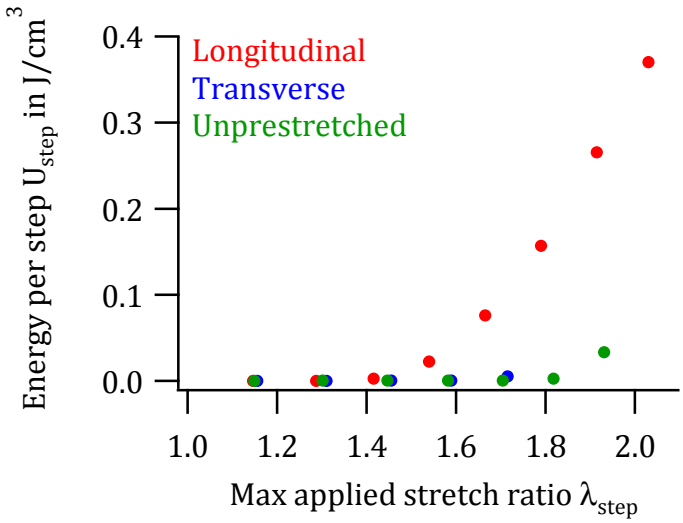

Figure 30: dissipated energy due to permanent damage in the example material from section 3.3.3 at each step.

Study of the energy dissipated per step

All double networks prepared with the ALA system are compared in Figure 31, with formulation groups separated with a vertical offset. **There is a clear threshold below which almost no energy is dissipated**. The position of this threshold primarily depends on the amount of ALA in the system. Within each formulation group, the same trends as before may be observed. **The 1.0 and 1.5 mol% groups show large amount of energy dissipated regardless of the direction, while in the 2.0 mol% group only the longitudinal direction damages. A directional effect may also be seen in the 1 mol% formulation group**, as the longitudinal direction seem to dissipate energy at lower strains than the transverse direction.

In order to go further in the analysis, the amount of lost energy per cycle is divided by the increase in deformation that has been applied during the cycle.

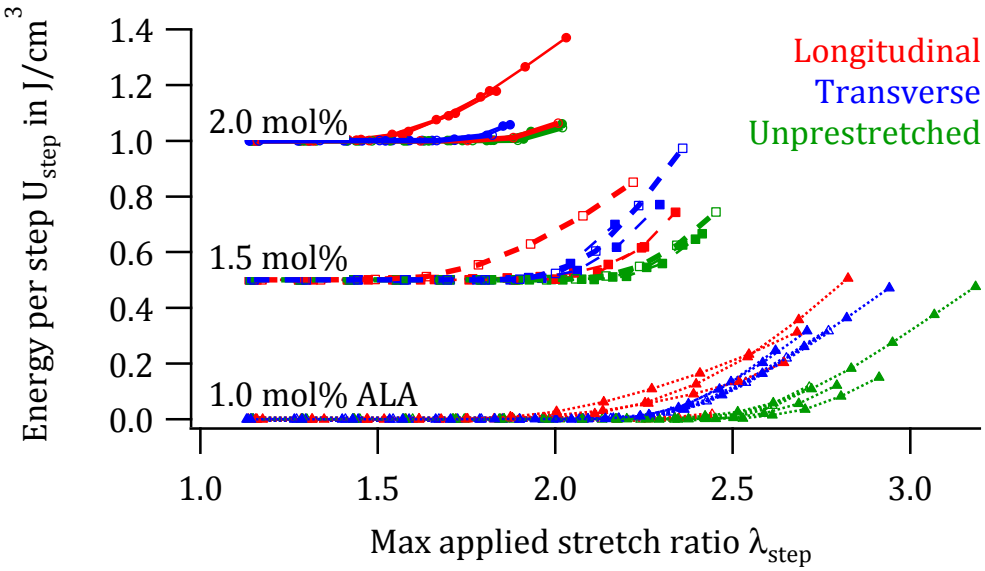

Figure 31: comparison of energy dissipation during damage for all double networks. Formulations at 1.5 and 2.0 mol% ALA have been shifted upward by 0.5 and 1 respectively. Open symbols/thicker lines are anomalous samples identified previously.

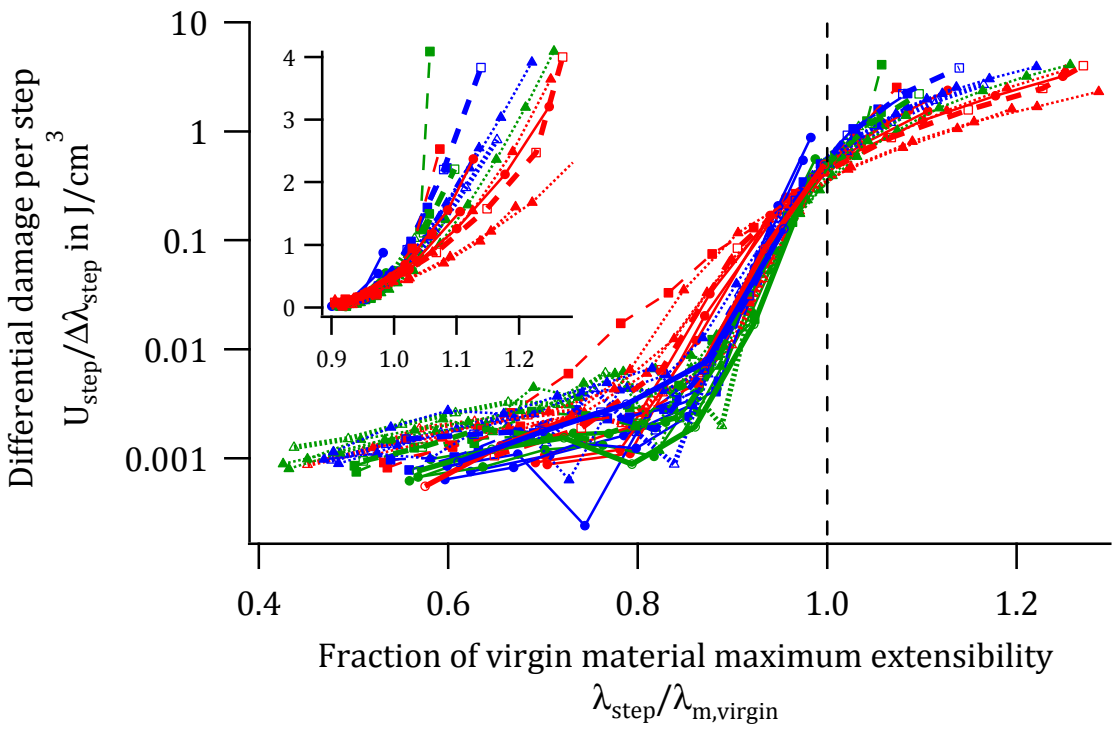

Figure 32: study of the "damage signature" for all double network samples. The increment of dissipated energy per added deformation is plotted again the distance with the maximum extensibility of the undamaged material, as estimated from Gent's model fits. The insert figure is a close up in the last part of the curve (above 0.9) in linear scale. Thicker lines/open symbols are anomalous samples identified previously. Red is longitudinal, blue transverse and green is unprestretched.

$$\mathcal{D}_{\text{step k}} = U_{\text{step k}}/(\lambda_{\text{step k}} - \lambda_{\text{step k-1}}) \qquad \text{Eq. 16}$$

This parameter $\mathcal{D}$ is referred to as differential damage and may be interpreted as the signature of the damage mechanism (i.e. the rate of damage). In order to compare the different formulations together, this parameter is plotted against a fraction of virgin extensibility. The latter is formally the ratio between the maximum applied stretch ratio at each step and the lower bound of the maximum extensibility fitted with Gent's model for low step stretch ratios. The increase in maximum extensibility of the damaged material begins when this ratio gets close to 1 (see 4.4.1).

The evolution of differential damage is plotted in Figure 32. Three regimes may be identified:

- **When the material is deformed far from the maximum extensibility of the virgin material, there is almost no damage and $\mathcal{D}$ is almost constant**. The absolute value of $\mathcal{D}$ in this regime is not meaningful and probably more representative of the experimental error associated to the measurement of U_{step}.
- **When the material is deformed at 90% of its virgin maximum extensibility, $\mathcal{D}$ increases steeply** by about 2 orders of magnitude. This is the real onset of damage, bonds start to break and the associated lost energy begins to be detectable.
- **Above 100% of the virgin extensibility, the material is fully into the permanent damage regime**. Energy is dissipated at a lower rate and is in the order of magnitude of 100 J/cm³/% regardless of the formulation or type of sub-sample.

It is worth pointing out that the rate of damage does not stabilize but instead keeps increasing when the material is stretched further. This is clearly visible in a linear scale, as in the insert of Figure 32. This is coherent with the idea that the material gets closer and closer to the maximum extensibility of the majority of the network strands once the shortest ones are broken. Therefore, more and more chains are broken as the material is stretched further.

Although all samples and directions share the same three-regime behavior, **a slight directional effect seem to be visible for the longitudinal direction**. Damage seems to begin at slightly lower fractions of virgin maximum extensibility (some samples start to damage from 70% instead of 90% of the maximum extensibility). After the material starts to really damage (i.e. above 100% of the virgin extensibility), the rate in the longitudinal direction is often smaller than in the other sub-samples. The latter point should however be nuanced by the fact that a significant part of the samples break before the main damage regime may be fully observed. Therefore, this observation is not necessarily representative of the overall behavior of longitudinal samples.

Study of total dissipated energy

Now that the incremental damage has been studied, the total amount of dissipated energy U_{tot} may be calculated by summing U_{step} at each step. The result of this is shown in Figure 33 and shows the same trends as before. **Final levels of dissipated energy reach values as high as 1.5 J/cm3**. These values of energy may be converted into a fraction of broken bonds in the material. In order to do this calculation, the total possible amount of dissipated energy is needed, and is estimated using Lake and Thomas' theory. Namely, one network strand may dissipate an energy $2U_bN_x$ where $2N_x$ is the number of bonds between two crosslinks and U_b is the energy borne by a bond. The amount of broken bonds in the material may thus be written as follows:

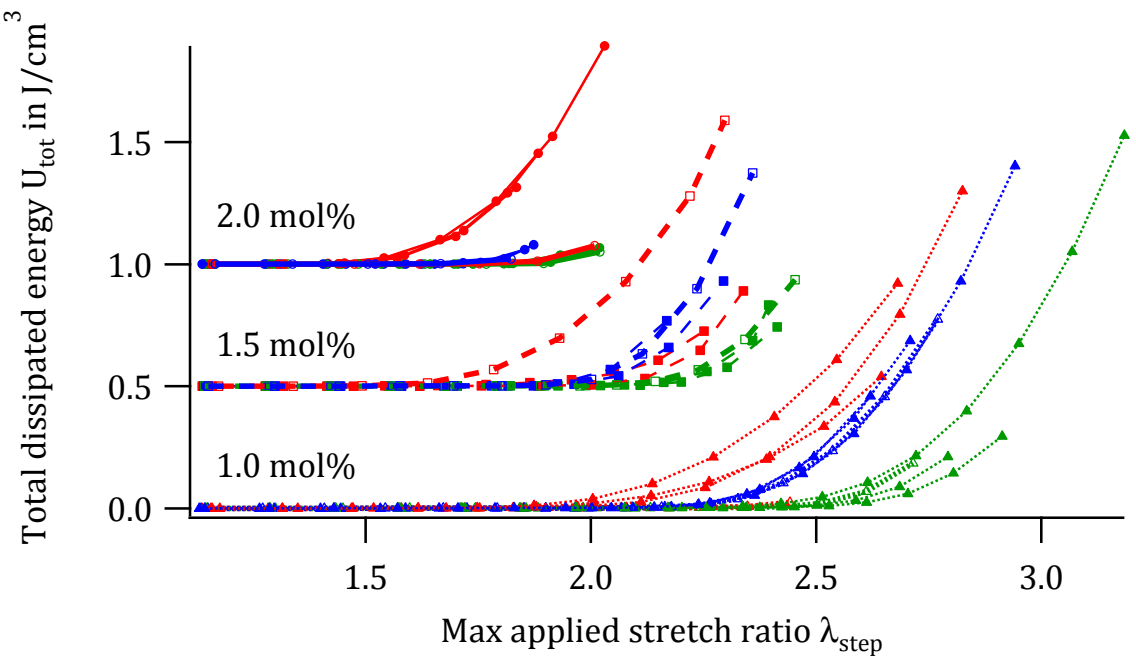

Figure 33: total amount of energy permanently dissipated at each step. Formulations at 1.5 and 2.0 mol% ALA have been shifted upward by 0.5 and 1 respectively. Thicker lines/open symbols are anomalous samples identified previously.

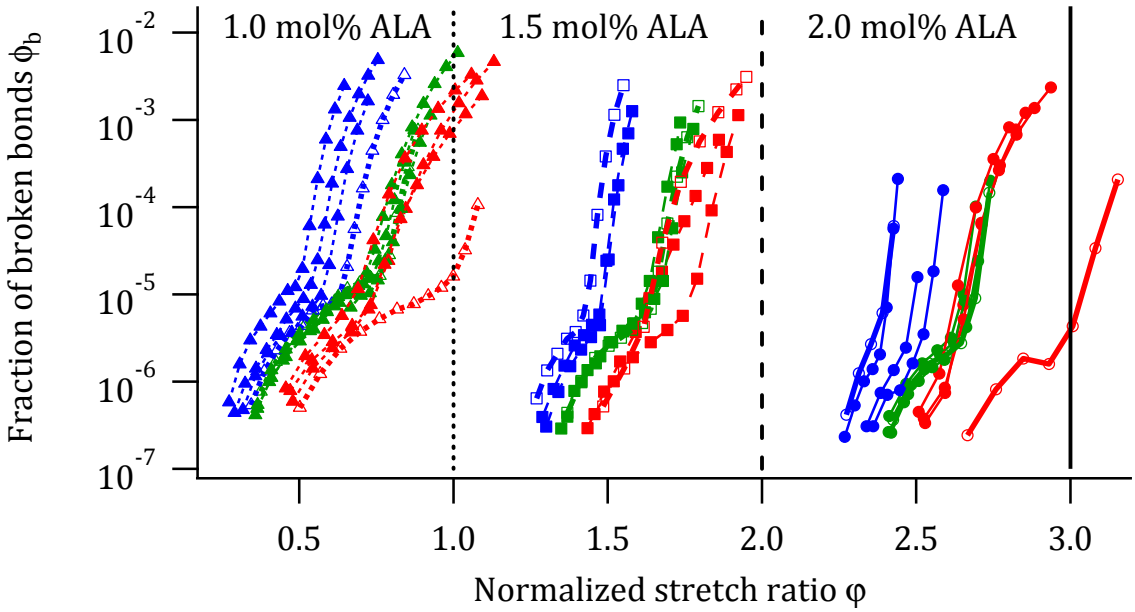

Figure 34: evolution of the amount of broken bonds estimated from Lake and Thomas' theory with the normalized stretch ratio defined in section 4.2.2. As a reminder, φ is the test stretch ratio (here λ_{step}) over the modelled stretch ratio at which the filler network strand should reach its maximum extensibility. Batches of curves corresponding to the 1.5 and 2.0 mol% ALA formulations have been shifted toward the right by 1 and 2 respectively.

$$\phi_b = \frac{U_{\text{tot}}}{U_{\text{entire filler network}}} = \frac{U_{\text{tot}}}{\nu U_b N_x} \qquad \text{Eq. 17}$$

where ν is the number density of filler network strands in the double network structure. The latter primarly depends on the swelling stretch ratio, since the volume fraction of first network in the double network structure is given by $1/\lambda^3_{\text{swelling}}$. Eventually, Eq. 17 may be rewritten into:

$$\phi_b = \frac{U_{\text{tot}}\, \mathcal{M}_0\, \lambda^3_{\text{swelling}}}{2\, U_{\text{C-C}}\, \rho_{\text{PEA}}} \qquad \text{Eq. 18}$$

where $\mathcal{M}_0 = 100.12$ g/mol is the monomer molar mass and $\rho_{\text{PEA}} = 1.12$ g/cm³ is the density of poly(ethyl acrylate). Regarding the value of U_b, Lake and Thomas use in their initial paper [8] the value of the dissociation energy of a carbon-carbon bond for U_b. In a recent article [9], Wang et al. suggest that a value of 60 kJ/mol would be closer to reality, and recent work from our group suggest that this value indeed gives more coherent values [10]. The value of 60 kJ/mol is therefore used here.

The result of this calculation is plotted in Figure 34 with respect to φ the ratio of the maximum stretch ratio applied over the predicted position of the maximum extensibility of the filler network. As a reminder, this ratio has been defined and used in sections 4.2.2 and 4.3.3 to compare the envelope curves of our materials to the extended version of Flory's model and prediction of the filler network maximum extensibility. $\varphi = 1$ corresponds to the expected position of the maximum extensibility of the average strand in the filler network. A strong increase in the fraction of broken bonds should therefore occur in the vicinity of the vertical unit line. This is what is obtained for the longitudinal and unprestretched sub-samples for all three formulations.

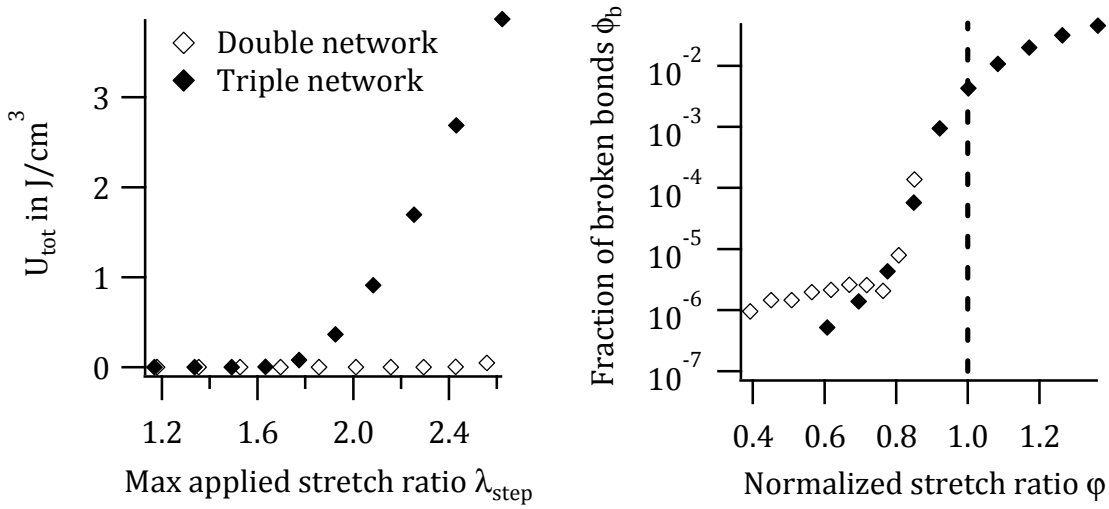

Figure 35: reproduction of data from Ducrot's PhD thesis on cyclic loading of pure poly(ethyl acrylate) double networks crosslinked with 1.45 mol% BDA. Samples were prepared with 50 vol% toluene and 1.16 mol% HMP. Left: total amount of dissipated energy in cyclic loading. Right: fraction of broken bonds calculated using Lake and Thomas' theory plotted versus the normalized stretch ratio (i.e. $\lambda\lambda_{swelling}/\lambda_{max}$ with λ_{max} the theoretical maximum extensibility of the filler network chains, calculated from the modulus of the filler network alone).

For the longitudinal and unprestretched directions, damage starts to increase significantly at about 80% of the filler network maximum extensibility and keeps increasing until the material breaks. Note that at 1.0 mol% ALA several samples overpass the theoretical limit of $\varphi = 1$ which indicate that the quality of the model used to calculate φ is probably less good for this formulation. This is consistent with the observations made on the envelope curves in section 4.3.3.

In the transverse direction of prestretched DN however, the onset of the increase in ϕ_b is located well below the position of $\varphi = 1$. This is an error of the model, since there is no reason why the filler network should start to break at lower fractions of its maximum extensibility in this direction specifically. Instead, this discrepancy should be seen as an additional proof that the maximum extensibility of the filler network in the transverse direction is not accurately predicted by the extended version of Flory's model.

Comparison with traditional double network elastomers

As a comparison, the same analysis may be performed on traditional double network elastomers, using results from Etienne Ducrot's PhD [6]. Figure 35-left shows the evolution of the total amount of dissipated energy during cyclic loadings in double and triple network elastomers, and Figure 35-right shows the amount of broken bonds. Immediately, it appears that **traditional double networks do not show significant hysteresis and damage**, as shown by the very low values of U_{tot}. The fraction of broken bonds remains also very low and only increases at the very end of the test, close to the maximum extensibility of the filler network (i.e. close to the vertical line at $\varphi = 1$). This onset of significant damage is similar between the double and triple networks, and occurs at around 80% of the maximum extensibility of the filler network. **In the triple network however, the final quantity of damage is much larger**, with final amounts of broken bonds similar to the ones that are observed in our double networks (about 1% at the theoretical limit of extensibility of the filler network).

Our double networks prepared with the UV system are therefore much closer to the traditional triple networks than double ones in terms of damage and breakage of covalent bonds, indicating that the details of the networks microstructure control the way the material damages in cyclic loading, more than the absolute value of the swelling stretch ratio.

Another similarity is that the fraction of broken bonds starts to increase strongly at about 70 to 80% of the filler network maximum extensibility. In our case however, when the filler network reaches 80% of its extensibility, there is already a fraction of broken bonds of at least 10^5, which is ten times larger than traditional multiple network elastomers. This is consistent with the presence of a significant amount of short network strands, which may break at very low extension ratios and cause some damage in the material in the early stages of the cyclic test.

These last comparisons gives the possibility to draw a few conclusions about how our double networks compare to the traditional ones from Etienne Ducrot's PhD. First, as shown in 4.2.1, double networks prepared with the UV dual-curing system are overall softer than the traditional ones, but their modulus is likewise controlled by the stiffness of the filler network. In the large strain regime (see section 4.2.2), the strain-hardening of traditional double networks is consistent with a theoretical model based on the prediction of the maximum extensibility of the filler network. In other words, the large strain behavior of Ducrot's double networks may be understood assuming affine deformation, independence of directions and global agreement with Neo-Hookean behavior far from the maximum extensibility of the filler network. This is also true to some extent for our double network elastomers (see section 4.3.3), at least for the unprestretched DN and the prestretched DN in the longitudinal direction, although the quality of the prediction is much poorer. In the transverse direction however, these assumptions fall down somehow and the large strain response of our materials shows a very large deviation to the model. Finally, study of cyclic loadings show a significant mechanical hysteresis and breakage of bonds in our double networks, while Ducrot's ones are almost perfectly elastic with no visible damage.

For all these reasons, it seems that the complexity of the microstructure of our materials profoundly affects their mechanical response, and that the simple modeling that has been used in the past for double networks cannot be used as it is to understand the behavior of our materials.

Comparison of hysteresis with the increase of extensibility

Damage in cyclic loading translates into two phenomena. On the one hand the breakage of bonds dissipates energy and gives some mechanical hysteresis. On the other hand, it increases the maximum extensibility of the double network, since the shortest chains break first. Energy dissipation and increase in extensibility should therefore be linked somehow.

In order to probe this link, the total amount of broken bonds when the material breaks is compared for each subsample with the increase in maximum extensibility, defined as follows:

$$\Delta\lambda_{\mathrm{m}} = \lambda_{\mathrm{m,\,fracture}} - \lambda_{\mathrm{m,\,virgin}} \qquad \text{Eq. 19}$$

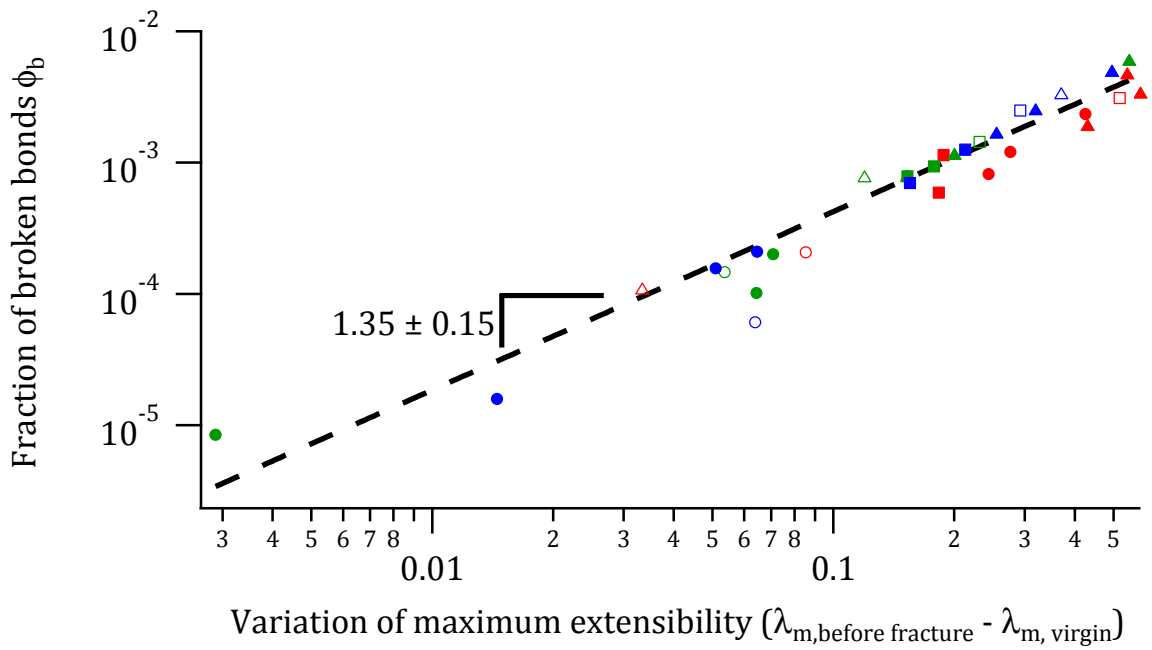

Figure 36: comparison of damage from the point of view of energetic hysteresis (fraction of broken bonds, left axis) and from the point of view of change in large strain behavior (increase in maximum extensibility, bottom axis). Open symbols are anomalous identified previously. The dotted line is a power law that has a slope of 1.35 with a standard deviation of 0.15.

The result of this comparison is shown Figure 36 and confirms the obvious correlation between the two parameters. A power law may be used to quantify this correlation and results an exponent of 1.3, although this value cannot easily be physically interpreted.

The dissipation of energy due to damage is thus clearly linked to the increase in maximum extensibility. Both phenomena are believed to relate to the breakage of short chains in the material.

4.4.3. Comparison with Mullins Effect in filled rubbers

The observed damage phenomenon shares some similarities with the well-known softening of filled elastomers. This phenomenon is commonly referred to as "Mullins effect" and has been extensively studied in the literature. Figure 37 is taken from the literature [11] and illustrates the main characteristics of this effect [12]:

- After an initial loading, the material softens significantly during unloading. This loss of stress is not recovered when the material is stretched again to the same level of extension.
- The material recovers the behavior of the virgin material when it is stretched above the maximum stretch it has ever experienced, and softens again when the force is removed.
- The loss of stress is accompanied by a decrease in the tangent modulus of the material
- The material shows a significant permanent set at zero force, which increases with the maximum applied stretch ratio.

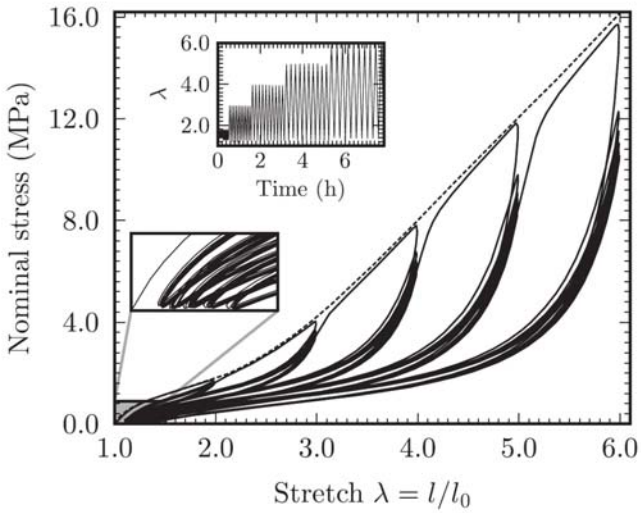

Figure 37: cyclic test featuring a pronounced Mullins effect on a typical filled rubber. Taken from (Merckel et al., 2012).

The two first characteristics at least are shared by our materials. But how close is this "Mullins-like effect" from the phenomenon observed in filled elastomers? To answer this question, we compare our material to styrene-butadiene rubber filled with carbon black and characterized in details by Merckel et al. [13]. In this subsection, we perform a similar treatment of the experimental data using the example from section 3 in order to identify potential differences.

First, the small strains are analyzed. The unloading curves are plotted and compared in Figure 38. A first noticeable difference is that **the decrease in modulus is much more pronounced in the filled rubber compared to our material**. To quantify this decrease, curves are fitted with a straight line and slopes are identified as tangent moduli. The results are given in Figure 39 both for our double network sample (left graph) and the filled rubber (right graph). In both cases, the decrease in stiffness is roughly linear with the Hencky strain. **In our case however, the decrease only starts from a certain threshold value of Hencky strain** (about 0.4). Besides, the relative

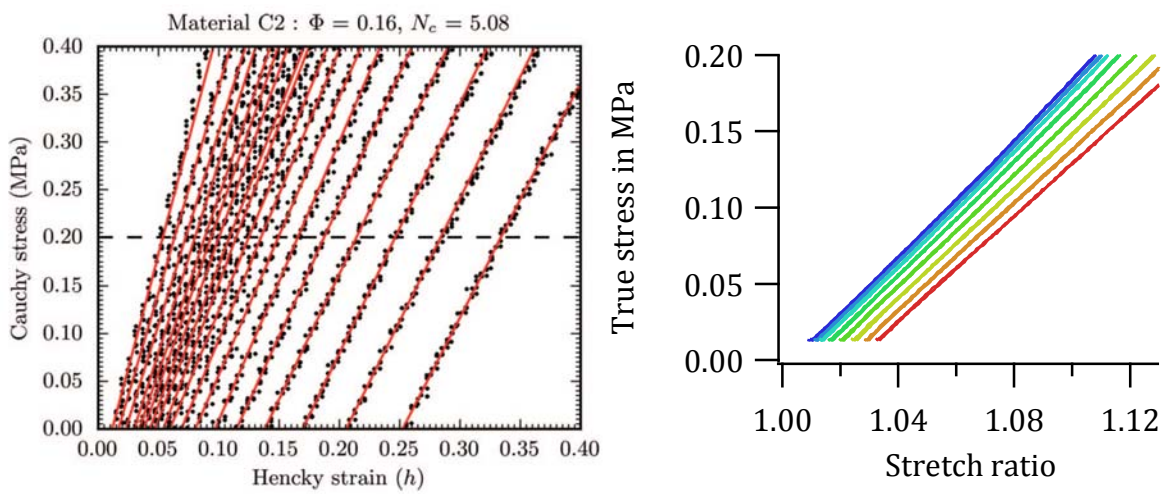

Figure 38: comparison of the small strain behavior of our prestretched double network elastomer in the longitudinal with a sulfur-vulcanized SBR elastomer filled with 50 phr of carbon black. In both cases, true stress is plotted and only unloading curves are shown. Left: a typical filled SBR rubber during a step-cyclic test. Hencky strain is the logarithm of the stretch ratio. Plot taken from (Merckel et al, 2011). Right: focus at small strain on the mechanical response of the test from Figure 10-B.

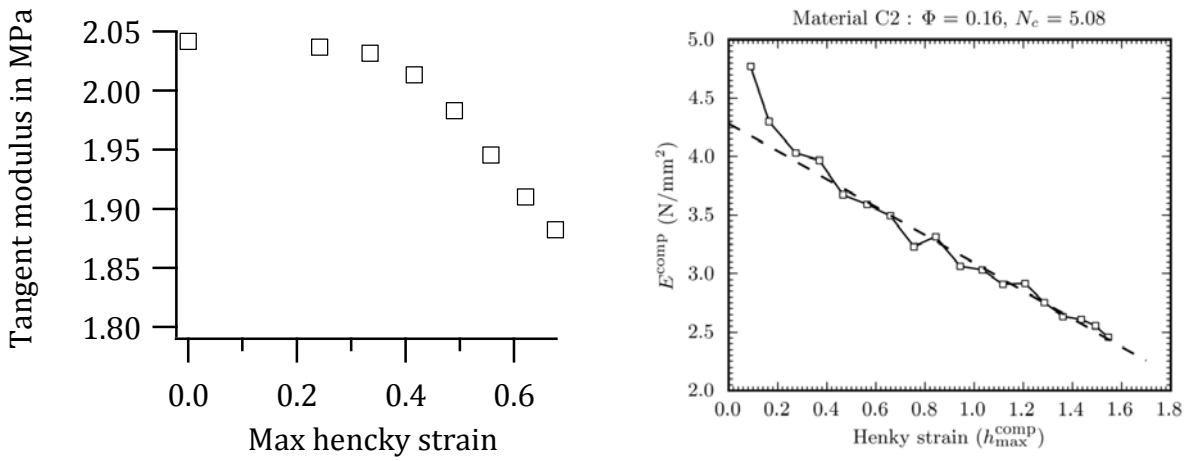

Figure 39: comparison of the decrease in modulis for our materials and for a typical filled rubber. In both graphs the bottom axis is the Hencky strain which is the natural logarithù of the stretch ratio applied at each step. Left: values of moduli extracted from the beginning of the stress strain curves from Figure 38. Right: loss of modulus observed in the filled rubber. Figure taken from (Merckel et al., 2011).

loss of modulus is fairly small (about 5 kPa/% of Hencky strain) compared to the case of the filled rubber (about 13 kPa/% of Hencky strain).

In the large strain regime, Hencky strains are first shifted in order to compensate the permanent set (albeit it remains very limited in our case). In our case, true stress is also shifted because our criterion for the end of each cycle is $F = 0.05$ N and not zero force. Then, strain hardening is characterized by constructing a master curve from the true stress vs Hencky strain plots, taking the first loading as a reference. Mathematically, this corresponds to applying correction factors to the Hencky strains at each step ($h_{\text{step k}}^{\text{rescaled}} = \alpha_{\text{step k}}\, h_{\text{step k}}$) and performing a least square optimization. Figure 40 shows the application of this process on our data, and compares it to the results obtained by Merckel et al. As shown in Figure 40-C, the curves collapse well onto each other. The resulting shift factors are shown in the insert and show once again **a threshold below which no shift needs to be applied**. This has already been stated in the previous sections: before the onset of damage, the curves of each cycle are superimposed, so scaling factor is not needed.

A damage parameter D may be defined in two different ways depending on the length scale. If the small strain regime, D is defined from the loss of modulus:

$$D_{\text{small strain}} = 1 - \frac{E_{\text{damaged}}}{E_{\text{virgin}}} \qquad \text{Eq. 20}$$

In the large strain regime, the damage parameter is defined from the rescaling factors calculated before:

$$D_{\text{large strain}} = 1 - \alpha \qquad \text{Eq. 21}$$

Damage parameters are calculated and plotted with respect to the maximum hencky strain of each step in Figure 41, with results from Merckel et al. reproduced for comparison. When comparing the damage parameters and thus the characteristics of Mullins effects from the two materials, two

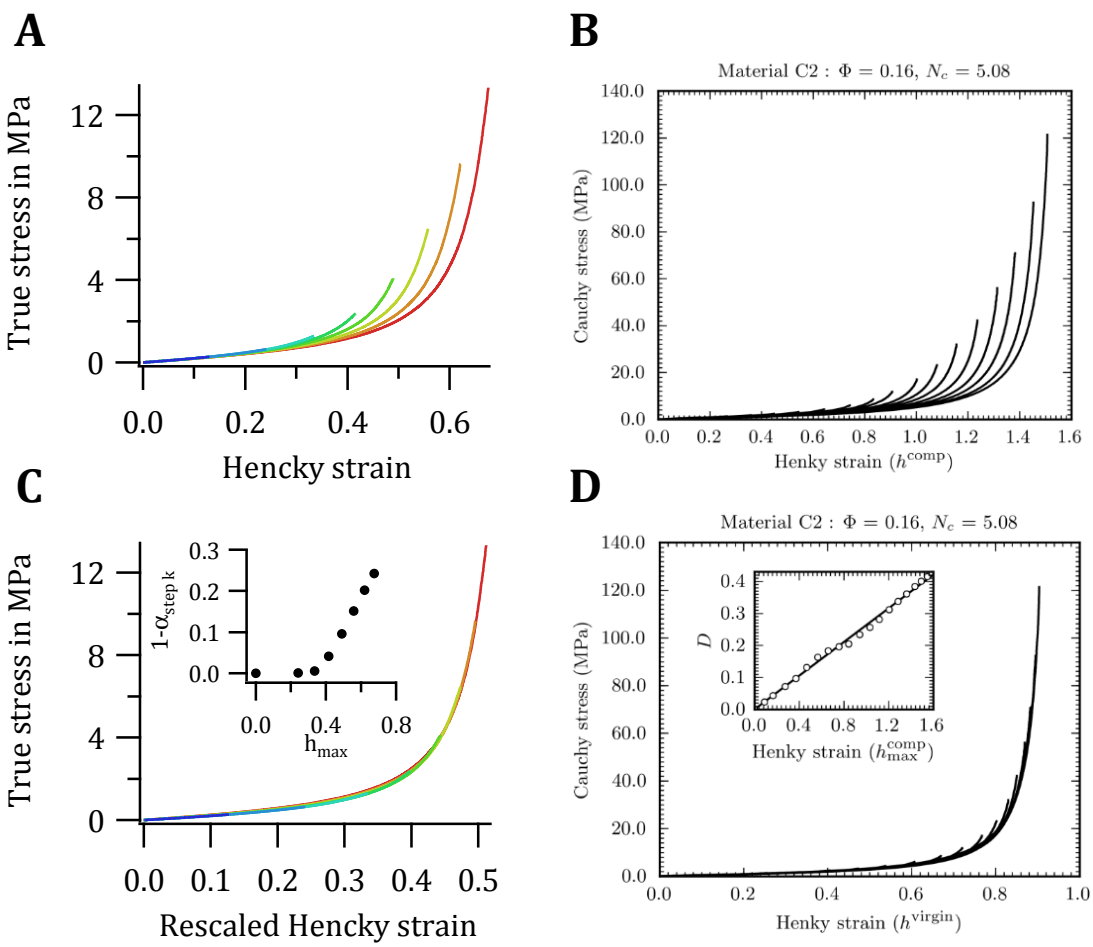

Figure 40: construction of master curves from the plots of true stress versus hencky strain, taking the virgin loading as a reference. A) Plots of true stress versus hencky strain for our material. B) Plots of true stress versus hencky strain for a filler SBR rubber (from (Merckel et al., 2011)). C) Master curve obtained by multiplying the hencky strains with a scaling factor $\alpha_{step\ k}$ at each step of the cyclic loading. The insert shows the evolution of scaling factors with the maximum applied hencky strain. D) Master curve obtained after data processing for a typical filled SBR rubber. The insert shows the damage parameter, defined as 1-α. Taken from (Merckel et al., 2011).

striking differences appear. First, **our material features a very visible threshold of strain below which virtually no Mullins effect is visible**. By opposition, the filled rubber shows a continuous and monotonous increase in damage parameter regardless of the method of calculation. This threshold effect in our case is linked to the fact that damage most probably comes from the rupture of the shortest chains of the material, and that these chains must be stretched enough to rupture.

The second and important difference concerns the two estimates of the damage parameter. In the case of filled rubbers, the two methods of calculation essentially give similar results and both damage parameters increase at a similar rate (see Figure 41-B). In other words, the small and large strains are correlated, and damaging the former impacts the latter. **In our case, the damage parameter measured from the large strain increases much faster than the one measured from the small strain behavior**. This corroborates the observation made previously about the fairly limited loss of modulus in our case. In other words, damage in our material primarily

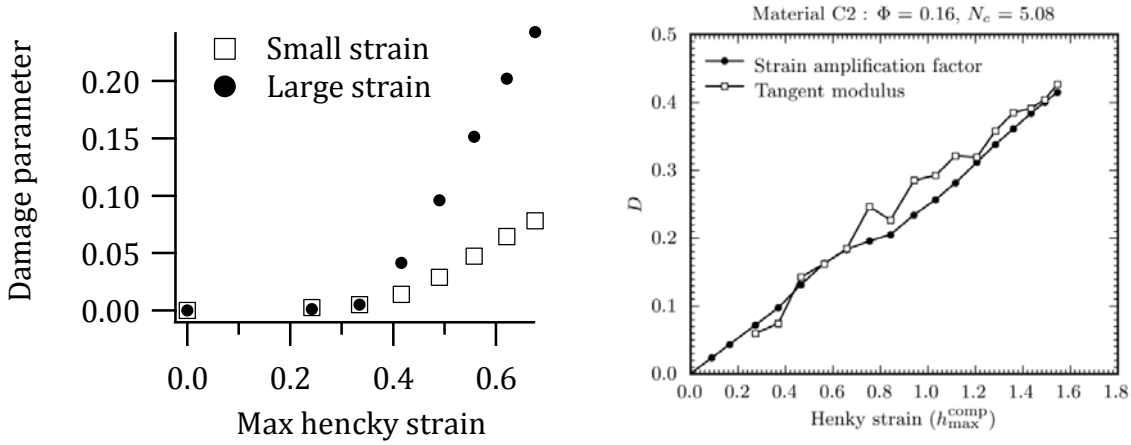

Figure 41: comparison of damage parameters calculated from either the small strain behavior (open symbols) or the large strain behavior (filled symbols). Left: application of the data processing method from (Merkel et al., 2011) on our materials. The small and large strain regimes do not respond to damage the same way. Right: results from (Merkel et al., 2011) showing that the two methods to evaluate D are equvalent in their case.

impacts the large strain properties of the materials, and only secondarily the small strain properties.

This difference may be at least in part explained by the fact that damage is believed to be caused by the fracture of short chains present in the filler network structure. These chains would be in large enough amount to be detectable by mechanical testing, but not too large so that the average properties of the material are not significantly affected. In our unfilled material, the small strain properties of the rubber are primarily given by average quantities such as the number density of chains. A minority of short chains should not have much impact on these properties, but will have a much bigger impact once they are stretched and ultimately broken.

To conclude, the “Mullins like” effect that is observed in dual-cured double networks shares some characteristics with the traditional Mullins effect observed in filled rubbers. Nevertheless, the two effects are not strictly equivalent. Traditional Mullins effect features a strong correlation between what is observed at large strain (a pronounced softening during unloading) and at small strain (a decrease in stiffness). In our case, the damage at large strain is much more pronounced than in the small strain regime. This difference may originate from the original source of damage, and in any case this observation sustains our hypothesis that damage originates from the breakage of a small amount of prestretched and short chains in the filler network architecture.

The next part therefore proposes a physical picture to reunite the different experimental results obtained with the UV system.

4.5. Suggested physical picture

We now aim to unify the results presented on double networks prepared with the UV system with a physical picture. In particular, it should explain at least qualitatively why some double networks show damage in cyclic loading while others do not, and how this feature can depend on prestretching, formulation and tested direction

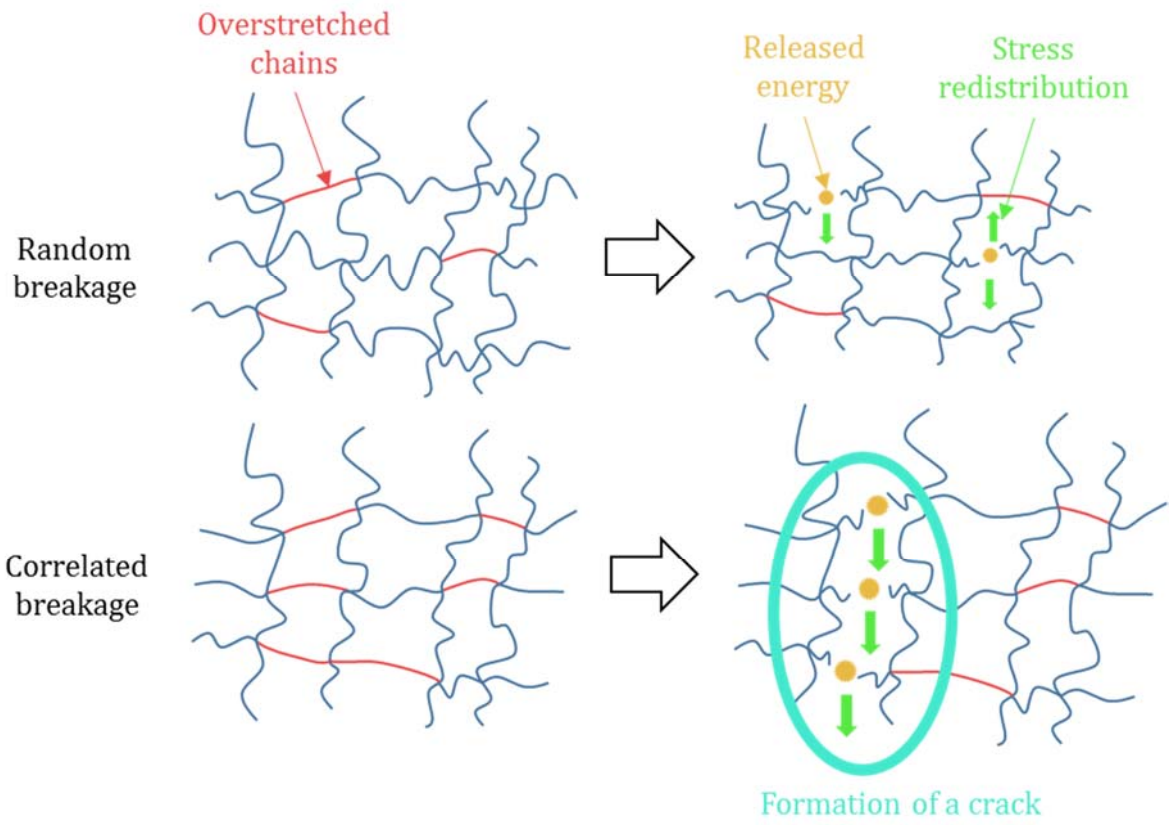

Figure 42: illustration of the concepts of random breakage and correlated breakage. Note that these schematic represent the filler network only, but in a double network structure. The matrix network is not represented but also takes back a part of the load when a chain breaks.

The idea behind the physical picture is to study the populations of chains in the filler network structure and consider their distribution in strand length and conformation. Three major assumptions are made in addition to affine deformation:

- Strain-hardening begins when the shortest strands of the filler network approach their maximum extensibility
- The probability for a chain to break strongly increases when it approaches its maximum extensibility, which is linked to the contour length of the chain
- The overall material breaks when too many chains start to break at the same time and in the same place, which nucleates a crack.

The third assumption is crucial to explain the presence of visible damage during cyclic damage. The latter is interpreted as the breakage of short chains that are diluted in the filler network architecture. These chains may therefore break independently from each other and dissipate energy. By opposition to this random breakage, chains start to break collectively when the material is stretched sufficiently so that many chains are loaded close to their maximum extensibility. At this point, the breakage of one chain releases significant energy, triggers the breakage of neighboring ones and correlated breakage starts. These two situations are illustrated in Figure 42. As the macroscopic loading rises, the mechanisms switches from one to the other situation by bringing more chains in an overstretched situation.

4.5.1. Dual-curing means two populations of chains

Our materials are double networks in which the filler network has been cured in two separate steps. At the end of the initial step, a fraction of the ALA units have reacted only on one side, and some other ones have reacted at both ends. The latter units form the initial crosslinks, and define network strands that can be stretched in the next dual-curing phase. There are therefore two populations of network strands in our filler networks, and they most certainly do not have the same length distribution nor the same orientation distribution, especially when prestretching is added.

In Figure 43, a schematic representation of the hypothetic end-to-end distances distribution of the filler network strands is given. The initial strands are polymer chains between crosslinks that are formed when the allyl groups copolymerize with acrylates. This copolymerization is certainly far from being statistical, since the reactivity of acrylate functions is very different from that of allyl ones. **The first population of network strands is thus probably quite heterogeneous in length**, so that the distribution of end-to-end distances of the initial network strands is probably broad. On the contrary, the positions of the second population of crosslinks is far less random since they are located where the allyl acrylate functions have reacted in the first stage. The incorporation of allyl comonomers via their acrylate function is probably statistical since the chemical functions are the same. Therefore, **the second population of crosslinks is probably fairly homogeneous in terms of number of monomer between crosslinks**, and the resulting strand length distribution is probably narrow.

Aside from the distribution of network strand length, there is also a distribution of end-to-end vectors orientations. In order to visualize it, one can plot diagrams that represent this distribution, such as shown in Figure 44. The distribution is represented in the two-dimensional plane of traction. The average strand length is represented by a plain line, and the limits of the distribution are represented by dotted lines. The latter may for instance represent the first and last centiles of the distribution. When a tensile force is applied on the material, the entire distribution is deformed under the affine assumption.

The usefulness of this this type of 2-D representation of end-to-end distances is that it enables the comparison of the two populations of network strands at different stages of the process, as shown

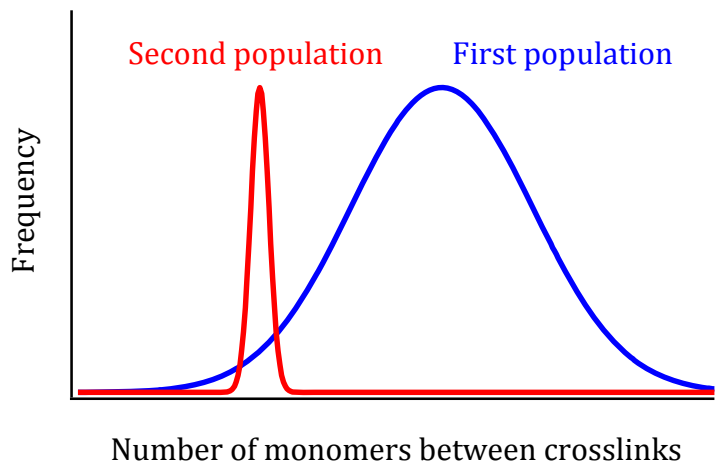

Figure 43: schematic representation of the hypothesized size distribution of network strands in the first (red curve) and second (blue curve) populations of crosslinks in the dual-cured filler network. The first network is believed to be much more heterogeneous because of the non-equivalent reacivities of acrylate and allyl groups.

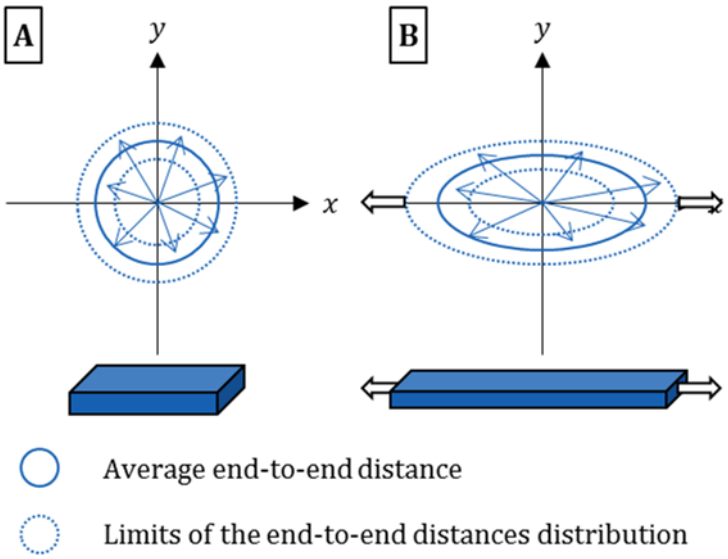

Figure 44: schematic representations of end-to-end vectors distributions before (subfigure A) and after (subfigure B) a tensile force has been applied in the x-direction.

in Figure 45. In the initial singly-cured state, chains may be assumed to be Gaussian and isotropic. All orientations are equiprobable and there is a circular distribution of end-to-end vectors. In the clamped state, the initial population of chains is extended in the x-direction and the second newly-generated one is isotropic. When the material is unclamped, it goes back partially toward equilibrium. In the relaxed state, the initial population of strands is extended in the x-direction and the second one in the y-direction. The passage from single to double network only adds an isotropic swelling stretch ratio.

In the end, the physical picture that is presented here is based on the two following differences between the two populations of filler network strands:

- **The distributions of strands lengths are different**, and the first population is assumed to be much more heterogeneous than the second one.
- **The distributions of orientations are different**, the first population of chains is mainly oriented in the x-direction while the second one is mainly oriented in the y-direction.

It is the combination of these two differences that give rise to the variety of mechanical behaviors in large strains that has been observed in the previous sections.

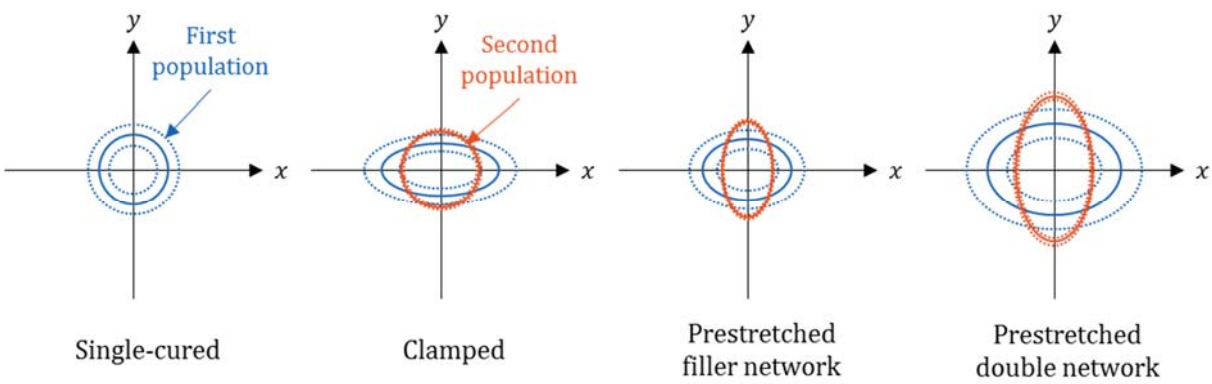

Figure 45: schematic representation of the end-to-end vector distributions of the filler network strands throughout the double network preparation process. The initial network strands correspond to the blue distribution, the second ones correspond to the orange one.

4.5.2. The origin of damage in cyclic loading

As stated before, the existence of damage during cyclic loading in double networks is believed to be linked to the distribution of end-to-end vectors in the filler network. **When the most heterogeneous population of chains reaches its maximum extensibility first, chains may break in a random fashion without threatening the survivability of the entire material**. To illustrate this situation, Figure 46-A shows the end-to-end vector of the first population of crosslinks superimposed with its limit of extensibility. The evolution of the distribution in the vicinity of the limit of extensibility is shown in Figure 46-B. Strain-hardening is typically expected to appear when the top situation is reached, i.e. when the least extensible chains approach their limit of extensibility. In the middle case, damage becomes visible on the cyclic loading curves. Because of the wide distribution of end-to-end vectors, some chains surpass their limit of extensibility and break. These chains however are in minority in the entire structure, so they break randomly here and there in the network. The material can therefore keep damaging and extend further before breaking. When the bottom case is reached, the average network strands reach their limit of extensibility. At this stage, correlated breakage is expected and the material would eventually break.

This first situation represents the case where the most heterogeneous network strands reach their maximum extensibility first. Instead, **if the second population reaches it first, then breakage should appear without any apparent damage in cyclic loading**. The distribution of end-to-end vectors is too narrow in this case. Once the least extensible chains start to break, the other ones are too close to their limit of extensibility to absorb the redistributed stress. Note that this second case basically corresponds to the case of traditional double network elastomers. Although there is some heterogeneity because of the free radical polymerization processing route, these materials are almost purely elastic in cyclic loading and virtually no damage is observed.

As an important clarification, note that regardless of its homogeneity, the filler network is embedded in a double network structure. As a result, some chains may and will break in a random way, even when the homogeneous population of crosslinks reaches its maximum extensibility first. As a proof of this, all double networks prepared with the UV system indeed show a pronounced strain hardening, which would not be the case if only correlated breakage of bonds was observed. The question is thus not about whether *some* chains may break randomly or not, but rather *how much* can break before the entire assembly of chains is too close to its maximum extensibility. If this number is large enough, then damage may be observed in cyclic loading. This is the case for instance when there is a broad distribution of network strand lengths, or in triple networks where the chains are diluted enough to be able to break individually in a large amount.

To sum up, in the frame of this physical picture, the presence or absence of significant damage depends on which population of strands approach their limit of extensibility first. If it is the first most heterogeneous population, then a large amount of bonds may break and significant damage is expected. If on the opposite the second most heterogeneous population reaches it first, then only a very small amount of bonds will break randomly before correlated breakage occurs. The presence or absence of damage in cyclic loading therefore depends on the prestretching and on

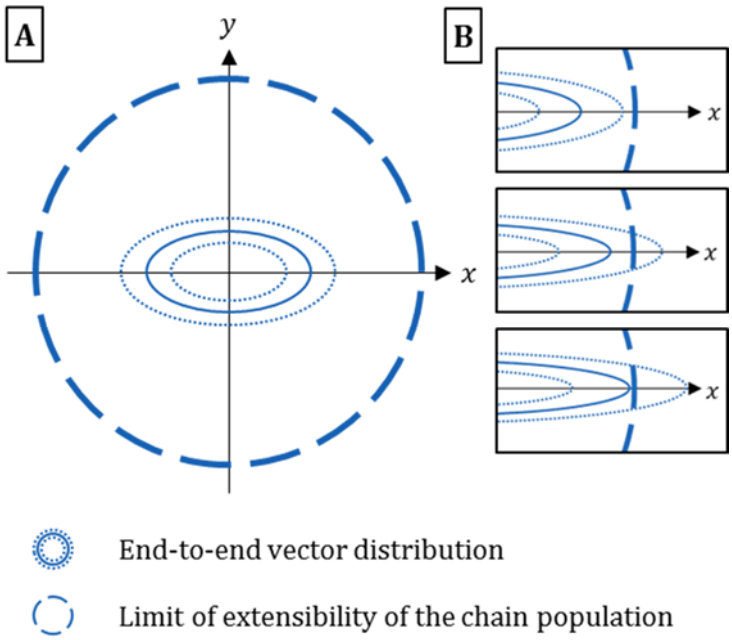

Figure 46: schematic represented of the end-to-end distribution (plain and dotted lines) and maximum extensibility (dashed line) of the filler network chains for the first population. In this situation, damage may be observed in cyclic loading.

the formulation via their effects on the end-to-end distributions of the two population of filler network strands.

4.5.3. The effect of prestretching and formulation

The case of low ALA contents

When taking a closer look at the values of Young's modulus, there is an important difference between the 1.0 and 1.5 mol% formulations on the one hand, and the 2.0 mol% on the other hand. In the two first cases, the difference in Young modulus is smaller than the initial modulus of the single-cured network. This means that the crosslinking density of the second population of chains is smaller than the initial one, therefore **the average strand length of the second population of crosslinks is longer than the initial one in this case**. As a result, the limit of the extensibility of the initial population of crosslinks is also smaller. This situation is represented schematically in Figure 47, for the unprestretched DN (on the left) and the prestretched one (on the right).

For low ALA contents, the initial population of filler network strands is ensured to reach its maximum extensibility before the second one in the unprestretched case and in the prestretched case in the longitudinal direction. As shown in Figure 47, stretching the distributions along the x-axis brings the edge of the initial network distribution at the level of the circle representing the maximum extensibility before the second population.

In the transverse direction, the average strand length is larger for the second population than for the initial one, as shown in the left subfigure of Figure 47. Therefore, it is not sure that the initial population of strands reach their limit of extensibility first. It all depends on how far this population is from its limit of extensibility compared to the second population. As shown in Figure 48, **there is a possibility that the initial population of strands break before the second one in the transverse direction**, provided the heterogeneity is large enough in the initial population of strands.

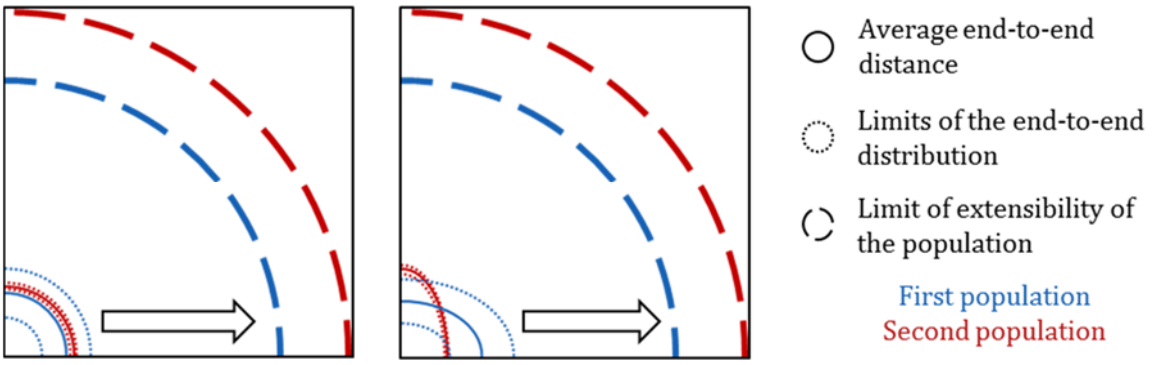

Figure 47: top-right corners of the end-to-end vector distributions in the case of the unprestretched DN (left) and prestretched DN (right) with low amount of ALA in the filler network formulation. In these two cases, stretching along the arrow ensures that the first population of chains reaches its maximum extensibility before the second one.

To sum up, using low levels of ALA in the formulation (1.0 or 1.5 mol%) is associated to a very moderate increase in modulus during the second curing. As a result, the average strand length of the initial population of filler network strands is smaller than the average strand length introduced with the second crosslinking step. In this case, the initial population of strands always reach its maximum extensibility before the second one provided its distribution of end-to-end vectors is broad enough. This would explain why damage in cyclic loading is always observed with these formulations.

The case of 2.0 mol% ALA

When a larger amount of ALA is used, the increase in modulus becomes much larger during the second curing. As a result, **the second population of network strands is shorter than the initial one on average** (but it is still less heterogeneous). Figure 49 shows the schematic representations of the end-to-end distributions in the initial state and during the tensile test both for the unprestretched and the prestretched case.

In the unprestretched case (left diagram on Figure 49), when the end-to-end vectors are stretched, the second population of crosslinks reach their limit of extensibility before the first one. If the heterogeneity of the initial population is larger, it is possible that some chains of the first population start to break before the second one, but this will only happen at the end of the test, very close to the fracture point. As a matter of fact, this is what has been observed on the example material from section 3.3.3.

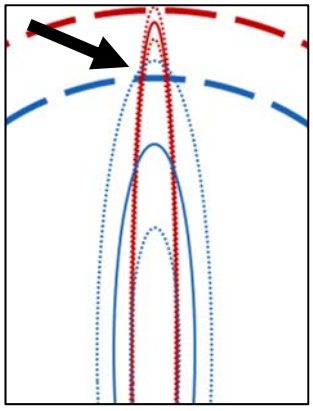

Figure 48: close up on the case of transverse loading on a prestretched DN with low amount of ALA in the formulation at the vicinity of the limit of extensibility of the filler network.

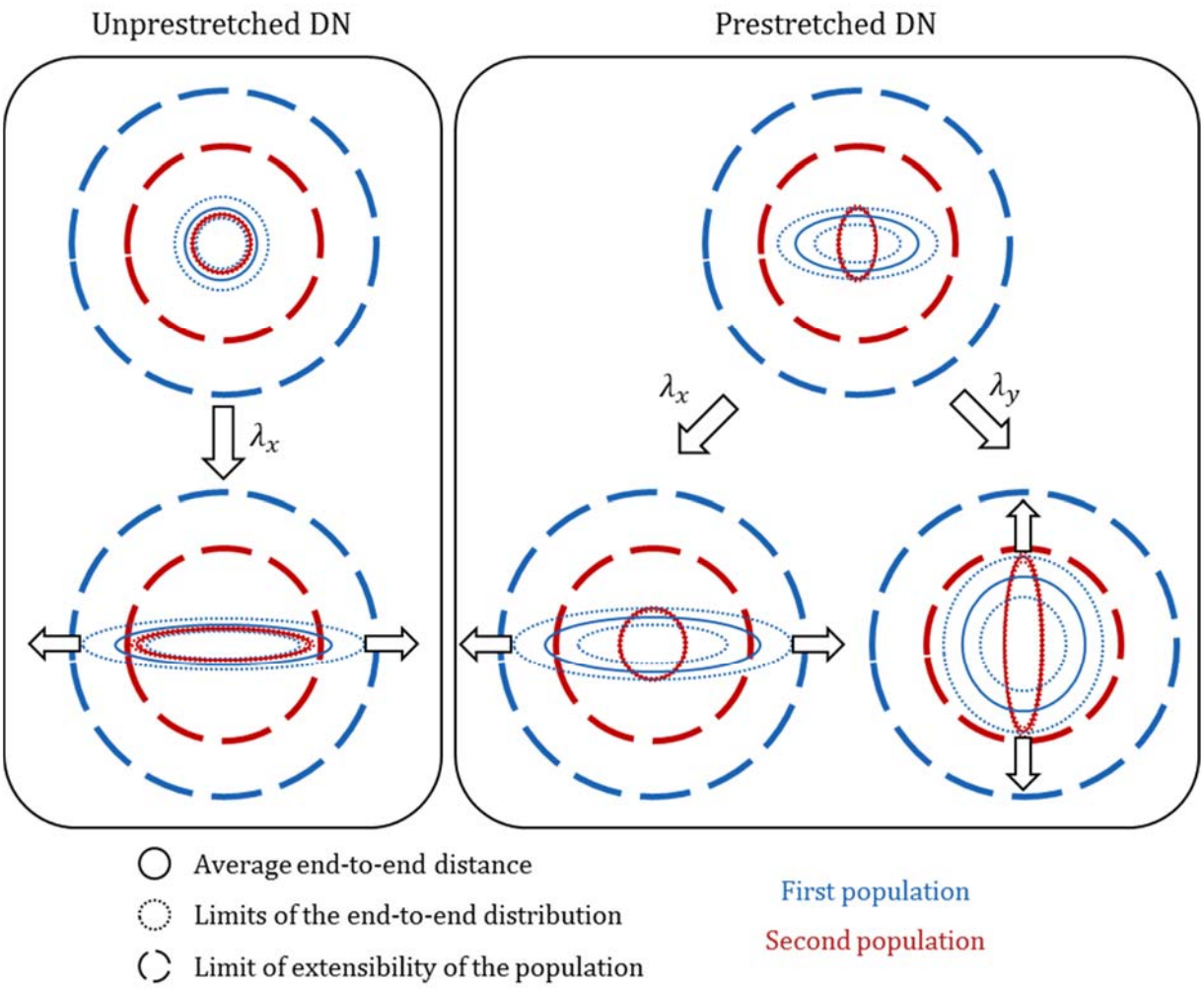

Figure 49: illustration of the end-to-end distributions of the filler networks in double networks prepared with 2.0 mol% ALA. The initial state is presented on the top line, and a tensile force is applied on the bottom line. Force directions are represented with arrows on the bottom line distributions.

In the prestretched case, in the transverse direction (right diagram in Figure 49), it is very clear that the second population of crosslinks will always reach its limit of extensibility first. The second population of strands is already partially extended and its maximum size is smaller because of the crosslinking density asymmetry. As a result, no visible damage in cyclic loading is expected, and this is indeed what is observed in most cases. **In the longitudinal direction however (middle diagram in Figure 49), thanks to the effect of prestretching, the filler network strands of the first generation are partially extended before the tensile test**. As a result, they are brought close enough to their limit of extensibility to induce damage in cyclic loading.

To summarize, the case of a large amount of ALA is the most interesting since in the absence of prestretching the average strand of the homogeneous population of crosslinks is closer to its maximum extensibility than the heterogeneous one. The presence of damage is made possible by the presence of prestretching, which brings the initial population of network strands closer to their maximum extensibility and the second strands further away from their maximum extensibility in the longitudinal direction.

4.5.4. Summary

The physical picture that is presented here relies on two physical ingredients and gives a way to rationalize the experimental results, and in particular the presence or absence of damage in cyclic loading:

- Damage in cyclic loading is believed to be due to the initial population of filler network strands. Because of the way the filler network is synthesized, this population should be more heterogeneous in terms of network strand length, and should therefore exhibit a broader distribution of end-to-end vectors.
- The presence or absence of damage is explained by the fact that the two populations of filler network strands are brought simultaneously toward their respective limits of extensibility. Depending on the extent of heterogeneity and on the prestretching, either population may reach its limit of extensibility first, and therefore the material may show damage or not

5. Influence of damage on mechanical properties for the UV system

5.1. Study of viscoelastic properties

To complete the study of mechanical properties, we analyze the viscoelastic properties of our materials in the small strain regime. The underlying question is to identify if the damage has an impact on the viscoelastic properties of the material. Only one sample has been tested, the characteristics of which are given in Table 8.

5.1.1. Study of undamaged materials

First, the linear regime of the material is identified. The unprestretched sample is used and tested in tensile mode with the DMA using the following set of parameters (see chapter 2 for explanations and definitions):

Parameter	Frequency	Static force	Forcetrack	Strain
Value	1 Hz	0.01 N	125 %	Variable

Results of strain sweeps at constant temperature are given in Figure 50. Tests at 25 and 80°C show a constant value of storage modulus E'. At -60°C, the value of E' decreases from 0.03% strain. This is normal given that the material is well into his glassy regime (poly ethyl acrylate glass transition is around -10°C). Therefore, **a value of strain of 0.015% will be used to measure the viscoelastic spectrum**, ensuring that the material is well into its linear regime throughout the temperature ramp.

Viscoelastic properties of virgin materials are then measured by DMA. The following set of properties is used in constant strain mode:

	Prestretched	Unprestretched
Formulation	2 mol% ALA 0.1 mol% HMP / 50 vol% AcOEt	
Synthesis yield	92.20%	
Infiltration swelling ratio	5.27	
λ_{clamp}	2.31	1
λ^*	1.52	1
$\lambda_{swelling}$	1.52	1.55

Table 8: Characteristics of the sample material tested in DMA for viscoelastic properties measurement. Based on the results from section 4.1, this sample is representative from the average trend observed in the 2 mol% group.

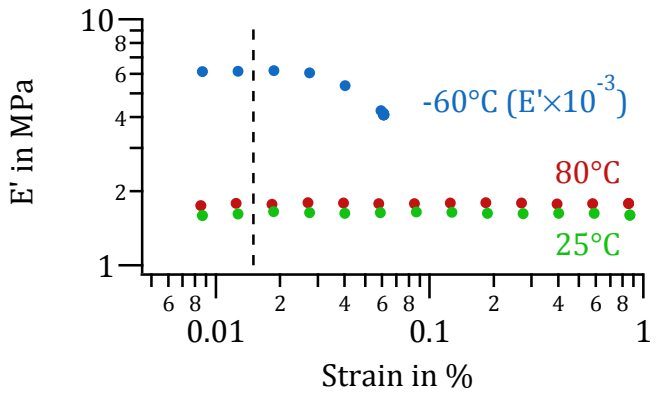

Figure 50: identification of the common linear regime for the temperatures tested in our materials. Storage modulus is plotted with respect to the strain. Note that modulus at -60°C has been multiplied by 10^{-3} on the graph.

Parameter	Frequency	Static force	Forcetrack	Strain	dT/dt
Value	1 Hz	0.01 N	125 %	0.015%	1°C/min

The resulting moduli and loss tangents are shown in Figure 51. Overall, **the global shape of the curves is the same for the three subsamples**. In particular, the position of the glass transition is the same, as well as the shape of the tan(δ) peak. The only visible difference is the value of the storage plateau modulus that is higher in the prestretched samples compared to the

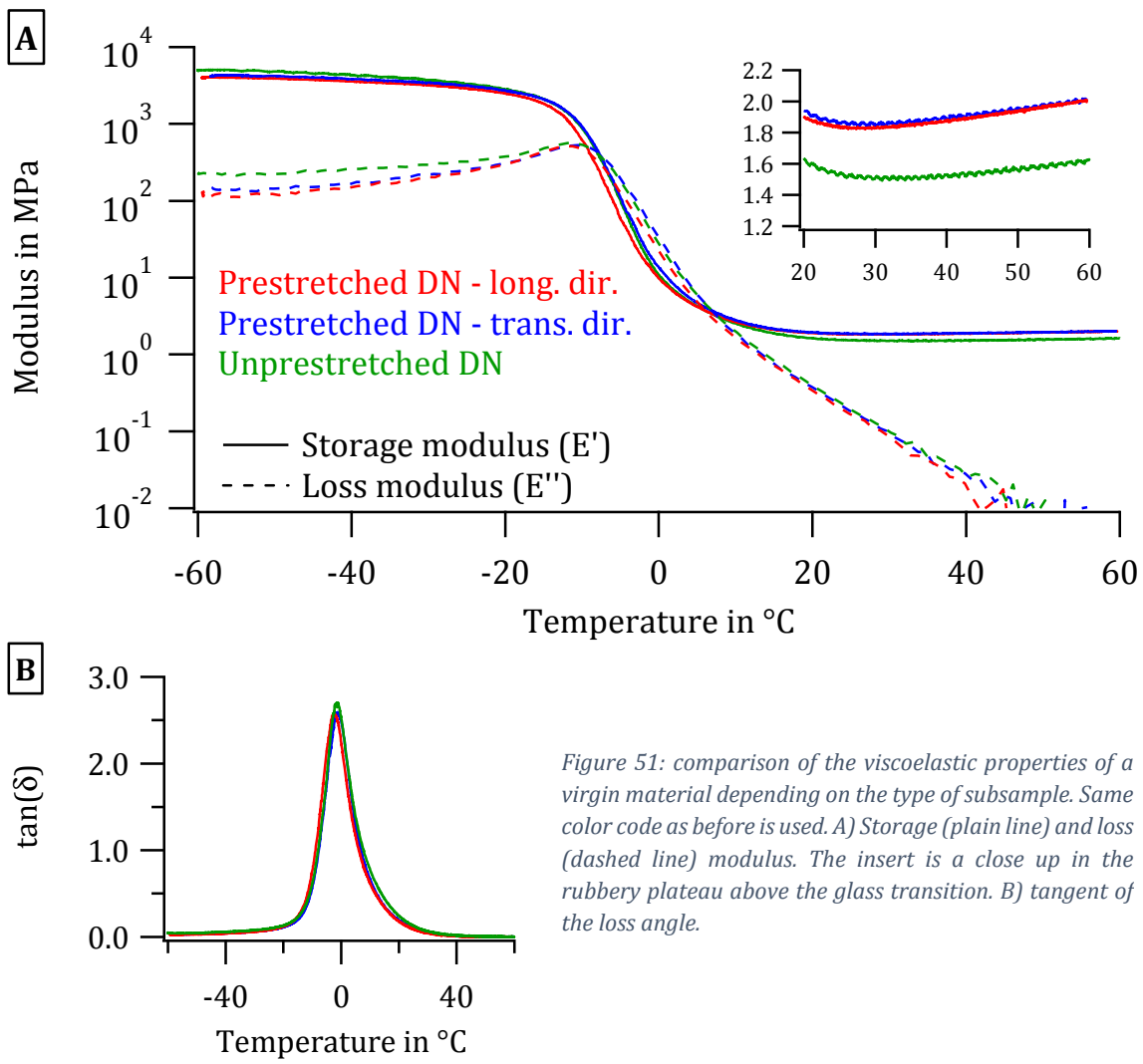

Figure 51: comparison of the viscoelastic properties of a virgin material depending on the type of subsample. Same color code as before is used. A) Storage (plain line) and loss (dashed line) modulus. The insert is a close up in the rubbery plateau above the glass transition. B) tangent of the loss angle.

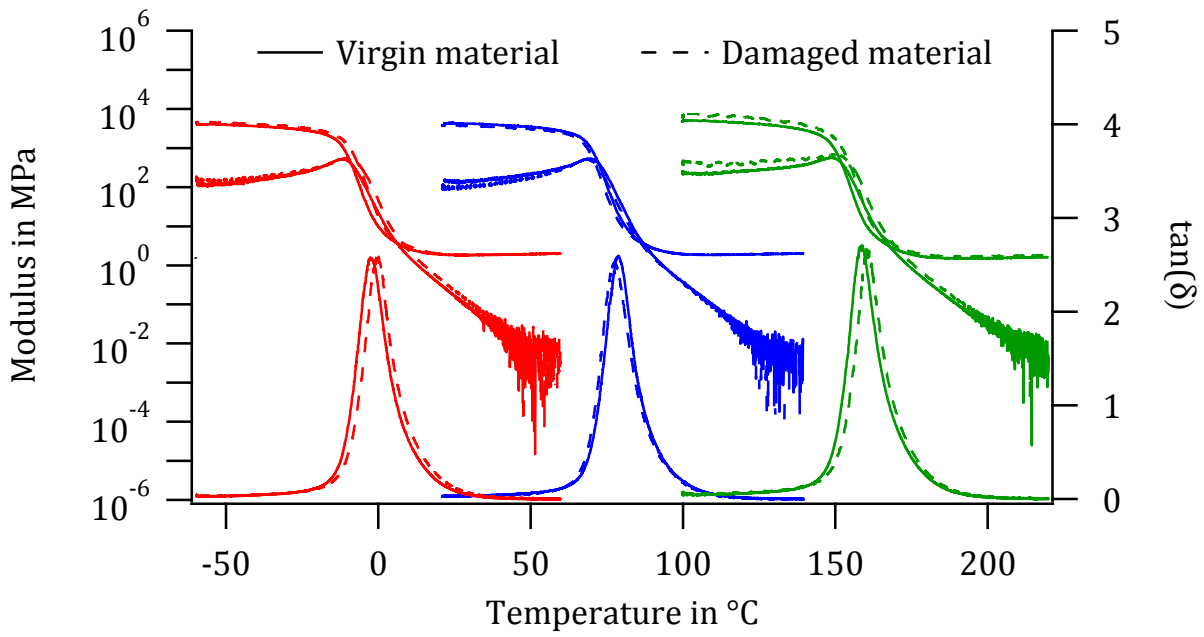

Figure 52: assessment of the effect of damage on the viscoelastic properties of our materials. The same legend as in Figure 51 is used. The top two curves for each subsample are the storage and loss moduli. The bottom bell-shape curve is the loss tangent. All experiments are performed between -60°C and 60°C, curves for the transverse and unprestretched subsamples (in blue and green respectively) and shifted toward the right for readability.

unprestretched one. This experimental fact has already been seen and explained before (see 4.3.2). Note that the storage modulus increases linearly with temperature in the plateau modulus. This is the expected behavior according to the entropic nature of rubber elasticity.

The resemblance between the three subsamples at (very) small deformations is not surprising, since the main difference between the samples is the degree of prestretching of the filler network chains. The latter are not expected to have any impact on the mechanical properties until they are stretched enough to be close to their limit of extensibility. At 0.015% strain, virtually all the chains in the network are well into their Gaussian regime, so no difference should be visible.

5.1.2. Study of damaged samples

What happens when the material is deformed and damaged? To answer this question, the same three samples are tested in cyclic loading up to stretch ratios between 1.9 and 2. After this, the central part of the samples is tested once again by DMA and a new viscoelastic spectrum is acquired with the same set of parameters.

The comparison of virgin and damaged samples is shown in Figure 52, with virgin samples in plain lines and damaged ones in dashed lines. Once again, there is no clear difference between the curves, **damage does not modify significantly the small strain behavior of the materials** (at least at this level of deformation).

If a difference can be distinguished, the unprestretched sample would be the sample showing the most dissimilar response between the virgin and damaged samples. The glass modulus is 1.5 times larger in the damaged sample. The same goes for the loss modulus that is 1.9 times larger in the undamaged sample. A difference of 2 degrees may also be seen in the position of the maximum of

the loss tangent. Values of rubbery plateau are only 12% larger though. All these differences are very minimal and may very well be due to clamping issues or small errors in the measurement of samples dimensions. Anyway, they are too small to account for a real difference in viscoelastic properties between the two types of subsamples.

To conclude, this small section on DMA experiments demonstrates that the damage mechanism in our materials mainly concerns the large strain properties of our materials. Breakage of short chains in the filler network are not expected to significantly impact the viscoelastic properties of the materials. This is understandable given the fraction of filler network in the double network structure (about 20 w%) and the very small fraction of broken bonds in the material (less than 1%).

5.2. Study of fracture properties

The fracture properties of materials prepared with the UV dual-curing system are now investigated. Fracture energy is measured by testing a notched sample in uniaxial traction, as described in 2.4. In short, the stretch ratio at which the pre-crack propagates is measured and then used to calculate the critical strain-energy density. Fracture energy is then calculated using Greensmith's formula [3].

In a first part, the fracture energy of virgin samples is tested. These values are then compared to samples that have been loaded cyclically and damaged in a second part.

5.2.1. Fracture study of virgin samples

The fracture energies of undamaged samples are compared in Figure 53. Error bars are confidence intervals at 95%, which enables safe comparison of formulation groups that do not contain the same number of tested samples. First of all, regardless of the formulation and type of subsample, **the fracture energy of all our samples is larger than 500 J/cm²**. This is well above the fracture energy of a typical unfilled elastomer (about 50 J/cm² [8]) and is directly due to the toughening effect of the double network architecture, as reported in previous studies on this type of architecture [5,14]. This reinforcing effect is thus still effective although an additional prestretching has been applied with the dual-curing mechanism.

In the 1.0 mol% ALA formulation group, a very large variability is observed and as a result no clear trend can be identified. In other words, prestretching does not have a large enough effect on the fracture properties to overcome the sample to sample variation. The two other formulation groups show clearer trends however. **The fracture energies of the prestretched samples in the longitudinal direction seem to be smaller than in the transverse direction and in the unprestretched sample**. Statistical comparison of the average values confirms the significance of the difference despite the large error bars, with p-values smaller than 2% (regardless of whether the comparison is made with the transverse subsample, the unprestretched subsample or both reunited in one group).

The explanation of this difference is challenging but may be linked to the short chains of the filler network structure. Basically, the fracture of any network means that all the chains in the plane of

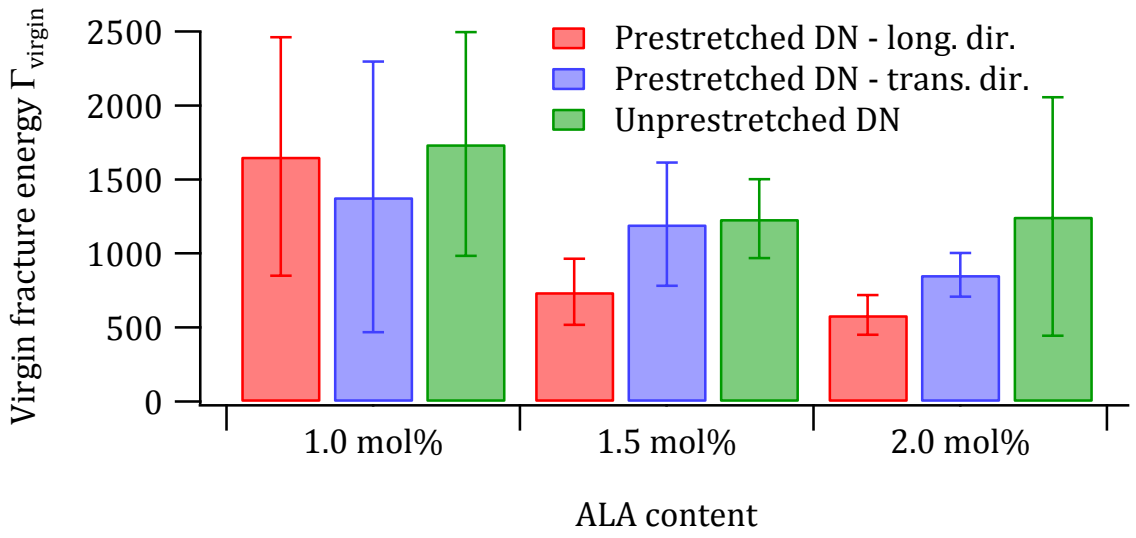

Figure 53: comparison of average values of fracture energies measured on virgin samples with different ALA contents. Error bars are confidence intervals at 95%.

the initial crack break. The overload of these chains comes from the stress concentration effect at the crack tip, so that when one strand breaks it leads to the breakage of its neighbor, and so on and so forth. The trick behind the reinforcing mechanism of double networks is that chains of the filler network are prestretched and break randomly in the bulk of the material (by opposition to correlated breakage that happens at the vicinity of the crack tip during crack propagation). These random covalent bond breaking events transfer the force from the filler network to the unstretched matrix network chains and avoid the premature and catastrophic propagation of the initial crack.

In our materials, the prestretching of the chains of the filler network depends at least partly on the direction. As seen in the previous sections, the addition of prestretching has an impact on the large-strain properties of the materials. It changes the potential of the filler network strands to further stretch toward their maximum extensibility. Therefore, it most certainly has an influence on the way the energy is redistributed in the filler network when the first strands start to break. For instance, one could imagine that because of the orientation of the chains in the prestretched direction the chains are on average closer to their maximum extensibility. The breakage and redistribution of stress to the neighboring chains is thus more likely to trigger a sequence of correlated breakage. However, the details of how prestretching may influence the propagation of a pre-crack are not easy to determine. The presence of two populations of networks strands and the presence of heterogeneity in the filler network structure certainly plays a role as well.

5.2.2. Effect of damage on fracture resistance

The presence of short chains in our materials is believed to be the origin of the prominent damage observed in cyclic loading. These chains may be broken at fairly low extensions, and their breakage dissipates energy. In a virgin material, this dissipation of energy probably participates to the overall fracture energy that is measured. What about damaged samples then? Should we observe a decrease in fracture energy once the material has been loaded and chains have been broken?

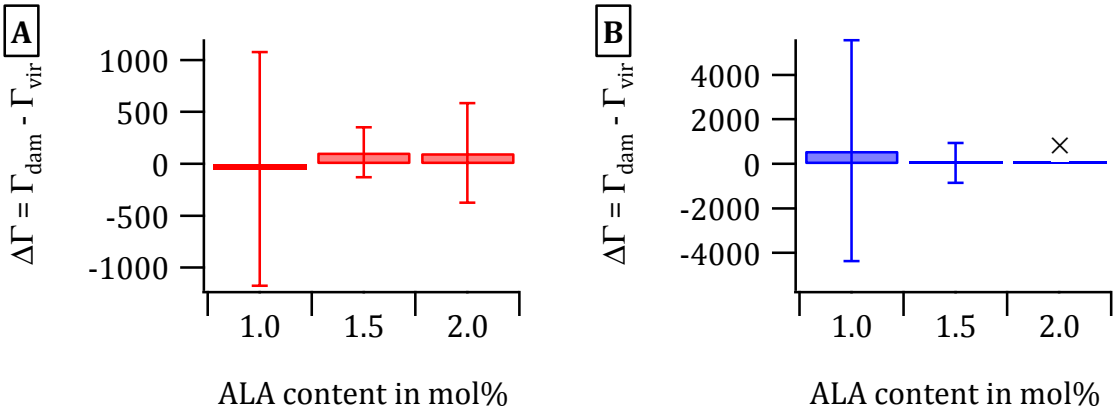

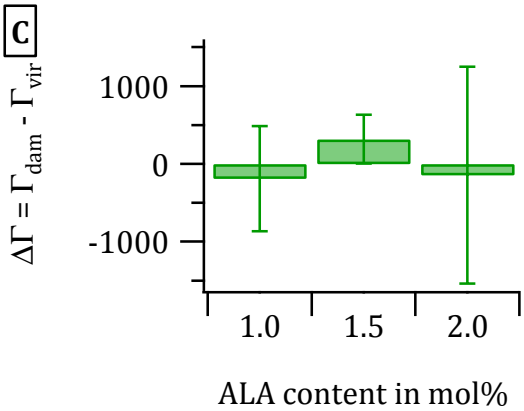

Figure 54: comparison of average values of fracture energy before and after a conditioning cycle. The difference in fracture energy is presented, averaged for each formulation group. Error bars are confidence intervals at 95%. Color represent the type of subsample: red/A is the prestretched DN in the longitudinal direction, blue/B is the transverse direction, and green/C is the unprestretched DN. The "x" on subfigure B is for a measurement where only one sample was tested before and after damage, therefore no variance could be calculated.

The impact of damage on fracture energy is shown in Figure 54 for the three formulation groups via the comparison of Γ_{virgin} and $\Gamma_{damaged}$. The difference $\Delta\Gamma = \Gamma_{damaged} - \Gamma_{virgin}$ is calculated for each sample and the values of $\Delta\Gamma$ are averaged within each formulation group and for each subsample. Each subfigure/color corresponds to a type of subsample (longitudinal/transverse/unprestretched), and virgin and damaged fracture energies are compared with confidence intervals at 95%. Note that due to the size of subsamples the transverse direction could not always be split in two strips of material to test both Γ_{virgin} and $\Gamma_{damaged}$. This explains in particular the very large error bar on Figure 54-B at 1.0 mol%, and the absence of error bar at 2 mol% (because only one sample could be tested).

Regardless of the direction, the fracture energy seems not to be significantly affected by damage. A larger amount of tested samples could help identifying a trend of course, but in any case the effect seems to be weak enough that it does not overcome the variability of the measurement of Γ. This result may appear surprising, since the toughening mechanism of double network has been attributed to the irreversible breakage of prestretched chains in the filler network structure. Therefore, breaking some of the short chains with damage might alter the ability of the material to resist fracture. This is at least what is claimed in the literature, and in several papers [14–16] authors claim that breakage of covalent bonds is a limitation to the use of these materials in applications that require good fatigue resistance (i.e. ability to resist fracture once damaged). As a matter of fact, recent studies on tough hydrogels by Suo et al. have shown that covalent bond scission is not incompatible with resistance to fracture in fatigue [17], and the present results seem to confirm this observation.

Actually, in double network elastomers, only a very small fraction of the bonds are broken during the deformation of an unnotched sample. The analysis presented in 4.4.2 has shown that 1% of filler network chains at most are broken during step-cyclic tests. This breakage occurs over the entire volume of the sample, and should be compared to the amount of filler network chains that are actually broken during the propagation of a crack. The latter is difficult to estimate, but recent research carried out in our group provides an estimation of the order of magnitude. Using mechanochemistry and fluorescence techniques, a recent PhD project conducted in our team [10] has estimated that the amount of broken bonds in a double network during crack propagation is about 4×10^{18} chains/m^2 and that the damage zone has a typical width of $L_{\text{dam}} = 20\ \mu m$. This result is for a double network with a poly(methyl acrylate) filler network and poly(ethyl acrylate) matrix network, which is as close as possible from our system. With the number density of chains in the filler network, one can derive the total number of filler network chains in the damage zone using L_{dam}:

$$\Sigma_{\text{filler, tot}} = \frac{\phi_{\text{filler}}\ E\ L_{\text{dam}}}{3\ k\ T} \qquad \text{Eq. 22}$$

with ϕ_{filler} the volume fraction of filler network (estimated from the swelling stretch ratio), E the Young modulus, k the Boltzman constant and T the absolute temperature. A numerical application of Eq. 22 gives an estimate of 7×10^{20} chains per square meter. This simple order of magnitude calculation shows that about 0.6% of the filler chains break in the damaged zone during the propagation of the crack.

To sum up, damage during cyclic loading breaks at most 1% of the filler network chains in the entire material. Since the ratio between the damaging zone volume and the entire volume of the sample is $L_{\text{dam}}/L_{\text{sample}} \approx 10^{-3}$ (the length of the sample being roughly 2cm), this means that **the damaging cycle breaks a fraction of 10^{-5} of the filler network chains in the future damaging zone**. Ultimately, during the propagation of a crack, 0.6% of filler network chains are broken in the damaging zone. Chains broken during the conditioning cycle are therefore just a drop in the ocean of the chains broken during the propagation of the crack. In light of these estimations, it is not so surprising that the effect of damage on fracture energy is so limited. The material may be damaged, but there is not enough broken chains in the damaging zone to really harm the ability of the material to resist the propagation of a crack, which is a localized event.

6.Conclusions

In this chapter, the prestretched dual-cured elastomers have been incorporated in double network structures. Prestretched networks from the two systems have been studied, mostly with tensile tests (monotonic and cyclic) and more occasionally using dynamic mechanical analysis or fracture tests. The first immediate conclusion is that the resulting materials are tough and show a mechanical response that is qualitatively similar to the standard double networks that have been studied so far. Therefore, the presence of prestretching does not seem to disturb the toughening mechanism. This study therefore confirms the universal aspect of the double network strategy and confirms that it should in theory be applicable to industrial elastomers that are not as perfect as lab-scale acrylic elastomers.

In our materials in particular, there is a fundamental distinction between the small and large strain behavior of the material. Regardless of the chemical system that is used to prestretch the filler network (thermal or UV), the small strain response of the resulting double network is mainly isotropic. All in all, the prestretching that is applied is not large enough to fundamentally change the statistics of the constituting chains of the filler network. At large strains however, the effect of prestretching becomes much more visible, as for example with the anisotropy in the maximum extensibility of the prestretched double network. This separation between the two scales is a specific feature of our materials and differs for instance from other types of tough elastomers.

Although the effect of prestretching on the large-strain properties of double network elastomers is fairly straightforward to observe, it is much more difficult to interpret it and model it using simple mean-field models. An extension of Flory's model to large strains gives a fairly good qualitative explanation of the results obtained in the longitudinal direction, but fails to predict the behavior in the transverse direction. This indicates that the details of the effect of prestretching on the mechanics of double networks are not fully understood. More importantly, this discrepancy probably result from cross-directional effects and/or strong influence of the highly non-Gaussian character of the chains once they come very close to their finite extensibility.

The two dual-curing systems that have been tested show some specificities that are mostly visible once the prestretched networks are incorporated in a double network structure. The thermal system for instance is characterized by a very problematic lack of reproducibility. The UV system on the other hand shows a visible and original damage mechanism that is only active at large strains. This damage mechanism is particularly visible in step-cyclic loading and is reflected in a stress softening and an increase in maximum extensibility, similar in some ways to the classical Mullins' effect of filled rubbers. This damage is original in the sense that it is not observed in traditional double network elastomers, which is attributed to the presence of a significant heterogeneity in our system.

The effect of damage on the material mechanical properties has also been studied. The study of viscoelastic and fracture properties reveals that although damage has a visible effect on the large strain response of the material, it does not significantly change its fracture properties nor its viscoelastic behavior in small strains. This is mainly explained by the fact that only a small fraction

of the filler network chains break during cyclic damage. These chains dissipate a significant amount of energy but are not numerous enough to really affect the material's viscoelastic response or its ability to resist the propagation of a crack.

To conclude, the prestretched double networks that have been prepared are original materials in the sense that subtle changes in their molecular structure induce visible changes in their large strain mechanical response, while leaving their small strain response globally unchanged.

7.References

1. Millereau P, Ducrot E, Clough JM, Wiseman ME, Brown HR, Sijbesma RP, et al. Mechanics of elastomeric molecular composites. Proc Natl Acad Sci. 2018 Aug 28;201807750.

2. Gent AN. A New Constitutive Relation for Rubber. Rubber Chem Technol. 1996 Mar 1;69(1):59–61.

3. Greensmith HW. Rupture of rubber. X. The change in stored energy on making a small cut in a test piece held in simple extension. J Appl Polym Sci. 1963 May 1;7(3):993–1002.

4. Millereau P. Large Strain and Fracture of Multiple Network Elastomers [PhD thesis]. [Paris]: Université Pierre et Marie Curie; 2017.

5. Ducrot E, Chen Y, Bulters M, Sijbesma RP, Creton C. Toughening elastomers with sacrificial bonds and watching them break. Science. 2014;344(6180):186–9.

6. Ducrot E. Innovative tough elastomers: Designed sacrificial bonds in multiple networks [PhD thesis]. [Paris]: Université Pierre et Marie Curie; 2013.

7. Ducrot E, Creton C. Characterizing Large Strain Elasticity of Brittle Elastomeric Networks by Embedding Them in a Soft Extensible Matrix. Adv Funct Mater. 2016 Apr 1;26(15):2482–92.

8. Lake GJ, Thomas AG. The Strength of Highly Elastic Materials. Proc R Soc Lond Math Phys Eng Sci. 1967 Aug 22;300(1460):108–19.

9. Wang S, Panyukov S, Rubinstein M, Craig SL. Quantitative Adjustment to the Molecular Energy Parameter in the Lake–Thomas Theory of Polymer Fracture Energy. Macromolecules. 2019 Apr 9;52(7):2772–7.

10. Slootman J. Quantitative detection of damage in soft materials using mechano-fluorescence [PhD thesis]. [Paris]: PSL Research University; 2019.

11. Merckel Y, Brieu M, Diani J, Caillard J. A Mullins softening criterion for general loading conditions. J Mech Phys Solids. 2012 Jul;60(7):1257–64.

12. Diani J, Fayolle B, Gilormini P. A review on the Mullins effect. Eur Polym J. 2009 Mar 1;45(3):601–12.

13. Merckel Y, Diani J, Brieu M, Gilormini P, Caillard J. CHARACTERIZATION OF THE MULLINS EFFECT OF CARBON-BLACK FILLED RUBBERS. Rubber Chem Technol. 2011 Sep;84(3):402–14.

14. Gong JP. Why are double network hydrogels so tough? Soft Matter. 2010;6(12):2583–90.

15. Haque MA, Kurokawa T, Kamita G, Gong JP. Lamellar bilayers as reversible sacrificial bonds to toughen hydrogel: Hysteresis, self-recovery, fatigue resistance, and crack blunting. Macromolecules. 2011;44(22):8916–24.

16. Chen Q, Yan X, Zhu L, Chen H, Jiang B, Wei D, et al. Improvement of Mechanical Strength and Fatigue Resistance of Double Network Hydrogels by Ionic Coordination Interactions. Chem Mater. 2016;28(16):5710–20.

17. Zhang W, Liu X, Wang J, Tang J, Hu J, Lu T, et al. Fatigue of double-network hydrogels. Eng Fract Mech. 2018 Jan 1;187:74–93.

Chapter 5

Toward glassy filler networks

Table of contents

1. Introduction and context 247
2. Materials preparation and characterization 249
2.1. Overall presentation of the preparation strategy 249
2.2. Materials preparation 250
2.2.1. Chemicals and formulations 250
2.2.2. PMMA network preparation 251
2.2.3. Filler network isolation and double network preparation 252
2.3. Dynamic Mechanical Analysis 254
2.3.1. Procedure and parameters 254
2.3.2. Specificities of PMMA samples and slippage phenomenon 255
2.3.3. Correction of slippage 255
2.4. Tensile tests 257
3. Results regarding the materials preparation 259
3.1. Overall overview of the synthesis 259
3.1.1. UV synthesis 259
3.1.2. Thermal synthesis 259
3.2. Quantitative parameters associated to synthesis 260
4. DMA characterizations 263
4.1. Effect of the nature of the crosslinker 263
4.1.1. UV synthesis / 1.5% crosslinker content family 263
4.1.2. UV synthesis / 3% crosslinker content family 266
4.2. Effect of crosslinker content / UV synthesis / BDMA crosslinker 268
4.3. Effect of initiation type 269
4.3.1. On filler networks 270
4.3.2. On double networks 271
5. Tensile characterizations 273
5.1. UV-polymerized DN with 0.75mol% BDMA 273
5.2. UV-polymerized DN with 1.5 mol% BDA 274
6. Conclusions 277
7. References 279

1. Introduction and context

The double network strategy is an effective toughening mechanism for elastomers that is based on a specific macroarchitecture. Specifically, it relies on the presence of not very extensible chains that are embedded in a soft matrix. This structure is similar to a molecular composite, with the combination of a filler network and a matrix network [1]. In principle, this strategy is not chemistry-dependent, in the sense that it may be adapted to any kind of filler network. The limit to this is that the filler network must be chemically compatible with the matrix monomer in order to swell and enable the in-situ synthesis of the matrix network.

In the literature, the vast majority of the strategies used to reinforce elastomers against fracture involve viscoelasticity (see chapter 1). The latter may be incorporated via polar groups or via the addition of fillers. In this case, the toughening is accompanied by a stiffening effect due to the use of hard inorganic particles. It however also changes significantly the appearance of the elastomer which becomes opaque and significantly denser. The idea of using viscoelasticity to toughen elastomers is fundamentally different from the double network strategy. The former is applicable to any network design but depends on the polymer chemistry, while the latter is applicable to any polymer but requires a specific design.

The idea in this preliminary study is to complement both approaches by studying double networks in which the filler network is not rubbery at room temperature. Until know, only moderate differences in T_g have been used in double network structures. Very notably, interpenetrated networks of poly(methyl acrylate) (PMA) and poly(ethyl acrylate) (PEA) are perfectly miscible at the molecular scale, resulting in a single glass transition observed either dynamic mechanical analysis or linear rheology [2–4]. When the asymmetry becomes larger (for example by using a PMA filler and a poly(butyl acrylate) matrix), two peaks are observed for the loss modulus in DMA, indicating the presence of phase-separation. The mechanical properties of the resulting materials in the fully-rubbery regime however are not significantly different from the homogeneous ones [2].

Here, we aim to push this asymmetry further. The idea is to incorporate a filler network that is glassy at room temperature into a matrix network that is purely elastomeric. Because of the large difference in dynamics, there are several possible situations that may arise when the two networks are interpenetrated. Three of them are now detailed and schematized in Figure 1:

- First, there is the possibility that the two networks form a perfectly miscible blend at the molecular scale (Figure 1-left). In this case, the matrix network would lower the T_g of the filler network and therefore reduce the molecular friction at room temperature. The resulting double network would therefore share some characteristics with standard purely elastic double networks, but with a glass transition temperature that is increased by the presence of the glassy filler network.
- In the opposite case, the two networks may phase-separate (Figure 1-right). If the affinity is bad enough between the two networks, the two phases may give microdomains that have significantly different dynamics, thus resulting into two glass transition

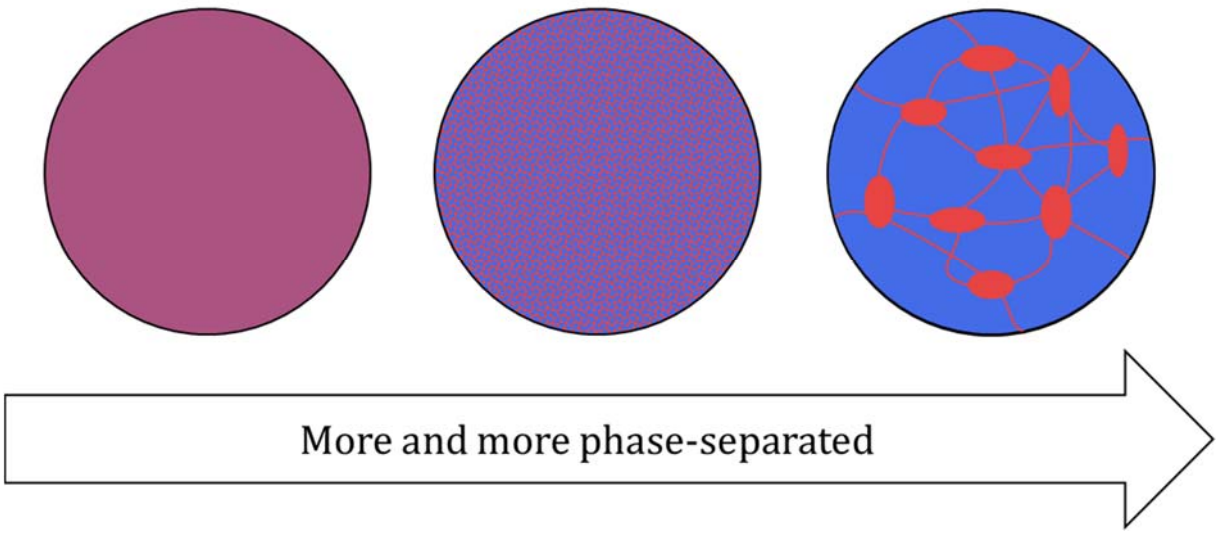

Figure 1: schematic representation of the three envisioned situations when a glassy filler network is incorporated in a double-network architecture. Left: completely miscible system, networks are mixed at the molecular scale. Middle: partly miscible system, there are separated domains of each networks, although at a small scale. Right: phase-separated system, there are well-defined and large-scale domains of filler networks within the matrix network.

temperatures. This situation would be similar to filled rubbers, with a hard phase dispersed in a soft matrix. The fundamental difference however would be that the filler phase would be continuous and percolating since it is made of a crosslinked network.

- In the intermediate case, there may be some partial mixture of the two networks (Figure 1-middle). In this case, there would be a large distribution of dynamics within the material, with regions that are more mobile than others depending on the local fraction of filler network. In this case, a broad glass transition is expected, resulting into a very dissipative material with time and temperature-depend mechanical behavior.

Depending on the details of the double network microstructure, very different mechanical behaviors are therefore expected. Interestingly, this type of material is much closer to traditional interpenetrated networks than the double networks that we usually study [5]. The main difference however remains that the filler network should be in minority and swollen by the matrix network in order to obtain a double network toughening effect. In other words, the filler network may be glassy when in the dry state, but it should remain at least partly mobile and extended in the double network architecture.

In the present chapter, the synthesis and first characterizations of this new type of double networks is presented. A screening of different formulations and synthesis conditions is presented, with small strain characterizations used to get an idea of the level of intermixing between the two networks. Specific formulations are then studied in more details with large strain characterizations.

Most of the experimental work presented in this chapter has been done by Maeva BALIMA, a former master student and research intern from our group.

2. Materials preparation and characterization

2.1. Overall presentation of the preparation strategy

Before studying the dynamics of these hybrid double networks, they first need to be synthesized. There is immediately a practical problem, since it is difficult to swell a glassy network with an organic solvent without damaging it. A possible solution to this problem is to prepare the crosslinked filler network in solution, so that the network is swollen with solvent at the end of the synthesis. On the one hand, the swollen gel may be placed in a bath of matrix monomer which can then diffuse in the mesh of the filler network and replace solvent molecules. After polymerization, this swollen glassy network would give a double network. On the other hand, the filler network may be isolated by carefully drying the swollen gel and progressively remove the solvent molecules. Figure 2 illustrates the overall approach that is followed in the rest of the chapter. Each synthesized PMMA network is thus separated in two parts, one that is used to isolate the filler network and one that is used to prepare the double network. Both materials therefore originate from the same synthesis, which is fundamental for comparisons.

The other question to address is the potential compatibility issue between the filler and matrix networks. In order to swell the filler network significantly during the double network preparation, we choose to remain in the family of acrylic polymers. Methacrylates in particular are known to exhibit high glass transition temperatures and good affinity with acrylates. This is for instance illustrated by the concept of rubber-toughened PMMA which incorporates acrylic rubber particles in a glassy methacrylic resin [6]. Choosing a PMMA filler network is therefore an easy way to ensure a high glass-transition temperature while maintaining good affinity with the poly(ethyl acrylate) rubbery matrix. The drawback of choosing a methacrylic filler network is that their

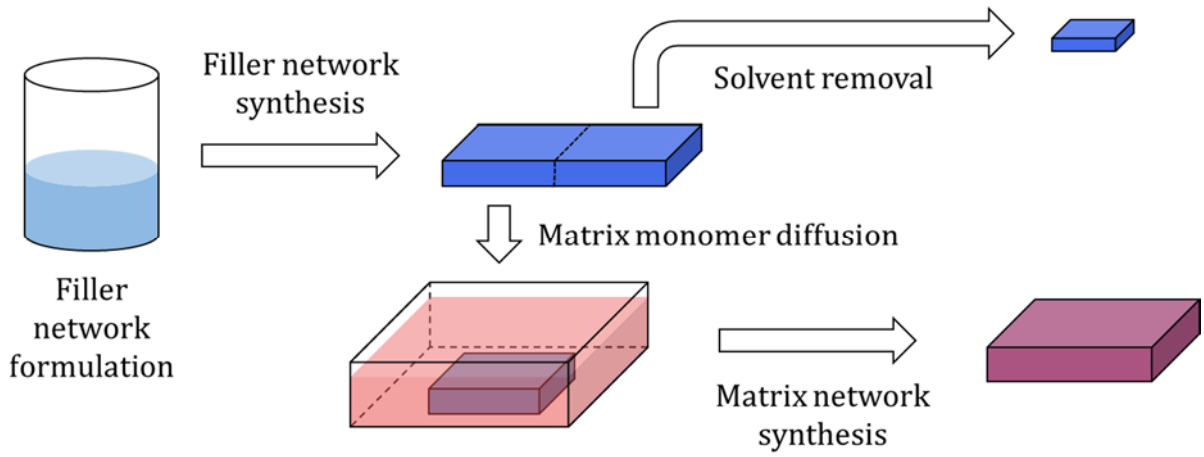

Figure 2: schematic representation of the preparatino process that is used here. The filler network is first prepared in the presence of solvent. The solvent is then either removed to isolate the filler network, or exchanged with matrix monomer to prepare the double network.

synthesis is known to be more complicated than acrylates, in particular because of their slower polymerization kinetics [3]. Some adjustments are therefore needed compared to the synthetic procedures presented in chapter 2.

2.2. Materials preparation

2.2.1. Chemicals and formulations

As in the previous chapters, all the materials that are presented and characterized in this study are made in the laboratory from commercial products. In addition to products presented in chapter 2, additional chemicals used in this chapter specifically are presented in Table 1. MMA is purified with basic alumina and liquids used in the glovebox are bubbled with nitrogen according to chapter 2. Formulations are presented in tables as in the rest of the manuscript (see chapter 2).

Samples are either prepared by UV or by thermal polymerization. Two different crosslinkers are studied in this chapter for the PMMA filler network. BDMA is a dimethacrylate crosslinker that is assumed to incorporate fairly randomly thanks to the chemical similarity between the monomer and crosslinker reactive functions. BDA is an acrylated crosslinker which may give more heterogeneous samples because of the difference in reactivity. Mixtures of the two crosslinkers are also used. In this case, the total molar fraction of crosslinker is split in two between BDA and BDMA.

To sum up and illustrate this, consider the example of PMMA samples prepared with a crosslinker molar percentage of 1.5 mol%. 6 different samples are obtained with this formulation overall, three by UV and three by thermal polymerization. For each type of polymerization, the three samples correspond to three possible crosslinking systems: one sample is prepared with 1.5 mol% BDA, one with 1.5 mol% BDMA and one with 0.75mol% BDA and 0.75 mol% BDMA so that the total crosslinker content is 1.5 mol%.

Abbrev.	Chemical name	Molecular formula	Purity	Origin	CAS
MMA	Methyl methacrylate	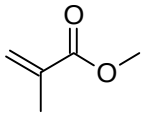	99%	Aldrich	80-62-6
BDMA	1,4-Butanediol dimethacrylate	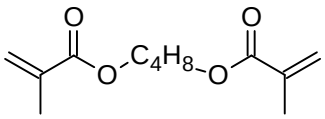	≥95%	Sigma-Aldrich	2082-81-7
AIBN	2,2′-Azobis(2-methylpropionitrile)	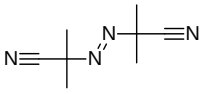	98%	Aldrich	78-67-1
Tol	Toluene	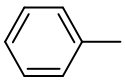	≥99.5%	Carlo Erba	108-88-3
MeOH	Methanol	$H_3C–OH$	≥99.9%	Honeywell	67-56-1

Table 1: information about chemicals used in this specific chapter

2.2.2. PMMA network preparation

Two different synthesis methods have been used for the preparation of the filler network. Namely, the free radical polymerization is either initiated by UV or by heating.

UV synthesis

UV synthesis is performed using the procedure described in chapter 2. The only difference with the procedure from chapter 2 is that UV irradiation is performed for 8 hours instead of 2. After the irradiation, the sample is left overnight in the glovebox without UV light until the next morning when the preparation process is resumed.

The following standard formulation is used:

Compound	MMA	AcOEt	BDA	BDMA	HMP
Role	Monomer	Solvent	Crosslinker	Crosslinker	Initiator
Quantity	/	50 vol%	0-3 mol%	0-3 mol%	10 mol%

The large initiator content is meant to ensure a high enough extent of polymerization and circumvent the low reactivity of methacrylates.

Thermal synthesis

For thermal polymerizations, the following formulation is used:

Compound	MMA	Toluene	BDA	BDMA	AIBN
Role	Monomer	Solvent	Crosslinker	Crosslinker	Initiator
Quantity	/	50 vol%	0-3 mol%	0-3 mol%	0.43 mol%

The day before the synthesis, the mold is first prepared (see Figure 3). Two glass slides are covered with PET sheets (stuck to the glass using adhesive tape) and separated by a PDMS spacer with a thickness of about 2 mm. Two needles are placed in between the slides and PDMS spacer to fill the mold and evacuate the gas. The mold is then sealed by applying silicone seal in between the PET sheets to insulate the mold as much as possible. This precautions aim to avoid air contamination and more importantly excessive evaporation of volatile compounds during the heating phase. The seal is left to dry overnight.

The day after, the formulation is first prepared out of the glovebox and bubbled with nitrogen. The solution is then poured in the mold in the glovebox. The sealed mold is taken out of the glovebox and heated for approximately 24 hours (between 21h and 26h). Heating is either done with an oven or with a water bath:

- In the former case, the mold is placed in the oven along with a 250mL Becker or dry ice which sublimates while the oven heats up. The dry ice helps ensuring a low oxygen content in the oven during the reaction.
- In the latter case, the mold is first sealed in a plastic bag in the glovebox and then placed in a pre-heated bath at 60°C.

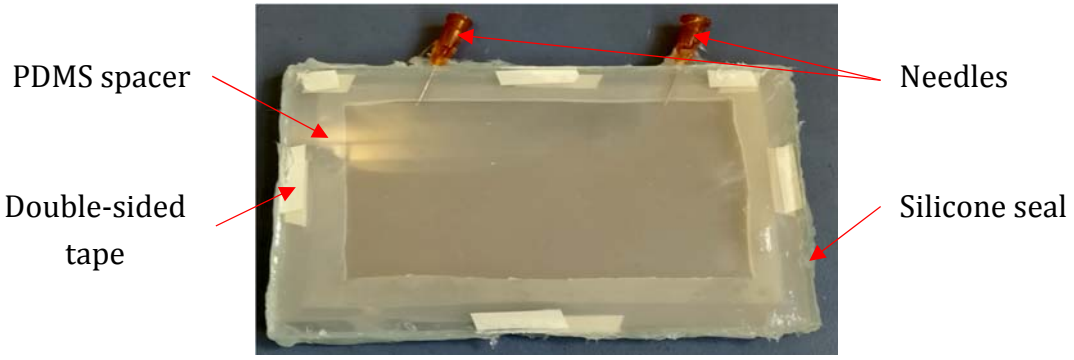

Figure 3: picture of the mold used for thermal synthesis.

Note that in both cases the polymerization is actually performed out of the glovebox, although some precautions are taken to ensure an initial atmosphere as inert as possible.

2.2.3. Filler network isolation and double network preparation

After completion of the filler network preparation, a swollen gel is obtained. The material is then cut in two parts. One third of the gel is used for the double network synthesis while the remaining two thirds are used to isolate the filler network.

Filler network isolation

The filler network is isolated by exchanging the synthesis solvent with methanol (which is a bad solvent for PMMA). This step washes the extractible species and synthesis solvent from the formed network, causing a progressive deswelling with hopefully little damage to the network.

The swollen filler network is first placed in a bath containing 100mL of pure ethyl acetate. At each step of the solvent exchange process, a volume V_n is taken from the bath and replaced by the same volume of methanol:

Step	0	1	2	3	4	5	6	7	8	9
V_n (mL)	/	20	25	33.3	25	33.3	25	33.3	50	100
c_{AcOEt} (v%)	100	80	60	40	30	20	15	10	5	0

At least one hour is left between each step in order to let the swelling equilibrate. After the last step, the sample is dried in vacuum at 60°C for at least one day.

A scheme of the relative proportion of the various masses involved in the filler network preparation and isolation process is presented in Figure 4:

- $m_{\mathrm{reactants}}$ and m_{solvent} are the mass of reactants (i.e. monomer, crosslinker and initiator) and solvent respectively that are used in the formulation. These masses are obtained by multiplying the actual masses used in the formulation by 2/3, since only two thirds of the swollen gel are used to isolate the filler network.
- m_{polymer} is the mass of filler network at the very end of the process, after dialysis and drying.

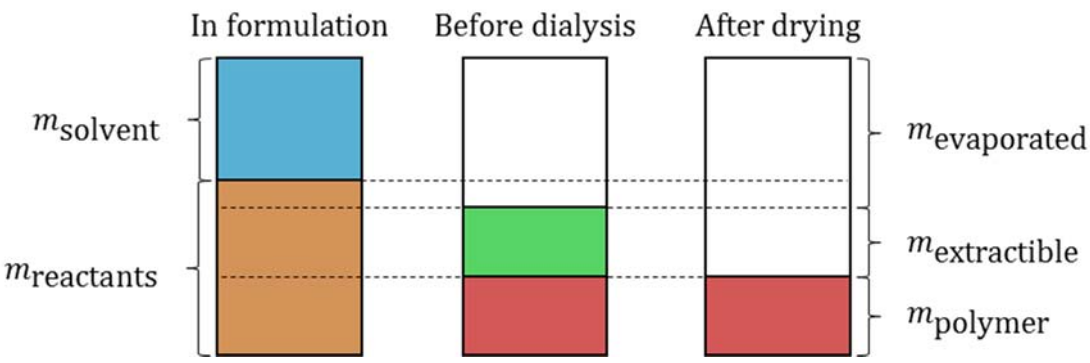

Figure 4: schematic representation of the repartition of masses between reactive species, solvent and polymer throughout the preparation process of the filler network. The full height of each box represents the mass of the formulation used for the filler network, i.e. two thirds of the total mass of the initial formulation.

- $m_{\text{extractible}}$ is the mass of species that are removed by the dialysis and drying processes. This mass is calculated by subtracting the mass of polymer to the mass of the swollen gel before dialysis ($m_{\text{before dialysis}} = m_{\text{extractible}} + m_{\text{polymer}}$). The extractible contains both unreacted species and residual solvent.
- $m_{\text{evaporated}}$ is the mass of volatile species that has evaporated between the beginning of the synthesis and the beginning of the dialysis.

Two quantitative parameters relative to the filler network synthesis are extracted from the measurement of masses throughout the process. The first one is the approximate yield of the polymerization reaction, which is calculated by dividing the final dry mass of the isolated filler network with the mass expected from the formulation:

$$\eta = \frac{m_{\text{polymer}}}{m_{\text{reactants}}} = \frac{m_{\text{after drying}}}{\frac{2}{3}(m_{\text{MMA}} + m_{\text{BDA}} + m_{\text{BDMA}} + m_{\text{HMP}} + m_{\text{AIBN}})} \qquad \text{Eq. 1}$$

The second parameter is the fraction of evaporated fraction which compares the mass of extractible that has actually been obtained with the mass that would have been obtained with the same synthesis yield if no vaporization had occurred:

$$\phi_{\text{evaporated}} = \frac{m_{\text{evaporated}}}{m_{\text{evaporated}} + m_{\text{extractible}}} \qquad \text{Eq. 2}$$

As an example, Table 2 gives numerical values of masses for the UV formulation with 1.5 mol% total crosslinker (mixture of BDA and BDMA). In the left column, values from the formulation and masses measured in the process are given. These masses are used to calculate the five masses defined above. From these calculated values, the two parameters may be calculated using the two equations. One finds in this case a yield $\eta = 56\%$ and an evaporated fraction $\phi_{\text{evaporated}} = 76\%$. This means that about half the monomers has reacted and almost all volatiles have evaporated before dialysis.

Measured values (in g)		Calculated values (in g)	
m_{MMA}	3.48	$m_{\mathrm{reactants}}$	2.77
m_{AcOEt}	3.34	m_{solvent}	2.23
$m_{\mathrm{BDA}} + m_{\mathrm{BDMA}}$	0.11	$m_{\mathrm{evaporated}}$	2.63
m_{HMP}	0.57	$m_{\mathrm{extractible}}$	0.82
$m_{\mathrm{before\ dialysis}}$	2.3666	m_{polymer}	1.55
$m_{\mathrm{after\ drying}}$	1.5484		

Table 2: numerical values of the various masses throughout the preparation process of the filler network based on the formulation with 1.5 mol% mixture of crosslinkers with UV polymerization method. Left column is measured or known values, right column is calculated values based on the definitions from Figure 4.

Double network preparation

The remaining third of the swollen filler network is used to prepare the double network, using ethyl acrylate as the matrix monomer. The same procedure as in chapter 4 is used, except that the swollen filler network is used and placed in the formulation bath. Drying is performed in vacuum at 60°C for at least one day. In all cases the variation of mass during drying is found to be lower than 2%, indicating that the yield of the matrix network polymerization reaction is high.

The prestretching of filler network chains is estimated from the measurement of thicknesses:

$$\lambda_{\mathrm{swelling}} = \frac{h_{\mathrm{double\ network}}}{h_{\mathrm{filler\ network}}} \qquad \text{Eq. 3}$$

where $h_{\mathrm{double\ network}}$ is the thickness of the dry double network $h_{\mathrm{single\ network}}$ is the thickness of the isolated dry filler network. This estimation assumes that swelling is homogeneous and isotropic and that the amount of extracted solid species during dialysis is low. If these two assumptions are true, then $\lambda_{\mathrm{swelling}}$ is representative of the stretch ratio applied on the chains of the filler network in the three principal directions.

2.3. Dynamic Mechanical Analysis

2.3.1. Procedure and parameters

Basics and working principles of Dynamic Mechanical Analysis have already been presented in chapter 2. For this project specifically, samples are cut into strips with dimensions of approximately 2.5 mm in width and 7 to 10 mm in length. Cutting of PMMA filler networks is done by heating the sample with a heat gun at 60 to 70 degrees while cutting it with sharp scissors. The heat avoids brittle fragmentation of the specimen and enables straight cutting.

The following set of parameters is used:

Parameter	Frequency	Strain	Static force	Forcetrack	Heating rate
Value	1 Hz	0.1%	0.05N	125%	1°C/min

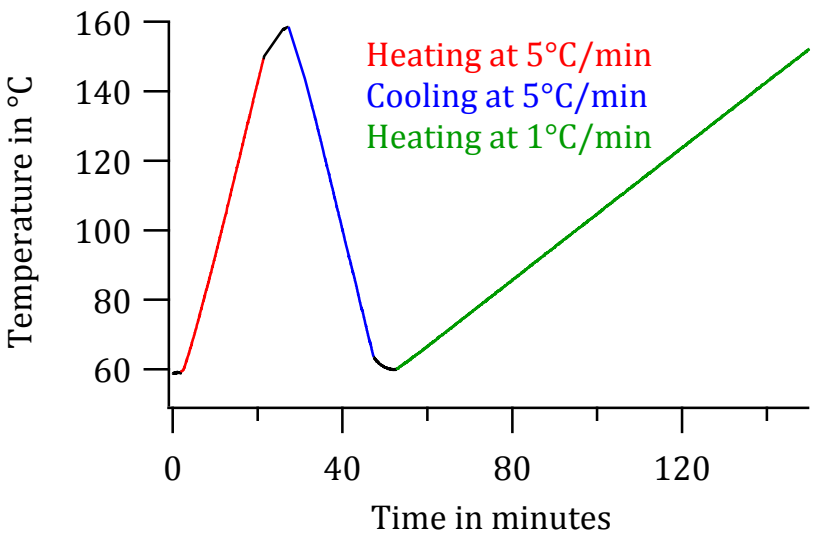

Figure 5: temperature profile applied for DMA characterizations. The measuring ramp is the last green one at 1°C/min. Black segments are transitions between the ramps when the temperature equilibrates.

2.3.2. Specificities of PMMA samples and slippage phenomenon

PMMA samples are glassy at room temperature. The measurement of the viscoelastic spectrum of the material is thus preceded by faster heating and cooling stages at 5°C/min. This pretreatment erases the thermal history of the material and removes potential residual stresses. The exact temperature profile that is applied is shown in Figure 5.

Bringing the clamped sample at elevated temperature also has the advantage of avoiding slippage during the last heating ramp. At the end of the first heating ramp, the material expands (because of thermal expansion) and softens. Clamps thus indent the sample and leave marks on it. When cooled down, the sample hardens and the clamps lock in place. During the last heating stage, they cannot slide any longer on the surface of the sample.

Before this locking takes place however, there may be some slippage occurring. As a matter of fact, there is direct evidence that the samples sometimes slip. As illustrated in Figure 6-left, the storage and loss moduli in the glassy regime are both significantly lower in the second heating stage than in the first one. There is no obvious physical reason behind such a loss of modulus in the glassy region, since there is no visible damage nor expectable change in the polymer chemical nature during the first thermal pre-treatment. Instead, this drop of modulus is believed to be due to slippage in the early stages of the test.

One could in principle imagine correcting the effect of slippage by taking into account the change in length. However, because of the way the experiment is performed this is not easily feasible (the main problem being that the static force changes with time because of the forcetrack correction, see chapter 2). Instead, we propose here a pragmatic and empirical approach to correct this experimental artifact.

2.3.3. Correction of slippage

Slippage is believed to affect the level of force that needs to be applied to reach the requested strain. Because of the way the DMA works, the measurement of $\tan(\delta)$ should not be much affected

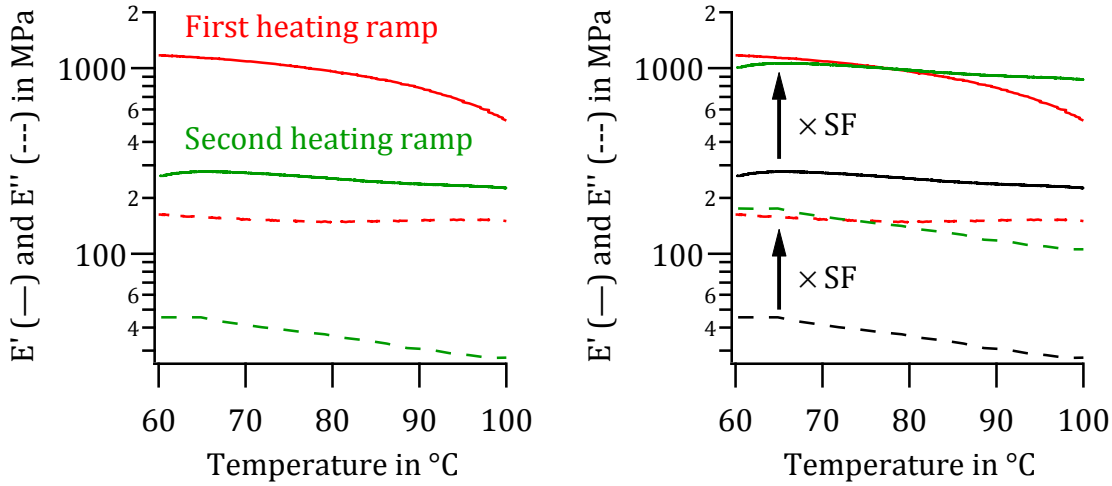

Figure 6: illustration of the slippage phenomenon in DMA and correction using slipping factor. Left: comparison of the beginning of the first and second heating ramps in the glassy plateau. Plain lines are storage moduli and dashed lines are loss moduli. Right: illustration of slippage correction. Storage and loss moduli are multiplied by a common factor to raise them to values coherent with the first heating ramp.

by slippage, since it relies on the measurement of the lag between the force and the applied displacement. Moreover, the DMA experiment is carried out in the linear regime so that the decrease in applied force should be proportional to the decrease in modulus. The loss tangent being the ratio of E'' over E', the correction of slippage can be done by multiplying both measured values by the same slipping factor. In our case, the latter can be estimated numerically by comparing the values of E' and E'' in the first and third heating stages.

The correction of slippage is therefore done in three steps. First the average values of storage and loss moduli are extracted at the beginning of the two heating ramps over a range of 6°C. Then, a slipping factor SF is calculated, which is formally the average multiplying factor that separates the first and heating stage moduli:

$$SF = \frac{1}{2}\left(\frac{E'_{\text{average first heating}}}{E'_{\text{average third heating}}} + \frac{E''_{\text{average first heating}}}{E''_{\text{average third heating}}}\right) \qquad \text{Eq. 4}$$

At last, the slipping factor is applied on the storage and loss moduli of the third heating stage. This gives values of E' and E'' that are coherent with the first heating stage (see Figure 6-right).

This correction is obviously very crude and probably does not permit to measure the exact absolute value of storage modulus in the third heating stage. It however enables qualitative comparison between samples. Additionally, it does not affect the presented values of the loss tangent.

Note that the first heating ramp is not necessarily neutral with respect to the glass transition of the material. Said differently, bringing the material at high temperature a first time may change the microstructure slightly and affect the position of the glass transition. For instance, the data in Figure 6 suggests that the decrease in storage modulus starts at lower temperatures in the first heating ramp than in the second one. This would imply that the glass transition has been shifted to higher temperatures after the first ramp. This aspect of how the material behaves and how the

viscoelastic spectrum is affected by cyclic thermal profiles has not been studied here. However, since the same thermal history is applied to all samples, this effect should not impact too much the results and in any case does not preclude comparison between samples.

2.4. Tensile tests

Step-cyclic tests have already been described in chapter 4. Tests are performed at 0.5 mm/sec with a lower bound of 0.5N for the end of the unloading cycles.

3. Results regarding the materials preparation

3.1. Overall overview of the synthesis

3.1.1. UV synthesis

The main observations made during the materials preparation by UV are given in Table 3. **Except for the sample with 0.75 mol% BDA, all the SN and DN could be prepared without too much trouble and could be characterized**. Note that:

- For the mixture with 0.75 mol% mixture crosslinker content, a flat piece of sample could still be cut for the DMA characterization although the entire DN sheet is not flat.
- For the mixture with 1.5 mol% mixture crosslinker, the presence of bubbles is probably due to the presence of too much residual solvent after the dialysis and drying step. This may be due to a problem with the desiccator that has been used.
- For the mixture with 3 mol% total crosslinker, the cracks are located on the edges of the sample, so that the central piece of double network is undamaged and may be used for characterization.

Still, the existence of these problems during the synthesis of the materials indicate that the preparation of swollen PMMA networks is not an easy task. More clever design of experimental conditions could help solve most of these problems.

Crosslinker content	Type of crosslinker		
	BDA	BDMA	Mixture 50/50
0.75 mol%	A		B
1.5 mol%			C
3 mol%			D

Legend / additional information	
A	Heterogeneous swelling during DN preparation
B	DN is curled after synthesis
C	Bubbles appeared during the DMA
D	Cracks appeared after DN swelling

Table 3: matrix summarizing the problems encountered during the preparation of the materials.

3.1.2. Thermal synthesis

As previously, Table 4 gives some qualitative information about the problems encountered during the preparation of the materials by thermal polymerization. **Most of the synthesis have not presented any major issue**. For two samples (3% BDA and 3% mixture), the swollen filler networks started to fracture around the edges before the end of the heating stage. This is most probably due to the evaporation of solvent, which takes place from the edges of the sample. The phenomenon is enhanced by the large crosslinking content which embrittles the material.

Crosslinker content	Type of crosslinker: BDA	BDMA	Mixture 50/50
0.75 mol%	A	A	A
1.5 mol%	A	B	A
3 mol%	A / C	A	A / C

Legend / additional information

A	Heating in water bath
B	Heating in the oven
C	The swollen gel was partially fractured on the edges after the the thermal synthesis

Table 4: matrix summarizing the information relative to networks preparation by thermal polymerization.

3.2. Quantitative parameters associated to synthesis

As explained in 2.2.3, three quantitative parameters can be obtained from the measurement of masses and dimensions throughout the preparation process. The values of these parameters when available are given for all the formulations and types of synthesis in Table 5.

η is an estimation of the yield of the polymerization reaction based on the sample mass that would be obtained if all reactive species from the formulation had reacted without evaporation. As shown in Table 5, **values of η are low for the UV synthesis, with reaction yields of 65% at most. Values are even lower for the thermal synthesis**. In other words, the actual mass of the filler networks that are obtained are much lower than what could be expected from the quantity of reactants used in the polymerization reaction. Two possible explanations may be given. First, the extended polymerization time and/or elevated temperature may induce a lot of evaporation of reactive species. The other possible explanation is that the polymerization reaction is hindered and does not proceed at a normal rate. This may typically be the case for the thermal polymerization, since the heating stage is performed out of the glovebox (although in an atmosphere as inert as possible).

The evaporated fraction represents the fraction of extractible species (unreacted monomer and solvent) that has evaporated during the polymerization process. **For both polymerization methods, values of $\phi_{evaporated}$ are extremely high**, above 90% in some cases (see Table 5). This is due to the fact that polymerization times are long and sometimes assisted with heating. However, although most of the extractible evaporates during the process, the obtained gels at the end of the synthesis are still swollen with enough solvents, "thanks" to the low polymerization yields. The obtained materials may therefore be placed in the matrix monomer bath without breaking. The polymerization conditions are therefore clearly sub-optimal, but they do not preclude the use of swollen filler networks in double network structures.

Finally, Table 5 shows the values of the swelling stretch ratios of double networks. Remember that this parameter is measured here using the ratio of double to filler network thicknesses and is therefore attached to a fairly large error margin. In particular, it is likely to be very sensitive to heterogeneous swelling. **Measured values of $\lambda_{\text{swelling}}$ are mostly centered on 1.3 and remarkably similar for different crosslinker contents**. The exceptions to this trend are the samples prepared by UV polymerization containing 1.5 mol% BDA and 0.75 mol% crosslinker

Parameter	Crosslinker content	UV synthesis			Thermal synthesis		
		BDA	BDMA	Mixture	BDA	BDMA	Mixture
"Yield" η	0.75 mol%	21%	65%	41%	25%	36%	34%
	1.5 mol%	40%	60%	56%	49%	69%	32%
	3 mol%	54%	44%	57%	42%	29%	25%
Evaporated fraction $\phi_{\text{evaporated}}$	0.75 mol%	90%	78%	79%	93%	90%	92%
	1.5 mol%	*	*	86%	87%	*	*
	3 mol%	81%	93%	80%	93%	94%	95%
DN prestretching $\lambda_{\text{swelling}}$	0.75 mol%	**	1.3	1.7	1.4	1.3	1.2
	1.5 mol%	1.8	1.4	1.2	**	1.3	1.4
	3 mol%	1.3	1.3	1.3	1.2	1.2	1.2

*Table 5: numerical parameters associated to the filler and double network synthesis for the two types of polymerization. * data not available because the mass before dialysis have not or could not be measured. ** data not available because the double network could not or have not been prepared.*

with a mixture of BDA and BDMA. These two samples feature much larger swelling ratios, which could indicate that the effective crosslinking density is very low in these samples and/or that the filler networks are very heterogeneous and swell non-isotropically.

To sum up, the synthesis of PMMA filler networks and PMMA/PEA double networks have been done. Despite some difficulties due to the low reactivity of methacrylates and to the synthesis of filler networks in solution, samples with several formulations have been obtained and are now going to be tested in their small strain regime by DMA.

4.DMA characterizations

In this section, we aim to give an overview of the results obtained by DMA on the filler and double networks presented before. The exhaustive and linear description of all the results is not really feasible, therefore some selected examples will be presented. These examples give a representative description of the materials responses in small strains. They also highlight some of the effects of formulation on the architecture and mechanical properties of the networks.

In order to avoid back-and-forths in the chapter and in order to give all the experimental details for the interested reader, values of the quantitative parameters of the synthesis are recalled in each section for the specific materials that are presented.

4.1. Effect of the nature of the crosslinker

4.1.1. UV synthesis / 1.5 % crosslinker content family

	BDA	BDMA	Mixture
η	40%	60%	56%
$\phi_{\text{evaporated}}$	/	/	86%
$\lambda_{\text{swelling}}$	1.8	1.4	1.2
$\phi_{\text{filler network}}$	17%	36%	58%

In order to illustrate the effect of the nature of the crosslinker, the results of UV-polymerized samples with 1.5 mol% crosslinker content are reviewed. Results are presented in Figure 7 for the two types of networks (filler network alone and double network). Values of $\lambda_{\text{swelling}}$ are given for the double networks. Note that the same scales are used for filler and double networks to enable comparison.

Let us first review the results of the isolated filler networks. **The three curves for the storage modulus are almost superimposed**, indicating that the materials are chemically fairly similar to each other. This is obviously expected since the formulations are different by only a few molar percents of crosslinker. Plots of E'' however show some differences with the type of crosslinker that is used. **The network crosslinked with BDA shows a clear and unique peak for the loss modulus, while the two other systems (BDMA and mixture) show more irregular curves**. This specificity of the BDA network is also visible on the loss tangent curves where one well-defined peak is visible. In contrast, the BDMA system shows a shouldering starting from about 100°C. The network crosslinked with a mixture of BDA and BDMA features a higher average value of $\tan(\delta)$ below the glass transition compared to the two other systems. The study of DMA patterns for the three crosslinking systems indicates that the network crosslinked with BDA is probably more homogeneous than the two other ones, with a clearer and better defined glass transition, corresponding to a narrower distribution of characteristic relaxation times.

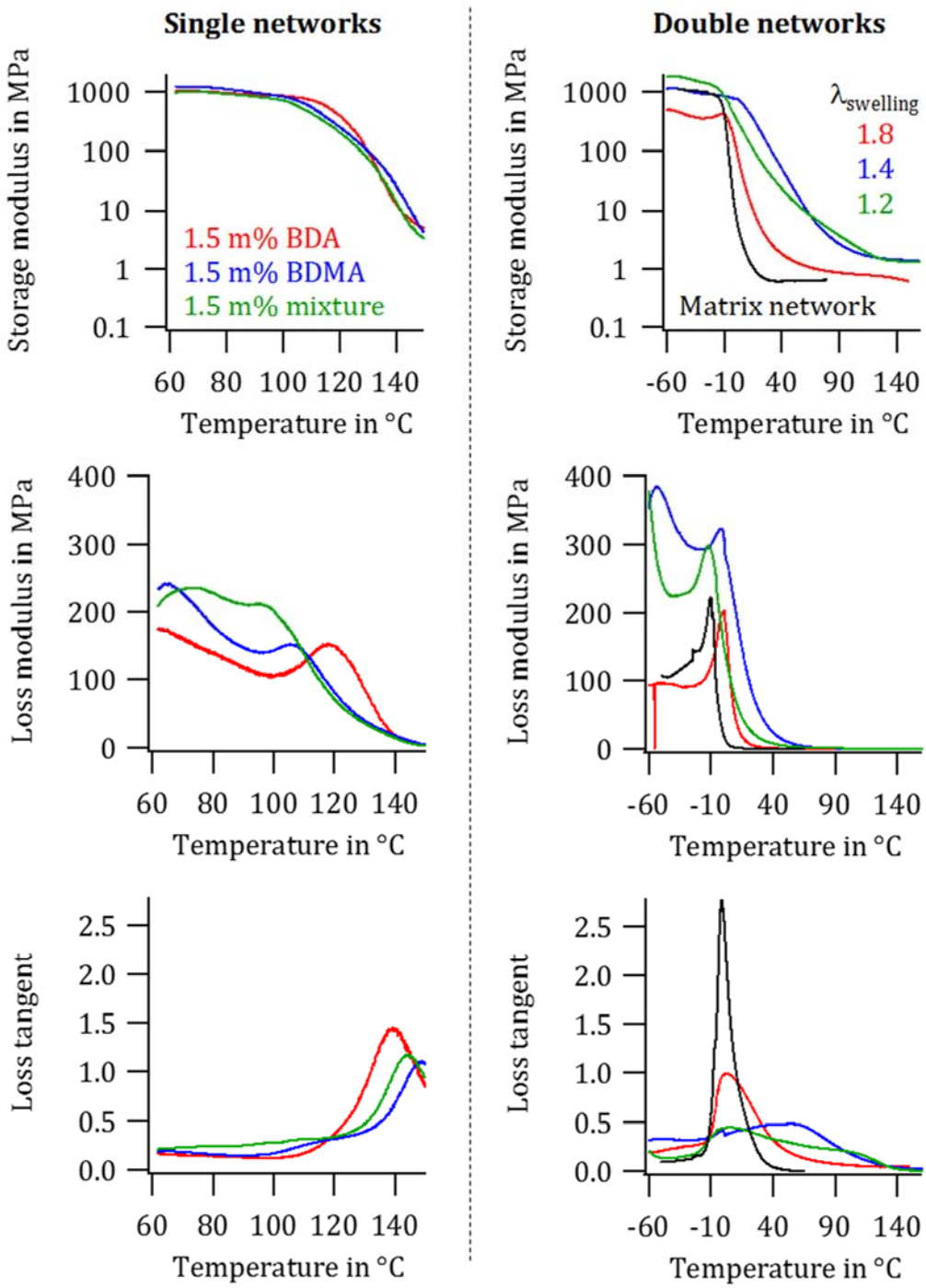

Figure 7: results of DMA characterization on the samples from the 1.5% crosslinker family. Left column is for filler networks and the right column is for double networks. Same legend for both columns. Corrected values are presented for the filler network. The viscoelastic spectrum of the matrix network alone has been added on the results of double networks for comparison.

The study of the viscoelastic properties of double networks reveals some large differences with the nature of the filler network crosslinker. **The BDA double network features a sharp decrease in storage modulus around 0°C, while the two other crosslinking systems give networks that soften much more gradually**. In particular, based on the DMA data, the mixture of BDA and BDMA gives a double network that does not exhibit a stable rubbery storage modulus

until the temperature reaches 140°C, which corresponds to the glass transition temperature of the filler network alone. These tendencies are confirmed by studying the loss tangent: **the BDA double network shows a well-defined peak whereas broad massive dissipative peaks are obtained for the two other crosslinking systems**. The miscibility of the filler and matrix network is therefore good for the BDA system but not for the two other ones. However, despite this incomplete miscibility, it is important to notice that there is no peak in the loss tangent in the region of the filler network alone (i.e. above 120°C). Although the mixing is incomplete, there is some partial miscibility and no clearly defined regions of pure PMMA are detected in the double network samples. The study of the loss modulus confirms these observations, since the three crosslinking systems give E'' peaks that are located close to each other, and close to the peak of the matrix network alone. This indicates that the temperature at which collective motion is activated in the material is similar for the three crosslinking systems, although the exact distribution of relaxation times may strongly differ.

In addition to these differences of miscibility and viscoelasticity, note that **there is a strong difference between the three double networks in terms of composition**. Despite the fact that the same amount of crosslinker is used in the three cases, swelling ratios of double networks are very different. This results in large differences in terms of filler network volume fraction in the double network structures. The fraction of PMMA in the double network is much smaller in the case of BDA (about 17%) than with the two other crosslinking systems (36% and 58% for the BDMA and mixed systems respectively). This strong compositional difference partly explains the fact that the glass transitions of the double networks are significantly different from each other, and that the decrease in storage modulus starts at much lower temperatures for the BDA double network, which is the richer in soft poly(ethyl acrylate) phase. The fact that a different mixing behavior is obtained for this crosslinking system most certainly has a link with this unexpectedly high swelling ratio.

We now take a closer look to the glass transition temperature of the double network sample that uses BDA as a crosslinker. Since the study of viscoelastic properties seems to indicate a good mixing between the two networks, one can attempt to use the Fox-Flory equation in order to predict the value of the glass transition temperature for the double network [7]. This semi-empirical equation has originally been developed to predict the glass-transition temperature of random copolymers but also gives good results when used for miscible double networks [2]. Mathematically, the T_g of the mixture of two polymers with respective glass transition temperatures of $T_{g,1}$ and $T_{g,2}$ may be written as follows:

$$\frac{1}{T_g} = \frac{w_1}{T_{g,1}} + \frac{1 - w_1}{T_{g,2}} \qquad \text{Eq. 5}$$

where w_1 (respectively w_2) is the mass fraction of polymer 1 (resp. 2). The latter may be estimated from $\lambda_{\text{swelling}}$ using the fact that PMMA and PEA have the same density [8]:

$$w_{\text{filler network}} = \frac{1}{\lambda_{\text{swelling}}^3} \qquad \text{Eq. 6}$$

		Max of E''	$\tan(\delta)$ peak
Measured values	Filler network	118 °C	139 °C
	Matrix network	-10 °C	-1 °C
	Double network	0°C	3°C
Predictions for DN T_g		5°C	7°C

Table 6: comparison of predictions of DN glass-transition temperatures with experimental values. Comparison is either done on the base of the maximum of the loss modulus, or on the base of the position of the peak of the loss tangent.

The values of $T_{g,1}$ and $T_{g,2}$ may be obtained by taking either the maximum of E'' or the maximum of $\tan(\delta)$ as the position of the glass-transition temperature. Corresponding predictions for the T_g of the double network are given in Table 6 and compared to experimental values from the DN viscoelastic spectrum. Regardless of whether E'' or $\tan(\delta)$ is used to estimate T_g, **Fox's equation returns the correct order of magnitude for the glass-transition temperature of the BDA-based double network**. This may not be considered as a proof that the two polymers (PMMA and PEA) are perfectly mixed at the molecular scale, but instead confirms that the viscoelastic response that we observe for the double network is consistent with the one of a material with a uniform average composition that corresponds to the relative mass fractions of filler and matrix networks.

To conclude, this family of samples based on a total crosslinker content of 1.5 mol% confirms that the microstructure of the double network strongly influences the final mechanical properties of the material. Although the differences are not very obvious when the filler network is studied alone, the heterogeneity of the network becomes much more visible when the filler network is incorporated in a double network structure. In this family of samples, the PMMA networks crosslinked with either BDMA or with a mixture of BDMA and BDA give heterogeneous filler network that only partially mix with the matrix network. The resulting double networks are globally hard at room temperature, very dissipative and their stiffness strongly depends on the temperature. On the opposite, the network crosslinked with BDA mix well with the PEA matrix and yields a globally elastomeric material with one visible glass-transition that can be predicted by Fox's equation.

4.1.2. UV synthesis / 3% crosslinker content family

	BDA	BDMA	Mixture
η	54%	44%	57%
$\phi_{\text{evaporated}}$	81%	93%	80%
$\lambda_{\text{swelling}}$	1.3	1.3	1.3
$\phi_{\text{filler network}}$	46%	46%	46%

For comparison, the family of samples prepared with 3 mol% crosslinker is shown in Figure 8. In filler networks alone, the sample crosslinked with BDMA shows a drop in storage modulus at higher temperatures. This agrees with positions of E'' and $\tan(\delta)$ peaks that are shifted toward

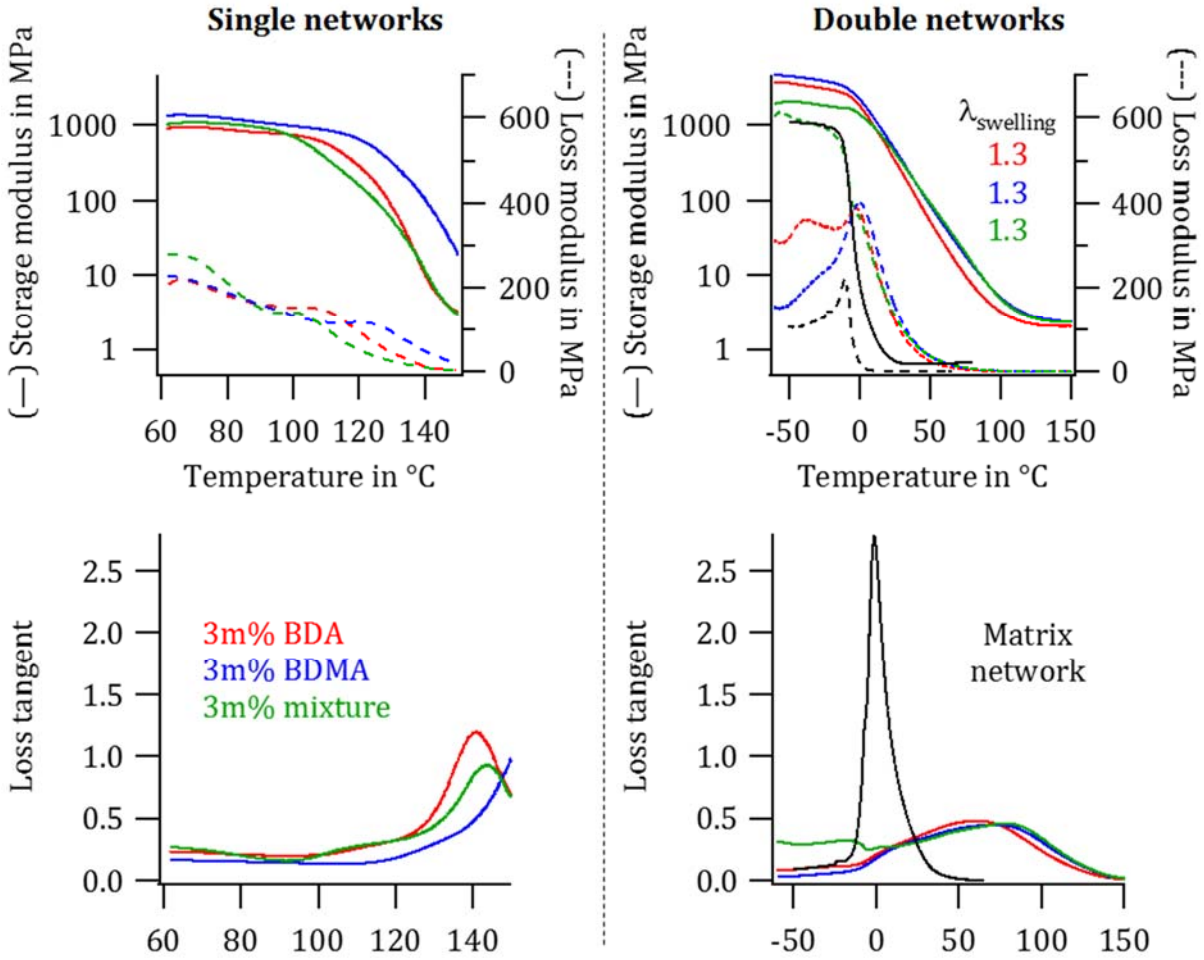

Figure 8: DMA characterization of filler and double network samples prepared by UV polymerization with 3 mol% total crosslinker content.

the right. **Aside from this small difference, the three filler networks are fairly similar to each other**.

Contrary to the 1.5 mol% family, **the three double network samples are almost undistinguishable**. The three samples show a broad and progressive glass transition, which probably means that the mixing is partial in the three cases. The case of BDA in the previous section should therefore be considered as an exception and not as the rule. In general, the mixing of a PMMA network with a PEA matrix gives a partially-miscible interpenetrated network. The original behavior of the sample with 1.5 mol% is probably the result of a coincidental small effective crosslinking density (which enable large swelling ratio) and good chemical affinity (i.e. low valuer of Flory χ parameter) between PEA and PMMA.

4.2. Effect of crosslinker content / UV synthesis / BDMA crosslinker

	0.75 m%	1.5 m%	3.0 m%
η	65%	60%	44%
$\phi_{\text{evaporated}}$	78%	/	93%
$\lambda_{\text{swelling}}$	1.3	1.4	1.3
$\phi_{\text{filler network}}$	46%	36%	46%

In this part, the family of UV-polymerized samples with BDMA used as a crosslinker is reviewed. The results of DMA characterizations are presented in Figure 9 for the filler and double networks.

Curves for the storage modulus and the loss tangent indicate that **the glass transition of the PMMA filler networks is shifted toward higher temperatures when the BDMA content in increased**. More precisely, the samples with 0.75 and 1.5 mol% BDMA show fairly similar responses, while the sample crosslinked with 3 mol% BDMA has a significantly higher T_g. Also, the curves of $\tan(\delta)$ show that there is a pronounced shouldering for the 0.75 and 1.5% samples that starts at around 100°C. This broadening of the peak is much reduced for the 3% sample and starts at higher temperatures (about 120°C). All in all, these observations suggest that **the sample prepared with 3 mol% BDMA is probably more homogeneous than the two other ones**.

The results obtained on filler networks correlates well with the mechanical responses of the double networks. First of all, **all the double networks show a single and broad glass transition**, which once again indicates a partial mixing between the filler and matrix networks. The quality of the mixing however seems to differ between the 3 mol% sample and the two other ones. When looking at the $\tan(\delta)$ curves, it appears that **the peak corresponding to the glass transition is slightly less broad for the 3 mol% sample**. Also, the beginnings of the peaks for the 0.75 and 1.5 mol% samples are located at the same position as the pure matrix. This indicates that in these double network structures there are regions that are almost pure in matrix network (and thus almost virgin in filler network). This feature is much less pronounced at 3 mol% of BDMA, which suggests that the network is much more homogeneously crosslinked at 3% BDMA than for lower amounts.

Finally, the amount of BDMA used to crosslink the filler network has a clear influence on the final stiffness of the double network materials. This is especially visible on the storage modulus curves, where **within and after the region of the glass transition the modulus of the double networks increases with crosslinker content**. Qualitatively speaking, this is consistent with the physics of rubber elasticity and expected behavior of double network structures. Quantitatively speaking though, the increase in modulus is not linear with the concentration of crosslinker. Besides, the increase in modulus for the double networks does not match with the almost constant value of $\lambda_{\text{swelling}}$ that is observed for the three materials. Swelling is therefore probably influenced by the larger extent of heterogeneity in the 0.75% and 1.5% samples and therefore does not correlate with the crosslinking density of the filler networks.

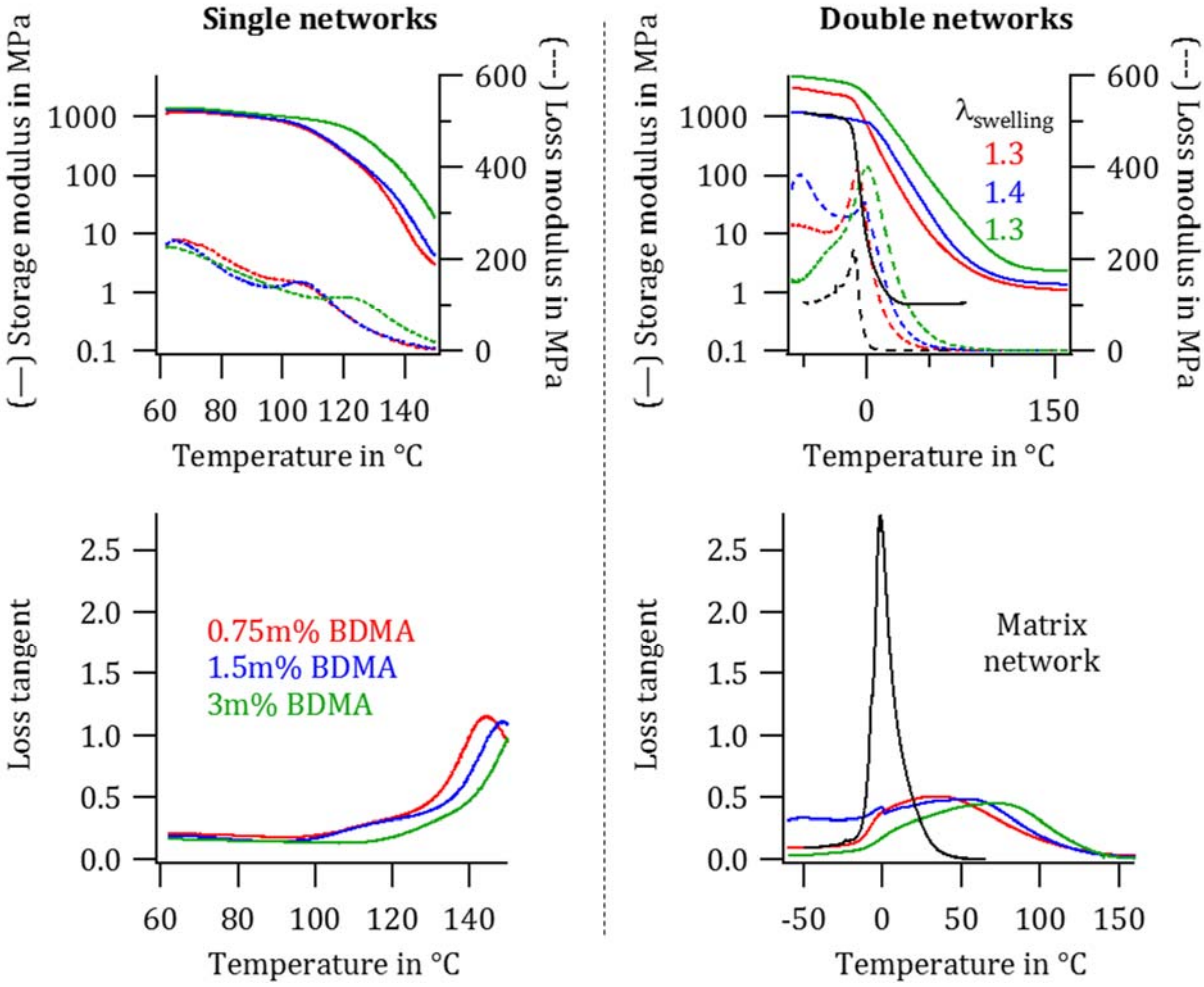

Figure 9: DMA characterization of filler and double network samples prepared by UV with a formulation using BDMA as crosslinker.

4.3. Effect of initiation type

In this subpart, we compare the same three samples presented in the previous section (i.e. UV-polymerized with BDMA as a crosslinker) with the same three formulations but prepared by thermal polymerization.

	UV synthesis			Thermal synthesis		
	0.75 m%	1.5 m%	3.0 m%	0.75 m%	1.5 m%	3.0 m%
η	65%	60%	44%	36%	69%	29%
$\phi_{\text{evaporated}}$	78%	/	93%	90%	/	94%
$\lambda_{\text{swelling}}$	1.3	1.4	1.3	1.3	1.3	1.2
$\phi_{\text{filler network}}$	46%	36%	46%	46%	46%	58%

4.3.1. On filler networks

The DMA characterizations of filler networks alone are presented in Figure 10, the type of line giving the type of polymerization. **Samples prepared by UV and thermal polymerization give very similar responses at small strains**, with glass transitions located close to each other. The main difference between the two polymerization methods is visible in the graph of the loss tangent. **Thermal samples show a pronounced shouldering that starts from 80°C**, very far from the maximum of the tan(δ) that is rather located around 140°C. The effect of this shouldering is also visible on the storage modulus: while on UV the storage modulus is almost constant in the glassy region and then decreases, the decrease is continuous for the thermal samples and the glassy plateau cannot really be identified. Since the filler networks are pure in PMMA, these differences in dynamics probably indicate that the network is less homogeneous when thermal polymerization is used, in the sense that the size distribution of the network strands is probably much broader.

The presence of a shouldering for tan(δ) at a temperature as low as 80°C is intringuing since linear PMMA is known to have a T_g much larger than that [8]. This could indicate that there are some short chains of PMMA in the filler network structure. Remember that the filler networks have been washed during the solvent exchange process, which means that these short chains are necessarily attached covalently to the network. The presence of PMMA oligomers within the network architecture could be due to the fact that thermal polymerization is not performed in a purely

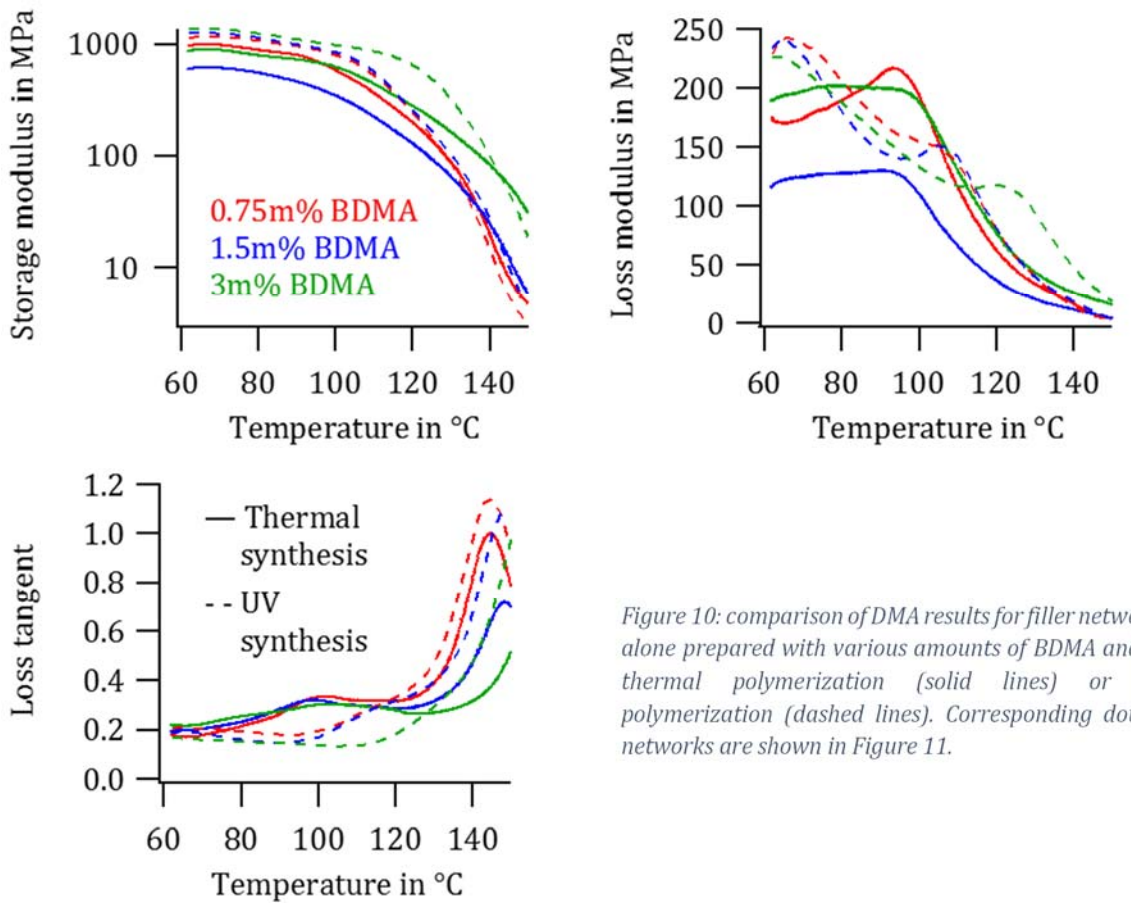

Figure 10: comparison of DMA results for filler networks alone prepared with various amounts of BDMA and by thermal polymerization (solid lines) or UV polymerization (dashed lines). Corresponding double networks are shown in Figure 11.

inert atmosphere. The presence of oxygen kills the growing radicals and inhibits the polymerization reaction, which may leave some short chains attached to the network structure.

4.3.2. On double networks

The DMA characterizations of the corresponding double networks are given in Figure 11. Overall, the same general mixing behavior is observed, namely a broad glass transition with a gradual decrease in modulus starting from 0°C up to 120-130°C. This indicates incomplete mixing between the two networks, hence **the mode of polymerization does not strongly impact the way the two networks blend together**. The relatively low influence of the way the reaction is initiated is also visible on the values of swelling stretch ratio that are similar to the UV synthesis, although on average slightly lower.

The main difference of the initiation type is visible on the decrease of the storage modulus. Samples prepared by thermal polymerization are systematically stiffer than their UV counterparts, and their rubbery modulus is also larger. Also, the glass transitions of thermal samples are shifted toward higher temperature. This feature is visible on the E' curve but also on the $\tan(\delta)$ profile. All these elements go in the direction of an overall larger crosslinking density for thermally-prepared samples, although the reason why is not clear.

Among the thermal double network samples, the one crosslinked with 0.75 mol% BDMA has an original response. The decrease in storage modulus occurs in two steps, the first one starting around 0°C and the second one around 110°C. This is also clearly visible on the loss tangent curve,

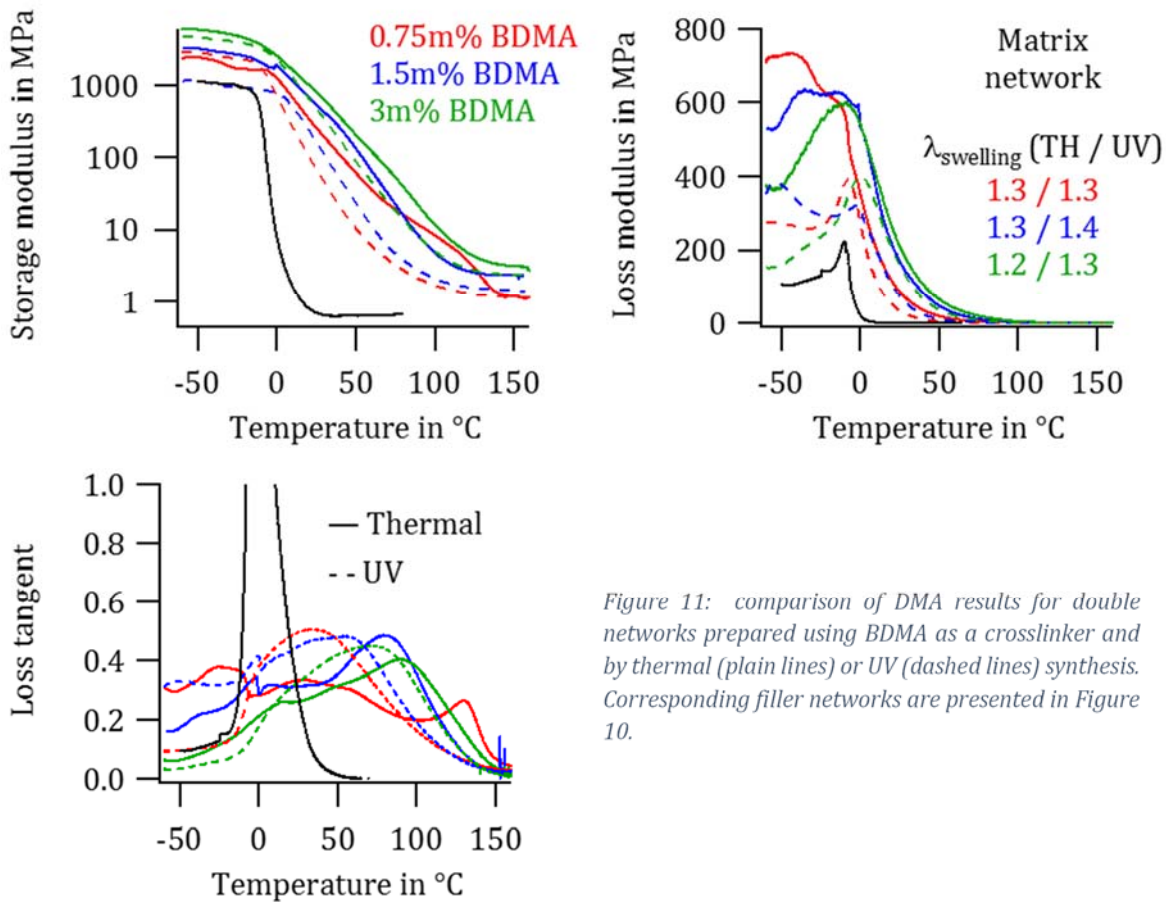

Figure 11: comparison of DMA results for double networks prepared using BDMA as a crosslinker and by thermal (plain lines) or UV (dashed lines) synthesis. Corresponding filler networks are presented in Figure 10.

with an evident peak located around 130C°. This secondary glass transition corresponds to the pure filler network, which means that there are regions in the double network sample that are very rich in PMMA. This is a very clear indication that the structure of the filler network is heterogeneous. There are probably regions of the filler network that are highly crosslinked and cannot be easily swollen by the matrix network. These regions exhibit a large glass transition temperature even if they are embedded in the matrix.

To sum up, preparing the filler networks by thermal synthesis instead of UV does not significantly change the behavior of the material. In both cases, a partial mixing is obtained and DMA results go in the sense of a heterogeneous filler network with a broad distribution of characteristic times of relaxation.

5.Tensile characterizations

Small strain characterization of hybrid double networks reveals that most of the tested formulations give very dissipative materials at room temperature. This is due to limited mixing at the molecular scale between the two networks, which results into a broad glass transition.

In this part, we study some of the materials shown previously in large deformation. Obviously, double networks with a high glass transition temperature cannot be tested in uniaxial traction. Although they could have been tested in large deformations with other geometries (flexion for example), we choose focus instead on samples that have a glass transition temperature not too far from room temperature. By increasing the test temperature, we can explore the viscoelastic spectrum of the material and see the effects on the large strain response of the material.

5.1. UV-polymerized DN with 0.75mol% BDMA

Figure 12 shows the result of a step-cyclic test performed at 500 µm/sec on the double network sample prepared from a filler network made by UV-polymerization with 0.75 mol% BDMA as crosslinker. As shown in 4.2, this sample features a partial mixing between the two networks and a broad glass transition.

At room temperature, the material behaves like an elasto-plastic material. The material is very stiff, shows a lot of mechanical hysteresis and a large residual strain when the sample is unloaded. This is entirely consistent with the high dissipation observed by DMA. **When the temperature is increased, the material gets closer to the perfect elastomeric case**. Hysteretic

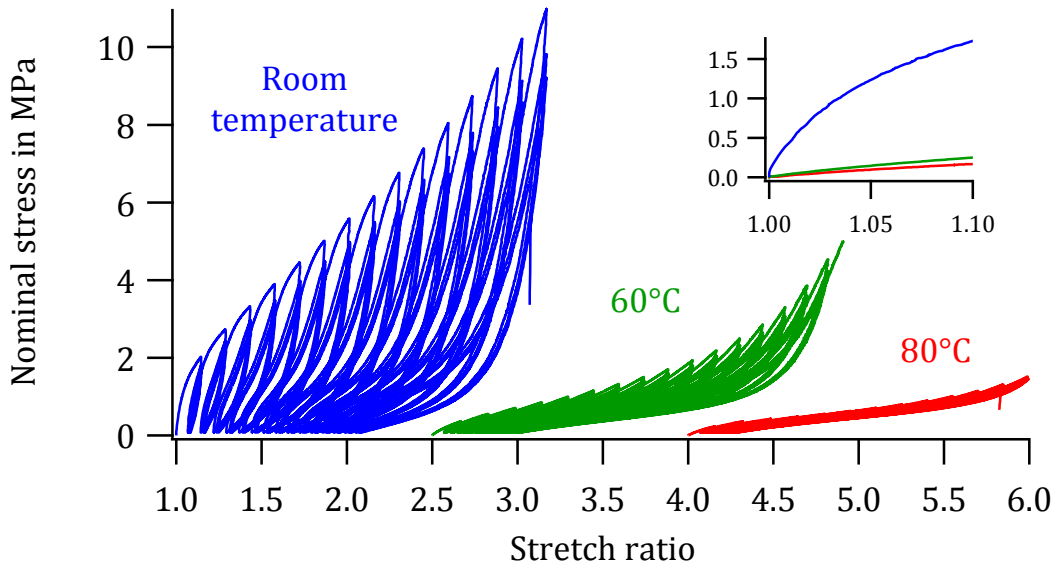

Figure 12: cyclic tensile test performed on the double network made from a filler network made by UV and crosslinked with 0.75 mol% BDMA. Tests are three different temperatures, tests at 60°C and 80°C have been shifted toward the right by 1.5 and 3 respectively. The insert shows a close-up of the beginning of the first stretching ramp.

cycles are smaller and so is the residual strain. Note that in all cases the material goes back to its initial shape when heated moderately at rest for a long time. This indicates that the residual strain is not the result of any damage but merely a result of the viscoelastic nature of the material. Interestingly, a strain-hardening is visible at 60°C which could indicate that the toughening mechanism of the double network strategy could still be active with a PMMA first network. This observation should however be confirmed by more systematic characterizations at higher temperature to extract the purely-elastic response of the material.

The type of large strain response reported here is very general of the double networks that are obtained with a PMMA filler networks. Other samples tested with different formulation show the same overall behavior, with sometimes an even more pronounced plastic behavior at room temperature when the PMMA fraction and glass transition are higher.

5.2. UV-polymerized DN with 1.5 mol% BDA

In the DMA characterization presented in section 4, the sample prepared by UV with 1.5 mol% BDA stand out from the other ones. In this sample, the mixing between the filler and the matrix network seems to be much better than with the other formulations. As a result, the viscoelastic response of the material is much simpler, with a well-defined glass transition peak centered around 0°C. This peak is broader than for the matrix network alone, but much narrower than for the other cases where only partial mixing is observed.

The step-cyclic test performed at 500 µm/sec on this material is presented in Figure 13. The same features as before are observed: the material is dissipative and there is a residual strain that reaches about 30% by the end of the test. The main difference however is that this test has been performed at room temperature, whereas for the sample presented in Figure 12 this behavior is observed at much higher temperatures. The good quality of the mixing ensures that the material

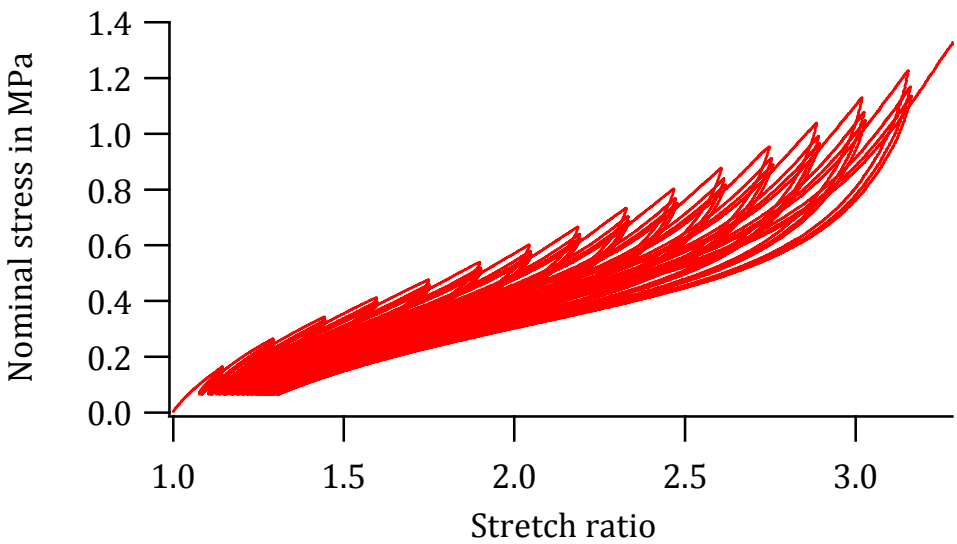

Figure 13: step-cyclic test of a sample using a filler network prepared by UV-polymerization with 1.5 mol% BDA. The test has been performed at room temperature.

is not too dissipative at room temperature. Obviously, increasing the temperature should decrease further the dissipation, but these experiments have not been carried out yet.

6.Conclusions

Until now, the study of double network elastomers has focused on materials in which the filler and the matrix networks are very similar. Both networks have originally been chosen in the (meth)acrylate family and with similar values of glass transition temperatures. It is however interesting to explore new types of filler networks, and this side-project indeed focuses on the use of a glassy filler network. These hybrid double networks could give rise to elastomeric materials that have viscoelastic dissipation, which could help enhancing their fracture properties.

PMMA filler networks with different types and quantities of crosslinkers have been prepared and incorporated into double network structures. The synthesis of these materials has turned out to be complicated, mostly because of the necessity to use a solvent and because of the lower reactivity of methacrylates.

The small strain characterization of these materials reveals that the intermixing between the filler and the matrix networks plays a very important role. In most cases, only partial mixing is obtained, which results into very dissipative materials with a broad glass transition and high stiffness at room temperature. Details of the filler network microstructure strongly influence the viscoelastic properties of the double networks. In some cases for example, the DMA response of the double networks suggests that the filler network contains defects such as regions that are very rich in PMMA or short dangling chains. The heterogeneity in crosslinking density implies heterogeneous swelling and therefore heterogeneity in composition in the double network structure.

For one specific set of parameters, a double network with a good mixing between the filler and matrix networks has been obtained. This material is soft and overall elastomeric, although its mechanical response at large strains in cyclic test features some hysteretic cycles and residual strain. Further studies could focus on the detailed study of these mechanical properties and on the identification of the reason why this specific set of parameter gives a better mixing.

7.References

1. Millereau P, Ducrot E, Clough JM, Wiseman ME, Brown HR, Sijbesma RP, et al. Mechanics of elastomeric molecular composites. Proc Natl Acad Sci. 2018 Aug 28;201807750.

2. Ducrot E. Innovative tough elastomers: Designed sacrificial bonds in multiple networks [PhD thesis]. [Paris]: Université Pierre et Marie Curie; 2013.

3. Millereau P. Large Strain and Fracture of Multiple Network Elastomers [PhD thesis]. [Paris]: Université Pierre et Marie Curie; 2017.

4. Slootman J. Quantitative detection of damage in soft materials using mechano-fluorescence [PhD thesis]. [Paris]: PSL Research University; 2019.

5. Sperling LH. Interpenetrating Polymer Networks and Related Materials [Internet]. Boston, MA: Springer US; 1981 [cited 2016 Dec 15]. Available from: http://link.springer.com/10.1007/978-1-4684-3830-7

6. Lalande L, Plummer CJG, Månson J-AE, Gérard P. Microdeformation mechanisms in rubber toughened PMMA and PMMA-based copolymers. Eng Fract Mech. 2006 Nov 1;73(16):2413–26.

7. Fox TG. Influence of Diluent and of Copolymer Composition on the Glass Temperature of a Polymer System. Bull Am Phys Soc. 1956;1:123.

8. Mark JE. Physical properties of polymers handbook [Internet]. Vol. 1076. Springer; 2007 [cited 2016 Oct 28]. Available from: http://link.springer.com/content/pdf/10.1007/978-0-387-69002-5.pdf

General conclusions and prospects

This research project is driven by the need to bridge the gap between the academic knowledge of double network elastomers and their use in industrial and applicative fields. In particular, mechanics of double network elastomers heavily relies on the stretch state of the filler network. This fundamental observation opens the way for new materials in which the filler network is prestretched in one direction specifically, by opposition to traditional double networks in which prestretching is isotropic and due to the osmotic equilibrium swelling of the matrix network.

A simple physical picture that requires a complex chemistry

This physical picture is indeed very simple, but its simplicity comes from the fact that it relies on one specific physical ingredient: the uniaxial orientation of the filler network. This specific feature has been found to be difficult to achieve in practice. Eventually, the solution we have found requires the design and use of a dual-curing system.

Conceptually, the difficulty to prepare oriented networks comes from the fact that chemistry is intrinsically isotropic, in the sense that a chemical reaction does not have in itself a preference for a given direction. In order to induce anisotropy at the molecular scale, an external force needs to be applied, and then the limitations of the materials truly limit the achievable prestretching.

In this project, it remains difficult and expensive in terms of time and resources to prepare filler networks that have just a limited amount of prestretching. An immediate improvement to the project would therefore be to find another chemical system, for instance by benefitting from an external expertise in polymer chemistry. Such a system should comply with the following non-exhaustive list of requirements: easy implementation with moderate chemistry equipment, compatibility with acrylates chemistry, fast and quantitative yield in mild conditions, versatility and tunability of experimental parameters (to vary the crosslinking density for example). Most importantly, the system should be effective in the bulk and dry state, in the absence of solvent. Such a set of requirements is not common in organic chemistry, and as a matter of fact it has been experimentally difficult to adress just a fraction of these requirements

The breakdown of the intuitive modelling approaches

Despite the experimental difficulties, prestretched filler networks have been obtained and incorporated in double network structures. The study of their mechanical properties gives some insights on the details of the mechanics of multiple network elastomers, and on some of the limitations of the existing modelling strategies.

Until now, the mechanical properties of double network elastomers have been successfully described by considering only the average stretch state of the filler network, always assuming that affine deformation applies and that the directions are fully independent. Once a dual-curing system is used and an anisotropic prestretching is added, such an approach is not valid any longer.

The most immediate proof of this is the fact that the strain-hardening of the prestretched DN in the transverse direction is always found to be located at strains smaller than the unprestretched DN. Yet, the relative changes of dimensions ensure that the filler network is on average more extended in the unprestretched state compared to the prestretched state in the transverse

direction. The solution to such a paradox has been found by extending Flory's model to large strains and by considering that second-curing is equivalent to having two populations of networks strands in the filler network. Modelling approaches based on the average stretch state of the filler network therefore break down, because the reference states of the two populations are not the same.

But even with this approach, there are some strong limitations. In all the prestretched DN studied in this manuscript, the transverse direction has been found to be very poorly described by the model. The first limitation of our approach is that we neglect all cross-directional couplings aside from Poisson's effect. The second one more fundamental lies in the fact that our modellings are based on a mean-field approach. Ultimately, the two populations of chains are considered separately and their contributions are simply added to predict the behavior of the entire network. In other words, our modelling approach may describe the behavior of a material in which some short chains are randomly dispersed in the structure, but breaks down as soon as these chains connect and form a percolative path. This is probably the reason why the transverse direction is so inaccurately described by our extended version of Flory's model.

Ultimately, what is needed is a model that takes into account the connectivity of the chains, i.e. molecular simulations. Some simulations are currently being developed in this direction, and it may be interesting to see if they are better than our model in catching the behavior of the transverse direction of prestretched double networks.

An original decorrelation between small and large strains

In terms of mechanical properties, the prestretched double networks that are presented in this research project show an overall isotropic behavior at small strains. This has been attributed to the fact that the extent of prestretching is in all cases fairly limited, so that the filler network chains remain Gaussian in the absence of significant deformation.

In the large strain regime however, several aspects of the mechanical response of our materials are directional-dependent. One of them is position of the onset of strain-hardening, which is related to the residual stretching capacity of the filler network to its maximum extensibility. The presence or absence of damage in cyclic loading is another one.

The damage that is observed in large strains in our materials gives us the opportunity to highlight some significant differences between our materials and the classical Mullins effect observed in tough elastomers based on a reinforcement with nanoparticles. In the latter case, a continuous damage is observed, starting at very small deformations and increasing with stretch. The damage at small strains (i.e. the decrease of the number of elastic strands) and the damage at large strains (i.e. the change in maximum extensibility) can be described by the same damage parameter. In our materials, damage only starts from a given deformation threshold, which indicates that filler network chains must be extended enough to break. Moreover, the damage at small strains is much smaller than in large strains. In our materials, some chains are indeed broken, but their contribution to the modulus is smaller than their contribution to the stress in large strains. Once again, this feature highlights the fact that our materials cannot simply be described by a mean-

field approach in which all chains are treated equally and simply added to obtain the modulus or the stress of the network.

Heterogeneity profoundly impacts the behavior in large strains

Qualitatively, the major difference between our materials and traditional double network elastomers is the presence of damage during cyclic loading. The presence of damage has been qualitatively explained by the presence of additional heterogeneity. In our dual-cured filler networks, the first crosslinking step results from the copolymerization of chemical functions with different reactivities. This most probably results in some non-random incorporation and strand length heterogeneity. This broad distribution of strand sizes results in a broad distribution of end-to-end vectors, which eventually results in a broad distribution of maximum extensibilities for the filler network strands. As a result, cyclic loading features some visible damage due to the presence of many less extensible chains in the structure. In contrast, there is indeed a distribution of end-to-end-vectors in traditional double network elastomers, but it is probably not broad enough to induce visible damage.

In our materials, this heterogeneity is fully uncontrolled, since it is the result of the way the material polymerizes. It may even vary significantly from sample to sample. One way to push this project forward would be to try to gain some control over the type and degree of heterogeneity. For instance, one could imagine using prepolymers with given molecular weight distributions in order to better control the filler network structure. The study of the influence of heterogeneity on the properties of double networks could be a way to study the initiation of cracks in polymeric networks, which remains one of the main gray areas in the field of soft materials fracture.

RÉSUMÉ

Les doubles réseaux élastomères sont composés de deux réseaux de polymères interpénétrés. Un « réseau de charge » fortement réticulé et pré-étiré isotropiquement est incorporé dans un « réseau matrice » mou. Les propriétés d'un tel composite moléculaire dépendent principalement de l'état d'étirement des chaines du réseau de charge qui dicte leur extensibilité maximale. Ici, nous introduisons une part d'anisotropie dans l'architecture des doubles réseaux en utilisant des réseaux de charge pré-orientés dans une direction en particulier. Ce pré-étirement uniaxial est obtenu en réticulant le réseau de charge en deux temps, le deuxième étant réalisée à l'état étiré. Deux systèmes de double réticulation sont conçus et activés soit par chauffage soit par UV. Des réseaux de charge pré-étirés sont ensuite obtenus et ne montrent pas d'anisotropie ni de module ni de gonflement. En revanche, les doubles réseaux préparés à partir de réseaux de charge pré-étirés ont un comportement anisotrope à grande déformation. En particulier, la direction transverse n'est pas prédite par des modèles de type champ moyen. Nous proposons un nouveau modèle basé sur la non-additivité des extensibilités limites des deux populations de points de réticulations afin de prédire semi-quantitativement le comportement en grande déformation de ces matériaux tenaces et anisotropes. Nous trouvons également que les endommagements visibles en petite et grande déformation sont découplés, contrairement aux élastomères chargés dans lesquels un seul paramètre d'endommagement suffit pour décrire les deux régimes. Au final, ces nouveaux doubles réseaux constituent un pas vers des applications pratiques, des matériaux et des situations qui sont plus proches de la réalité.

MOTS CLÉS

Elastomère, réseaux multiples, double réticulation, anisotropie, mécanique, fracture

ABSTRACT

Double network elastomers are composed of two interpenetrated polymeric networks. A highly-crosslinked and isotropically prestretched filler network is embedded into a soft matrix network. The properties of such a molecular composite primarily depend on the state of stretch of the filler network chains, which dictates their maximum extensibility. Here, we introduce some anisotropy into the double network architecture by using uniaxially pre-oriented filler networks. This prestretching is obtained by crosslinking the filler network in two steps, the second one being performed in the stretched state. Two dual-curing systems are designed, activated either by heating or by UV. Prestretched filler networks are then prepared and do not show any anisotropy in modulus nor swelling ratio. However, double networks prepared from prestretched filler networks show a pronounced anisotropic behavior in large strain. In particular, the transverse direction is not predicted by mean-field models. We propose a new model based on the non-additivity of the finite extensibility for both populations of crosslinks to predict semi-quantitatively the large strain behavior of these anisotropic tough materials. Interestingly we find also that the damage in small and large strain are decoupled, as opposed to conventional filled rubbers where a single damage parameter is sufficient for both regimes. All in all, these new double network elastomers based on more complex network topologies represent a new step toward practical applications, materials and situations that are closer to real life situations.

KEYWORDS

Elastomer, multiple network, dual-curing, anisotropy, mechanics, fracture